



The  
University  
Of  
Sheffield.

# **Subcellular information processing in the olfactory system**

A thesis submitted to The University of Sheffield  
in partial fulfilment of the requirements for the degree of  
Doctor of Philosophy

The University of Sheffield  
Faculty of Science  
Department of Biomedical Science

By Hoger Amin

Registration number: 160101157

January 2020

## Table of contents

<b>Preface</b> .....	4
<b>Summary</b> .....	5
<b>List of Abbreviations</b> .....	6
<b>Acknowledgements</b> .....	8
<b>1. General introduction</b> .....	9
1.1 Local computation in the nervous system.....	9
1.1.1 The rise of graded potentials and local computations .....	9
1.1.2 Mechanisms of encoding information.....	10
1.1.3 The basis of local computations.....	14
1.1.4 Dendritic release of neurotransmitters .....	18
1.1.5 Local computations facilitate stimulus-specific adaptation and branch-specific plasticity ..	19
1.1.6 The case for using <i>Drosophila melanogaster</i> to study local computations .....	21
1.2 Olfactory processing in <i>Drosophila</i> .....	22
1.2.1 The challenge of processing olfactory sensory information .....	22
1.2.2 Anatomy and physiology of the <i>Drosophila</i> early olfactory system .....	23
1.2.3 Stereotyped PN-LH connectivity implies that the LH uses predictive sampling .....	26
1.2.4 The LH utilises predictive sampling to drive innate responses .....	28
1.2.5 Identifying the MB as a locus of olfactory learning .....	29
1.2.6 The arbitrary nature of PN-KC connectivity and KC odour responses provide a basis for associative learning .....	31
1.2.7 Integration of stimulus identity and valence in the mushroom body facilitates memory formation.....	34
1.2.8 The MB integrates information from sensory pathways and the fly's internal state to generate context-specific innate and learned behaviour .....	40
1.2.9 Network-level recurrent activity and compartment-crosstalk underlie post-learning processing.....	44
1.2.10 The case for studying the APL neuron in the context of localised processing .....	48
1.2.11 Tools for imaging neuronal activity.....	56
1.2.12 Tools for local, artificial activation of neurons.....	60
1.2.13 Parallels between the mushroom body and the vertebrate nervous system .....	61
<b>Focus of this thesis</b> .....	64
<b>2. Materials &amp; Methods</b> .....	65
2.1 Materials.....	65
2.1.1 Fly rearing.....	65

2.1.2 Fly stocks .....	65
2.1.3 Equipment .....	67
2.1.4 Reagents .....	68
2.1.5 List of filters used for widefield and two-photon microscopy.....	70
2.2 Methods.....	71
2.2.1 Fly preparation .....	71
2.2.2 Functional imaging .....	72
2.2.3 Odour delivery .....	72
2.2.4 Picospritzer local drug application.....	73
2.2.5 Electric shock.....	73
2.2.6 Aversive conditioning .....	73
2.3 Analysis.....	74
2.3.1 Analysis of imaging data.....	74
2.3.2 3D-skeletonization .....	76
2.4 Molecular biology .....	79
2.4.1 Gel electrophoresis.....	79
2.4.2 Generation of new DNA constructs .....	79
2.4.3 Strategy .....	79
<b>3. Input to the APL neuron remains localised, but its output has a widespread effect .....</b>	<b>82</b>
3.1 Overview of the chapter.....	82
3.2 Results.....	83
3.2.1 Activity arising in the lobular and calyceal projections of the APL neuron are spatially segregated.....	83
3.2.2 Whole-MB characterisation of activity attenuation in the APL neuron .....	87
3.2.3 Local activation of the APL neuron has a largely local inhibitory effect on KC baseline activity.....	93
3.2.4 Local stimulation of the APL neuron inhibits KC odour responses beyond the spatial extent to which it is activated .....	102
3.2.5 Local puffing of GABA and local activation of the APL neuron have similar effects on KC activity.....	120
3.2.6 Comparison of activity or effect spread vs red dye spread .....	125
3.3 Discussion .....	129
3.3.1 Whole-MB characterisation of activity spread in the APL neuron.....	129
3.3.2 Local and distal effects of APL activation on KC activity .....	131
<b>4 Characterising electric shock responses and plasticity in the APL neuron.....</b>	<b>134</b>
4.1 Introduction.....	134
4.2 Results.....	135
4.2.1 APL neuron ES responses are spatially differential.....	135

4.2.2	Characterising plasticity in the APL neuron .....	137
4.3	Discussion .....	139
4.3.1	Characterisation of electric shock responses in different regions of the APL neuron .....	139
4.3.2	No plasticity observed in the APL neuron following electric shock-odour coupling .....	140
<b>5</b>	<b>Local muscarine application differentially affects KC subsets</b> .....	<b>142</b>
5.1	Introduction .....	142
5.2	Results .....	144
5.2.1	Muscarine differentially affects the baseline activity of KC subsets, but overall inhibits odour responses throughout the MB .....	144
5.3	Discussion .....	149
<b>6</b>	<b>Discussion</b> .....	<b>153</b>
6.1	Summary of findings .....	153
6.2	Localised activity in the APL neuron .....	154
6.3	Determining the spatial extent of the APL neurons output .....	155
6.4	Plasticity in the APL neuron .....	155
6.5	Expanding upon my findings and improving the experimental approach .....	158
6.5.1	Optical imaging of neuronal activity .....	158
6.5.2	Local activation of neurons .....	161
6.5.3	Measuring plasticity in the APL neuron .....	164
6.6	The implications of my findings for APL neuron function in the MB .....	165
6.7	Comparisons to other systems .....	167
	References .....	169

## Preface

This thesis and all the results presented in it stem from my own work and writing except where it is indicated otherwise in the text, with editorial comments from my supervisor. This thesis has not previously been submitted to this or any other university

Certain parts of this work have previously been published in the following papers:

AMIN, H. & LIN, A. C. 2019. Neuronal mechanisms underlying innate and learned olfactory processing in *Drosophila*. *Curr Opin Insect Sci*, 36, 9-17

BIELOPOLSKI, N., AMIN, H., APOSTOLOPOULOU, A. A., ROZENFELD, E., LERNER, H., HUETTEROTH, W., LIN, A. C. & PARNAS, M. 2019. Inhibitory muscarinic acetylcholine receptors enhance aversive olfactory learning in adult *Drosophila*. *Elife*, 8

I declare that the parts of these publications that are reproduced in this thesis are based on my own work or writing. Where this is not the case, the respective publications have been referenced.

## Summary

The nervous system is tasked with the challenge of processing a variety of sensory stimuli from the environment with limited coding space and energy consumption. Recent findings challenge the traditional view of the neuron as the elementary functional unit of the nervous system, in which dendrites mainly serve as input sites, and action potential propagation through axons generates output. Instead, individual neurites have emerged as the single functional unit capable of computing inputs and generating outputs locally.

Despite recent advances, the link between the mechanisms that facilitate local computations and their behavioural relevance remains unclear. I addressed this problem in *Drosophila Melanogaster*. The anatomical organisation of the mushroom body, a brain region associated with learning, has a compartmentalised architecture that forms the basis for local computations. My project studied subcellular signalling in the mushroom body and its role in memory formation, with emphasis on the non-spiking APL neuron that is involved in sparse odour coding and memory formation, to determine if it operates locally. To investigate this, I addressed the following points.

1. I investigated the nature of activity spread in the APL neuron. I found that input to the APL neuron evokes activity that attenuates as it propagates, supporting local computations.
2. I characterised the spatial nature of inhibition from the APL neuron onto mushroom body neurons. I found that the inhibition had a strong local effect that diminished with distance.
3. I sought to determine if there are spatial differences in the APL neuron's response to electric shock, and if plasticity in the APL neuron is similarly spatially distinct. I found that electric shock responses are spatially distinct, but my data on plasticity was inconclusive.
4. I investigated the effects of local muscarine signalling on Kenyon cell odour responses. I found that muscarine signalling has spatially distinct effects.

## List of Abbreviations

AL	Antennal lobe
APL	Anterior paired lateral
ATP	Adenosine triphosphate
Ca <sup>2+</sup>	Calcium
CaCl	Calcium chloride
CS	Conditioned stimulus
dAC	dorsal accessory calyx
DAN	Dopaminergic neuron
DBD	DNA binding domain
DNA	Deoxyribonucleic acid
dNPF	<i>Drosophila</i> neuropeptide F
dNTP	deoxynucleoside triphosphate
Dop1R1	Dopamine 1-like receptor 1
Dop1R2	Dopamine 1-like receptor 2
Dop2R	Dopamine-like receptor 2
DPM	Dorsal-paired medial
GABA	$\gamma$ -aminobutyric acid
GAD	Glutamate decarboxylase
GECI	Genetically encoded calcium indicator
GEVI	Genetically encoded voltage indicator
GtACR	<i>Guillardia theta</i> anion channelrhodopsin
HCl	Hydrogen chloride
KC	Kenyon cell
KCl	Potassium chloride
IAA	Isoamyl acetate
IALT	lateral antennal lobe tract
LH	Lateral horn
LHIN	Lateral horn input neuron
LHN	Lateral horn neuron
LHON	Lateral horn output neuron
LTM	Long-term memory

mAChR	Muscarinic acetylcholine receptor
mALT	medial antennal lobe tract
MB	Mushroom body
MBON	Mushroom body output neuron
MCH	4-methylcyclohexanol
MgATP	Magnesium ATP
MgCl <sub>2</sub>	Magnesium chloride
MgSO <sub>4</sub>	Magnesium sulfate
NaCl	Sodium chloride
NaH <sub>2</sub> PO <sub>4</sub>	Monosodium phosphate
ORN	Olfactory receptor neuron
OCT	3-octanol
PAM	protocerebral anterior medial
Ped	Pedunculus
PN	Projection neuron
PPL	paired posterior lateral
Rdl	Resistance to dieldrin
SNARE	Soluble N-ethylmaleimide sensitive factor (NSF) attachment <b>protein</b> receptors
STM	Short-term memory
TES	<i>N</i> -tris(hydroxymethyl)methyl-2-aminoethanesulfonic acid
UAS	Upstream activation sequence
vAC	ventral accessory calyx

## Acknowledgements

This work would not have been possible without the guidance, help, and support of many people both inside and outside University of Sheffield.

First, I would like to thank my supervisor, Andrew Lin, who has been invaluable for guidance, help with techniques, encouragement, and developing ideas together over afternoon-long discussions. I also want to thank Andrew for genuinely giving thought to any ideas I came up with. I could not have hoped for a more patient, calm, and intelligent supervisor.

I would like to thank all current and former colleagues of our group who have offered helpful feedback on the work I have done and provided practical assistance when needed.

I give my thanks to my colleagues at The Bateson Centre who have provided helpful feedback on my results.

I would like to thank the staff, especially Katherine Whitley, at the fly facility in The Bateson Centre for the great work they are doing and the service they provide with fly maintenance.

I thank Darren Robinson for the services and support provided at The Light Microscopy Facility.

I am grateful for the support and encouragement my parents have given me throughout my studies.

Finally, I give my deep-felt gratitude to my fiancée, Angela Ibler, for the encouragement, love, and support that she has given me throughout my PhD. I am very grateful for all the emotional support she gave me, intellectual discussions we had, but also the cooking, laundry, grocery shopping, and all other practical work that she took care of while I was deeply submerged in the writing waters. Most of all, I was simply grateful for her presence.

# 1. General introduction

## 1.1 Local computation in the nervous system

### 1.1.1 The rise of graded potentials and local computations

Our understanding of the nervous system is continuously expanding. Broadly speaking, a brain allows an animal to gather information from its surroundings, integrate this information with its internal state, and generate context-specific behaviour. All of this can be tempered by previous experience, which the brain can store and recall. Much of this does not require a nervous system to accomplish. A single receptor tied to a molecular pathway can store information from the environment through a protein modification that signifies a change in state, leading to further downstream signalling and action. By making the modification transient, the information can be stored as a ‘memory’, and by interacting with other signalling pathways that represent the internal state, external and internal information can be integrated (Laughlin and Sterling, 2015).

However, decision-making often involves multimodal sensory input, conflicting or incomplete information, and state-dependent physiological needs. Under such circumstances, the ability of the nervous system to integrate information at high capacity and complexity becomes essential. Doing so requires individual neurons to process and convey information between each other.

Information is encoded as graded- and action potentials. Of the two, the action potentials, also known as ‘spikes’, have by far received the most attention and are traditionally considered the main mechanism of encoding information. The emphasis on action potentials is particularly evident in vertebrate research, where action potentials are more prevalent than in small invertebrates (Alle and Geiger, 2006, Bialek et al., 1997). However, studies from the last few decades have demonstrated that spatially restricted activity, whether it is graded potentials or locally restricted spikes, are widely used in sensory systems of both vertebrates and invertebrates, and also in invertebrate central circuit neurons (Burrows and Siegler, 1978, Burrows, 1980, Jahr and Nicoll, 1980, Roberts and Bush, 1981, Juusola et al., 1996, Zhou and Fain, 1996, Grimes et al., 2010, Chen et al., 2017, Liu et al., 2017), and a theoretical framework is developing for the significance of graded potentials or localised activity in information processing (Grimes et al., 2010, Sardi et al., 2017, Branco and Häusser, 2010, Wybo et al., 2019). Nevertheless, the significance of subcellular information

processing for higher brain function and behaviour remains largely unknown and calls for further studies in a genetically tractable system with well-established behavioural readouts.

The compartmentalised architecture of memory formation in the olfactory system of *Drosophila* provides a great opportunity to study this question. The anterior paired lateral neuron (APL), a non-spiking  $\gamma$ -aminobutyric acid (GABA)-synthesising (GABAergic) neuron, is part of the fly olfactory circuit, and widely innervates the mushroom body (MB) (Pitman et al., 2011, Papadopoulou et al., 2011, Tanaka et al., 2008), the central brain region where olfactory associative learning takes place. Memories are formed in discrete regions in the MB (Aso et al., 2014a, Hige et al., 2015). The APL neuron ensures sparse odour coding by Kenyon cells (KCs) through feedback inhibition, and memory formation induces plasticity in the APL neuron (Lin et al., 2014a, Liu and Davis, 2009, Zhou et al., 2019). However, the spatial nature of the feedback inhibition and learning-induced plasticity remain unknown. This study aimed to characterise propagation of neuronal activity in the APL neuron, determine the nature of its inhibitory feedback onto KCs, and establish if learning induces spatially differential plasticity in the APL neuron.

### 1.1.2 Mechanisms of encoding information

Neuronal signalling relies on the polarised nature of the cell membrane. A net negative charge on the cytoplasmic side arises from an actively maintained difference in intracellular and extracellular ionic concentrations, of which sodium, potassium, chloride, and calcium are the most influential. This charge separation results in a resting membrane potential that largely depends on the composition of ion channels in the cell membrane (Kandel, 2013).

This occurs through graded potentials or action potentials, and in some cases both (Pasztor and Bush, 1982, Alle and Geiger, 2006, Kandel, 2013). Graded potentials are analogue signals that arise from chemical or sensory synaptic inputs that activate receptors specific to the sensory stimulus or neurotransmitter. Depending on the sensory system, activation of these receptors directly or indirectly leads to a change in the membrane potential due to closing or opening of ion channels. Graded potentials propagate through the neuronal projections by passive spread, leading to attenuation of the membrane depolarisation as the signal spreads (Roberts and Bush, 1981) (**Fig. 1.1 A**). Signal attenuation limits the distance to which a neuron can transmit signals through graded

potentials. To overcome signal attenuation across large distances, neurons generate action potentials, also known as spikes (Kandel, 2013).

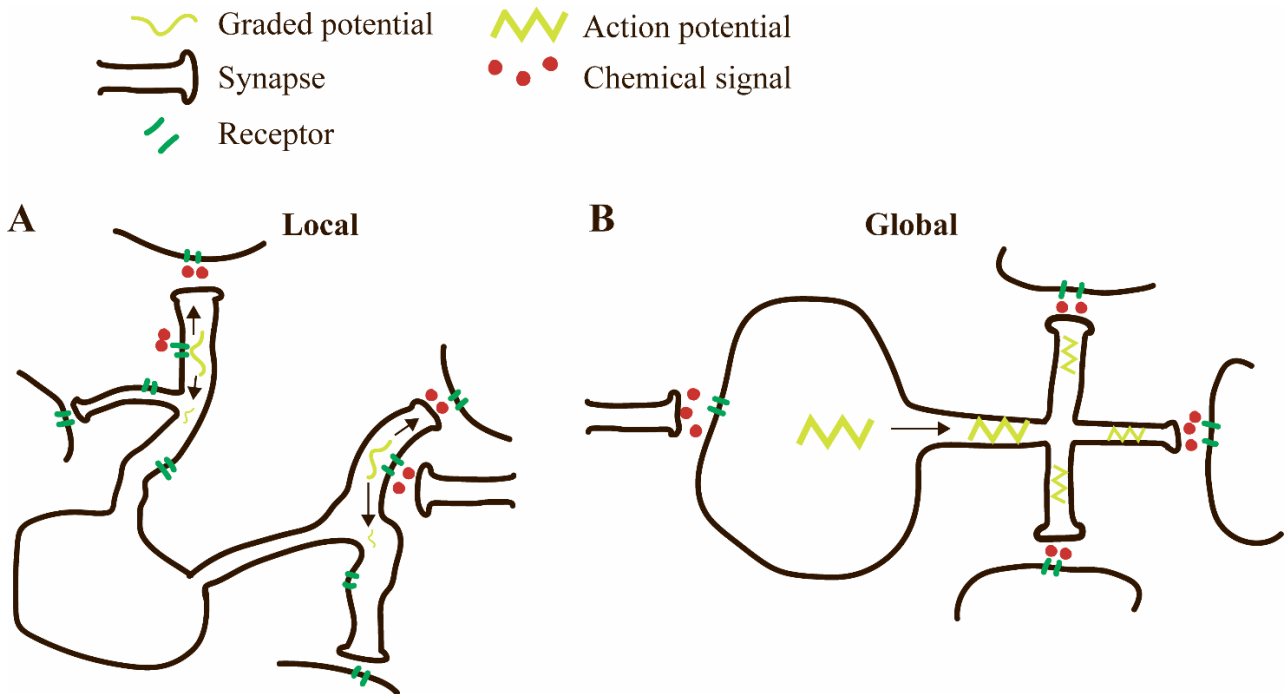


**Figure 1.1 Local and global signalling**

Schematic of local and global signalling. **(A)** Graded potentials attenuate as they propagate, only evoking neurotransmitter release (chemical signal) from nearby synapses. **(B)** The regenerative nature of action potentials means that the signal can spread far, leading to release of neurotransmitters from nearby and distal synapses.

Action potentials are all-or-none events that are generated in neurons with voltage-gated sodium channels. Synaptic inputs locally depolarise the cell membrane, leading to opening of voltage-gated sodium channels. The influx of sodium creates a positive feedback loop, leading to opening of more sodium channels. This inward current passes a threshold when it becomes strong enough to overcome outward currents that keep the membrane polarised, leading to generation of an action potential. This process occurs at the axon initial segment (AIS), which has a high density of sodium channels. **(Fig. 1.1 B)**. Depolarisation causes an influx of calcium through voltage-gated calcium channels clustered at synapse terminals, the region where pre- and post-synaptic neurons make contact and transmit signals. Here the signal is transformed from electrical to chemical signalling. Synapse terminals contain docked vesicles loaded with neurotransmitters. These vesicles are bound to the cell membrane through Soluble N-ethylmaleimide sensitive factor (NSF) attachment **protein** receptors (SNAREs). The calcium influx increases the intracellular concentration 100-fold, which

causes another protein, synaptotagmin, to bind calcium, which interacts with the SNAREs to fuse the vesicle with the cell membrane, releasing neurotransmitters into the synaptic cleft. The neurotransmitters bind to specific ligand-gated receptor ion channels on the postsynaptic neuron, transforming the signal back to an electrical form.

A key feature of neuronal anatomy is the characteristic extension of the cell membrane and cytoplasm to form projections that brings them into proximity of other neurons. These projections, collectively referred to as neurites, are subdivided into dendrites and axons. Dendrites are traditionally considered the input sites of neurons, comprising the postsynaptic side of the synaptic cleft. They form elaborate, thin branches, with sections as low as 0.05  $\mu\text{m}$  in diameter. Axons are the output sites, and generally form thicker projections, typically in the range 0.2-4  $\mu\text{m}$  for sensory neurons, but up to 1 mm in the extreme case of the squid giant axon. (Laughlin and Sterling, 2015).

The diameter of a neurite is an important measure for passive propagation of currents in neurons, affecting both the conduction velocity of electric signals in neurons, and the distance it can cover. The thinner a neurite, the higher the resistance through the conducting cytoplasm, core, also known as axial resistance,  $r_i$ . Together with the membrane resistance,  $r_m$ , which depends on the ion channel composition in the cell membrane, these two parameters give the length constant,  $\lambda$ . This parameter largely determines how far a signal reliably can be transmitted. The time it takes for the signal to

decay to 37% of its initial amplitude is given by  $\lambda = \sqrt{\frac{r_m}{r_i}}$

Being relatively thin, dendrites have high axial resistance. Consequently, they are usually less than 1 mm long. For insect brains, this is not a significant limitation for transmission across “large” distances. As an example, the fruit fly brain measures less than 600  $\mu\text{m}$  in its largest dimension.

The speed of a signal conveyed by passive spread is limited by the rate of current flow, as the ions carrying charge must navigate between molecules in the cytoplasm. Increasing neurite diameter allows higher current flow, reducing axial resistance, which leads to increased conduction velocity. Furthermore, changes in membrane potential do not instantaneously reach a peak value. Like a capacitor, the cell membrane can store charge, determined by its capacitance,  $c_m$ . The greater the membrane surface area, the more charge it can store. For current to flow, charge must be deposited on the membrane. Therefore, the change in membrane potential reaches its peak only after a delay.

This delay is given by the time constant,  $\tau$ , which denotes the time it takes for a change in membrane potential to reach 63% of its peak value, given by  $\tau = r_m \times c_m$

With these parameters in mind, what are the main differences between graded- and action potentials?

Due to the sharp and high current generated by action potentials, they are much better suited than graded potentials for signalling across large distances at high velocity. Action potentials can reach conduction velocities higher than 1 mm/ms, while graded potentials only reach up to 50  $\mu\text{m}/\text{ms}$  (Laughlin and Sterling, 2015).

However, graded potentials are analogue signals that can gradually change to represent many different response levels, whereas an action potential encodes information by digital signalling, representing spaced changes of membrane potential between two levels. Graded potentials can transmit information at a rate higher than 2000 bits/s, while action potentials are limited to 500 bits/s or less. Furthermore, sending information with graded potentials is energetically more efficient than action potentials, as a single action potential requires a change in membrane potential of  $\sim 100$  mV for 1 ms, whereas graded potentials can transmit information by changing the membrane potential by a few mV. The larger the change in membrane potential, the costlier the subsequent transport of sodium out of, and potassium into, the cell required to repolarise the membrane potential. Additionally, the diameter of projections required for transmission of action potentials are larger than those used for graded potentials, increasing maintenance costs and utilising more space (Laughlin and Sterling, 2015). Thus, the maximum speed and distance of activity propagation that neurons can achieve are balanced by costs in energy expenditure and utilised space.

These differences between the two modes of signalling, and the relatively small size of the insect nervous system, can explain why analogue signalling is commonly observed in insects, including *Drosophila melanogaster* (Pasztor and Bush, 1982, Juusola et al., 1996).

Action potentials have long been considered the prevailing mode of information coding and transmission in the nervous system, and further studies into action potentials are revealing nuances in this mode of transmission (Alle and Geiger, 2006, Bean, 2007). However, in sensory systems, and many central circuits in insects and other invertebrates, graded potentials, or spatially restricted

synaptic potentials, are commonly the means of encoding information (Pasztor and Bush, 1982, Juusola et al., 1996, Heidelberger, 2007, Castro and Urban, 2009, Marder, 2006). Recent studies also suggest that graded potentials can modulate neurotransmitter release elicited by action potentials (Alle and Geiger, 2006, Zbili et al., 2016). Finally, there are numerous studies from various animals showing that localised signalling facilitates local computations in individual neurites (Branco and Häusser, 2010, Wybo et al., 2019, Ludwig et al., 2016, Medan et al., 2018, Cichon and Gan, 2015, Bayley and Hedwig, 2018, Ogawa and Oka, 2015) These findings demonstrate that graded potentials, or spatially restricted synaptic potentials, are an essential mechanism for encoding and transmitting information in the nervous system and warrant further study to understand their role in ultimately generating decision making.

The following sections will cover the theoretical rationale for localised information processing, the actual studies that demonstrate the prevalence of local computations in the nervous system, and its functional significance physiologically and behaviourally.

### 1.1.3 The basis of local computations

The beautiful illustrations of the nervous system published by Ramón y Cajal established the canonical view of neurons as the functional units of the nervous system (Swanson and Swanson, 1995), which was further cemented by the characterisation of action potentials by Hodgkin and Huxley (Hodgkin and Huxley, 1952). In this view neurons are unidirectional. The dendrites act as input sites that collect information, and convey a signal to the axon initial segment, where these signals are integrated to generate action potentials for further transmission of the information.

Our understanding of information processing has expanded upon this view to recognize that the action potential is not the only way for neurons to convey information. Neuronal input and output generation can occur locally, independently of action potentials. Dendritic branches can function as independent units that locally compute inputs, and release neurotransmitters onto specific postsynaptic targets. There are numerous studies that demonstrate the use and importance of local information processing for sensory processing and task-specific memory formation in vertebrate model systems (Branco and Häusser, 2010, Wybo et al., 2019, Ludwig et al., 2016, Medan et al., 2018, Cichon and Gan, 2015). However, the importance of local processing for extraction of different sensory features, or processing of input from different sensory channels, in spatially

segregated branches has also been observed in invertebrates (Dan et al., 2018, Liu et al., 2017, Yang et al., 2016, Zhang et al., 2019, Elyada et al., 2009), implying that local computations are widely utilised across the nervous system of organisms. What are the implications of localised computations in neuronal projections?

- (1) Instead of operating as a single processing unit, a neuron takes on the role of a network, vastly increasing the computational power of a single neuron. By limiting activity spread to a branchpoint or even more locally within a branch, a single neuron can perform computations in spatially segregated compartments (Branco and Häusser, 2010, Wybo et al., 2019).
- (2) A single neuron facilitates independent computations and output signalling to multiple postsynaptic targets. Inputs originating from different parts of the brain, e.g. different sensory channels, can be processed independently. In turn, local processing would lead to local output, targeting specific postsynaptic targets relevant to the type of input (Branco and Häusser, 2010, Wybo et al., 2019).
- (3) Energy and space constraints posit that information should be processed utilising as little space as possible (Laughlin and Sterling, 2015). If inputs, computations, and outputs all occur locally within a dendritic branch, there is no need to spend energy on conveying the information to other parts of the neuron before reaching the postsynaptic target. Thus, local processing optimizes energy expenditure.

Localised information processing relies on the ability to restrict activity spread. How can activity in neuronal projections be spatially restricted? Activation of ligand-gated ion channels evoke graded potentials in neurites. Graded potentials exponentially decay with distance. Consequently, activity decays rapidly in dendritic branches (as thin as  $0.05\ \mu\text{m}$ ) due to their high axial resistance (Laughlin and Sterling, 2015). Thus, one way to compartmentalise analogue signals is simply to transmit through thin neurites.

Modelling studies suggest that inhibition is also an important mechanism for compartmentalization of activity in dendritic branches. Inhibition onto dendritic branches would serve not only to restrict the spread of activity within a branch, but also differentially affect computations in the branch depending on where along the branch the inhibitory synapse is localised (Wybo et al., 2019, Bloss et al., 2016). Several studies have confirmed that inhibition facilitates functional compartmentalisation, (described below) (Poleg-Polsky et al., 2018, Chen et al., 2017). In summary,

restricting spread of activity through passive conductance and inhibition are ways to facilitate local computations

What are the functional roles of local computations? Branch-specific computations have been extensively characterised in the vertebrate visual system. Studies on amacrine cells, who have no defined axonal projections, have elegantly demonstrated that computations occur within individual dendritic branches (Losonczy et al., 2008, Grimes et al., 2010, Vlasits et al., 2016, Poleg-Polsky et al., 2018). Starburst amacrine cells have numerous dendritic projections radiating from the cell soma that provide GABAergic input to neighbouring dendrites of direction-selective ganglion cells (DSGCs). The dendrites of starburst amacrine cells are selective for outward-moving, or ‘centrifugal’, stimulus (Euler et al., 2002). DSGCs receive non direction-selective excitatory input from bipolar cells. In turn, the GABAergic output from the starburst amacrine cell dendrites specific to stimulus direction inhibits their neighbouring DSGC dendrites, cancelling out the null-direction excitation (Mauss et al., 2017).

Direction-selectivity in the starburst amacrine cell dendrites is thought to arise from lateral inhibition, where dendrites with opposed direction-selectivity inhibit each other, and from organizing excitatory inputs to the dendrites so that temporal summation is strongest when excitatory input arrives outwardly, from the cell soma to the end of the dendrites (Fransen and Borghuis, 2017, Ding et al., 2016). This lateral inhibition is also thought to enhance compartmentalization between individual dendritic branches, improving direction-selectivity (Poleg-Polsky et al., 2018). Thus, lateral inhibition is crucial for establishing direction-selectivity but promoting compartmentalization, which allows individual neurites to specifically encode stimulus that follows a certain pattern.

The significance of passive spread and synaptic inhibition as facilitators of spatially segregated computations between dendritic branches has also been illustrated in glutamatergic amacrine cells. These cells are presynaptic to both ON- and OFF-pathways in the visual system. However, they maintain the parallel processing of the pathways by computing input and generating output to and from the two pathways in spatially segregated compartments of their dendrites. This spatial segregation is in part due to attenuation of synaptic potentials through passive spread, but also due to synaptic inhibition (Chen et al., 2017).

How do neurons that receive multimodal sensory input maintain the origin or identity of the inputs? Local dendritic computations facilitate independent processing of such inputs. The giant cricket interneuron, descending brain neuron ipsilateral 1-2, provides a great example of this. This neuron responds to visual stimulus, touch to the antennal flagellum, and stimulation of strain receptors at the antennal base. Each type of stimulus evokes distinct, localised calcium influx. For touch stimulus, the calcium influx is further refined to match a topographic map of the antenna. (Bayley and Hedwig, 2018). This is enabled by spatially restricting activity within neurites.

The Mauthner cells of the goldfish are another example of a neuron where dendritic compartmentalization facilitates multimodal computation of inputs from the visual and auditory system. Active conductance selectively allows postsynaptic potentials evoked by auditory inputs to reach the dendrites that receive visual input, but not the other way around, demonstrating how variations in ion channel expression selectively can facilitate asymmetric cross-compartmental signalling and computations (Medan et al., 2018).

Rather than processing multimodal sensory input in the same neuron, some neurons integrate different features of the same stimulus in segregated branches. Serotonergic neurons in *Drosophila* project to both the antennal lobes and the lateral horn. Odour stimulus elicits an inhibitory response in the neurites that innervate the antennal lobes in an odour-invariant manner, while the same stimulus evokes an excitatory response in the lateral horn projections in an odour-dependent manner. However, these projections are asymmetrically separated, as inhibition from the antennal lobe neurites reaches the lateral horn neurites, but not vice versa (Zhang et al., 2019). The inhibitory input to the serotonergic neuron's projections in the antennal lobe scales with odour concentration (Zhang, 2016). This serves as a gain control that allows the odour identity-specific excitation the serotonergic neurons receive in the lateral horn to be less concentration-dependent (Zhang et al., 2019).

In summary, local computations are facilitated by passive spread of activity, actively restricted dendritic spikes, and inhibition onto individual neurites. This serves a variety of sensory computations and numerous studies have demonstrated how local computations facilitate multimodal or feature-specific information processing in a single neuron.

#### 1.1.4 Dendritic release of neurotransmitters

For dendritic branches to be considered truly independent functional units, they should be able to not only integrate inputs, but also generate outputs. Dendrites can release conventional neurotransmitters like GABA and glutamate (Castro and Urban, 2009, Duguid et al., 2007), but also neuromodulators and numerous peptides (Zilberter et al., 1999, Patel et al., 2009, Duguid et al., 2007, Ludwig et al., 2016).

What facilitates dendritic neurotransmitter release? Dendrites harbour the different intracellular membrane compartments associated with secretory trafficking and exocytosis: endoplasmic reticulum, Golgi membranes, endosomes, and vesicles containing neurotransmitters can be found in dendrites (Kennedy and Ehlers, 2011). Synaptic potentials evoke calcium influx in dendritic branches (Yuste and Denk, 1995, Jackie et al., 1998). Dendritic release of glutamate, GABA, and dopamine is mediated by calcium influx (Zilberter et al., 1999, Patel et al., 2009, Castro and Urban, 2009, Jeffry, 2001). This has been linked to a requirement for SNARE proteins, suggesting that dendritic release depends on the exocytosis pathway (Ludwig and Stern, 2015, Duguid et al., 2007, Branco and Häusser, 2010). It has yet to be determined if these findings from specific neurons are generalizable, or if there are other mechanisms that serve a similar function in other neurons or organisms.

What is the physiological and behavioural functions of dendritic neurotransmitter release? There is little knowledge on this matter. One of the proposed functions of dendritic release is feedback inhibition to maintain neuronal activity within a certain range through retrograde or autocrine signalling (Regehr et al., 2009).

One example of this is from the auditory system. Auditory neurons of the lateral superior olive release GABA upon activation, which retrogradely regulates its excitatory and inhibitory inputs through GABA-B receptor signalling. It is proposed that this allows the auditory neurons to regulate the excitation/inhibition balance to accommodate the auditory stimulus they receive (Magnusson et al., 2008). Autocrine regulation of activity is mediated by dopamine signalling. Dopaminergic neurons in the substantia nigra pars compacta release dopamine from their dendrites, which regulates their activity through D2 auto receptors, and also targets downstream GABAergic neurons, increasing their release of GABA, and ultimately regulating motor behaviour (Rice and Patel, 2015).

Dendritic neurotransmitter release plays an important role in sensory processing. Dendrodendritic signalling between mitral and granule cells of the olfactory bulb mediate dendritic release of GABA from granule cell, onto mitral cells (Isaacson and Strowbridge, 1998, Jahr and Nicoll, 1982). Granule cells lack axons and instead release GABA from their dendritic projections. Behaviourally, the dendrodendritic feedback inhibition regulates the latency of olfactory discrimination. Increasing the GABA-mediated feedback inhibition reduces the latency of odour discrimination, while reducing GABA signalling has the opposite effect (Abraham et al., 2010).

Similar to granule cells, the GABAergic APL neuron in the *Drosophila* olfactory system has no defined axons, but instead expresses pre- and post-synaptic markers throughout its extensive projections (Wu et al., 2013). Depending on stimulus strength, this neuron provides local or global feedback inhibition to a population of neurons that encode multimodal sensory information (Yagi et al., 2016, Vogt et al., 2016, Kirkhart and Scott, 2015, Marin et al., 2020, Turner et al., 2008), known as KCs (Inada et al., 2017). This feedback inhibition maintains sparse odour coding in the KC population (Lin et al., 2014a).

In summary, local computations and dendritic neurotransmitter release enables single neurites to operate as independent functional units.

### 1.1.5 Local computations facilitate stimulus-specific adaptation and branch-specific plasticity

Behavioural adaptation to a changing environment relies on stimulus-specific learning. What are the implications of local computations in terms of memory formation and storage capacity? Theoretical work suggests that a neuron with dendritic branches that have independent thresholds for synaptic inputs has much greater storage capacity than a neuron with linear summation of inputs to its dendrites. When these two neuronal types were trained with different patterns of stimulus, the linear summation model neurons could respond to 600 patterns, while the non-linear, independent thresholding model neurons learned 27000 patterns (Poirazi and Mel, 2001). Practically speaking, the level of noise at individual dendritic branches might limit to what extent they can operate independently, depending on the number of active synapses at each branch.

Another hypothesis posits that local computations in branches underlies stimulus specific adaptation. By segregating representations of different stimulus types or parametric values into different dendritic regions or branches, adaptation can be stimulus specific, maintaining the nervous system's ability to detect novelty (Prešern et al., 2015). What is the physiological and behavioural significance of localised plasticity and adaptation?

Spatial segregation of dendritic computations facilitates branch-specific plasticity or adaptation (Losonczy et al., 2008, Prešern et al., 2015, Cichon and Gan, 2015, Ogawa and Oka, 2015). A well-described example of this is from motor control in rodents. Branch-specific plasticity is crucial for maintaining parallel memory formation in rodent motor cortex pyramidal neurons. Different motor-related learning tasks evoke calcium influx in distinct dendritic branches of these pyramidal neurons. The spatial segregation of dendritic computations is enabled by inhibition. Blocking inhibition disrupts the spatial segregation, which makes memory formation for otherwise separately-encoded motor tasks overwrite each other (Cichon and Gan, 2015).

In the olfactory system of *Drosophila melanogaster*, dopaminergic neurons (DANs) encode reward and punishment and induce plasticity in synapses between the KCs that encode sensory stimulus and the mushroom body output neurons (MBONs) that are postsynaptic to KCs. This occurs within discrete regions of the mushroom body, where DANs and MBONs innervate segregated compartments (Aso et al., 2014a). The DANs only induce plasticity locally in the compartment they innervate, selectively suppressing excitatory drive to MBON that guide approach or avoidance behaviour, depending on the valence of the stimulus (Hige et al., 2015, Cohn et al., 2015). This topic is discussed in detail in sections **1.2.6-1.2.9**.

Stimulus specific adaptation has been observed in various insect sensory systems. TN-1 neurons of the conehead katydid, *Neoconocephalus triops*, undergo stimulus-specific dendritic adaptation. These neurons receive inputs from auditory sensory neurons that are tonotopically distributed across the dendrites of TN-1 neurons such that different regions of the dendritic field are excited by stimulus with specific carrier frequencies. Adaptation preferentially occurs in dendritic regions specific to a carrier frequency (Prešern et al., 2015).

Wind-sensitive giant interneurons in crickets undergo stimulus specific adaptation. Repeated exposure to air currents from a given direction leads to branch-specific increase in calcium influx, which was correlated with increased wind-evoked avoidance behaviour (Ogawa and Oka, 2015).

These examples demonstrate how localised computations facilitate stimulus-specific encoding of sensory input and subsequent adaptation or plasticity following repeated exposure or learning.

### 1.1.6 The case for using *Drosophila melanogaster* to study local computations

The discoveries outlined above clearly demonstrate that dendrites are not merely linear summation input sites from which inputs are integrated to generate spikes, but instead can operate independently, locally computing information and signalling to other neurons. In some cases, dendrites in neurons devoid of axons are the sole input and output sites, locally computing information and signalling to other neurons (Inada et al., 2017, Grimes et al., 2010, Isaacson and Strowbridge, 1998, Castro and Urban, 2009). These local computations facilitate multimodal processing of sensory information (Bayley and Hedwig, 2018, Medan et al., 2018), stimulus specific adaptation (Prešern et al., 2015, Ogawa and Oka, 2015), and branch-specific plasticity (Cichon and Gan, 2015, Losonczy et al., 2008).

However, most of these studies were conducted in model systems where the nervous system has complex connectivity and many neurons, with limited tools for accessing specific neurons (Cichon and Gan, 2015) (Abraham et al., 2010, Castro and Urban, 2009, Isaacson and Strowbridge, 1998, Grimes et al., 2010), or with limited tools for genetic manipulations (Ogawa and Oka, 2015, Prešern et al., 2015).

While some of these studies demonstrate the behavioural significance of local computations (Cichon and Gan, 2015) (Abraham et al., 2010), the link between local computations and their behavioural significance remains unclear. To understand the link between the molecular basis for localised activity and the behavioural relevance of local computations, we need tools that:

- (1) Allow us to characterise genetic expression on single-neuron or neuron-subtype level
- (2) Record neuronal activity on whole-neuron level, rather than only recording from part of a neuron as with electrophysiology
- (3) Label single neurons or neuron-subtypes for manipulation of neuronal activity
- (4) Clear behavioural paradigms that allow us to link physiological changes in the nervous system to changes in behaviour

*Drosophila melanogaster* fulfils all these criteria to study the physiological and behavioural significance of local computations. There is a variety of genetic tools available that are widely used and continuously improved to characterise, image, and manipulate the nervous system (Venken et al., 2011), and multiple established behavioural paradigms to evaluate the effect of alterations in the nervous system (Pitman et al., 2009).

The olfactory system of the fruit fly has been extensively characterised on the anatomical level (Tanaka et al., 2008, Aso et al., 2014a, Takemura et al., 2017, Xu et al., 2020, Zheng et al., 2018), revealing an associative memory centre, the mushroom body, associative conditioning leads to formation of memory traces in spatially segregated compartments (Hige et al., 2015, Cohn et al., 2015). The APL neuron innervates all these compartments, and receives input from both the Kenyon cells that carry odour identity and the dopaminergic neurons thought to signal stimulus valence (Takemura et al., 2017, Lin et al., 2014a, Zhou et al., 2019, Xu et al., 2020). A previous study suggested that it is a non-spiking neuron, raising the possibility that activity is compartmentalised within the APL neuron (Papadopoulou et al., 2011). However, it remains unclear if this neuron locally computes information, and what functional significance it would have.

The following sections describe our current knowledge of how the fly olfactory system is organised, how this ties together with its physiological function, and how it facilitates olfactory associative condition, which ultimately drives behaviour towards olfactory cues. Finally, I will emphasise why this system is of interest with regards to local computations, and why the APL neuron is a good candidate for studying local computations.

## 1.2 Olfactory processing in *Drosophila*

### 1.2.1 The challenge of processing olfactory sensory information

Sensory systems allow organisms to gather information from their surroundings and make decisions on this basis. To accomplish this, it is necessary for the sensory system to classify the stimulus it receives. An inherent challenge in any sensory system is the limited coding space available to represent different types of stimulus. For olfaction there is no parameter, like the wavelength of visual stimulus or the frequency of auditory stimulus, by which to distinguish the stimulus type.

Instead, olfactory perception relies on discrimination of odours by a wide array of receptors corresponding to identities of odourant molecules. The olfactory systems of both vertebrates and invertebrates are organised into glomeruli that each represent an individual odour channel, determined by the olfactory receptor expressed by its cognate olfactory receptor neurons. In mice, there are ~1800 such glomeruli, while *Drosophila* has ~50 (Mombaerts et al., 1996, Laissue et al., 1999). These glomeruli converge in higher brain regions where neurons sample information from multiple odour channels. Animals can encounter complex stimuli that involve any combination of these channels, presenting too large a number for the limited coding space of the brain (Su et al., 2009).

How does the brain address this problem? One option is for the higher order neurons to unbiasedly sample from the glomeruli, with each brain using its limited coding space to sample a random set of glomerular combinations. Another approach is predictive sampling, where stereotyped combinations of glomeruli are over-represented across flies, signifying that certain type of stimuli are predicted to be behaviourally significant (Jeanne et al., 2018). Two higher brain regions in the fly receive input from the glomeruli, known as the MB and lateral horn (LH). The sections below will illustrate how these two regions differ in which of the two sampling approaches they utilise, and how this ties together with their behavioural roles.

### 1.2.2 Anatomy and physiology of the *Drosophila* early olfactory system

In *Drosophila*, stimulus discrimination takes place in three orders of neurons. First order neurons are known as ORNs, the second order neurons are called projection neurons (PNs), with the third order neurons consisting of two distinct cell populations, KCs and lateral horn neurons (LHNs).

ORNs are localised in the antennae and maxillary palps. Each antenna contains ~1200 ORNs (Stocker et al., 1990). These are covered by sensilla, where the dendrites of the ORNs reside. There are ~50 ORN types, each expressing mostly one of ~60 olfactory receptors (Benton et al., 2009, Couto et al., 2005, Fishilevich and Vosshall, 2005). Each receptor has varying affinity for different sets of odourant molecules (Hallem and Carlson, 2006), representing the first level of sensory discrimination. Some ORN types are broadly tuned to a variety of odourant molecules, while others respond to a select few, and some ORNs respond to the same odourant at different concentration levels, with high concentrations recruiting more ORNs, resulting in overlapping receptive fields

(Hallem and Carlson, 2006). ORNs show spontaneous spiking, with the average firing rate depending on the type of receptor a given ORN expresses (Hallem and Carlson, 2006). Notably, many odourants simultaneously excite some ORNs while inhibiting the spontaneous firing rate of others. Thus, any odourant molecule is encoded in the first order neurons by a pattern of excitatory and inhibitory responses across multiple ORN types.

ORNs extend their projections to glomeruli in the antennal lobes (**Fig. 1.2**). All ORNs of a given type innervate the same glomerulus, with a few types innervating more than one glomerulus (Vosshall et al., 2000, Grabe et al., 2016). ORNs synapse onto PNs, the cholinergic second order neurons, in the glomeruli.

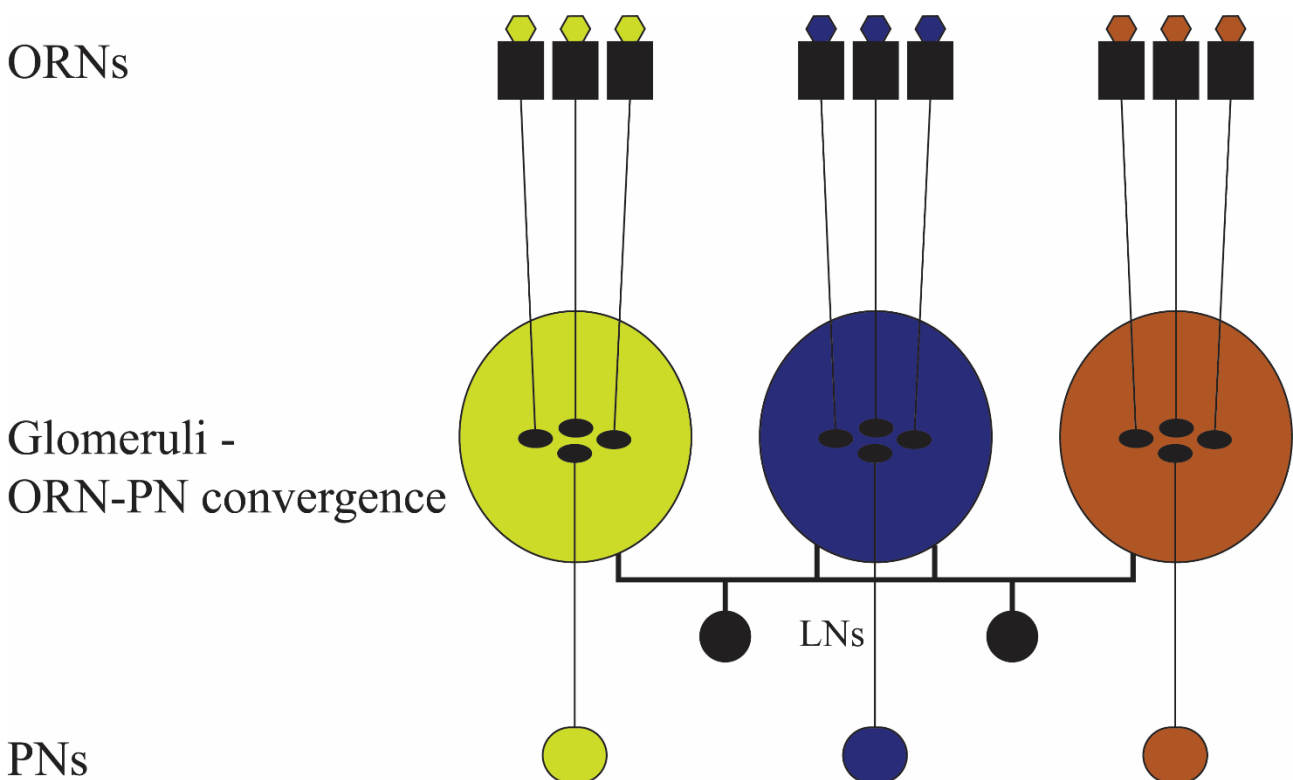


**Figure 1.2 Organisation of the fly early olfactory system**

Schematic of olfactory channels in the fly olfactory system. Each ORN expresses a unique type of olfactory receptor (indicated by different colours). ORNs expressing the same receptor project their axons to the same glomerulus. Likewise, projection neurons send their dendrites to a single glomerulus. Local neurons (LNs) laterally connect the glomeruli, mainly providing inhibition. Thus, ORN axons and PN dendrites converge in glomeruli in a manner that maintains the specificity of olfactory receptors, giving rise to spatially segregated unique olfactory channels.

Like the ORN axons, the dendrites of individual PNs only innervate a single glomerulus, maintaining the anatomical segregation of odour-specificity encoded by ORNs (Vosshall et al.,

2000, Grabe et al., 2016) (**Fig. 1.2**). Multiple PNs innervate the same glomerulus, referred to as sister PNs, and each PN receives input from every ORN within the same glomerulus (Vosshall et al., 2000). Thus, ORN-PN connectivity is stereotyped, and gives rise to ~50 odour channels. Because of similarity of input origin and the convergence of multiple ORNs onto each PN, sister PNs have highly correlated odour responses compared to the ORNs they receive input from. (Kazama and Wilson, 2009).

What is the functional advantage of transmitting the encoded odour stimulus to a second layer of neurons where the coding space is reduced (~1200 ORNs to ~200 PNs)? Although recordings from ORNs and PNs innervating the same glomeruli have revealed that their responses are similar in terms of which odours they respond to, there are significant differences in their response properties. The convergence of multiple ORN inputs onto each PN means that the latter averages its inputs. (Bhandawat et al., 2007). This reduces the level of noise, improving trial-to-trial variability of individual PNs compared to ORNs, and ultimately means that PNs more reliably fire when the fly is subjected to a specific odourant (Bhandawat et al., 2007). For the same reason, they are highly sensitive to weak odour stimulus, displaying a sharp increase in firing rates in response to small increases in odour concentration, but also saturating at lower concentrations than their cognate ORNs. Furthermore, each ORN axon forms multiple synapses onto the dendrites of each cognate PN. These synapses have a high vesicle release probability. This contributes to the reliable firing of PNs and their sensitivity to low odour concentrations (Kazama and Wilson, 2008).

The glomeruli also house the projections of predominantly GABAergic (a few cholinergic) local neurons (LNs) that form connections across glomeruli, of which many innervate all glomeruli (Ya-Hui et al., 2010). In contrast to the stereotyped connectivity of PNs and ORNs, LNs show great variability in glomerular innervation patterns, and equally diverse odour response properties (Ya-Hui et al., 2010). The main role of LNs seems to be mediation of odour-evoked lateral inhibition between glomeruli.

Both ORNs and PNs receive lateral inhibition, although ORN axons seem to be the most prominent targets. Lateral inhibition has been proposed to serve two roles. First, it broadens the range of stimulus strength that PNs can encode by reducing the sensitivity of PNs to input from ORNs at high levels of total ORN activity (Olsen et al., 2010). Second, lateral inhibition decorrelates activity between different glomeruli (Olsen et al., 2010), which improves naïve odour discrimination by third order neurons in the lateral horn (Parnas et al., 2013, Liang et al., 2013). It is known that

lateral inhibition generally increases with the total level of ORN activity (Olsen et al., 2010), and a recent study found that the level of inhibition between different glomeruli is odour invariant, but that each glomerulus has a specific level of sensitivity to lateral inhibition (Hong and Wilson, 2015).

Even less is understood of the cholinergic LNs in the antennal lobes (Wilson, 2013). They evoke depolarisations in PNs, seemingly not through synaptic release of acetylcholine, but rather through gap junctions (Olsen et al., 2007, Root et al., 2007, Shang et al., 2007, Yaksi and Wilson, 2010).

At this point in the olfactory circuit, the PNs branch out to two regions that are generally associated with innate and learned behaviours, known as the lateral horn (LH) and mushroom body (MB), respectively. These will be described in the following sections. We will see that there are structural and functional differences between the neurons of the LH and MB that receive input from PNs, and how these play into their distinct, but in some cases overlapping, physiological and behavioural functions.

### 1.2.3 Stereotyped PN-LH connectivity implies that the LH uses predictive sampling

Traditionally, the lateral horn has been considered the fly central brain region that mediates innate behavioural responses to primarily odourant stimulus. What anatomical organisation underlies such functionality? Several older studies found that PN-LH connectivity is rather stereotypic (Marin et al., 2002, Tanaka et al., 2004), and more recent ones have characterised this to greater extent.

The LH has no clear boundaries, but instead is delineated by the PN axons that terminate in this region. Three major PN axonal tracts have been identified. The majority of PNs extend their axons towards the MB and LH through the medial antennal lobe tract (mALT). These axons pass through the MB calyx and from there extend further to the LH (Jefferis et al., 2007, Tanaka et al., 2012). Other PNs' axons extend through the mediolateral antennal lobe tract (mlALT) which bypasses the MB calyx, directly going to the LH (Tanaka et al., 2012). The third tract, the lateral antennal lobe tract (lALT), is comprised of PN axons that directly innervate the LH, some of which branch from there to the MB lobes. PNs extending their axons through these nerve fibres are mainly uniglomerular (innervates a single AL glomerulus with their dendrites) and cholinergic, while some

are multiglomerular and GABAergic (Parnas et al., 2013, Liang et al., 2013). These PN axons synapse onto local lateral horn neurons (LHNs), which themselves can be excitatory or inhibitory.

What is the relationship between the PN-LHN synapses and the olfactory channels that these PNs represent, and what does this tell us about the sampling approach utilised by LHNs? LHNs are postsynaptic to PN presynapses from combinations of glomeruli, and the same type of LHNs have similar, but not identical, inputs (Jeanne et al., 2018). On average, a glomerulus makes connections to 13% of LHNs, with some narrowly-tuned glomeruli making an exceptionally higher number of connections (Jeanne et al., 2018).

Rather than converging independently onto LHNs, certain combinations of glomeruli converge onto specific LHN types. Notably, glomeruli that are part of a combination that converge have low odour tuning correlations. Instead, there is a tendency for such glomerular combinations to be tuned to odours associated with specific behaviours (egg laying, courtship, fruit volatiles) (Jeanne et al., 2018). As mentioned before, a hallmark of predictive sampling is biased, or stereotyped, connectivity that is over-represented across individuals. Such anatomical organisation implies that certain stimulus features or identities are predicted to serve a specific function or role. These anatomical findings strongly suggest that PN-LHN connectivity is stereotyped, suggesting that PN-LH connectivity utilises predictive sampling (Jeanne et al., 2018).

Little was known about the inputs and outputs to and from the LH from non-AL brain regions (Frank et al., 2015, Kim et al., 2015) until the recent work by Dolan et al. and Frechter et al., who published a large set of split-Gal4 drivers that allow researchers to dissect the role of the LH in olfactory processing by monitoring neuronal activity and manipulate specific types of LH neurons (Dolan et al., 2019). The authors extensively characterised the anatomy of LHNs, dividing them into lateral horn local neurons (LHLNs), lateral horn input neurons (LHINs), and lateral horn output neurons (LHONs) types. In total, they estimated the size of the LH population at ~1400 LHNs (Frechter et al., 2019).

The authors found novel LHIN inputs that originate from the visual, auditory, gustatory and mechanosensory pathways. These multimodal inputs innervate a restricted, ventral region of the LH, which is largely devoid of inputs from the AL (Dolan et al., 2019). LHONs mainly project their axons to the superior lateral protocerebrum, but also to the superior intermediate protocerebrum and the superior medial protocerebrum (Dolan et al., 2019). A subset of ~30% LHONs project axons

that overlap with DAN dendrites or MBON axons, suggesting that innate responses in the LH play a role in memory formation, and are integrated with output from the MB onto downstream targets (Dolan et al., 2019). Finally, the LH receives input from the MB. Several MBONs project axons to the LH or other areas where LHN dendrites reside (Tanaka et al., 2008, Aso et al., 2014a, Dolan et al., 2018, Dolan et al., 2019, Séjourné et al., 2011)

The anatomical findings showing stereotyped connectivity between PN-LHNs support the notion of the LH utilising predictive sampling to drive innate behaviour, but the crosstalk between DANs, MBONs and LHNs suggests that the MB and LH are not separate entities driving learned and innate behaviour in parallel.

#### 1.2.4 The LH utilises predictive sampling to drive innate responses

How are the anatomical findings of PN-LHN connectivity reflected in the odour responses of LHNs?

LHONs are more broadly tuned to odours than PNs. While PNs respond to 12% of odours, LHONs respond to 35%. This is possibly due to convergence of PNs from multiple glomeruli onto LHONs. There is higher correlation between odour responses of different LHON types than the odour responses of PNs. It has been proposed that this could be due to inhomogeneous sampling of glomeruli. This is evident from the finding that LHONs respond to odours categorized by chemical structure (i.e. amines, acetates). Both LHONs, and LHLNs to a lesser extent, encode odour categories to a stronger degree than PNs (Frechter et al., 2019). There are regions in the LH and superior protocerebrum that receive innervations from projections of LHONs that encode either of the odour categories amines, esters, aldehydes, and carboxylic acids, suggesting that processing of odour categories is regionalized (Frechter et al., 2019).

How are inputs from multiple glomeruli integrated? This has been addressed behaviourally by stimulating single or pairs of olfactory channels and observing if this promotes attraction or repulsion. For certain pairs, linear summation was observed, while other pairs showed sublinear summation. Activation of olfactory channels with opposing sign led to repression of the attractive effect (Bell and Wilson, 2016).

These findings demonstrate that LHNs are more broadly tuned towards odours than PNs, and receive inputs from glomeruli pairs that either encode odours from the same chemical category, or odours that are associated with a specific behavioural response, strongly suggesting that LHNs encode the predicted behavioural significance of a given stimulus rather than its identity. This is coherent with predictive sampling being suitable for stimuli who are predicted to be behaviourally significant.

How is this reflected in the fly's behavioural responses to different odour stimuli? There are several concrete examples of this. Egg-laying in *Drosophila* can be suppressed by activating a subset of glomeruli (Chin et al., 2018). The PNs that innervate these glomeruli project their axons to a specific region in the LH, suggesting the presence of hard-wired connectivity that suppresses egg-laying upon stimulation by the odour(s) they are tuned towards, such as geosmin (Chin et al., 2018). CO<sub>2</sub> exposure, which specifically activates the V glomerulus, evokes avoidance behaviour in flies (Suh et al., 2004). Artificial activation of this glomerulus opposes the attractive effect of activating other glomeruli. Conversely, activation of ORNs that are tuned to detect odourants associated with citrus fruits promotes egg-laying, presumably because citrus fruits are an ideal egg-laying site (Dweck et al., 2013). More specifically, artificial activation of different glomeruli alone or in pairs either evokes approach or avoidance depending on which pairs are co-activated. This is further supported by experiments that have demonstrated the ability of certain LHNs subtypes to elicit approach or avoidance, or elicit context-dependent motor programmes (Dolan et al., 2019).

To summarize, anatomical studies have found that different glomeruli that convey stimuli with ethologically similar implications converge on the same LHNs. This stereotypic connectivity supports predictive sampling. Physiologically, LHNs are broadly tuned to odour stimuli, suggesting that they do not encode identity, but rather odour categories. This supports the rationale behind predictive sampling. Finally, activation of LHNs drives approach or avoidance behaviour, suggesting that responses evoked in LHNs by their cognate odour category elicits stereotyped response. These findings establish the link between predictive sampling and innate behavioural responses.

### 1.2.5 Identifying the MB as a locus of olfactory learning

The LH has largely been determined to govern innate behavioural responses. However, animals will face changes in their environment that call for behavioural adaptation. Flies demonstrate the ability to learn to a variety of stimuli. They can learn to use visual cues for navigation (Ofstad et al., 2011), colour recognition (Vogt et al., 2014), and pattern recognition (Marcus et al., 1993). The males establish social hierarchies based on aggressive bouts (Yurkovic et al., 2006) and undergo courtship conditioning following failed mating attempts (Siegel and Hall, 1979).

One of the most widely studied forms of learning in *Drosophila* is olfactory learning. Flies can associate the presence of an odour with either reward (sugar) (Tempel et al., 1983) or punishment (electric shock) (Quinn et al., 1974). This requires learned olfactory discrimination. If flies experience a specific odour paired with reward (e.g., sugar) or punishment (e.g., electric shock), they learn the association and thereafter approach/avoid the trained odour, but not untrained odours (Keene and Waddell, 2007). This process requires the brain to (1) form unique representations of odours or odour scenes, (2) assign valence (reward/punishment) to these representations, and (3) drive attraction or avoidance based on stimulus valence. In *Drosophila*, it is widely understood that the MB is the central brain region responsible for this process (McGuire et al., 2005, Keene and Waddell, 2007, Hige, 2018, Cognigni et al., 2018, Aso et al., 2014a).

Historically, associative learning in *Drosophila* was initially studied on the molecular level. These studies relied on the chemical mutagenesis approach pioneered by Seymour Benzer (Benzer, 1967) to identify mutant flies with impaired learning. The first learning paradigm utilised for olfactory learning relied on flies running into a tube with a light source and a grid that could deliver electric shocks (unconditioned stimulus) paired with an odour (conditioned stimulus, CS). The learning efficiency was assessed by scoring the fraction of flies who subsequently went into a tube with an unpaired odour vs the fraction who went into a tube with the paired odour to obtain a performance index (Quinn et al., 1974). The early classic learning deficiency mutants, *dunce* (Dudai et al., 1976), *rutabaga* (Livingstone et al., 1984) *cabbage* (Aceves-Piña and Quinn, 1979), and *amnesiac* (Quinn et al., 1979) were identified using this approach. However, this learning paradigm was not robust, with relatively low performance index (0.3), presumably because not all flies went into the tube used for training (McGuire et al., 2005).

This led to the development of the T-maze method (Tully and Quinn, 1985), where the flies are subjected to electric shock and odour pairing using vacuum to draw the odour into the training tube, ensuring that all flies are subjected to both shock and odour. This method produced more robust

learning, with performance index scores of 0.7-0.9 (McGuire et al., 2005). Many additional mutations that impair learning have been identified since then (McGuire et al., 2005, Keene and Waddell, 2007).

These important findings shed light on the molecular basis of olfactory learning but left the question open if learning occurs in a particular brain region. What were the initial findings that implicated the MB in olfactory learning? By staining the brain of mutant flies with structural deficiencies and a process of elimination, researchers were able to pin down that alteration of the MB structure, but not other brain regions, was correlated with impaired olfactory associate learning (Heisenberg et al., 1985).

### 1.2.6 The arbitrary nature of PN-KC connectivity and KC odour responses provide a basis for associative learning

Associative learning posits that the animal can assign valence to an arbitrary stimulus. As described in the previous section, flies are capable of associative olfactory learning, implying that *Drosophila* can encode arbitrary stimuli. How does it achieve this? This will first be addressed from the anatomical perspective, followed by the physiological basis. Parts of section 1.2.6-1.2.8 are based on my personal contributions to a published review paper, Amin and Lin, 2019.

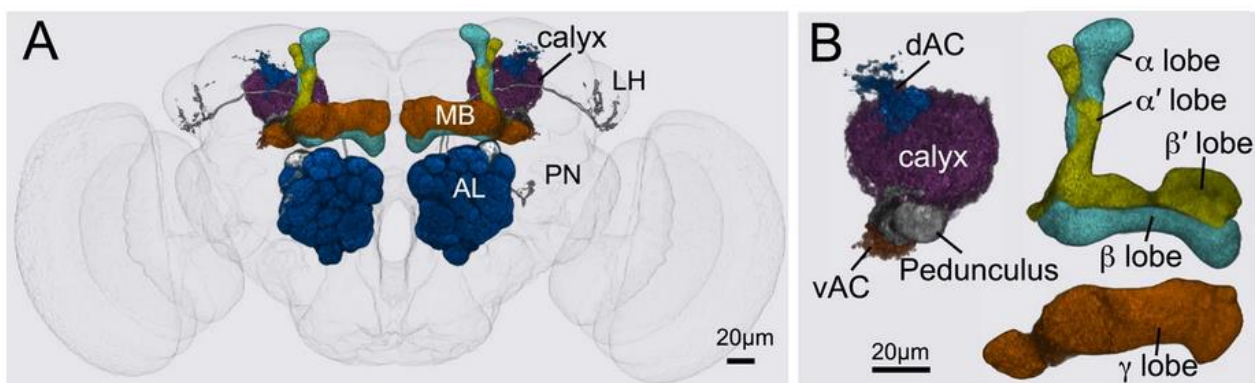


**Figure 1.3 Anatomy of the olfactory system**

Adult fly female brain generated using 3D image rendering software. The antennal lobes (AL) are shown in blue. PNs project to the MB, which consists of the MB lobes, pedunculus, and the calyx. The lobes are composed of KC axons and are subdivided into the  $\alpha\beta$  (teal),  $\alpha'\beta'$  (yellow), and  $\gamma$  lobes (orange), based on the KC subtypes that constitute each lobe. The calyx (purple) is composed of KC dendrites and is divided into the main calyx, the dorsal accessory calyx (dAC), and the ventral accessory calyx (vAC). Taken from Aso et al., 2014a.

PN axons carry odour information to the MB, where they synapse onto the dendrites of KCs (**Fig. 1.3 A**). These cholinergic neurons (Barnstedt et al., 2016) are divided into three main subtypes;  $\alpha\beta$ ,  $\alpha'\beta'$ , and  $\gamma$  KCs (Tanaka et al., 2008, Lee et al., 1999, Aso et al., 2014a) (**Fig. 1.3 B**). The MB is comprised of the dendritic and axonal projections of the KCs, with their dendrites giving rise to the calyx and their axons forming the horizontal and vertical lobes (Tanaka et al., 2008, Aso et al., 2014a). The dendrites of different KC subtypes occupy partially segregated areas of the calyx. PN projections from the same glomerulus are similarly regionalized (Lin et al., 2007, Leiss et al., 2009). The dendrites of several KCs form a microglomerulus. These are comprised of actin-rich, claw-like structures with 2-11 claws each (Caron et al., 2013). The microglomeruli can be comprised of different KC subtypes (Leiss et al., 2009). PNs synapse onto KC dendrites in the calyx of the MB in the centre of the microglomeruli, where multiple claws wrap onto the same PN bouton (Leiss et al., 2009). Thus, a PN bouton can synapse onto multiple KC claws from multiple subtypes, and a KC can receive input from PNs that originate from distinct glomeruli.

Does PN-KC connectivity suggest unbiased sampling? One study found there was no structure in PN-KC connectivity for PNs from the same glomerulus, implying that connectivity between KC and PNs is stochastic (Caron et al., 2013). This is in contrast with previous studies suggesting regionalized PN projections (Lin et al., 2007, Leiss et al., 2009) and a recent EM study that found strong regionalization for projections of PNs from the same glomerulus (Zheng et al., 2018). Additionally, a functional connectivity study also found that intra-KC claw responses are more similar than inter-KC claw responses (Gruntman and Turner, 2013). Together, these findings suggest that PN-KC connectivity is probabilistic, but regionalized/structured to some extent. By sampling multiple odour channels each, KCs give rise to a combinatorial code for odour input in the fly brain.

How do KC odour responses reflect this anatomical structure? Theoretical work suggests that associative learning based on stimulus discrimination is optimized by sparse coding (few neurons encoding a given stimulus type) and expansion of the coding space, which makes stimulus representations more distinct and describes the stimulus more specifically (Olshausen and Field, 2004, Marr, 1969). Sparse odour coding can be observed in KCs. While PN inputs to KCs respond broadly to odours (Bhandawat et al., 2007), only 5-10% of KCs respond to a given odour (Honegger et al., 2011, Perez-Orive et al., 2002, Turner et al., 2008, Ito et al., 2008). However, the degree of sparseness in KCs still allows generalisation of associative learning to similar odours (Hige et al., 2015, Campbell et al., 2013). Theoretical work suggests that the fly olfactory circuit

drives learned behaviour towards stimuli that is similar to previously conditioned stimuli using a variant of the computer algorithm called “locality-sensitive hashing” (Dasgupta et al., 2017).

Sparseness relies on inhibition from the GABAergic APL neuron. This non-polarised, non-spiking neuron has post- and pre-synapses throughout the MB (Papadopoulou et al., 2011, Wu et al., 2013) and forms reciprocal connections with KCs (Lin et al., 2014a, Inada et al., 2017). The GABAergic feedback inhibition from the APL neuron onto KCs is mediated by both the ionotropic GABA<sub>A</sub> and the metabotropic GABA<sub>B</sub> receptors (Inada et al., 2017). Blocking the APL neuron’s activity broadens odour representation in KC somata and impairs learned discrimination of similar odours (Lin et al., 2014a). The extensive arborisations of this neuron cover the entirety of the MB (**Fig. 1.4**). Considering its non-spiking nature, this anatomical organisation has interesting implications for the spatial extent of activity propagation within the APL neuron. This is further discussed in section **1.2.10**.

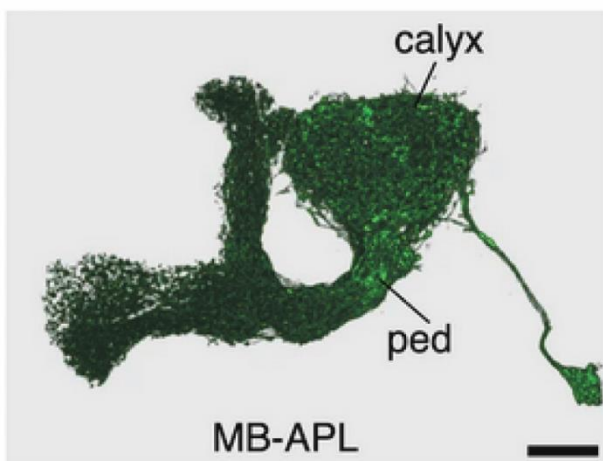


**Figure 1.4 Anatomy of the APL neuron**

Expression of spaghetti-monster GFP in the APL neuron using MultiColour-FlpOut (Nern et al., 2015). The calyx and pedunculus (ped) are highlighted. Scale bar is 20  $\mu\text{m}$ . Taken from Aso et al., 2014a.

Another contributing factor to sparseness is that KCs mainly spike when they receive multiple dendritic inputs simultaneously (Gruntman and Turner, 2013). This integration of dendritic inputs reflects the drift-diffusion model of evidence accumulation, which posits that decision-making is based on evidence accumulation in neurons. Only when enough evidence has been accumulated to meet a threshold does the neuron spike. This model explains the nature of animals’ reaction times based on the ambiguity of the stimuli it faces: when the stimuli are easily discriminated, evidence accumulation quickly passes the threshold, while noisy or ambiguous stimuli leads to prolonged evidence accumulation (Shadlen and Kiani, 2013).

A recent study elegantly demonstrated that stimulus integration in  $\alpha\beta_c$  KCs follows the drift-diffusion model of evidence accumulation. This KC subtype integrates information from subthreshold synaptic inputs over time.  $\alpha\beta_c$  KCs take longer to reach spiking threshold the more ambiguous the stimulus (Groschner et al., 2018). The authors had previously found that mutation of the gene encoding forkhead box P transcription factor in flies, a transcription factor that is widely involved in developmental processes in both humans and flies (Santos et al., 2011, Castells-Nobau et al., 2019), affected reaction times in discrimination tasks (Dasgupta et al., 2014). Mutation of this transcription factor was found to regulate expression of a voltage-gated potassium channel, *Shal*, which reduced the intrinsic excitability of  $\alpha\beta_c$  KCs reaction times, increasing the latency from stimulus onset to the first spike. Indeed, this latency accurately predicted how long it took flies to decide (Groschner et al., 2018).

The probabilistic nature of PN-KC connectivity allows KC to form sparse representations of arbitrary combinations of odour stimulus, while their ability to accumulate evidence from olfactory input allows them to more accurately discriminate ambiguous stimuli. Together, this forms the basis for olfactory associative learning.

Although the main topic discussed here is related to olfactory sensory processing, it should be noted that the MB is more broadly connected to sensory modalities. In addition to the main calyx, the calyx consists of accessory calyces (Fig. 1.3 B). Like the main calyx, these accessory calyces harbour KC dendrites. However, instead of olfactory input, the dendrites receive input from visual, gustatory, and thermosensory pathways (Yagi et al., 2016, Vogt et al., 2016, Kirkhart and Scott, 2015, Marin et al., 2020). Thus, the MB is a brain region with much broader function than merely processing of olfactory, instead serving as a centre where multimodal sensory input converges for further processing. What further processing entails will be outlined in the sections below.

### 1.2.7 Integration of stimulus identity and valence in the mushroom body facilitates memory formation

How is valence assigned to the sparse odour representations held by KCs, and how does coupling of valence and stimulus identity guide learned behaviour? The current understanding in the field is that DANs extrinsic to the MB respond to the unconditioned stimulus and 'label' the stimulus as either appetitive or aversive. DANs are subdivided into two clusters, protocerebral anterior medial (PAM,

mainly reward), and paired posterior lateral (PPL, mainly punishment) DANs. Different DANs respond to either reward (sugar) or punishment (electric shock) (Cohn et al., 2015, Burke et al., 2012, Liu et al., 2012, Mao and Davis, 2009) Artificial activation of DANs coupled to odour stimulus (conditioned stimulus) substitutes for either reward or punishment (unconditioned stimulus) (Liu et al., 2012, Aso and Rubin, 2016, Aso et al., 2010, Aso et al., 2012, Burke et al., 2012, Claridge-Chang et al., 2009, Hige et al., 2015), while blocking DANs prevents memory formation (Lin et al., 2014b, Huetteroth et al., 2015, Yamagata et al., 2015). These findings have established that signalling from DANs is crucial for labelling sensory stimulus as either appetitive or aversive, acting as the reinforcement signal during memory formation.

Because of the way DANs and MBONs are matched, learning is mediated by depression of behavioural drive opposed to the stimulus valence: when an odour is coupled with a reward, DANs that encode appetitive stimulus valence depress synapses between KCs and avoidance MBONs in their cognate compartment, skewing the balance between approach and avoidance towards approach. Likewise, DANs encoding aversive stimulus depress approach KC-MBON synapses, increasing the behavioural drive towards avoidance (Hige et al., 2015, Cohn et al., 2015, Berry et al., 2018). When the fly subsequently encounters a reinforced stimulus, the memory is recalled by activation of the MBON through the depressed KC-MBON synapse.

These findings have led to the current hypothesis in the field that olfactory learning in *Drosophila* depends on a balance between the behavioural drives for approach and avoidance towards a given stimulus. DANs suppress the ‘wrong’ or opposite behavioural drive relative to the stimulus valence they encode, skewing the behavioural drive towards approach or avoidance (**Fig. 1.5 A**). This is due to the way MBONs direct behaviour. Stimulus identity and valence is read out by both approach- and avoidance-directing MBONs. Thus, it is the balance between these two opposing forces that determines if the fly will approach or avoid an odour. This is apparent in forced-choice tasks, where the fly must choose between two odours. However, these opposing forces can also regulate naïve preferences observed in single odour tasks, as observed when flies choose to approach a pure air stream over an odour they have naïve aversion towards: when output from the avoidance-directing MBON- $\beta^2mp$  and MBON- $\gamma 5\beta'2a$  is blocked, the flies instead approach the odour (Owald et al., 2015).

The tuning of KC-MBON synapses ultimately affects the output of MBONs. What is the function of MBON output? Artificial activation of MBONs drives flies towards approach or avoidance (Owald et al., 2015, Aso et al., 2014b), while blocking MBON output can prevent a memory from

being recalled when the fly subsequently encounters the conditioned stimulus (Owald et al., 2015, Aso et al., 2014b, Perisse et al., 2016, Felsenberg et al., 2017, Berry et al., 2018), suggesting that they are important for guiding fly behaviour based on associative conditioning.

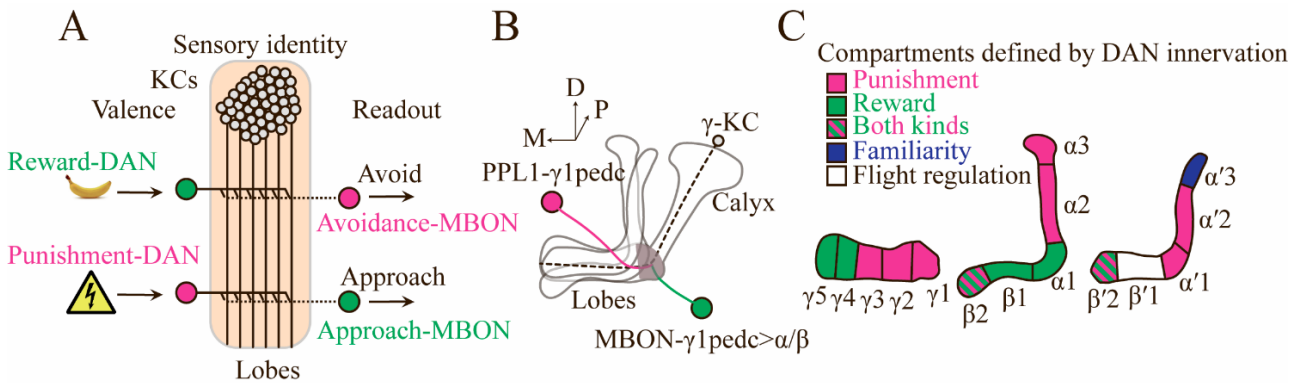


**Figure 1.5 Mushroom body architecture**

(A) Schematic of the compartmentalised architecture of the MB. KC axons carry sensory identity to the individual compartments, where DANs that respond to rewards (green) or punishment (pink) synapse onto the KC axons. In turn, the KC axons synapse onto MBON dendrites. DAN signalling depresses KC-MBON synapses within their respective compartments during conditioning. Because of the opposing pairing of reward-DANs with avoidance-MBONs and punishment-DANs with approach-MBONs, reward signals reduce excitatory drive to avoidance-MBONs, while punishment signals reduce excitatory drive to approach-MBONs. (B) Example of DAN-KC-MBON connectivity. The PPL1- $\gamma$ 1pedc is a punishment-DAN that innervates the  $\gamma$ 1-compartment and depresses the synapses between  $\gamma$ -KCs and MBON-  $\gamma$ 1pedc> $\alpha/\beta$  during aversive conditioning. (C) Schematic of the MB lobes divided into the KC subtypes and subdivided into colour coded compartments according to the type of DANs that innervate them (pink for punishment, green for reward), or other known functions they are implicated in. Striped colouring indicates that the compartment is innervated by both types of DANs. Adapted from (Amin and Lin, 2019)

Importantly, the timing between the sensory stimulus and the reinforcement signal can skew fly behaviour towards either approach or avoidance, regardless if it is a reward or punishment signal. When sensory stimulus precedes or coincides with punishment (forward pairing) the flies will avoid the sensory stimulus on subsequent exposure. However, if the punishment precedes the conditioned stimulus (backward pairing) the flies are attracted by the conditioned stimulus (Tanimoto et al., 2004, König et al., 2018, Vogt et al., 2015, Handler et al., 2019). The latter is thought to signify that the conditioned stimulus indicates the cessation of punishment, and thus becomes appetitive to the fly. This can be demonstrated by differentially timing artificial activation of DANs with sensory stimulus (König et al., 2018, Handler et al., 2019). What is the physiological basis of the DAN signal, and how does it regulate fly behaviour?

The DAN signal is believed to form a memory trace that is read out by another set of MB-extrinsic neurons, known as MB output neurons (MBONs). KCs are presynaptic to MBONs, providing excitatory input to MBONs during sensory stimulus. Odour stimulus coupled to unconditioned stimulus depresses KC-MBON synapses, reducing MBON odour response (Cohn et al., 2015, Oswald et al., 2015, Séjourné et al., 2011, Hige et al., 2015, Berry et al., 2018). This occurs in a timing-dependent manner, so that the depression only occurs when the odour stimulus precedes or coincides with the unconditioned stimulus (Hige et al., 2015, Cohn et al., 2015). Likewise, some evidence suggests that backward pairing can reverse this depression of a KC-MBON synapse, or potentiate the synapse, compared to pre-conditioning response levels (Handler et al., 2019). Even in the absence of odour stimulus, DAN signalling alone can potentiate its cognate KC-MBON synapses (Berry et al., 2018, Cohn et al., 2015).

What is the mechanistic basis of the temporally specific bidirectional tuning of KC-MBON synapses? It is thought to be mediated by dopamine 1-like receptor 1 and 2 (Dop1R1 and Dop1R2), which are expressed in KCs (Han et al., 1996, Kim et al., 2003, Handler et al., 2019). These receptors signal through different pathways. Dop1R1 activates the G protein G<sub>s</sub>, which initiates signalling by cAMP through a calcium-dependent adenylyl cyclase, Rutabaga. This functions as a coincidence detector between odour-mediated calcium-influx and the dopamine signal during learning (Levin et al., 1992, Himmelreich et al., 2017, Gervasi et al., 2010). In contrast, Dop1R2 activates Rac1 and Scribble through the G protein G<sub>q</sub> G to drive release of calcium from the ER (Himmelreich et al., 2017, Cervantes-Sandoval et al., 2016, Shuai et al., 2010, Berridge, 1993).

What does signalling through these receptors convey about the temporal order of sensory stimulus and reinforcement? Although cAMP production is at its max when KC activation slightly precedes or is synchronized with DAN activation, its production does not strictly depend on the temporal order of neuronal activation, suggesting that Dop1R1 signalling does not provide information about the temporal order of stimulus and reinforcement pairing. Instead, endoplasmic reticulum release of calcium mediated by Dop1R2 signalling is dependent on the temporal order of odour and reinforcement pairing, being released from the endoplasmic reticulum only with backward pairing (i.e. DAN activation precedes KC activation). With forward or synchronized pairing, cAMP production is at its highest, endoplasmic reticulum release of calcium is at its lowest, and the KC-MBON synapses are depressed. Conversely, when learning is done with backward pairing, ER release of calcium is at its highest, cAMP production is comparatively lower, and the KC-MBON

synapse becomes potentiated. Mutation of Dop1R1 abolishes the increase in cAMP production and depression of KC-MBON synapses induced by learning, while mutation of Dop1R2 abolishes ER release of calcium and potentiation of KC-MBON synapses induced by backward pairing (Handler et al., 2019).

Thus, the concerted action of signalling through two distinct dopamine receptors in KCs are required for bidirectionally tuning the KC-MBON synapses according to the temporal order of sensory stimulus and the reinforcement signal.

How do these three elements – stimulus representation, valence, and readout – come together? The neuronal processes of KCs, DANs and MBONs converge in the MB lobes, forming a highly compartmentalised structure that lays the foundation for stimulus-specific learning (Tanaka et al., 2008, Aso et al., 2014a, Takemura et al., 2017, Zheng et al., 2018). KCs extend their axons from the calyx, giving rise to the MB peduncle and lobes. The lobes are divided into 15 compartments (**Fig. 1.5 B**), defined by the DANs and MBONs that innervate each compartment. This has led to the classification and naming of the DANs and MBONs based on the anatomical segregation of their projections into specific compartments or regions (Aso et al., 2014a, Tanaka et al., 2008). Individual DANs and MBONs typically innervate only a single MB compartment. DANs and MBONs that innervate the same compartment encode opposite valence (i.e., appetitive DAN + avoidance MBON; aversive DAN + approach MBON) (**Fig. 1.5 B**). Within these compartments, DANs form axoaxonal synapses with KCs, while KCs are presynaptic to dendritic projections of MBONs (Takemura et al., 2017, Zheng et al., 2018). DAN signalling operates locally, inducing plasticity in KC-MBON synapses only in the compartment they innervate (Hige et al., 2015, Cohn et al., 2015).

How does MBON output drive behaviour? Anatomical studies suggest that information from the MBONs converge in higher brain regions that integrate information from sensory pathways and the animal's internal state. However, some MBON axonal projections also overlap and synapse onto LHN dendrites within and outside the LH (Dolan et al., 2019, Tanaka et al., 2008, Aso et al., 2014a, Dolan et al., 2018). One of these is MBON- $\alpha$ 2sc, an approach-MBON whose output is required for aversive memory recall (Hige et al., 2015, Séjourné et al., 2011). MBON- $\alpha$ 2sc is presynaptic to the LH neurons PD2a1 and PD2b1. Punishment suppresses olfactory drive to MBON- $\alpha$ 2sc (Hige et al., 2015). In line with this, punishment leads to decreased odour responses in PD2a1/b1, presumably due to the reduced output from MBON- $\alpha$ 2sc. Like MBON- $\alpha$ 2sc, their output is required for

aversive memory recall (Dolan et al., 2018). PD2a1 and PD2b1 are additionally postsynaptic to PNs and other LH neurons and are required for unlearned attraction to certain odours, suggesting that they fulfil a dual function that involves both innate, and learned responses.

These findings suggest that PD2a1 and PD2b1 integrate information from both innate and olfactory learning pathways to drive behaviour (Dolan et al., 2018). It is possible that future functionality studies will find that more of the MBON-LH connections can play a role in olfactory memory recall (Dolan et al., 2019), and elucidate how MBON output ultimately translates to goal-oriented motor output.

What could be the purpose of having multiple MB compartments? While having one compartment that encodes reward/avoidance and one for punishment/approach could in theory suffice, the many compartments in the MB allow storage of memories with differences in terms of the type of training required (single session vs multiple), memory duration, capacity to store multiple memories, and how easily the memory trace is erased (Yamagata et al., 2015, Aso and Rubin, 2016, Hige et al., 2015, Aso et al., 2012). In these terms, the diversity across compartments could be instrumental for the fly to prioritise what information to store based on stimulus identity and intensity, and the reliability of odour-valence pairing. Indeed, different kinds of rewards and tastes (water, sweet, nutritious, bitterness) are encoded by distinct DANs, and the memories formed by signalling from different DANs have different levels of stability (Huetteroth et al., 2015, Yamagata et al., 2015, Lin et al., 2014b, Burke et al., 2012, Felsenberg et al., 2017, Felsenberg et al., 2018, Kirkhart and Scott, 2015).

Unsurprisingly, there is greater anatomical and functional complexity to the MB than the relatively simple above depiction of the MB may give the impression of. Within MB compartments, KCs form reciprocal connections with both MBONs and DANs, while DANs also synapse onto MBONs in addition to KCs (Takemura et al., 2017, Xu et al., 2020). Some MBONs project axons to multiple compartments (Aso et al., 2014a), synapsing onto other MBONs (Felsenberg et al., 2018). The functional significance of these variations on MB connectivity will be covered in section 1.2.9.

MBON function is also broader than simply driving approach or avoidance behaviour. One study found that some MBONs have little or no effect in terms of approach or avoidance when activated on their own (Aso et al., 2014b). MBONs that do not drive approach or avoidance behaviour could have other, context-specific functions, such as MBON-a'3, which only responds strongly to novel

odours and evokes alerting behaviour (Hattori et al., 2017), or MBON- $\beta$ '1 which regulates the duration of flight bouts (Manjila et al., 2019). It is possible that the MBONs have other, yet to be discovered functions.

There are several lines of evidence suggesting that KC subsets are differentially required for memory acquisition, consolidation, and retrieval (Krashes et al., 2007, Perisse et al., 2013, Yamazaki et al., 2018, Trannoy et al., 2011). These KC subtype-specific requirements for different aspects of learning are possibly linked to subtype-specific innervations of different compartments (Aso et al., 2014a, Tanaka et al., 2008).

Finally, some findings suggest there are exceptions to the general observation that a given compartment is innervated by DANs encoding either appetitive or aversive stimuli, and not both types of DANs. The  $\beta$ 2 and  $\beta$ '2 compartments receive dopaminergic input from PAM- $\beta$ 2 $\beta$ '2a whose activation can substitute for negative reinforcement to form short-term aversive memories (Aso et al., 2010). These compartments also receive input from other DANs that provide reward signals and substitute for positive reinforcement for memory formation (Huetteroth et al., 2015).

The next section will elaborate on how the MB integrates information from sensory channels with information from the fly's internal milieu, and how this plays into the fly's behaviour.

### 1.2.8 The MB integrates information from sensory pathways and the fly's internal state to generate context-specific innate and learned behaviour

How an organism responds to sensory input such as that encoded in the MB depends on its internal state. An organism's energy level limits what it is capable of, and all physiological processes require energy expenditure, including the act of foraging to replenish energy levels. To respond appropriately to external cues, notably food odours, the fly brain must integrate this information with its internal state. The DANs that innervate the MB seem to play an important role for this purpose. They do not only provide reinforcement signals during associative learning, but also encode satiety state and arousal (Tsao et al., 2018, Cohn et al., 2015, Lin et al., 2019, Plaçais and Preat, 2013, Perisse et al., 2016, Krashes et al., 2009).

A well-characterised example of coupling between the fly's motivational state and physiological response to external cues is the satiety state-dependent role of PPL1- $\gamma$ 1pedc DANs and MBON- $\gamma$ 1pedc $>\alpha/\beta$  in appetitive memory performance. Flies that are fed after appetitive conditioning show poor memory performance compared to starved flies when they are subsequently tested for the strength of the formed memory, suggesting that satiety state affects memory performance (Krashes et al., 2009). This satiety-associated memory recall becomes potentiated by activation of neurons that release *Drosophila* neuropeptide F (dNPF), an ortholog of mammalian neuropeptide F (Brown et al., 1999) that regulates feeding behaviour (Clark et al., 1984, Stanley and Leibowitz, 1985), onto PPL1- $\gamma$ 1pedc DANs. Likewise, blocking output from PPL1- $\gamma$ 1pedc strengthens appetitive memory recall, while activation of PPL1- $\gamma$ 1pedc blocks expression of appetitive memory even in starved flies. This suggests that the hunger signal from *Drosophila* neuropeptide F suppresses PPL1- $\gamma$ 1pedc activity.

How does this translate to stronger or weaker memory recall? This happens through regulation of the balance between approach and avoidance drive from the MBONs. The MB compartment that PPL1- $\gamma$ 1pedc innervates harbours dendrites from the approach-promoting MBON- $\gamma$ 1pedc $>\alpha/\beta$ . Starvation increases the odour drive to this MBON, and artificially activating this neuron increases appetitive memory performance in fed flies. In contrast, blocking its output disrupts expression of appetitive memory (Perisse et al., 2016). MBON- $\gamma$ 1pedc $>\alpha/\beta$  is GABAergic, synapsing onto the avoidance-promoting MBON- $\beta$ '2mp and MBON- $\gamma$ 5 $\beta$ '2a (Felsenberg et al., 2018). This configuration means that starvation strengthens the inhibitory drive from MBON- $\gamma$ 1pedc $>\alpha/\beta$  onto avoidance-MBONs, skewing the balance towards approach.

Output from PPL1- $\gamma$ 1pedc regulates this MBON configuration. PPL1- $\gamma$ 1pedc activity is higher in fed flies compared to starved flies (Plaçais and Preat, 2013). Artificial activation of PPL1- $\gamma$ 1pedc depresses olfactory drive to MBON- $\gamma$ 1pedc $>\alpha/\beta$  (Hige et al., 2015). This suggests that the increased activity of PPL1- $\gamma$ 1pedc in fed flies would similarly depress MBON- $\gamma$ 1pedc $>\alpha/\beta$  odour responses, effectively decreasing the inhibition from MBON- $\gamma$ 1pedc $>\alpha/\beta$  onto the avoidance-promoting MBON- $\beta$ '2mp and MBON- $\gamma$ 5 $\beta$ '2a.

The hunger signal from *Drosophila* dNPF-positive neurons presumably suppresses PPL1- $\gamma$ 1pedc, potentiating olfactory drive to MBON- $\gamma$ 1pedc $>\alpha/\beta$  and skewing the balance between approach and avoidance towards approach by increasing feedforward inhibition onto the avoidance-promoting MBON- $\beta$ '2mp and MBON- $\gamma$ 5 $\beta$ '2a.

In this way, the fly's motivational state and previous experience is connected to external cues. An odour that previously has been associated with a reward drives approach behaviour. This interaction between motivational state, and external, appetitive cues exemplifies how neuronal function in the MB tempers the behavioural drive that arises from associative conditioning according to the fly's needs: re-exposure to the appetitive external cue evokes a strong attractive response in starved flies, whereas fed flies are only weakly attracted, if at all.

Another study found that MBON- $\gamma$ 1pedc $>\alpha/\beta$  and PPL1- $\gamma$ 1pedc, amongst numerous other DANs and MBONs, mediate innate yeast food-seeking behaviour (Tsao et al., 2018). *Drosophila* is strongly attracted to yeast, which is present in naturally occurring food sources like ripe fruits. The presence of yeast in the food substrate promotes egg-laying, and has a strong impact on adult size, reproduction, survival, and food preference (Becher, 2012, Palanca et al., 2013, Grangeteau et al., 2018, Scheidler et al., 2015).

Flies seek out yeast-containing food sources when they are starved. The longer they are starved, the faster they locate a drop of yeast in a circular petri dish (Tsao et al., 2018). This food-seeking behaviour relies on olfactory reception and output from all KC subsets. Output from multiple pairs of MBONs and DANs that innervate specific MB compartments associated with either approach or avoidance are required for flies to seek out yeast. The yeast odour responses of these MBONs are modulated by the satiety state of the fly, suggesting that MBONs or DANs that regulate the odour responses receive hunger or satiety signals (Tsao et al., 2018). Knockdown of receptors in DANs for hunger and satiety cues like dNPF, serotonin, and insulin-like peptides affects yeast food-seeking behaviour, but it does not establish functional connectivity between e.g. serotonergic or peptidergic neurons and the DANs they presumably regulate.

In summary, food-seeking behaviour seems to involve multiple DANs and MBONs that drive both approach and avoidance, but it is unclear how the individual MBONs and DANs contribute to the behaviour, or which neurons establish the link between the fly's satiety state and the various DANs and MBONs identified in Tsao et al., 2018.

Brains allow organisms to navigate environments that present conflicting cues, determining when it is desirable to approach an area with potential rewards, even in the presence of danger. Flies innately avoid CO<sub>2</sub> (Suh et al., 2004), a cue that is released by stressed flies, possibly signalling

danger to other flies. CO<sub>2</sub> is also generated by fermentation, which is prevalent in fly food sources like rotting fruits. How is innate repulsion and appetitive cues from the same food source weighed to guide behaviour?

Although CO<sub>2</sub> avoidance responses can be processed in the LH (Varela et al., 2019), it can also be modulated by satiety state, in an MB-dependent manner (Bräcker et al., 2013, Lewis et al., 2015). This involves the previously mentioned avoidance-promoting MBON-β'2mp and MBON-γ5β'2a, that both respond to CO<sub>2</sub>. Interestingly, this response decreases in the co-presence of vinegar (Lewis et al., 2015). Blocking MBON-β'2mp and MBON-γ5β'2a output reduces CO<sub>2</sub> avoidance behaviour in fed flies (Lewis et al., 2015). These findings suggest that MBON-β'2mp and MBON-γ5β'2a mediate innate CO<sub>2</sub> avoidance behaviour, but also are regulated by satiety state and odours that signify food.

How does satiety state regulate CO<sub>2</sub> avoidance? A DAN that innervates the same MB compartment, PAM-β'2a, strongly responds to some food-related odours, more so in starved flies. Knockdown of the dNPF receptor, which mediates the NPF hunger signal, in PAM-β'2a leads to weaker yeast food-seeking behaviour (Tsao et al., 2018). Furthermore, activation of PAM-β'2a abolishes CO<sub>2</sub> avoidance behaviour (Lewis et al., 2015), but promotes yeast food-seeking behaviour (Tsao et al., 2018). These findings suggest that PAM-β'2a activity plays a role in fly approach behaviour towards food sources even in the presence CO<sub>2</sub> by suppressing CO<sub>2</sub> avoidance behaviour. However, Lewis et al., 2015 lacks important experimental evidence to determine if PAM-β'2a activation can modulate MBON-β'2mp and MBON-γ5β'2a responses to CO<sub>2</sub>. Thus, it is unclear how, or if, satiety state is functionally connected through PAM-β'2a (either directly from PAM-β'2a, or indirectly through KCs) to these MBONs whose output is required for innate CO<sub>2</sub> avoidance behaviour.

As MBON-β'2mp and MBON-γ5β'2a receive feedforward inhibition from MBON-γ1pedc>α/β (Perisse et al., 2016), it is possible that CO<sub>2</sub> avoidance behaviour is modulated cross-compartmentally through the hunger-regulated function of MBON-γ1pedc>α/β and PPL1-γ1pedc described above. In starved flies, the increased olfactory drive to MBON-γ1pedc>α/β would potentiate feedforward inhibition onto MBON-β'2mp and MBON-γ5β'2a, effectively reducing the behavioural drive for CO<sub>2</sub> avoidance.

These examples illustrate how various MB compartments are involved in different physiological processes and behaviours and demonstrate that the MB operates as an integrator of both external and internal cues to guide fly behaviour. However, more work is required to determine how satiety state is functionally connected to MBONs, and how MBONs are physiologically regulated in different contexts.

Although this section has solely focused on MB function with regards to the fly's energy state and food-associated behaviours, MB function is clearly important for a variety of other behaviours and physiological processes that are not covered here, such as courtship conditioning (Keleman et al., 2012, Lim et al., 2018), memory formation resulting from aggression bouts (Kim et al., 2018), temperature preference (Shih et al., 2015), distinguishing novel stimuli from familiar ones (Hattori et al., 2017), flight regulation (Manjila et al., 2019), and visual memory formation (Vogt et al., 2014, Vogt et al., 2016), but should be mentioned to highlight the diverse functions of the MB as an integrative centre of sensory information and the fly's internal state.

### 1.2.9 Network-level recurrent activity and compartment-crosstalk underlie post-learning processing

How are memories processed once they are established? Olfactory memories have different durations depending on the robustness of the association between the odour stimulus and the reinforcement, in the sense that repetition forms longer-lasting memories. Single training sessions with electric shock form aversive short-term memory (STM), which decays within a day. Multiple, spaced training sessions form long-term memory (LTM) in a protein-synthesis dependent manner, which remains strong for multiple days (Tully and Quinn, 1985, Tully et al., 1994). In contrast, a single session of appetitive learning with sugar as reinforcement leads to formation of LTM (Krashes and Waddell, 2008, Colomb et al., 2009). Being qualitatively different, it is not possible to make direct comparisons between sugar and electric shock reinforcement, but the requirement for multiple spaced sessions with electric shock vs a single session with sugar suggest that different types of reinforcement are differentially weighted in the context of conditioning.

What mechanisms facilitate memory consolidation? Several lines of evidence suggest that recurrent activity, persisting beyond the time of memory acquisition, is required for memory consolidation (Cognigni et al., 2018). One of the initial findings came from studies on the learning-impairing

*amnesiac* mutation and its expression in the DPM neuron (Waddell et al., 2000), an MB extrinsic neuron that widely innervates the MB lobes, forming pre- and post-synaptic connections with DANs, MBONs, and KCs (Takemura et al., 2017). Output from the DPM neuron is required for both appetitive and aversive memory consolidation (Waddell et al., 2000, Keene et al., 2004, Keene et al., 2006), for which  $\alpha'\beta'$  KCs are also important (Krashes et al., 2007), while the other KC subtypes are required for all or some aspects of olfactory learning (Trannoy et al., 2011, Yamazaki et al., 2018, Krashes et al., 2007, Perisse et al., 2013). Intriguingly, the KC subset-specific roles in memory formation match the requirement for output from the MBONs in the compartments innervated by these KCs, suggesting the two are linked in some cases at least (Shyu et al., 2017, Ichinose et al., 2015).

Recurrent activity between DANs, KCs and MBONs is essential for olfactory learning. Consolidation of appetitive conditioning to LTM relies on recurrent activity between the components of the  $\alpha 1$  compartment. Anatomical characterisation suggests that MBON- $\alpha 1$  axons synapse onto the dendrites of PAM- $\alpha 1$  in the superior intermediate, and lateral protocerebra (Ichinose et al., 2015). Blocking output of either of these neurons or the  $\alpha/\beta$  KCs disrupts memory consolidation, while knockdown of the D1-like dopamine receptor in  $\alpha/\beta$  KCs, but not MBON- $\alpha 1$  also disrupts consolidation.

Another configuration of recurrent activity is axoaxonic connectivity, which has been observed between DANs and KCs in the  $\alpha 2\alpha'2$  compartment. Cholinergic feedback from KCs to PPL1- $\alpha 2\alpha'2$  modulates its ongoing activity and is required for appropriate levels of dopamine release from PPL1- $\alpha 2\alpha'2$ , which seems to be required for memory acquisition. Thus, a recurrent PAM- $\alpha 1 > \alpha/\beta$  KC > MBON- $\alpha 1 > PAM-\alpha 1$  circuit facilitates consolidation of appetitive memories in the  $\alpha 1$  compartment (Ichinose et al., 2015), while a recurrent loop between KCs and DANs in the  $\alpha 2\alpha'2$  compartment is required for memory acquisition (Cervantes-Sandoval et al., 2017).

How is LTM mechanistically gated? A clue to this question has been provided by studies into aversive LTM consolidation. LTM requires ongoing oscillatory activity in PPL1- $\gamma 1$ ped in a temporally specific window (Plaçais et al., 2012). These oscillations are modulated by GABAergic input to PPL1- $\gamma 1$ ped from MBON- $\gamma 1$ pedc >  $\alpha/\beta$ . This GABAergic input is required 30-60 minutes post memory acquisition. Artificially activating MBON- $\gamma 1$ pedc >  $\alpha/\beta$  before this period disrupts memory consolidation (Pavlovsky et al., 2018). The oscillatory activity in PPL1- $\gamma 1$ ped depends on output from a pair of serotonergic neurons. depends on activity from a pair of serotonergic

projection neurons. Output from these serotonergic neurons is regulated by Dnc, a phosphodiesterase that, at baseline level, inhibits PKA/cAMP activity. Spaced training disinhibits PKA/cAMP activity, leading to increased signalling from the SPNs onto the DANs. This facilitates the oscillatory activity required in PPL1- $\gamma$ 1ped for memory consolidation (Scheunemann et al., 2018). Thus, serotonergic gating of LTM and recurrent activity between MBONs and DANs form the basis for consolidation of aversive memories.

As environmental conditions change, organisms may find that their associative memories are poor predictors of stimulus valence. What happens when a fly is re-exposed to a conditioned odour and the expected outcome is not met? When the fly is exposed to an odour that was previously associated with punishment, but now in the absence of punishment, the old memory undergoes 'extinction'. Instead of erasing the old memory, however, the unexpected lack of punishment acts as a 'reward', leading to formation of a new memory of opposite valence in parallel that counteracts the old memory (Felsenberg et al., 2018). What is the physiological basis of this process?

Aversive memory formation suppresses MBON- $\gamma$ 1pedc $\alpha/\beta$  responses to the conditioned stimulus, an approach MBON that provides feedforward inhibition to MBON- $\gamma$ 5 $\beta$ '2a and MBON- $\beta$ '2mp (Perisse et al., 2016). Extinction does not completely erase this memory trace. Instead, the dendrites and axons of MBON- $\gamma$ 5 $\beta$ '2a, but not MBON- $\beta$ '2mp, show decreased responses to the conditioned stimulus, suggesting that a parallel, appetitive memory trace is formed. How is this parallel memory trace formed?

Aversive memory extinction in flies requires output from reward-signalling PAM DANs (Felsenberg et al., 2018). Some of these DANs are functionally connected to the avoidance-directing MBON- $\beta$ '2mp and MBON- $\gamma$ 5 $\beta$ '2a, their dendrites overlapping with the axons of these MBONs (Aso et al., 2014a). Interestingly, activation of these MBONs evokes a strong excitatory response in PAM DANs that project axons to the  $\gamma$ 5 compartment, and to a smaller extent in  $\beta$ '2m and  $\beta$ '2p, suggesting that output from MBON- $\beta$ '2mp and MBON- $\gamma$ 5 $\beta$ '2a can drive activity in DANs that could potentially suppress the KC presynapses in the very same MBON compartments (Felsenberg et al., 2018). Output from MBON- $\beta$ '2mp and MBON- $\gamma$ 5 $\beta$ '2a is necessary to drive aversive memory extinction.

A similar configuration seems to drive appetitive memory extinction, where output from approach-directing MBONs that innervate the  $\alpha$ 2sc,  $\alpha$ '1,  $\alpha$ 2p3p,  $\alpha$ '3ap and  $\alpha$ '3m compartments recruit punishment-signalling PPL1 DANs that project their axons to the very same compartments

(Felsenberg et al., 2017). This suggests that both aversive and appetitive memory extinction in flies relies on functional MBON-DAN connectivity. Due to the increased excitatory drive of avoidance-directing MBONs after aversive conditioning, the MBON network presumably recruits reward-DANs more strongly than punishment-DANs, forming an appetitive ‘extinction’ memory when re-exposed to the conditioned odour in absence of punishment (Felsenberg et al., 2018). The extinction memory that is formed after aversive memory extinction is therefore like an appetitive memory trace. How is the original aversive memory and the appetitive extinct memory integrated?

MBON- $\gamma 1pedc > \alpha / \beta$  forms inhibitory synapses along the primary neurite, and the root of the dendritic tree, on MBON- $\gamma 5\beta'2a$ , while synapsing onto the distal dendritic branches of MBON- $\beta'2mp$ . This difference between the localisation of inhibitory synapses suggests that MBON- $\gamma 5\beta'2a$  could integrate input from the original aversive memory through feedforward inhibition from MBON- $\gamma 1pedc > \alpha / \beta$  and the putative depression arising from reward-DAN signalling to the  $\gamma 5$  compartment. Blocking reward-DANs provides compelling evidence that DAN signalling is required for extinction memory formation (Felsenberg et al., 2018), but the case could be made stronger by determining whether activation of a smaller subset of reward-DANs can suppress MBON- $\gamma 5\beta'2a$  odour responses.

Thus, the connectivity between DANs, KCs and MBONs serves not only to form and retrieve memories, but also to evaluate their accuracy. When the expected outcome is no longer met, MBONs seemingly drive DANs to form an extinction memory of opposite valence.

Behaviourally, the fly avoids the conditioned odour to a lesser extent after extinction. Thus, the fly brain forms parallel memory traces of conflicting information, which can be integrated to guide decision-making (Felsenberg et al., 2018).

Section 1.2.6-1.2.9 have elaborated on the function of the MB as a brain region that encodes sensory information and internal cues to shape associative learning, driving, or suppressing both innate and learned behaviours in conjunction with the LH. To summarise, KCs encode arbitrary combinations of sensory information to serve as the substrate for associative learning. KC axons comprise the MB lobes, where they form *en passant* synapses onto MBONs. DANs synapse onto the KC-MBON synapses to locally label, or categorise the sensory input, tempered by internal cues of the that are thought to regulate DAN activity. MBONs out this label in their respective compartment to guide the fly’s behaviour towards the external cues. This information processing

can take place on a local level, due to the spatial nature of DAN and MBON innervation of the MB lobes, where individual DANs and MBONs occupy distinct MB compartments. Details are emerging of the variety of behaviours that MBONs regulate other than approach or avoidance behaviour towards sensory stimulus, such as responding to novel stimuli and flight regulation. Recent studies highlight the complexity of functional connectivity between DANs, KCs and MBONs that goes beyond DAN-KC and KC-MBON synapses, and the role of various synaptic arrangements for memory formation and re-evaluation of memories.

Much remains unknown about the neuronal identity and function of the inputs that DANs receive, and how MBON output translates into regulation of motor output to steer behaviour. On a broader level, little is known about state-dependent memory recall except in the context of hunger state. When in different locomotor states, e.g. during flight, when walking, or when stationary, do flies recall certain memories strongly, while others are suppressed? This could be sensory modality-dependent, as the different behavioural states have an impact on the sensory cues the fly would experience, and act upon. Another question is whether memories that arise from different sensory modalities can be integrated. Can flies combine e.g. visual and olfactory cues to guide behaviour?

Large-scale connectome studies (Takemura et al., 2017, Zheng et al., 2018, Xu et al., 2020), combined with development of drivers to label subsets of neurons to probe for functional connectivity will help determine the function of pre- and post-synaptic partners of MB neurons for fly behaviour. Whole-brain imaging of freely moving flies offers the potential of recording neuronal activity during different states or behavioural contexts, which could shed light on state-dependent modulation of MB function (Grover et al., 2020).

#### 1.2.10 The case for studying the APL neuron in the context of localised processing

In the context of the compartmentalised structure and function of the MB, the APL neuron presents an interesting candidate to study localised computations for the reasons outlined below.

1. The APL neuron widely innervates the MB
2. There is some evidence suggesting that the APL neuron is non-spiking, implying that activity could be localised

3. Its output is required for sparse odour coding by KCs, but is also thought to be involved in memory formation

Below I will outline what is known about this neuron and emphasise the gaps in our knowledge about this neuron's function and emphasise why this is interesting to study with regards to local information processing.

The anatomy of the APL neuron, together with the possibility that it is a non-spiking neuron, is intriguing in the context of local computations. The GABAergic APL neuron extensively innervates the MB lobes, forming parallel neurites that follow the KC axons, but also innervates the calyx (Liu and Davis, 2009, Pitman et al., 2011, Aso et al., 2014a, Tanaka et al., 2008), forming reciprocal synapses with KCs in both regions (Takemura et al., 2017, Xu et al., 2020, Zheng et al., 2018). It is pre- and post-synaptic to the DPM neuron, while in the  $\alpha$  lobe it is known to be post-synaptic to DANs and mainly pre-synaptic to MBONs (Takemura et al., 2017, Lin et al., 2014a, Inada et al., 2017). Thus, it is connected to other parts of the olfactory system that govern sensory coding and associative conditioning. What is known about the APL neuron's function in the MB?

Its reciprocal connections to the KCs are required for maintaining sparse coding of odour stimuli by providing feedback inhibition to the KCs (Lin et al., 2014a). Depending on the odour concentration of the stimulus, the feedback inhibition can operate globally or locally. Blocking a specific KC subset is not sufficient to abolish the feedback inhibition – only when all subsets are blocked is the inhibition disrupted (Lin et al., 2014a). However, at lower stimulus strength the feedback inhibition seems to become subset-specific (Inada et al., 2017). There is some evidence that the APL neuron is non-spiking (Papadopoulou et al., 2011) supporting the notion that the APL neuron can operate differentially depending on the excitatory drive it receives.

What remains unclear is to what extent activity in the APL neuron remains localised. This is of great interest because there are clear spatial distinctions in the organisation of KC neurites in different parts of the MB. First, KC dendrites all reside in the calyx, while their axons give rise to the lobes. Second, the dendrites of different KC subtypes are largely intermingled in the calyx, while the KC axons are strictly segregated into different lobes (Takemura et al., 2017, Xu et al., 2020, Aso et al., 2014a). Does the APL neuron inhibit KCs in both the MB lobes and calyx? The anatomical data suggests it could, but there is a lack of functional evidence to confirm this. If it does, and activity in the APL neuron is spatially segregated between the calyx and the lobes, where

KC input and output sites reside, respectively, it would suggest that feedback inhibition in these two regions can operate independently and serve different purposes. Thus, it is first necessary to determine if activity in the APL neuron is localised. If this is case, the next step is to determine where in the MB the APL neuron can inhibit KCs, and characterise how locally its inhibitory output operates

Another interesting observation, although not in the scope of the work conducted for this thesis, is that the APL neuron could encode multimodal sensory stimulus. As some KCs receive input from the accessory calyces of other sensory modalities than olfaction (Yagi et al., 2016, Vogt et al., 2016, Kirkhart and Scott, 2015), and connectome data (Xu et al., 2020) shows that these KCs form connections with the APL neuron (query of connectome data available on <https://neuprint.janelia.org/>), it seems plausible that the APL neuron also encodes information other sensory modalities than olfaction. If activity in the APL is localised, it would raise the question to what extent input to the APL neuron from different sensory modalities remain spatially segregated, or if they are in fact integrated. Strong integration would imply that the APL neuron mediates cross-inhibition between sensory modalities.

Finally, the APL neuron's connections with MBONs and DANs are interesting in the context of associative learning, as the APL neuron has been implicated in memory formation and expression. It responds to electric shocks (Liu and Davis, 2009, Zhou et al., 2019), which is often used for aversive conditioning in flies. Aversive conditioning can suppress the APL neuron's response to the conditioned odour, suggesting that a 'memory trace' is formed, which seems to involve signalling through dopamine receptors (Liu and Davis, 2009, Zhou et al., 2019). Some evidence suggests that this dopamine signal to the APL neuron has an effect on the strength of immediate memory expression (Zhou et al., 2019).

What is the nature of dopamine signalling to the APL neuron? Zhou et al. used a G protein-coupled receptor-activation-based DA sensor (GRAB<sub>DA</sub>) (Sun et al., 2018) and P2X2-mediated activation of PPL1 DANs to show that the APL neuron receives signals from DANs through the DA sensor, suggesting that there are functional connections between DANs and the APL neuron (Zhou et al., 2019). Using genetically encoded calcium sensors (discussed in section **3.1.2**) to record neuronal activity while perfusing dopamine onto the brain evoked an increase in calcium signal at the tip of the vertical lobe and a decrease in the stalk and heel regions. Adding tetrodotoxin to block neurotransmission blocked the dopamine-evoked increase in calcium signal at the tip of the vertical

lobe (Zhou et al., 2019). Artificial activation of PPL1 DANs (broadly labelled by TH-GAL4) while imaging the APL neuron in the presence of tetrodotoxin and an acetylcholine receptor antagonist (added to block cholinergic input to the APL neuron) increased the calcium signal in the APL neuron (Zhou et al., 2019). This suggests that direct or indirect dopamine signalling has spatially differential effects on the APL neuron activity, where some parts of APL are inhibited by the dopamine signal, and others are excited.

How is the DAN signal conveyed to the APL neuron? The DAN-APL signalling seems to be mediated in part by the dopamine 2-like receptor (Dop2R). Knockdown of this receptor, or pharmacological blocking, weakened the dopamine perfusion-evoked suppression of the calcium signal in the ‘stalk’ and ‘heel’ region of the vertical lobe. Blocking Dop2R increased the APL neuron’s response to artificial activation of PPL1 DANs. Electric shock was also found to elicit an excitatory response in the APL neuron, which was increased by blocking Dop2R (Zhou et al., 2019). These findings suggest that there is both an excitatory and inhibitory component to DAN signalling onto the APL neuron, possibly mediated by different receptors, in different regions.

What is the functional role of DAN signalling to the APL neuron? Behaviourally, knockdown of Dop2R in the APL neuron slightly decreased learning performance of flies subjected to aversive conditioning as measured straight after conditioning (Zhou et al., 2019). Physiologically, knockdown of Dop2R abolished training-induced suppression of the APL neuron’s response to conditioned stimulus in flies subjected to aversive reinforcement using electric shock. The suppression of the APL neuron’s response was abolished both during, and after, conditioning (multiple odour-electric shock pairings). This suggests that dopamine signalling to the APL neuron is required during conditioning, after conditioning, or both, for suppression of the APL neuron’s response to conditioned stimulus and has an impact on immediate memory expression. As dopamine signalling was constitutively impaired by knockdown of the Dop2R receptor, it is not possible to say from this study if dopamine signalling is specifically required during conditioning for the APL neuron’s role in immediate memory expression.

Importantly, it remains unknown if the ‘memory trace’ induced in the APL neuron by aversive conditioning is spatially restricted to one or more MB compartments, or if it adheres to the compartmental division at all. This was not addressed by Zhou et al., as they quantified the APL neuron’s responses during and after conditioning in a single plane of the vertical lobe, referred to as the ‘lower stalk of the vertical lobe’. Their quantification of the APL neuron’s responses to artificial

activation of DANs and electric shock were also limited to single planes of the vertical lobe. Due to these limitations, the study provides no knowledge of the spatial nature of the APL neuron's in any of the above-mentioned contexts. This is an essential point to address, because our current understanding of fly olfactory learning is that plasticity is induced in a compartment-specific manner by having DANs that respond to the unconditioned stimulus suppress the KC-MBON synapses specifically in the compartments they innervate (Hige et al., 2015, Cohn et al., 2015). The APL neuron innervates the MB compartments, receives input from dopaminergic neurons, and responds to electric shocks. Since the plasticity imposed on KC-MBON synapses by DAN signalling occurs in a compartment-specific manner, it seems plausible that the plasticity in the APL neuron should also occur in this manner.

Another limitation of the study is that they only determine if the APL neuron responds to artificial activation of PPL1 DANs. Whether the APL neuron responds to activation of PAM DANs, and if its response is spatially uniform, remains unknown.

What could be the function of learning-induced suppression in the APL neuron, and how does this depend on whether inhibition from the APL neuron works locally or globally?

One possibility is that inhibition from the APL neuron onto KCs works as a gating mechanism for learning. Disinhibition would then allow the memory to be formed. What could be the mechanistic basis of inhibition from the APL neuron working as a gating mechanism? Perhaps it is necessary to reduce inhibition from the APL neuron onto KCs during learning to increase the level of calcium influx evoked by odour stimulus. This could be required for the coincidental detection of calcium and the reinforcing dopamine signal by the calcium-dependent adenylyl cyclase, Rutabaga (Levin et al., 1992, Himmelreich et al., 2017, Tomchik and Davis, 2009, Gervasi et al., 2010). If the inhibition from the APL neuron restricts calcium influx through voltage-gated calcium channels to an extent that it is not detected by Rutabaga, perhaps the APL must be suppressed to disinhibit KCs, thereby increasing calcium influx.

There is some evidence in support of this theory. Zhou et al. reported that they observed a suppression of APL neuron's response to conditioned stimulus both during and after conditioning. This suppression was abolished when Dop2R was knocked down in the APL neuron. These findings suggest that dopamine signalling is required for suppression of the APL neuron during and after learning. Furthermore, knockdown of Dop2R in the APL neuron impaired immediate memory recall (Zhou et al., 2019). This finding suggests that suppression of the APL neuron could be

required either during training, after training, or both, for the APL neuron's effect on immediate aversive memory recall. This possibility would also explain the observation that knockdown of GAD or Rdl in the APL neuron or KCs, respectively, improves learning performance (Liu and Davis, 2009).

Would this proposed function work with local or global inhibition? If suppression of the APL neuron is required specifically during training to gate memory formation, then it could work either locally or globally. Even if inhibition from the APL neuron is global, it should only affect memory formation where KCs synapses coincidentally receive the dopamine teaching signal and increased calcium influx.

However, if suppression of the APL neuron is required after training for memory recall, it is difficult to envision how it would work if inhibition from the APL neuron is global, equally affecting approach and avoidance compartments. In this case, suppression of the APL neuron would potentiate KC odour responses, increasing the excitatory drive to both approach and avoidance MBONs.

Interestingly, another study found that output from the APL neuron is required after training for 3 h appetitive memory recall (Pitman et al., 2011). The authors suggested that output from the APL neuron might be required for maintaining synaptic specificity of learning-associated recurrent activity. It was not in the scope of this study to determine if output from the APL neuron is required during training, nor if appetitive learning led to formation of a memory trace in the APL neuron. Thus, it is unclear if the role for the APL neuron in relation to 3 h appetitive memory is related to what happens to the APL neuron during aversive conditioning. Nevertheless, their finding suggests that learning-induced suppression of the APL neuron could be short-lasting, or that its level of output must be narrowly controlled for memory recall.

Another possibility is that suppression of the APL neuron's response to the conditioned stimulus counteracts the suppression of KC-MBON synapses induced by conditioning, due to the reduced inhibition from the APL neuron onto KCs (Concept proposed by Andrew C. Lin, personal communication). Consider the scenario where there is no inhibition from the APL neuron (no GABA release from APL, or no GABA receptors in KCs) and the fly is subjected to aversive conditioning. This suppresses excitatory drive from KCs to approach MBONs, strongly skewing the balance towards avoidance (**Fig. 1.6 A**).

Now compare this to the default scenario where the APL neuron does provide feedback inhibition to KCs. Aversive conditioning suppresses KC-MBON synapses to approach-MBONs. It also suppresses the APL neuron's response to the conditioned stimulus (Liu and Davis, 2009, Zhou et al., 2019), which would presumably reduce the strength of feedback inhibition onto KCs. The result would be that conditioning inhibits MBONs by suppressing KC-MBON synapses, but also indirectly potentiates KC-MBON synapses by reducing inhibition from the APL neuron onto KCs, increasing the excitatory drive from KCs to MBONs. It is a skew in the balance in excitatory drive to the approach and avoidance MBONs that drives behaviour. Thus, if inhibition from the APL neuron operates **locally** and it is only suppressed locally to the conditioned stimulus, this would counteract the depression of KC-MBON synapses in the approach compartment, but maintain the default level of inhibition onto KCs in the avoidance compartment, effectively counteracting the strength of the aversive memory. In other words, local suppression of the APL neuron's response to the conditioned stimulus would work as an 'anti-memory', working in opposition to the DAN-induced suppression of the KC-MBON synapse (**Fig. 1.6 B**).

If aversive conditioning suppresses the APL neuron globally, or if inhibition from the APL neuron operates globally, however, inhibition from the APL neuron should not influence the strength of the memory, because it would equally affect the KC odour responses in both approach and avoidance compartments (**Fig. 1.6 C**), just as though there was no inhibition from the APL neuron altogether (**Fig. 1.6 A**). This is under the assumption that inhibition from the APL neuron has a linear effect in different compartments. If inhibition from the APL neuron has nonlinear effects in different compartments, then even global inhibition could differentially affect compartments.

Under the assumption that the APL neuron operates locally, this 'anti memory' model could explain the previous observations that knockdown of GAD in the APL neuron or Rdl in KCs leads to stronger memory expression (Liu and Davis, 2009), and impairs reversal learning (Wu et al., 2012). Fly reversal learning involves an initial training cycle where flies are subjected to one odour-reinforcement pairing, and a second unpaired odour, followed by a cycle where the second odour is paired with reinforcement and the first odour is unpaired.

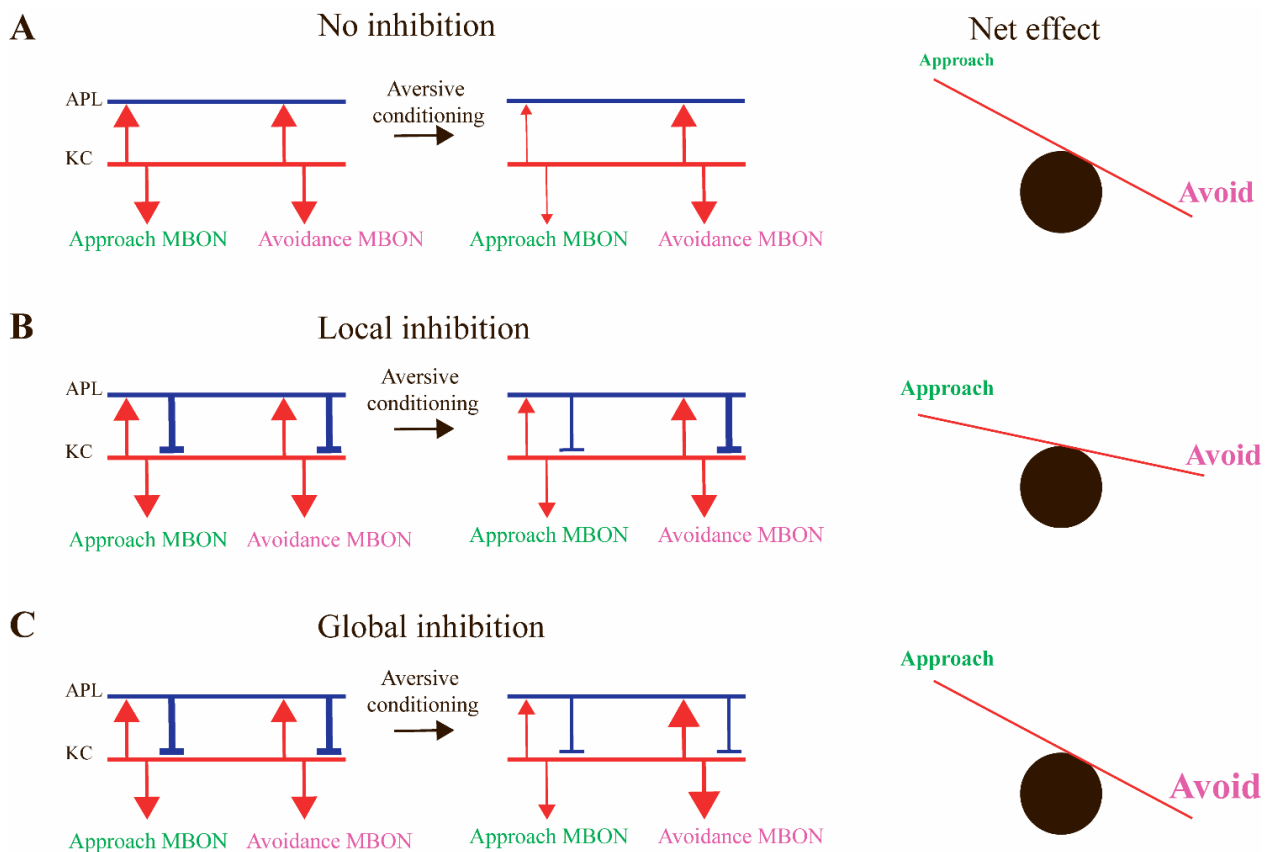


**Fig. 1.6 Local vs global inhibition in the context of APL neuron plasticity**

Cartoon showing the predicted effects of local vs global inhibition of KCs by the APL neuron in the context of learning-induced plasticity. Blue lines represent the APL neuron's neurites, while red lines represent KC axons. **(A)** If there is no inhibition from the APL neuron, aversive conditioning will simply suppress KC synapses to approach MBONs, skewing the balance towards avoidance (right). **(B)** Aversive conditioning suppresses the APL neuron and KC synapses to approach MBONs. If inhibition from the APL neuron onto KCs is local, the learning-induced suppression of the APL neuron will locally increase KC activity in the approach compartment, but not the avoidance compartment, mitigating the skewed balance towards avoidance. **(C)** If inhibition from the APL neuron is global, suppression of the APL neuron should equally affect KCs in approach and avoidance compartments, and thus have no effect on the balance between the opposing forces.

If inhibition from the APL neuron onto KCs is impaired (Rdl or GAD knockdown), there would no longer be the 'anti-memory' effect from suppressing the APL neuron in the same compartment as the suppressed KC-MBON synapse, shifting the excitatory drive to avoidance MBONs relative to approach MBONs further towards avoidance (**Fig. 1.6 A**). Another contributing factor could be that the lack of inhibition from the APL neuron broadly increases KC odour responses, leading to depression of more KC-MBON synapses. This would presumably strengthen memory expression. Because of the stronger initial memory formation, reversal learning could be more difficult and require multiple reversal training sessions to achieve.

The potentially local function of the APL neuron in associative conditioning, combined with its non-spiking nature and ubiquitous innervation of the compartmentalised MB structure makes it an interesting candidate for studying local computations relevant to essential behavioural output.

### 1.2.11 Tools for imaging neuronal activity

In this and the next section, I will outline the technical requirements of the experiments I conducted and explain why the tools I used were suitable for the task. I also briefly mention alternative methods that I considered using while conducting my experiments. Since then there have been advances and improvements of genetic tools used for recording neuronal activity (Dana et al., 2019, Kannan et al., 2019), but as these were not available at the time of my experimental work, they will not be considered here.

The conventional method of recording neuronal activity is known as patch clamping. For electrophysiological recordings of neuronal responses to stimuli, the common approach, known as whole-cell patch clamping, is to bring a patch pipette into contact with the target neuron and create suction to rupture the cell membrane, creating a tight seal. This connects the electrode solution with the cell interior, allowing for intracellular recordings of both subthreshold voltage deflections and action potentials. For population-level recordings, multi-electrode arrays can be utilised, where each channel records local extracellular changes in ionic currents (Obien et al., 2014). Although this method offers the most accurate and sensitive measure of neuronal activity, it has several limitations.

The invasive nature of electrophysiological recordings can potentially compromise cell physiology, as subsequent diffusion of solutes between the recording electrode and the cytoplasm can potentially change the kinetics or amplitude of responses, especially for extended recordings.

More importantly, electrophysiological recordings lack spatial resolution both on a single-neuron level, but also population wise, as activity is recorded from an individual neuron, typically at the cell soma. Recording from a single site is problematic because neurons with elaborate branching can receive inputs from spatially distal sites that are electrically segregated (Grimes et al., 2010, Medan et al., 2018) Furthermore, it can be technically difficult, if not impossible, to record from individual neurites due to their small sizes. Global electrophysiological recordings can be achieved using multi-electrode arrays, consisting of hundreds of individual electrode channels. While multi-

electrode arrays circumvent the limitation of recording from a single neuron at a time, they still suffer from low spatial resolution due to the inherent difficulty of assigning neuronal activity to individual neurons (Hilgen et al., 2017, Carlson and Carin, 2019).

The limitations of spatial resolution with electrophysiological recordings were not compatible with the experiments I had to conduct, as they required a means of recording neuronal activity from specific neurons in the entire MB volume in intact flies. For this purpose, optical imaging of neuronal activity is superior to electrophysiological recordings.

*In vivo* imaging of a neuronal activity presents a great challenge in terms of signal-to-noise ratio (SNR, peak signal during stimulus period over the standard deviation of the signal in a pre-stimulus period) due to background fluorescence, light scattering, and signal attenuation when recording from deep brain regions. When acquiring recordings from multiple imaging planes (volume imaging), fewer frames are acquired from each imaging plane compared to single plane imaging. Therefore, it is not possible to down-sample the framerate to average the signal to the same extent when acquiring a volume as it is for single plane recordings.

Optical imaging can be achieved using fluorescence-based genetically encoded calcium or voltage indicators (GECIs and GEVIs, respectively). GECIs and GEVIs can be expressed in neurons using the yeast binary transcription-activation system comprised of GAL4 and upstream activation sequence (UAS). GAL4 is a transcription factor that recognises and binds to the UAS, initiating transcription of genes downstream of the UAS. This system has been repurposed to drive tissue-specific expression of transgenes in *Drosophila melanogaster* (Brand and Perrimon, 1993). By placing the Gal4 sequence under control of enhancer fragments (either through targeted or random insertion into the genome), the expression pattern of GAL4 can be restricted to subsets of cells. By crossing a fly that harbours the Gal4 sequence to another fly that carries the UAS, the offspring that receive both elements will express the gene of interest specifically in the cells where both GAL4 and UAS are present (Brand and Perrimon, 1993) (**Fig. 1.7**) This system has led to development of large libraries of fly lines with distinct GAL4 expression patterns (Jenett et al., 2012, Aso et al., 2014a, Kvon et al., 2014, Tirian and Dickson, 2017, Hayashi et al., 2002).

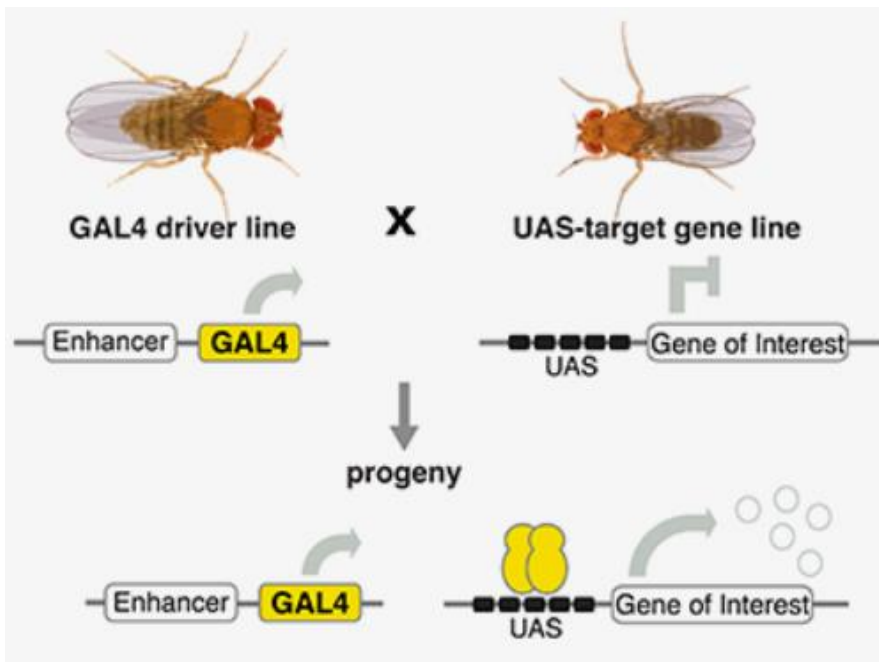


**Fig. 1.7 The GAL4/UAS system.**

Enhancer fragments drive the expression of GAL4, a transcription factor that binds to UAS and initiates transcription of downstream genes of interest. Crossing flies that express GAL4 with ones that harbour UAS yield progeny that can have both elements, driving expression of the gene of interest in cells where both GAL4 and UAS are present. Taken from

<https://andreabrandlab.org/gal-4-system>

Depending on the genetic construct, a GECI or GEVI can be ubiquitously expressed throughout the neuron's cytoplasm, including its neurites, or more specifically localised to synaptic sites (Cohn et al., 2015). The ability to ubiquitously express an activity indicator fulfilled the requirement of my experiments to record activity throughout entire neurons.

Optical imaging of a genetically encoded indicator dispenses of the need for an invasive procedure to record neuronal activity and circumvents the technical difficulty of targeting a single neuron or neurite inherent to whole-cell patch clamping, greatly increasing throughput. Combined with cell-type specific expression of an indicator, optical imaging allows you to simultaneously record neuronal activity across a defined population of neurons, revealing differences in responses not only between neurons, but also in individual neurites of a single neuron (Yang et al., 2016, Cohn et al., 2015). Thus, optical imaging of a genetically encoded indicator seemed ideal for my purposes.

For my experiments I used a GECI known as GCaMP6f (Chen et al., 2013). This indicator consists of a circularly permuted enhanced GFP that is linked to calmodulin, a calcium-binding protein, and the calmodulin-binding peptide known as M13 (Crivici and Ikura, 1995, Nakai et al., 2001). Calcium indicators rely on the ~100-fold increase in cytosolic calcium levels evoked by depolarisation (Grienberger and Konnerth, 2012) to report neuronal activity. Subsequent calcium binding by calmodulin induces conformational changes in the construct that alters the chemical

environment around the GFP chromophore, increasing fluorescence intensity (Wang et al., 2008, Akerboom et al., 2009). Thus, they provide an indirect measure of neuronal activity.

Several studies have aimed at optimising the initial GCaMP construct (Nakai et al., 2001) to increase sensitivity (lowest level of activity that the sensor can report), dynamic range (amplitude of fluorescence change for different levels of stimulus), and kinetics (rise to peak and decay to half intensity times) (Tian et al., 2009, Akerboom et al., 2012, Chen et al., 2013). At the time that these experiments were conducted, the GCaMP6 indicators were the most optimised variants available. This family consists of GCaMP6s (slow), m (medium), and f (fast), referring to their response rise and decay times, with the slower variants having higher sensitivity (Chen et al., 2013).

Although my goal was mainly to spatially characterise activity spread and inhibition, I also sought to capture differences between MB regions in terms of the kinetics of activity spread, as faster or slower temporal decay of activity could explain why activity propagates farther from certain regions, but not others. Thus, I used GCaMP6f as my activity reporter, because it has the fastest rise (~50-200 ms, time to peak from stimulus onset) and decay (~200-600 ms, time to half peak activity) times of all three variants while still offering improved sensitivity and dynamic range compared to its predecessor, GCaMP5 (Chen et al., 2013).

An alternative optical imaging approach is to use a GEVI. This emerging method directly reports neuronal activity by linking voltage fluctuations to a change in fluorescence signal. Voltage indicators consist of a voltage-sensing domain, derived from proteins such as ion channels, voltage-sensitive phosphatases, or opsins, coupled to a fluorescent protein. Fluctuations in membrane potential induce conformational changes in the voltage-sensing domain, or protonation of the rhodopsin chromophore, retinal, modulating the fluorescence signal of the connected fluorophore (Kannan et al., 2019). By directly measuring voltage fluctuations, these voltage indicators can report any change in membrane potential, even if there is no concomitant change in calcium levels (subthreshold changes or hyperpolarisation). Voltage indicators also address the limited temporal resolution of GECIs. Whereas GCaMP6f at best resolves spikes up to a rate of 20 Hz, some voltage indicators resolve spikes at rates higher than 100 Hz (Kannan et al., 2019).

The use of GECIs and GEVIs with respect to my experimental findings are discussed in section **6.5.1**.

### 1.2.12 Tools for local, artificial activation of neurons.

The other requirement of my experiments was to locally activate or inhibit neurons in the MB. The challenges involved with this task are how to limit the manipulation to a specific type of neurons, how to titrate the effect to the desired level, and how to spatially restrict the local activation or inhibition to a small region in the MB. Cell-type specific targeting can be achieved by using a ligand-gated ion channel. Importantly, the ligand-gated ion channel should not be endogenously expressed, so that only the neurons that express it are directly activated by application of the ligand. By adjusting the ligand concentration, it is possible to adjust the stimulation strength, and by coupling delivery of the ligand solution to a pressure system, it is possible to restrict bulk flow to a small region in the brain.

These requirements can be fulfilled using ATP-mediated activation of neurons expressing P2X2, a ligand-gated ion channel that belongs to the family of purinergic receptors (Valera et al., 1994, Brake et al., 1994) and mainly conducts calcium and sodium currents upon ATP binding (Liu and Adams, 2001, Evans et al., 1996). Signalling through this receptor family is involved in various processes, such as cell migration, differentiation, and neuronal signalling in the nervous system (Burnstock, 2018). Due to lack of endogenous expression of P2X2 in the *Drosophila* genome (Littleton and Ganetzky, 2000), it is possible to selectively stimulate neurons labelled by a GAL4 line that drives expression of P2X2 using ATP application.

For direct suppression of neurons, I instead applied GABA, a major inhibitory neurotransmitter in the insect central nervous system, to the MB (Enell et al., 2007).

To deliver ATP or GABA, a patch pipette filled with drug solution and coupled to a pressure ejection system (Picospritzer) was manually brought to the desired stimulus site in the MB. By adjusting the duration and pressure applied to the patch pipette, it was possible to locally apply the drug solution in the MB.

To estimate how widely the patch pipette solution dispersed, I co-ejected a red dye to approximate how widely the ejected drug disperses. I identified Setau-647 (Seta Biomedicals) and Alexa Fluor 647 (Fischer) as potential candidates. The molecular weights of ATP and GABA are 507.18 g/mol and 103.12 g/mol, respectively, while Alexa Fluor 647 is 1155.06 g/mol, and Setau-647 is 1461 g/mol. Thus, based on molecular weight, Alexa Fluor 647 would be a better approximation of ATP

and GABA dispersion, but Setau-647 has a higher quantum yield and total brightness across a range of dye-to-protein ratios. For some of my recordings, the red dye signal was less than 2%  $\Delta F/F$ , so a dimmer dye would possibly have caused complications due to low signal-to-noise ratio. Therefore, I chose Setau-647. The reliability of the red dye as an approximation of drug spread is discussed in section **3.3.1**.

Another popular approach for artificial activation of neurons is coined ‘optogenetics’ (Deisseroth, 2015). This method relies on genetically expressing photon-gated ion channels, known as channelrhodopsins, in the neurons of interest and using a laser to activate the ion channels, which depolarises the neurons through influx of cations (Deisseroth, 2015). In *Drosophila melanogaster*, the blue light-gated (~480 nm) channelrhodopsin-2 was the first variant used to study neuronal function (Simpson and Looger, 2018). However, this approach was severely limited by the penetrance of blue light through the fly cuticle (~1%) (Inagaki et al., 2014), omitting its use for deep-brain stimulation. To overcome this limitation, red-shifted variants, such as ‘red-activatable channelrhodopsin’ (~610 nm) (Lin et al., 2013) or Chrimson (~590 nm) (Klapoetke et al., 2014) can be utilised, as red wavelengths can penetrate the cuticle up to ten-fold more strongly than blue light (Inagaki et al., 2014). For simultaneous optical stimulation of select regions and calcium imaging, two lasers with different wavelengths are required to avoid cross-activation of the channelrhodopsin by the scanning laser (Packer et al., 2013).

In section **6.5.2**, I discuss the advantages and drawbacks of different artificial stimulation approaches in light of my experimental findings

### 1.2.13 Parallels between the mushroom body and the vertebrate nervous system

What can the fly olfactory system teach us about sensory processing and learning in the vertebrate brain? Fruit flies display a wide array of motor and social behaviours (courtship, aggression, foraging), including experience-dependent behaviours, suggesting that their nervous system carries out complex processes that are required for similar behaviours in vertebrates. With regards to the olfactory system, the numerically simpler brain of the fly and the wide array of genetic tools available allows us to study how sensory information is encoded at different levels throughout the nervous system. The anatomical segregation between innate (section **1.2.2-1.2.4**) and learned (section **1.2.5-1.2.9**) responses lends itself well to studying the differences in sensory processing

between predictive and unbiased sampling, respectively, but also to understand how these two paths converge and interact to shape fly behaviour.

There is a striking similarity between the anatomical organisation of the fly and rodent olfactory systems. Like the fly ORNs, these neurons express one specific olfactory receptor and project only to a single or two distinct glomeruli in the rodent olfactory bulb, maintaining odour identity in separate channels (Mombaerts et al., 1996, Godfrey et al., 2004). Mitral and tufted cells receive input in the olfactory bulb and project to the piriform cortex where they synapse onto pyramidal neurons (Price and Powell, 1970). Odourants evoke responses in a sparse, unique ensemble of neurons in the piriform cortex with no apparent spatial clustering (Stettler and Axel, 2009, Iurilli and Datta, 2017, Poo and Isaacson, 2009), similarly to what has been observed for KCs in the mushroom body (Honegger et al., 2011, Perez-Orive et al., 2002, Turner et al., 2008, Ito et al., 2008). Sparse odour coding in the piriform cortex is thought to be maintained by inhibition originating from interneurons that receive broadly tuned olfactory input (Poo and Isaacson, 2009, Large et al., 2016), similar to the importance of feedback inhibition from the APL neuron onto KCs for sparse coding (Lin et al., 2014a, Inada et al., 2017).

Thus, there are clear similarities between the mouse and fly olfactory system in terms of sensory discrimination. The value of studying sensory discrimination in the fly is the numerically simpler nervous system, exemplified by the single APL neuron per hemisphere versus the multiple types of interneurons in the piriform cortex. This makes it much simpler to study the function of a neuron or neuronal type, by selectively manipulating that neuron using the wide selection of genetic tools available for flies.

How does the compartmentalised nature and its importance for olfactory learning in the mushroom body relate to associative conditioning in vertebrates?

There is little knowledge of this with regards to the piriform cortex. Network activity in the piriform cortex changes after associative olfactory learning, and artificial stimulation of ensembles of piriform cortex neurons is sufficient to drive learned behaviours, suggesting that the piriform cortex encode memories (Chen et al., 2011, Sevelinges et al., 2004).

However, there is another structure in the vertebrate brain, the cerebellum, which has striking functional and structural similarities to the mushroom body. The cerebellum is thought to process

multimodal information in parallel, facilitating associative learning (Apps et al., 2018, Xiao and Scheiffele, 2018).

Structurally, the cerebellum consists of granule cells that form parallel fibres akin to KC axons. Granule cell dendrites form claw-like shapes onto which mossy fibre afferents form connections within well-defined glomeruli, or 'rosettes', reminiscent of the microglomeruli structures where PNs and KCs form connections. Granule cells receive multimodal sensory or motor input from mossy fibres, with each granule cell receiving multiple inputs, suggesting that they encode representations or associations between sensory and motor information (Xiao and Scheiffele, 2018). The granule cell parallel fibres heavily converge onto Purkinje cells, similarly to the convergence of KC parallel axons onto MBONs (Farris, 2011).

Functionally, parallel fibres receive broad, lateral feedback inhibition from Golgi cells in the cerebellum (D'Angelo et al., 2013), like the feedback inhibition from the APL neuron onto KCs. The synapses between parallel fibres and Purkinje cells can undergo both long-term potentiation (LTP) and long-term depression (LDP) (Coemans et al., 2004), similarly to how KC-MBON synapses undergo plasticity through DAN signalling.

To summarize, there is the same fan-out fan-in architecture for both brain structures, suggesting that this architecture is recurrent throughout nervous systems. Importantly, the cerebellum is also thought to operate in modular units, processing different types of information in parallel (Apps et al., 2018). Both structures decorrelate information from the previous layer, PNs to KCs for the MB, and mossy fibres to granule cells for the cerebellum, and then converge onto efferent neurons that undergo LTP and LDP. Although the mushroom body and the cerebellum process different types of input (with the piriform cortex being more related to the MB in this regard), the fact that they share structural similarities and process multimodal information in parallel suggests that this organisation serves a specific mode of information processing. Indeed, this architecture has been proposed as a suitable substrate for associative learning (Marr, 1969, Albus, 1971).

The strength of the fruit fly as a model system is exemplified by the extensive knowledge already obtained about the compartmentalised architecture of the mushroom body and how convergence of sensory identity and teaching signals onto efferent neurons drives behaviour. The compartmentalised, or modular, nature of the cerebellum, and the requirement for feedback

inhibition in vertebrate structures such as the piriform cortex and the cerebellum highlight the potential in studying the APL neuron.

Unravelling the mechanistic basis of local computations in the fly olfactory system, will further our understanding of how neurons process information from different origins. Linking this to learning and decision-making will demonstrate the importance of local computations in the nervous system. From there, future studies in vertebrates can develop our understanding of learning and decision-making in the human brain.

## Focus of this thesis

To investigate the gaps in our knowledge about the function of the APL neuron and whether it operates locally, I set out to address the following questions.

1. How does activity propagate within the APL neuron? Does depolarisation in the APL neuron propagate throughout its neurites (from lobes to calyx) or stay localised?
2. What is the nature of feedback inhibition from the APL neuron to KCs? Does the spatial extent of feedback inhibition correspond to activity spread in the APL neuron?
3. What are the spatial dynamics of plasticity in the APL neuron? Are there spatial differences in its electric shock response, and how does this relate to where a memory trace is formed following aversive conditioning?

During my PhD, I was also offered the opportunity to take part in a study on the role of signalling through muscarine receptors in KCs on olfactory learning. The part of the study that I contributed was to determine where in the MB muscarine receptors played a role, and if there were KC subset-specific effects of muscarine signalling. This was of great interest to me, as it involved a question similar to the ones I was addressing in my own project: what is the role of subcellular signalling in olfactory learning?

## 2. Materials & Methods

### 2.1 Materials

#### 2.1.1 Fly rearing

Fly stocks and crosses were kept at 25 °C or 18 °C (long-term stock maintenance) on a 12L:12D (light/dark) cycle in vials containing the following food mix:

H <sub>2</sub> O	1 L
Medium Cornmeal	80 g
Dried Yeast	18 g
Soya Flour	10 g
Malt Extract	80 g
Molasses	40 g
Agar	8 g
10% Nipagin in Absolute Ethanol	25 ml
Propionic Acid	4 ml

#### 2.1.2 Fly stocks

Designation	Reference	Availability
OK107-GAL4	(Connolly et al., 1996)	BDSC:854
MB247-DsRed	(Riemensperger et al., 2005) FLYB:FBtp0022384	
UAS-GCaMP6f (VK00005)	(Chen et al 2013), FLYB: FBst0052869	BDSC:52869
UAS-GCaMP6f (attP40)	(Chen et al 2013), FLYB: FBst0042747	BDSC:42747
tub-FRT-GAL80-FRT	(Gordon and Scott, 2009; Lin et al., 2014)	BDSC:38880

MB247-LexA	(Lin et al., 2014; Pitman et al., 2011), FLYB:FBtp0070099	Gift from S. Waddell
LexAop-P2X2	Unpublished	Gift from A. Lin
LexAop-GCaMP6f	(Barnstedt et al., 2016)	Gift from S. Waddell
GH146-FLP	(Hong 2009), FBtp0053491	
UAS-mcherry-CAAX	(Kakihara et al., 2008; Lin et al., 2014), FLYB:FBtp0041366	
NP2631-Gal4	(Tanaka 2008)	DGRC:104266
UAS-P2X2	(Lima and Miesenbock 2005), FLYB: FBtp0021869	BDSC:76032
UAS-P2X2(attP40)	(Clowney et al., 2015)	Gift from V. Ruta
UAS-Ort	(Rister et al., 2007) FLYB:FBrf0201203	Gift from C.Lee
VT43924-Gal4.2	(Lin lab, unpublished)	VDRC:v201194
VT43924-LexAp65	(Lin lab, unpublished)	VDRC:v201194
LexAop2-jRGECO1a	(Sun et al., 2017) FLYB: FBst0064426	BDSC:64426
UAS-CD8::GFP??	(Lee et al., 1999), FLYB: FBst0005130	BDSC:5130
R82C10LexA	(Jenett et al., 2012), FLYB: FBst0054981	BDSC:54981
R48H11LexA	(Jenett et al., 2012), FLYB: FBst0052745	BDSC:52745
R48B03LexA	(Jenett et al., 2012), FLYB: FBst0054214	BDSC:54214
R30G08LexA	(Jenett et al., 2012), FLYB: FBst0052679	BDSC:52679
474-Gal4	(Gohl et al., 2011)FBst0063344	BDSC:63344
MB077B	(Aso et al., 2014) FBrf0227179	BDSC:68283

### 2.1.3 Equipment

Equipment	Vendor
Leica S8 APO stereomicroscope	Leica
Narishige PC-10	NARISHIGE GROUP
DSP controller LC.400 (1-Channel)	npoint
Pockels amplifier 350-80LA	conoptics
Microscope movement controller MPC200	Sutter Instrument
PXIe-1073	National Instruments
Sutter Resonant scan box MDR-R	Sutter Instrument
Sutter Moveable Objective Microscope	Sutter Instrument
Shutter controller SC10	Thorlabs
GO-5000M-USB camera	Jai
DALSA GENIE NANO-M1280-NIR	Stemmer
Double PatchStar Micromanipulator System - One Cube	Scientifica
Mai Taie eHP DeepSee Ti:S laser	Spectra-Physics
Thermorack 401	Solid State Cooling Systems
2-Channel PicoSpritzer III 0-30PSI	MCI
Constant current isolated stimulator DS3	Digitimer
Watson-Marlow 120S/DM2 pump	Scientifica
Nanodrop ND+1000	Fisher

DS3 Constant Current Isolated Stimulator	Digitimer Ltd.
USB6059 Digital I/O Device	National Instruments

## 2.1.4 Reagents

Material	Model/Reference	Vendor
TES	T5691-100G	Sigma
KCl 500 g	10735874	Fisher
CaCl <sub>2</sub>	21115-100ML	Sigma
MgCl <sub>2</sub>	M1028-100ML	Sigma
NaH <sub>2</sub> PO <sub>4</sub>	S5011-100G	Sigma
4-methylcyclohexanol	153095-250ML	Sigma
3-octanol	218405-50G	Sigma
Trehalose	T9531-100G	Sigma
proteinase K	P2308-10MG	Sigma
D-(+)-Glucose (aka dextrose)	G8270-1KG	Sigma
histamine dihydrochloride, 5g	H7250-5G	Sigma
SeTau-647-NHS	K9-1949	Seta Biomedicals

1 M HCl	15676840	Fisher
MgATP	A9187-500MG	Sigma
GABA	A5835-10G	Sigma
Muscarine (mAChR agonist)	M6532-5MG	Sigma
GeneJET Plasmid Miniprep Kit	K0503	Fisher
Library Efficiency® DH5α™ Competent Cells	18263-012	Fisher
One Shot® MAX Efficiency® DH5α™-T1R Competent Cells	12297-016	Fisher
One Shot®ccdB Survival™ 2 T1R chemically competent cells	10733874	Fisher
CutSmart Buffer	B7204S	New England Biolabs
KpnI-HF	R3142S	New England Biolabs
HindIII-HF	R3104S	New England Biolabs
EcoRV-HF	R3195S	New England Biolabs
EcoRI	R3101T	New England Biolabs
SYBR Safe DNA Gel Stain	S33102	Fisher

Gel Loading Dye Purple (6X)	B7024S	New England Biolabs
Platinum™ Pfx DNA Polymerase	11708013	Fisher
Qiaquick gel extraction kit	101676Z	Qiagen
Invitrogen™ T4 DNA Ligase (5U/uL)	10443242	Fisher
Clonase II LR enzyme mix Gateway(TM) 20	10134992	Fisher
Carbogen gas tank	131-J	BOC
Zero grade compressed air	270028-L	BOC

## 2.1.5 List of filters used for widefield and two-photon microscopy

### Widefield:

#### GFP filter cube

49002 from Chroma

excitation: 470/40

dichroic: long-pass 495

emission: 525/50

#### dsRed filter cube

49004 from Chroma

excitation: 545/25

dichroic: long-pass 565

emission: 605/70

Cherry filter cube

LED-mCherry-A-000 from Semrock / Laser2000

excitation: 578/21

dichroic: long-pass 596

emission: 641/75

Far red filter cube

49311 from Chroma

excitation: 599/13

dichroic: long-pass 612

emission: 632/28

Two-photon:

Zeiss filter holder (91015 ZEISS AXIO 2-5 Cube)

Green filter

525/50 from Semrock / Laser2000

Dichroic 565dcxr CO-O551400 25.6 x 36 x 1 mm (Chroma)

## 2.2 Methods

### 2.2.1 Fly preparation

Flies were cold-anesthetized and mounted in a preparation chamber covered with aluminum foil with a hole in the middle, using wax and dental floss, such that the fly's dorsal and ventral sides were kept on opposite sides of the hole. The dorsal part was then immersed in carbogenated (95% O<sub>2</sub>, 5% CO<sub>2</sub>) external solution (103 mM NaCl, 3 mM KCl, 5 mM trehalose, 10 mM glucose, 26 mM NaHCO<sub>3</sub>, 1 mM NaH<sub>2</sub>PO<sub>4</sub>, 3 mM CaCl<sub>2</sub>, 4 mM MgCl<sub>2</sub>, 5 mM N-Tris (TES), pH 7.3). The cuticle from the back of the fly's head was carefully removed using forceps, followed by removal of fat tissue and trachea. During experiments, the brain was continuously perfused with carbogenated (95% O<sub>2</sub>, 5% CO<sub>2</sub>) external solution using a Watson-Marlow pump (model 120S DM2).

### 2.2.2 Functional imaging

The brains were initially inspected using widefield microscopy (Moveable Objective Microscope, Sutter) and a xenon-arc lamp (model LAMBDA LS, Sutter). Functional imaging was carried out using two-photon laser-scanning microscopy (Ng et al., 2002; Wang et al., 2003). Fluorescence in the brain was excited using the microscope (Moveable Objective Microscope, Sutter), coupled to a Ti-Sapphire laser (Mai Tai eHP DS, 70 fs pulses, Spectra-Physics) set to 910 nm (or other if specified in figure legends), which was attenuated by a Pockels cell controller by a voltage amplifier (model 350-80LA, Conoptics), and connected to a galvo-resonant scanner (model MDR-R, Sutter). Excitation was focussed using a 1.0 NA 20X objective (Olympus). Emitted light was captured and detected by GaAsP photomultiplier tubes (model PS-2LV, Hamamatsu Photonics) whose currents were amplified (TIA-60, Thorlabs) and transferred to the computer used for imaging. Volume imaging was carried out using a piezo objective stage (nPFocus400, nPoint). Volume images were acquired at 5 Hz using ScanImage 5 software. Recordings from brains that sustained injury, as observed by sudden, repetitive MB-wide surges in calcium signal were discarded.

### 2.2.3 Odour delivery

$10^{-3}$  odour dilutions delivery ( $\sim 10$  ppm measured at odour tube exhaust) of 4-methylcyclohexanol (MCH), 3-octanol (OCT), and isoamyl acetate (IAA) was carried out by switching mass-flow controlled carrier and stimulus streams (Sensirion) via software-controlled solenoid valves (The Lee Company). This odour concentration was previously determined to evoke robust responses. Delivery rates were 0.5 or 0.8 l/min at the exit of the odour tube, which was positioned  $\sim 1$  cm from the fly's head. Labview 2015 (National Instruments) software on the image acquisition computer was used to control odour delivery. Odour pulses lasted 5 s. At the end of each recording where odour pulses were given, the tubes were purified by passing pure air through. A tube connected to a pump was positioned behind the fly to deplete the air of odours remaining after the odour pulse.

#### 2.2.4 Picospritzer local drug application

ATP, GABA or muscarine at the concentrations indicated in figure legends, together with a red dye for visualisation of fluid ejection, were applied locally by pressure ejection from patch pipettes (resistance ~10 M $\Omega$ ; capillary inner diameter 0.86 mm, outer diameter 1.5 mm - Harvard Apparatus 30-0057) coupled to a Picospritzer III (Parker) (puff duration 10 ms, pressure 12.5 psi). The patch pipette was mounted on a micromanipulator with a control cube (Patchstar, Scientifica). The Picospritzer trigger was controlled using Labview 2015 software. The patch pipette was carefully brought down to the brain and pushed into the brain to be positioned at the tip of the vertical lobe, close to the junction point in the horizontal lobe, or in the central part of the calyx. Before initiating recording, fluid was manually ejected to ensure that the pipette was not blocked. For experiments where ATP or GABA were applied during odour stimulus, the fluid ejection was set to trigger the same time as the odour pulse, whereas for muscarine application the fluid ejection was set to occur one second before the odour pulse. The brain was continuously perfused with carbogenated external solution during the experiment.

#### 2.2.5 Electric shock

Electric shocks were applied to the fly by bringing a rectangle of stacked copper plates coupled with wires to a DS3 Constant Current Isolated Stimulator (1.2 s, 32 mA, Digitimer Ltd.) into contact with the fly's abdomen. The fly's physical reaction to shock was observed with a Genie Nano-M1280 camera (Stemmer) coupled to the computer used for image acquisition.

#### 2.2.6 Aversive conditioning

Flies were subjected to aversive conditioning by pairing odour stimulus with delivery of electric shocks.

For the negative reinforcement control experiment where MBON $\gamma$ 2 $\alpha$ '1 responses were measured (**Fig. 4.2**), flies were exposed to OCT for 5 s, then MCH for 5 s, with a 10 s interval between the two odour pulses. After approximately 90 s (partially the time it takes for the script to finish after the last odour pulse, and the variable time it takes to select the next script, prepare the imaging

software for the next recording, and visually inspect the setup to confirm that the copper plates are still touching the fly and no water has leaked through) the flies were subjected to the training protocol, which consisted of 12x electric shocks (1.2 s pulse every 5 s) coupled to 60 s of OCT exposure, followed by 60 s MCH exposure, with a 45 s interval between the two odour pulses. This was followed by a post-conditioning test that was identical to the pre-conditioning protocol.

The same protocol was applied for the negative reinforcement experiment where I measured the APL neuron's responses (**Fig. 4.3**), except that the pre- and post-conditioning tests included a 5 s pulse of IAA: OCT for 5 s, then MCH for 5 s, and finally IAA for 5 s, with a 10 s interval between each odour pulse.

## 2.3 Analysis

### 2.3.1 Analysis of imaging data

$\Delta F/F$  calculation in ImageJ was done as follows:

$$F(t) = F_{ROI}(t) - F_{Bkgnd}(t)$$

$$F_0(t) = F_{mean}(t) \text{ over the user-defined pre-stimulus window}$$

$$\Delta F/F = [F(t) - F_0(t)]/F_0(t)$$

Where  $F(t)$ , the fluorescence signal at time  $t$ , is given by the difference between the fluorescence signal in the user-defined ROIs,  $F_{ROI}(t)$  and the fluorescence signal in the user-defined background ROI,  $F_{Bkgnd}(t)$ .

$F_0(t)$  is the baseline fluorescence, given by the mean fluorescence signal in the user-defined ROIs during the user-defined pre-stimulus period,  $F_{mean}(t)$ .

For experiments that show quantification of neuronal responses not involving 3D-skeletonization, the raw  $\Delta F/F$  was obtained in ImageJ by manually drawing ROIs around the MB (further specified below) on a montage of all captured z-slices, and an ROI in an empty region from the deepest slice to get an accurate measure of background fluorescence. All manual drawings of ROIs were based on MB landmarks revealed by expression of DsRed in the entire MB using MB247-DsRed (Riemensperger et al., 2005).

For **Fig. 3.1** ROIs were drawn around the tip of the vertical lobe and the central region of the calyx, where the ATP was applied, judging by a co-ejected red dye ((SeTau-647, SETA BioMedicals) (Podgorski et al., 2012).

For **Fig. 4.1** and **4.3** the raw  $\Delta F/F$  was obtained in ImageJ based on ROIs drawn around (V) the first four imaged planes from the tip of the vertical lobe, (S) the lower part, or stalk, consisting of the remaining vertical lobe imaging planes until the horizontal lobe becomes visible, ( $\gamma$ ) the  $\gamma 1$ - $\gamma 3$  compartments, and the remainder of the horizontal lobe (H). See **Fig. 2.2** for a schematic. Data was analysed in Igor Pro, where neuronal response traces from recordings were smoothed by a moving average over a 1 s window. For **Fig. 4.1** the average  $\Delta F/F$  responses were quantified by taking the average  $\Delta F/F$  over a 2.5 s time window starting from onset of electric shock. This was further averaged across all 3 electric shocks given during the recordings. For **Fig. 4.3** the responses for each odour were calculated by taking the mean  $\Delta F/F$  over a 3.5 s time window starting 0.5 s into the odour pulse. This time window captured the most significant portion of the response across stimulus all regions, taking into account the delay from triggering odour delivery to a neuronal response. The following equation describes how the change in odour responses between pre- and post-conditioning was quantified (CS+ example):

$$\frac{\Delta F/F (CS +_{post})}{\Delta F/F (IAA_{post})} - \frac{\Delta F/F (CS +_{pre})}{\Delta F/F (IAA_{pre})}$$

For recordings where an ROI had an IAA response that was within 1 standard deviation of the noise level (measured as the mean fluorescence signal during the pre-stimulus period), the data point for that ROI was excluded.

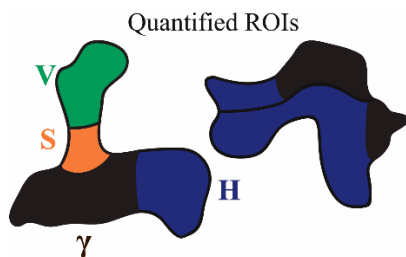


**Fig. 2.2 Schematic of ROIs for quantification of electric shock response**

Schematic showing the ROIs used to quantify the APL neuron's responses to electric shocks and pre- and post-conditioning odour responses. The same schematic is shown in **Fig. 4.1** and **4.3**.

For **Fig. 4.2** ROIs were drawn around all neurites visible by GCaMP6f fluorescence in all the imaged planes. Data was analysed in Igor Pro, where neuronal response traces from recordings were

smoothed by a moving average over a 1 s window. The responses for each odour were calculated by taking the average  $\Delta F/F$  over a 3.5 s time window starting 0.5 s into the odour pulse. The following equation describes how the change in odour responses between pre- and post-conditioning was quantified (CS+ example):

$$\frac{\Delta F/F (CS +_{post})}{\text{Max } \Delta F/F (CS +_{pre})} - \frac{\Delta F/F (CS +_{pre})}{\text{Max } \Delta F/F (CS +_{pre})}$$

For **Fig. 5.1** and **5.2**, the raw  $\Delta F/F$  was obtained in ImageJ based on ROIs drawn around each KC subset in both the vertical and horizontal lobe. Data was analysed in Igor Pro, where neuronal response traces from recordings were smoothed by a moving average over a 1 s window and responses were calculated as the average or maximum  $\Delta F/F$  in the time windows specified in the panels or figure legend.

### 2.3.2 3D-skeletonization

The following is based on MATLAB code mainly conceptualized by Andrew Lin. I mainly contributed to conceptualization, troubleshooting, and bug fixing, and writing of the part required for interpolation and plotting of the time series (further described below).

To visualise the whole brain structure of interest and characterise neuronal responses in 3D throughout this structure, a custom-written MATLAB code was used to generate a 3D-skeleton of the brain structure. This code loads the movie recording and creates an ‘activityMap’ class with a set of parameters relevant to the recording (number of dimensions, dimension lengths, number of slices, pixel calibration, frame rate), which calculates and stores  $\Delta F/F$  data for ScanImage recordings. Another class, ‘activityMapParams’, holds all the parameters required to create an activityMap object.

The movie is displayed as a montage, with z-slices shown in individual windows. The user draws ROIs around the brain structure in all the windows, creating a mask of it. This mask, shown as a montage, is used to manually set points along the structure, creating a connected series of points that correspond to a branch. Here, we drew two branches. The first one from the tip of the vertical lobe to the tip of the calyx, and the second one starting from the junction between the lobes and to the tip of the horizontal lobe. The user then defines a zero point from which a skeleton of the whole structure is generated. Here, the zero point corresponds to the junction between the horizontal and

vertical lobes. From this point, the skeleton is drawn as evenly spaced nodes of user-defined spacing, consisting of the designated branches (**Fig. 2.3**)

For multiple movies from experiments on the same fly (individual recordings of responses to: odour alone, odour+drug, and drug alone, at different puff sites: vertical, horizontal, or calyx), the code loads all the movies together, using the first movie as a template to superimpose the other movies onto, and runs cross-correlation to find offsets that describe how much each movie must be moved to have the highest correlation with the template. From this an average image is constructed, on which the user draws a mask that is used to generate a skeleton that is common for all those movies.

In order to compare neuronal responses in the MB from different experiments (different genotypes with the same or different stimulus) we expanded the code to normalize the dimensions of the MB from any recording to a set of averaged dimensions. The code calculates the average length of the vertical lobe, horizontal lobe, and the peduncle based on all recordings. These average values are used to stretch or squish each individual recording to match the averages, whereby we can match responses of different recordings at any given distance from the zero point of the skeleton (junction).

The code calculates the background signal in a user defined channel and ROI (for each recording I chose a region outside the MB in the deepest z-slice). The loaded movie is smoothed in the in x-y plane using a Gaussian filter and smoothed in time by using a moving average window of 5 frames. The background is subtracted after filtering. The user sets a pre-stimulus period which is used for calculating  $\Delta F/F$ . With a user-defined stimulus time-window, the code calculates  $\Delta F/F$  for each skeleton node, generating a  $\Delta F/F$  vs distance plot, indicating which branch the node belongs to, with each node represented as a set distance away from the zero point. It also generates a time series plot, displaying  $\Delta F/F$  for each node vs time.

For recordings from multiple experiments (different genotypes, different stimulus) that have been analysed together, the code calculates  $\Delta F/F$  separately for the different conditions and generates CSV files where  $\Delta F/F$  is plotted vs distance. In this case the code treats the tip of the calyx as the ‘zero distance point’ and generates separate files for calyx-vertical lobe and calyx-horizontal lobe plots (**Fig. 2.3**). For the spatial analysis of the normalized inhibitory effect shown in **Fig. 3.20-3.22, 3.25, and 3.27**, the calculation was done as follows:



For the spatial analysis shown in **Fig. 3.20-3.22, 3.25, and 3.27**, the normalized inhibitory effect was calculated the same way, but instead of calculating the effect at each time point, it was calculated as the mean  $\Delta F/F$  response in a 2.5 s time window from the onset of odour stimulus, or the onset of ATP stimulation for recordings with ATP alone.

## 2.4 Molecular biology

### 2.4.1 Gel electrophoresis

Gel electrophoresis was carried out using 0.7-1.0% agarose gel containing 1  $\mu\text{g/mL}$  ethidium bromide or 1% Sybr safe (Fisher), and 1x Gel Loading Dye Purple (6X) (New England Biolabs) in 1x TBE buffer at 80 or 100V.

### 2.4.2 Generation of new DNA constructs

#### **Plasmids**

pBPGUw was a gift from Gerald Rubin (HHMI Janelia Research Campus, 19700 Helix Dr, Ashburn, VA 20147, United States) (Addgene plasmid # 17575; <http://n2t.net/addgene:17575>; RRID: Addgene\_17575)

pUAST-ZipLexADBD was a gift from Chi-hon Lee (Institute of Cellular and Organismic Biology, Academia Sinica, 128 Academia Road, Section 2, Nankang, Taipei, 115, Taiwan) (Ting et al, 2011) The following enhancer constructs were gifts from Gerald Rubin: VT049483, VT039550, VT030604, GMR35B12, GMR12F03, GMR44E04, GMR45H04, GMR21D08, GMR16A06, GMR13F02 (Jenett et al., 2012)

### 2.4.3 Strategy

The following work was carried out to generate enhancer-ZipLexADBD lines for split-LexA labelling of KC subsets. The outline below describes the strategy to reach the final step of creating a Zip-LexADBD construct with a Gateway cassette in front, and subsequently use the Gateway LR clonase reaction to swap the cassette for the different enhancer-sequences.

1. Amplify the ZipLexADBD fragment from the pUAST-ZipLexADBD plasmid
2. Replace the Gal4 sequence in PBGUw with ZipLexADBD by restriction digest and subsequent ligation reaction

- Use Gateway LR clonase reaction to insert the various enhancers in front of ZipLexADBD in the PBGUw-ZipLexADBD construct

### Amplification of Zip-LexADBD

The following primers 5'-ATTAGGTACCATGCTGGAGATCCGCGCC-3' (forward) and 'GCTAAAGCTTTTACAGCCAGTCGCCGTT' (reverse) were used to amplify ZipLexADBD from the pUAST-ZipLexADBD vector (Ting et al., 2011) using Platinum™ Pfx DNA Polymerase (Invitrogen, Fisher). The reaction mix consisted of:

1x Pfx amplification buffer	5 µL
10 mM dNTPs	1.5 µL
10 µM forward primer	1.5 µL
10 µM reverse primer	1.5 µL
50 mM MgSO <sub>4</sub>	1 µL
DNA template	1 µL
Platinum Pfx DNA polymerase	0.4 µL
dH <sub>2</sub> O	39 µL

PCR program:

1x 94°C	94°C, 180 s
30x	94°C 15 s
	55°C 30 s
	68°C 60 s
1x	68°C 420 s

Transformation of PBGUw in One Shot®ccdB Survival™ 2 T1R chemically competent cells (Fisher), and pUAST-ZipLexADBD in One Shot® MAX Efficiency® DH5α™-T1R Competent Cells (Fisher) was carried out as follows:

For each transformation, a vial of the cells was thawed on ice. 0.5 µL of DNA of interest and 1 µL of the pUC19 control plasmid were added to a vial each and gently mixed. The vials were incubated on ice for 30 min, then heat-shocked for 30 s at 42 °C, and subsequently put on ice for 2 minutes. 250 µL S.O.C Medium was added to each vial. The vials were shaken horizontally at 37 °C at 225 rpm for 1 h. 10 (PBGUw, pUC19) and 100 µL (PBGUw, pUC19, and pUAST-ZipLexADBD) or

20  $\mu$ L and 200  $\mu$ L (PBGUw-ZipLexADBD ligation reaction product) from each transformation was spread on pre-warmed selective plates. Plated were incubated overnight at 37 °C.

The enhancer constructs were transformed in Library Efficiency® DH5 $\alpha$ ™ Competent Cells (Fisher) similarly to transformation of PBGUw as described above.

Single colonies were transferred to individual 4 mL liquid cultures with 4  $\mu$ L ampicillin (100 mg/mL) and 4  $\mu$ L chloramphenicol (25 mg/mL) (PBGUw, PBGUw-ZipLexADBD ligase reaction product) or 4  $\mu$ L ampicillin (100 mg/mL) (pUAST-ZipLexADBD) and incubated overnight at 37 °C.

### Replacing Gal4 sequence with Zip-LexADBD

PBGUw was subsequently restriction-digested with Kpn1-HF and HindIII-HF using Cutsmart buffer (all from New England Biolabs) by 1 h incubation at 37 °C.

PBGUw digest and ZipLexADBD PCR products were purified from a gel using Qiaquick gel extraction kit (Qiagen). ZipLexADBD was subsequently digested with Kpn1-HF and HindIII-HF using Cutsmart buffer, run on a gel, and purified using Qiaquick gel extraction kit.

The reaction mix consisted of:

5x Ligase reaction buffer	4 $\mu$ L
Vector DNA (PBGUw)	5 $\mu$ L
Insert DNA (ZipLexADBD)	0.5 $\mu$ L (3:1 insert to vector ratio)
T4 DNA ligase	1 $\mu$ L
dH <sub>2</sub> O	9.5 $\mu$ L

The reaction was incubated for 1 h at 24 °C. A similar reaction was prepared for a vector-only control. The reactions were subsequently transformed in One Shot®ccdB Survival™ 2 T1R chemically competent cells as previously described, plated and incubated overnight at 37 °C. 6 individual colonies were transferred to liquid cultures, from which minipreps were carried out using GeneJET plasmid Miniprep kit (Fisher). The isolated plasmids were restriction digested with EcoRV-HF **and** HindIII-HF using Cutsmart buffer. The ligase reaction products were verified by gel electrophoresis. One of these verified plasmids was sent for sequencing with the primers 5'- CCGCTGCCTTCGTTAATA-3' (forward)  
5'-TTTAAAACTTAAGCCAGG-3 (reverse)

Enhancer vectors were isolated using GENEJET plasmid Miniprep kit, and DNA concentrations were determined using a Nanodrop ND-1000 (Fisher).

### **LR clonase reaction**

LR clonase reaction was carried out with the enhancer vectors as donors and PBGUw-ZipLexADBD as the destination vector, using Clonase II LR enzyme mix Gateway(TM) 20 (Fisher). This was done according to manufacturer's protocol, with the exception that:

- (1) All components were scaled down to half the indicated volume.
- (2) Transformation was carried out with Library Efficiency® DH5 $\alpha$ ™ Competent Cells.

The clonase reaction products were restriction digested using EcoRI-HF (New England Biolabs) and EcoRV-HF for verification of products and sent to Bestgene for fly injection.

## **3. Input to the APL neuron remains localised, but its output has a widespread effect**

### **3.1 Overview of the chapter**

This chapter covers a series of experiments I conducted to determine (1) whether activity in the APL neuron can remain localised, (2) to what extent it attenuate as it propagates, (3) where in the MB the APL neuron inhibits KCs, and (4) how widespread its inhibitory effect is on KC activity.

Section **3.2.1** addresses (1), where I investigate whether APL neuron activity evoked by local stimulation in the vertical lobe or the calyx attenuates before it reaches the other region.

In section **3.2.2** I use a novel method to characterise temporal and spatial decay of activity in the APL neuron in the entire MB using imaging using a custom written MATLAB code.

I address (3) and (4) in section **3.2.3** and **3.2.4** by quantifying how local stimulation of the APL neuron in the MB lobes and calyx affects KC activity spatially to determine how widespread the APL neuron's inhibitory effect is.

In section **3.2.5** I investigate whether the spatial extent of the APL neuron's inhibitory effect on KC activity can be reproduced by local GABA application, or if GABA application has a more limited effect. This indirectly addresses how reliable my estimate of activity spread in the APL neuron is.

Finally, section **3.2.6** addresses one of the main challenges with my experimental approach, trying to estimate the extent of drug dispersion from the patch pipette.

## 3.2 Results

### 3.2.1 Activity arising in the lobular and calyceal projections of the APL neuron are spatially segregated

Section 1.2.10 highlighted the anatomical and functional features of the APL neuron that makes it an interesting candidate for studying local computations. One of the main questions to be addressed is whether activity remains localised in the APL neuron. The previous finding suggesting that the APL neuron is non-spiking (Papadopoulou et al., 2011), combined with the extensive arborisations of the APL neuron in the MB strongly point towards the possibility that input to the APL neuron would evoke a local, not global, response.

I initially sought to determine if there was spatial segregation between activity in the APL neuron's projections in the MB lobes and the calyx (henceforth referred to as lobular and calyceal projections, respectively). Determining this would establish if there is spatial segregation of activity in the APL neuron on a broader level. The actual characterisation of activity spread in the entire MB is presented in section **3.3.2**.

Segregated activity between the APL neuron's lobular and calyceal projections has implications for its role in sparse coding of KC odour responses. It is unclear whether the inhibition required for sparse odour coding observed in KC cell soma (Lin et al., 2014a) arises from inhibition of KC axons in the lobes, the calyx or both. As the APL neuron forms reciprocal synapses to KCs throughout the MB (Xu et al., 2020), the feedback inhibition onto KCs could impose sparseness on odour responses in any part of the MB.

The lobes and cell soma are distal to the KC putative AIS (Trunova et al., 2011). Presumably, sparseness would have to be imposed before KCs fire action potentials, as it is difficult to envision how the responses observed in the KC cell soma could be sparse otherwise. This makes it unlikely that the sparseness observed in KC cell soma is due to feedback inhibition in the MB lobes, as KCs would have to spike for activity to reach the MB lobes. If instead the APL neuron imposes sparseness on KC odour responses by feedback inhibition through its reciprocal synapses with KC dendrites, any activity that reaches the cell soma and lobes would be sparsened. This idea is supported by the finding that KC dendrites can release vesicles (Christiansen et al., 2011).

Thus, for the sparseness observed in KC cell soma, it follows that if there is spatial segregation of activity between the APL neuron's lobular and calyceal projections, it would suggest that the APL neuron can impose sparseness on KC odour responses locally in the calyx. Of course, this would not exclude the possibility that feedback inhibition from the APL neuron's lobular projections also contributes to sparse coding of odour responses in the KC axons.

To investigate whether there is spatial segregation of activity in the APL neuron, I initially decided to determine if local input from KCs to the APL neuron would evoke activity that propagates from the calyx to the tip of the vertical lobe, or vice versa, as this is the longest distance between two points along the neurites of the APL neuron. Because KCs generate action potentials (Perez-Orive et al., 2002, Turner et al., 2008), but their lobular projections are distal from their putative AIS (Trunova et al., 2011), I thought that local stimulation of KCs in the calyx and the lobes might have different effects, with only calyceal stimuli likely to generate spikes and concurrent widespread activity in the APL neuron. To do this, I expressed P2X2 in the KCs using the MB247-LexA driver. By driving expression of GCaMP6f (Chen et al., 2013) in the APL neuron, I could image its responses to activation of KCs in different parts of the MB.

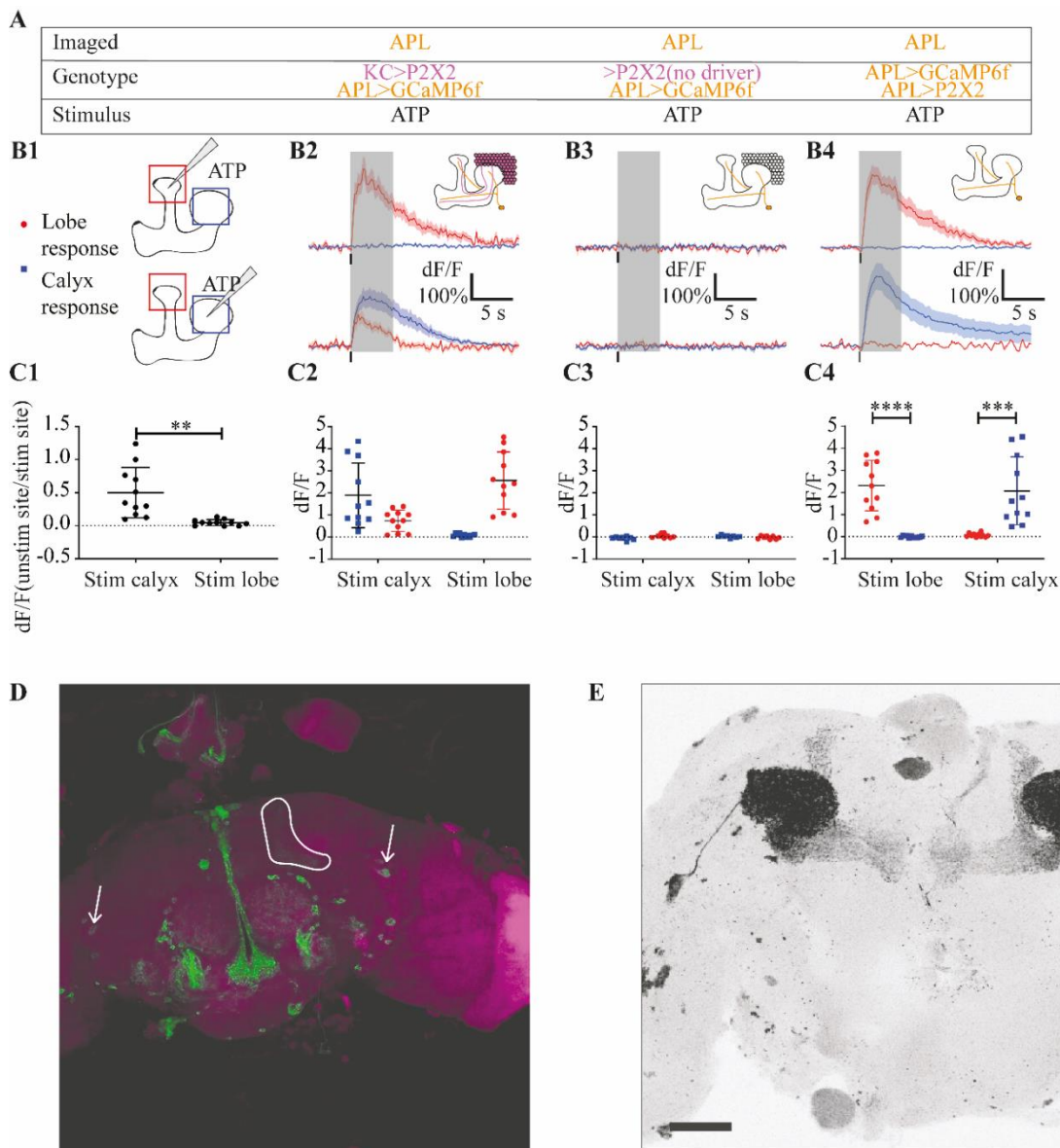


### Figure 3.1 Activity in the APL neuron is spatially restricted

Imaging responses of the APL neuron to ATP stimulation of: **(B2)** KCs in 474-Gal4>UAS-GCaMP6f, MB247-LexA>LexAop-P2X2 flies or **(B3)** 474-Gal4>UAS-GCaMP6f, MB247-LexA (negative control), **(B4)** or ATP stimulation of the APL neuron in tubP-FRT-Gal80-FRT, GH146-FLP, NP2631-Gal4>UAS-GCaMP6f, UAS-P2X2 flies with 1.5mM ATP (100 ms pressure ejection at 12.5 psi) in the tip of the vertical lobe or the calyx, as indicated in the schematics and tables. Response curves show the average across all flies with SEM shading. Scatter plots show individual data points, quantifying responses for 5s (grey shading) from stimulus onset (vertical black bar). **(A)** Table showing which neuron was imaged, what the genotype of the flies were, and what type of stimulus was used. **(B1)** MB schematics showing the ROIs where responses were quantified, and where ATP was applied (arrow). **(B2-B4)** Response curves of the APL neuron to ATP stimulation of KCs or the APL neuron, as indicated in the table. **(C1)** Scatter plot showing the ratio of the average responses of the APL neuron in the unstimulated region to the stimulated region. **(C2-C4)** Scatter plots showing the average response of the APL neuron. **(D)** Expression pattern of 474-Gal4>UAS-GFP (adapted from inSite database, accessed 06.11.2019). The outline shows expression of GFP in the APL neuron's projections, while the arrows indicate the cell bodies. **(E)** Expression pattern of NP2631-GAL4>UAS-mCherry, tubP-

FRT-Gal80-FRT, GH146-FLP, MB247-LexA>LexAop-GCaMP3. Scale bar is 50  $\mu$ m (adapted from Lin et al., 2014). n (B2, C2) = 11 (7 flies), n (B3, C3) = 8 (4 flies), n (B4, C4) = 11 (9 flies). Statistics: (C1) paired t-test, \*\*p<0.01. (C2) Two-way ANOVA, interaction factor \*\*\*\*p<0.0001. (C3) Two-way ANOVA, interaction factor = \*p<0.0394. (C4) Multiple t-tests with Holm Sidak multiple comparisons correction, \*\*\*p<0.001.

Using patch pipettes coupled to a pressure ejection system, I locally puffed ATP on the tip of the vertical lobe. This elicited activity at the tip of the vertical lobe, and possibly elsewhere in the APL neuron's lobular projections, but not the calyx, while ATP application in the calyx evoked activity in both the calyceal and lobular projections of the APL neuron (**Fig. 3.1 B2, C1, C2**). The same stimulation of flies without the KC driver for P2X2 elicited no detectable response in any case (**Fig. 3.1 B3, C3**). These results are consistent with the notion that calyceal stimulation would lead to integration at the KC AIS and generate spikes, eliciting widespread activity in the APL neuron, while lobular stimulation only locally depolarises the KCs and in turn elicits local activity in the APL neurites.

A more direct approach to the question would be to image the APL neuron while directly stimulating the APL neuron. To do this I expressed P2X2 and GCaMP6f in the APL neuron, and puffed ATP on the same regions as described above. Because the 474-Gal4 driver (Gohl et al., 2011) used in **Fig. 3.1 B, C** labels other neurons close to the MB, I decided to use an intersectional approach to achieve more sparse labelling for specific activation of the APL neuron (**Fig. 3.1 D vs E**). GH146-FLP (Weizhe et al., 2009) and NP2631-Gal4 (Tanaka et al., 2008) both label the APL neuron. Combined with tubP-FRT-Gal80-FRT, the Gal80 will be expressed ubiquitously, except in the neurons labelled by the GH146 driver, where expression of FLP will excise the Gal80. Thus, Gal4 will only be expressed in neurons labelled by both GH146 and NP2631, leading to specific labelling of the APL neuron (**Fig. 3.1 E**).

Stimulation of the APL neuron in either region evoked no activity in the unstimulated region (**Fig. 3.1 B4, C4**). These findings establish that activity arising in the APL neuron in either of the regions described above does not propagate to the other region. This suggests that sparsening of KC somata odour responses by feedback inhibition from the APL neuron might be independent of the APL's lobular projections.

This approach provided no information about the extent to which activity propagates in the APL neuron throughout the MB, only that it does not propagate from the tip of the vertical lobe to the

calyx, and vice versa. Characterising activity spread in the APL neuron in the entire MB would show to what extent activity arising from different parts of the APL neuron propagates. Depending on how localised activity in the APL neuron is, it could be differentially affecting KC activity between different MB compartments. The findings to this question could expand our understanding of how the APL neuron operates in the context of memory formation in the MB.

One way to approach this task would be to manually draw ROIs throughout the entire MB for every recording. However, this could introduce great variability in the way ROIs are drawn from one recording to another, and make it difficult to compare responses in different parts of the MB between recordings from flies where the shape or size of the MB varies due to the brains of different flies being slightly compressed or stretched. A semi-automated approach that takes into account differences in MB size and shape across different recordings would generate more robust results in considerably less time.

### 3.2.2 Whole-MB characterisation of activity attenuation in the APL neuron

To achieve this goal, Dr. Andrew Lin and I developed a MATLAB code (henceforth referred to as ‘skeleton code’) to analyse the MB as a 3D ‘skeleton’ of the MB. This 3D skeleton is based on user-drawn ROIs outlining the MB (based on the MB-specific anatomical marker MB247-DsRed (Riemensperger et al., 2005)) in individual z slices from the two-photon microscopy recordings. The software constructs a 3D skeleton from these ROIs, divides the skeleton into evenly spaced segments, and calculates the change in GCaMP signal for each segment during a defined period (see **Methods** section 2.3.2 for detailed description) (**Fig. 3.2**).

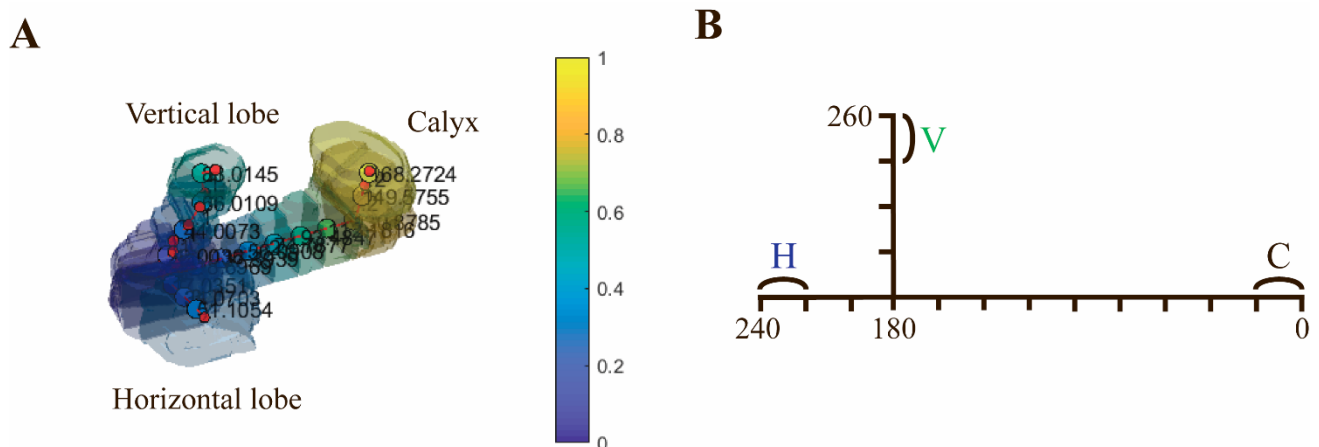


### Figure 3.2 Example 3D skeleton and anatomical reference for quantification of responses

(A) The image is generated from user-drawn ROIs of the MB, using MB247-DsRed as landmark, divided into equally spaced segments, and colour-coded for distance. In this example, the junction between the horizontal and vertical lobe was set as the origin. Higher intensity indicates greater distance (scale on right). (B) Cartoon showing a simplified representation of the 3D skeleton with distance coordinates and letters indicating the two distalmost segments of the calyx (C, black), the vertical lobe (V, green), and the horizontal lobe (H, blue). These three coloured letters are henceforth used to represent the described segments in figures and text below.

There will be differences between the length of the vertical and horizontal lobular branches and the peduncle from one fly to another. To be able to match neuronal responses of flies from different experiments, the skeleton code calculates an average length of the vertical and horizontal lobe, and the peduncle. For every recording, the code stretches or compresses the lengths of these parts to match the average lengths. This allowed us to characterise neuronal activity throughout the MB, but also to make comparisons between different experiments. For these experiments I added a red dye to the patch pipette to be able to approximate how far the ATP puff spreads. I identified Setau-647 (Seta Biomedicals) and Alexa Fluor 647 (Fischer) as potential candidates. The MW of ATP is 507.18 g/mol, while Alexa Fluor 647 is 1155.06 g/mol, and Setau-647 is 1780 g/mol. Thus, based on MW, Alexa Fluor 647 would be a better approximation of ATP spread, but Setau-647 has a higher quantum yield and total brightness across a range of dye-to-protein ratios, and therefore I chose the latter. For some of my recordings, the red dye signal was less than 2%  $\Delta F/F$ , so a dimmer dye would possibly have caused complications due to low signal-to-noise ratio.

A previous student in Andrew Lin's lab, Raquel Suarez-Grimalt, developed a new APL driver, VT43924-Gal4.2, based on the original VT43924-Gal4 (Tirian and Dickson, 2017). This line showed more reliable expression than the original VT line and didn't have stochastic labelling like the intersectional approach described above. It also labels fewer neurons near the MB compared to 474-Gal4, making it applicable for ATP stimulation of the APL neuron. For this reason, I used VT43924-Gal4.2 for the following experiments.

Looking at the time courses, localised artificial activation of the APL neuron elicited a strong local response that attenuated as it propagated throughout the neuron, with higher concentration of ATP leading to prolonged and larger responses (**Fig. 3.3 A1-A3 vs B1-B3 and C1-C3**). For puffing on the horizontal lobe, there were no strong differences between the different segments in terms of how persistent the evoked responses were (**Fig. 3.3 A1-C1**).

Imaged	APL	APL	APL
Genotype	APL>GCaMP6f APL>P2X2	APL>GCaMP6f APL>P2X2	APL>GCaMP6f APL>P2X2
Stimulus	0.3 mM ATP	0.75 mM ATP	1.5 mM ATP

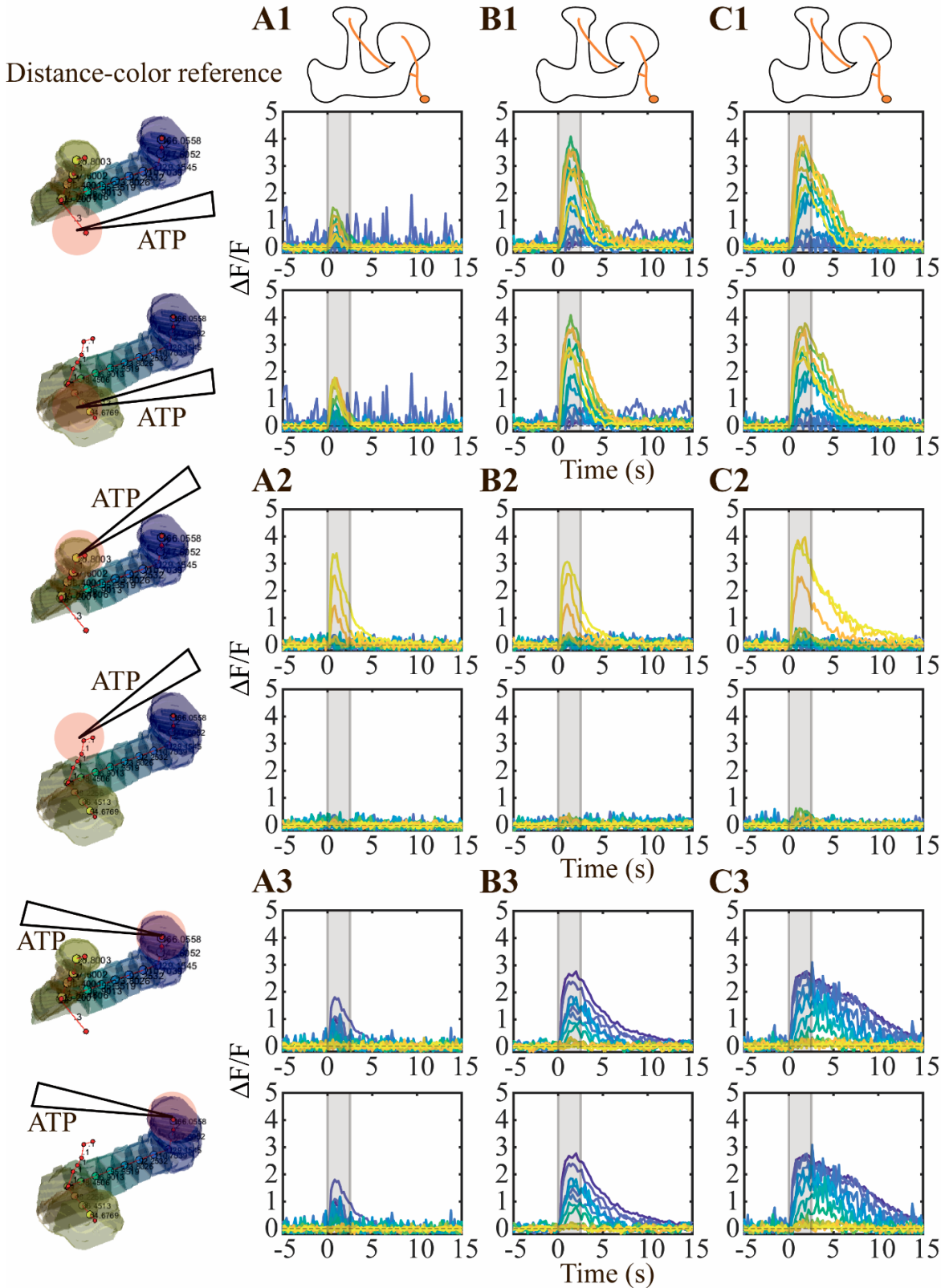


### Figure 3.3 Time courses of the APL neuron's responses to local artificial activation

Imaging responses of the APL neuron to ATP stimulation (10 ms pressure ejection at 12.5 psi). (A-C) top: Table showing which neurons were imaged, fly genotype, and stimulus type, with MB schematics below showing which neuron expresses what transgene(s). Left: Example 3D-skeletons divided into the vertical (top) and horizontal (bottom) lobular branches, with distance-coloured segments, and an arrow showing where the ATP was puffed. Right: The curves show the  $\Delta F/F$  vs time averaged across all recordings with the same conditions (ATP concentration and puff site) in the branch indicated by the 3D-skeleton on the left across time. Each curve shows the response of its colour-matched segment. (A1-A3) 0.3 mM, (B1-B3) 0.75 mM, and (C1-C3) 1.5 mM ATP stimulation. Stimulation occurred at 0 s. Grey shading indicates the time window used for quantification of the matching plots in **Fig. 3.4**. Fly genotype: VT43924-Gal4.2>UAS-GCaMP6f, UAS-P2X2, MB247-DsRed. n (A1) = 8 (5 flies), n (A2) = 7 (4 flies), n (A3) = 4 (4 flies), n (B1, B2) = 10 (6 flies), n (B3) = 6 (4 flies), n (C1, C2) = 9 (6 flies), n (C3) = 5 (4 flies).

In contrast, activity evoked by puffing ATP on the vertical lobe and calyx were most persistent in the proximal segments (**Fig. 3.3 A2-C2** and **A3-C3**).

To get a clear picture of the extent of activity spread, I carried out spatial analysis of the 3D skeleton by quantifying the responses for each segment in a time window that I deemed would capture the greatest part of the effect across different concentrations and puff regions (0-2.5 s from stimulus onset), highlighted by the grey shading in the figures. Furthermore, I chose to make statistical comparisons of the tip of the two lobular branches and the calyx (referred to as V, H, and C), depicted in the cartoon in **Fig. 3.2**, comparing the responses at the stimulated site to the unstimulated ones (**Fig. 3.4**).

For stimulation of the horizontal lobe, I found that 0.3 mM ATP stimulation elicited a statistically significantly lower response at the tip of the vertical lobe and the calyx, whereas at higher concentrations the difference was only significant compared to the calyx (**Fig. 3.4 A1-C1**).

Calyceal stimulation elicited a statistically significantly lower response at the tip of the lobular branches (V and H, as shown in **Fig. 3.2**) only with 0.75 mM ATP. Although this was not the case for 0.3 and 1.5 mM, the trend was clear, with very little variation in the data, and more repeats would likely confirm this (**Fig. 3.4 A3-C3**).

In comparison, stimulation of the vertical lobe showed pronounced attenuation, eliciting a small response in the junction only at the highest concentration, and no detectable response in the calyx or the tip of the horizontal lobe (**Fig. 3.3** and **3.4, A2-C2**).

Imaged	APL	APL	APL
Genotype	APL>GCaMP6f APL>P2X2	APL>GCaMP6f APL>P2X2	APL>GCaMP6f APL>P2X2
Stimulus	0.3 mM ATP	0.75 mM ATP	1.5 mM ATP

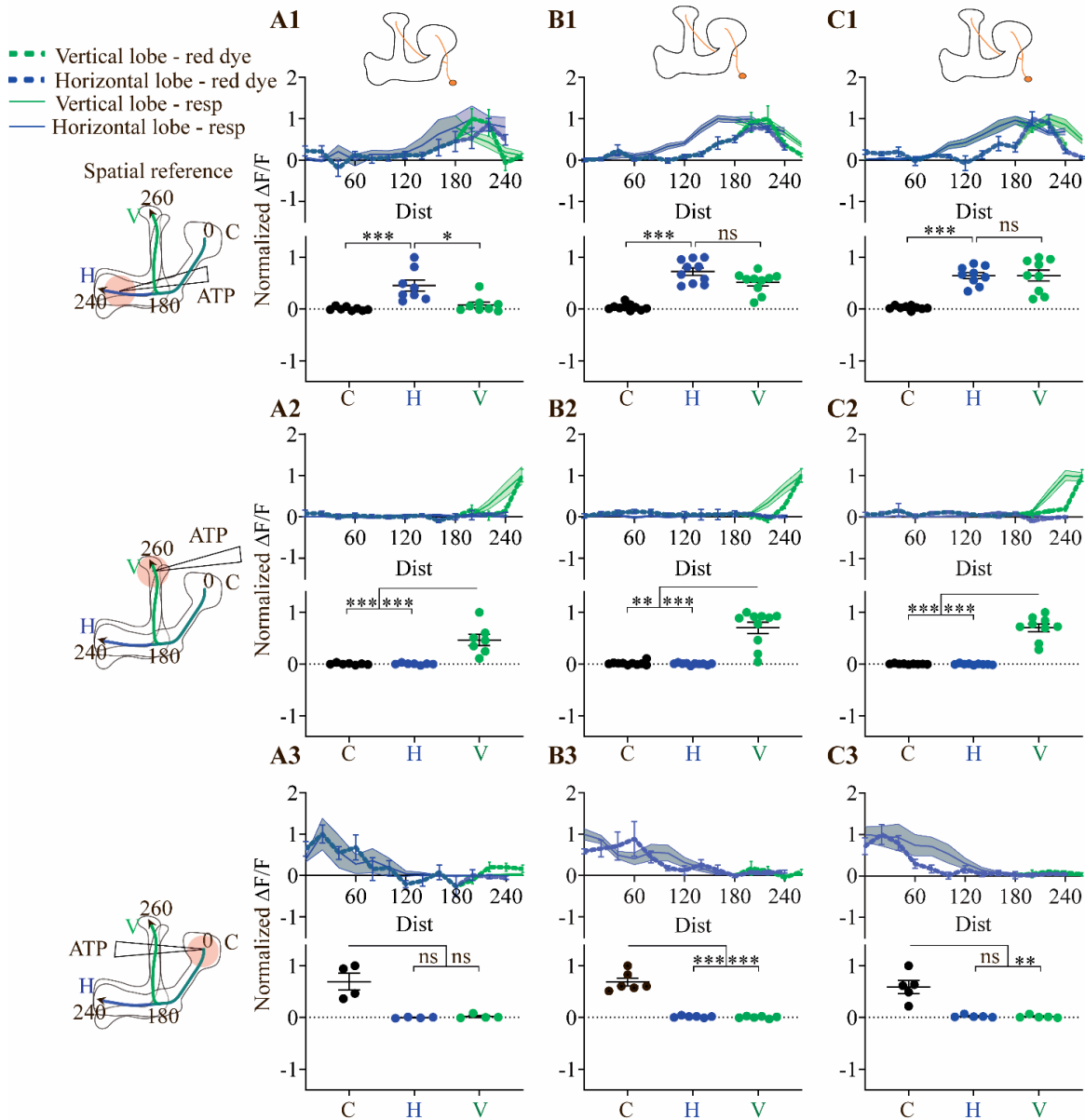


**Fig. 3.4 Spatial quantification of the APL neuron's responses to local artificial activation**

(A-C) top: Table showing which neurons were imaged, fly genotype, and stimulus type, with MB schematics below showing which neuron expresses what transgene(s). Left: MB schematics showing the 3D-skeleton distance measurements, with the calyx represented by 0 (origin), and the vertical and horizontal branches represented in green and blue colours, respectively. Top panels: Response curves showing mean  $\Delta F/F$  responses of the imaged neuron to the indicated stimuli, vs distance from the calyx to the tip of the two lobular branches, in the grey-shaded periods shown in Fig. 3.3 (2.5s from stimulus onset). The colour of the curves matches the vertical (green) and horizontal (blue) lobular branches depicted in the schematics shown on the left. Data shown is the average across all flies for that condition

$\pm$ SEM shading. Bottom panels: Scatter plots showing the average response of the two most distal segments of the calyx (C), vertical (V), and horizontal lobe (H), quantified from the same period as the top panels. Each dot represents an individual recording. Data shown is mean. Error bars show mean  $\pm$ SEM. Fly genotype: VT43924-Gal4.2>UAS-GCaMP6f, UAS-P2X2, MB247-DsRed. n (A1) = 8 (5 flies), n (A2) = 7 (4 flies), n (A3) = 4 (4 flies), n (B1, B2) = 10 (6 flies), n (B3) = 6 (4 flies), n (C1, C2) = 9 (6 flies), n (C3) = 5 (4 flies).

Calyceal stimulation elicited the longest lasting activity (**Fig. 3.3 A3-C3**), possibly due to the ATP taking longer to wash away in the calyx, nevertheless the activity did not spread farther than the peduncle (**Fig. 3.4 A3-C3**). Possible explanations for regional differences in activity propagation are discussed in section 3.3.1.

How does this artificial activation of the APL neuron compare to more naturalistic stimulus in terms of stimulus strength? The extent of activity spread in the APL neuron to odour stimulus could be higher if odour stimulus evokes a stronger response than what I observe with artificial activation, meaning that my experiment would underestimate activity spread in the APL neuron in a more physiologically relevant context.

Imaged	APL
Genotype	APL>GCaMP6f
Stimulus	IAA

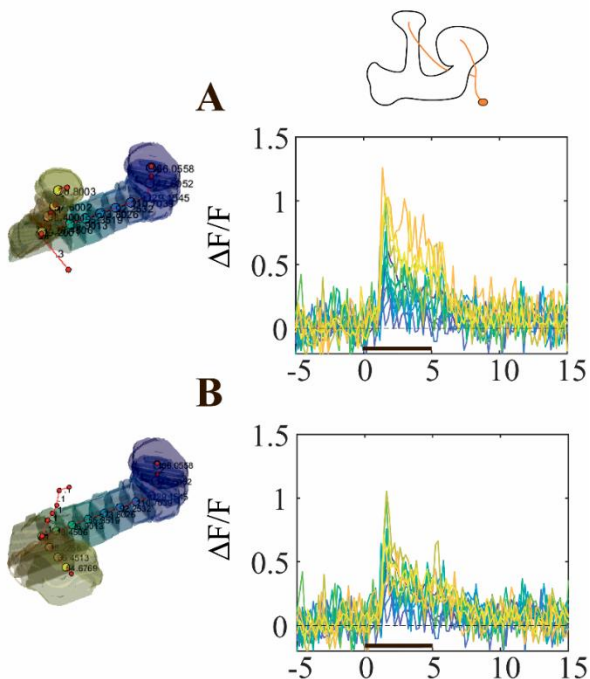


**Figure 3.5**

### Imaging responses of the APL neuron to odour stimulus

(A-B) Left: Example 3D-skeletons divided into the vertical (A) and horizontal (B) lobular branches, with distance-coloured segments. Right: The curves show the average of all recordings in the branch indicated by the 3D-skeleton on the left across time. Each curve shows the response of its colour-matched segment. The thick black horizontal bar indicates the onset and duration of IAA stimulus. Fly genotype: VT43924-Gal4.2>UAS-GCaMP6f. n = 6 (5 flies).

However, if artificial activation elicits a stronger response than odour stimulus, it would suggest that activity spread in the APL neuron is more restricted than my data indicate. To determine this, I recorded activity in the APL neuron while providing the flies with odour stimulus (**Fig. 3.5**).

Compared to odour responses, the ATP stimulation elicited a stronger local response in the APL neuron at either of the stimulus sites (**Fig. 3.3 vs 3.5**). 0.3 mM ATP stimulation was most similar in amplitude to odour responses, except for stimulation of the vertical lobe, where the local response was more than twice as high with ATP stimulation. Thus, it is unlikely that local KC input to the APL neuron during odour stimulus evokes more widespread activity in the APL neuron than what I observed with ATP stimulation.

In summary, activity propagation was generally observed to be more widespread with higher ATP concentration, but it was evident that the activity was attenuating from the stimulation site and outwards. These findings established that activity originating from different regions of the lobes or the calyx in the APL neuron is spatially restricted, in agreement with a previous study suggesting that the APL neuron is non-spiking (Papadopoulou et al., 2011). Spatially segregation of inputs suggests that the APL neuron could locally compute information.

### 3.2.3 Local activation of the APL neuron has a largely local inhibitory effect on KC baseline activity

My next aim was to investigate how widely the inhibition from the APL neuron affects KCs. If the inhibitory effect attenuates as it propagates from the stimulus site, it would indicate that the APL neuron can function locally. This is an intriguing possibility in the context of the anatomically segregated MB compartments formed by MBON and DAN neuronal processes (Aso et al., 2014a). If inhibition from the APL neuron locally affects KC responses, it could match the MBON compartment-specific plasticity that occurs during olfactory learning (Hige et al., 2015, Oswald et al., 2015, Perisse et al., 2016). In this context it is most interesting to characterise the inhibitory effect of the APL neuron in the lobes, as this is where the MBON compartments are situated. However, as an extension of determining how localised activity spread in the APL neuron is, and to get a comprehensive picture of the effect of feedback inhibition originating from different parts of the APL neuron, I decided to also stimulate the APL neuron in the calyx.

Throughout the remainder of the chapter, there will be tables providing an overview of the numerous figures making various comparisons between different experiments or groups within experiments to help orient the reader. **In some figures there will be data from puffing GABA on the MB. They are shown together with the ATP puffing data for the sake of comparison in section 3.2.5, and not duplicated to avoid redundancy and excessive use of space.**

Fig#	Type	Neurons imaged	APL>P2X2?	Odour?	Stim	ATP conc
3.6	Traces	KC	Y	N	ATP, GABA	various
3.7	Quantification (3.6)	KC	Y	N	ATP, GABA	various
3.8	Quantification (3.11-12)	APL v KC	Y v N	N	ATP	0.3 mM
3.9	Quantification (3.13-14)	APL v KC	Y v N	N	ATP	0.75 mM
3.10	Quantification (3.15-16)	APL v KC	Y v N	N	ATP	1.5 mM

**Table 3.1 Overview of figures below**

The table shows an overview of the figures described in the text below. “Fig#” indicates the number of the figure. “type” indicates whether the figure shows traces or quantification of traces. “Neurons imaged” shows whether KCs, the APL neuron, or both, were imaged. “APL>P2X2?” indicates whether P2X2 was expressed or not “Odour?” indicates whether the flies were given an odour stimulus or not. “Stim” indicates the type of stimuli given to the flies. “ATP conc” indicates which concentration(s) of ATP were used.

I initially stimulated the APL neuron while imaging KCs in absence of any odour stimulus to determine if this would affect the neurons’ baseline activity, as it has previously been reported that there is subthreshold activity and spontaneous spikes in KCs (Gu and O’Dowd, 2006, Turner et al., 2008). To do this I expressed P2X2 in the APL neuron, and GCaMP6f in the KCs. Additionally, I looked at the time courses of the recordings to observe if there were temporal differences between the responses of individual segments.

ATP stimulation of the APL neuron in either of the three puff regions in absence of any odour stimulus revealed that there is a level of baseline activity in KCs which decreases upon stimulating

the APL neuron (**Fig. 3.6**). This was observed at all ATP concentration levels. This decrease in baseline activity could originate from spikes, (Turner et al., 2008), subthreshold spontaneous activity (Gu and O'Dowd, 2006), or a combination of both.

Higher concentrations elicited a stronger and longer lasting decrease in baseline activity (**Fig. 3.6 A1-A3 vs B1-B3 vs C1-C3**). Stimulation of the horizontal lobe seemed to have a stronger effect than stimulation of the vertical lobe (**Fig. 3.6 A1-C1 vs A2-C2**) and was more widespread (**Fig. 3.6 A1-C1 and A2-C2 horizontal branch vs vertical branch**).

Surprisingly, puffing ATP on the calyx elicited a local increase in calcium influx, while having the opposite effect in the lobes of KCs. This is likely due to leaky expression (uncontrolled expression of the gene of interest, discussed further below). The effect of puffing on the calyx lasted longer than that for the other puff sites (**Fig. 3.6 A1-C1 vs A2-C2 vs A3-C3**). There was no striking difference between the time courses for different segments of the 3D skeleton for any given puff site.

To get a clear picture of the spatial extent of the APL neuron's inhibitory effect on KC baseline activity and make direct comparisons between the V, H, and C segments of the 3D skeleton (**Fig. 3.2**), I carried out spatial analysis as I did for activity spread in the APL neuron. **Fig. 3.7** compares spatial analysis across the different ATP concentrations to determine differences due to stimulus strength. For each puff site, the responses are normalized to the largest absolute value within that group (**A1-D1, A2-D2, and A3-D3, in Fig. 3.7**), for comparisons across concentrations (and later comparison to GABA application). The subsequent three figures show side-by-side spatial analysis comparisons of activity spread in the APL neuron elicited by ATP stimulation (**Fig. 3.8-3.10 A1-A3**), the effect of APL activation on KC baseline activity (**Fig. 3.8-3.10 B1-B3**), and the negative control without a P2X2 driver (**Fig. 3.8-3.10 C1-C3**). These figures emphasise how activity spread in the APL neuron relates to the inhibitory effect of locally stimulating the APL neuron on KC baseline activity. For each puff site, the response plots for the experimental and negative control flies were normalized to the largest absolute value in the experimental fly plots (**C1 to B1, C2 to B2, C3 to B3, in Fig. 3.8-3.10**) to make comparisons between the experimental and negative control flies.

Imaged	KC	KC	KC	KC
Genotype	KC>GCaMP6f APL>P2X2	KC>GCaMP6f APL>P2X2	KC>GCaMP6f APL>P2X2	KC>GCaMP6f
Stimulus	0.3 mM ATP	0.75 mM ATP	1.5 mM ATP	7.5 mM GABA

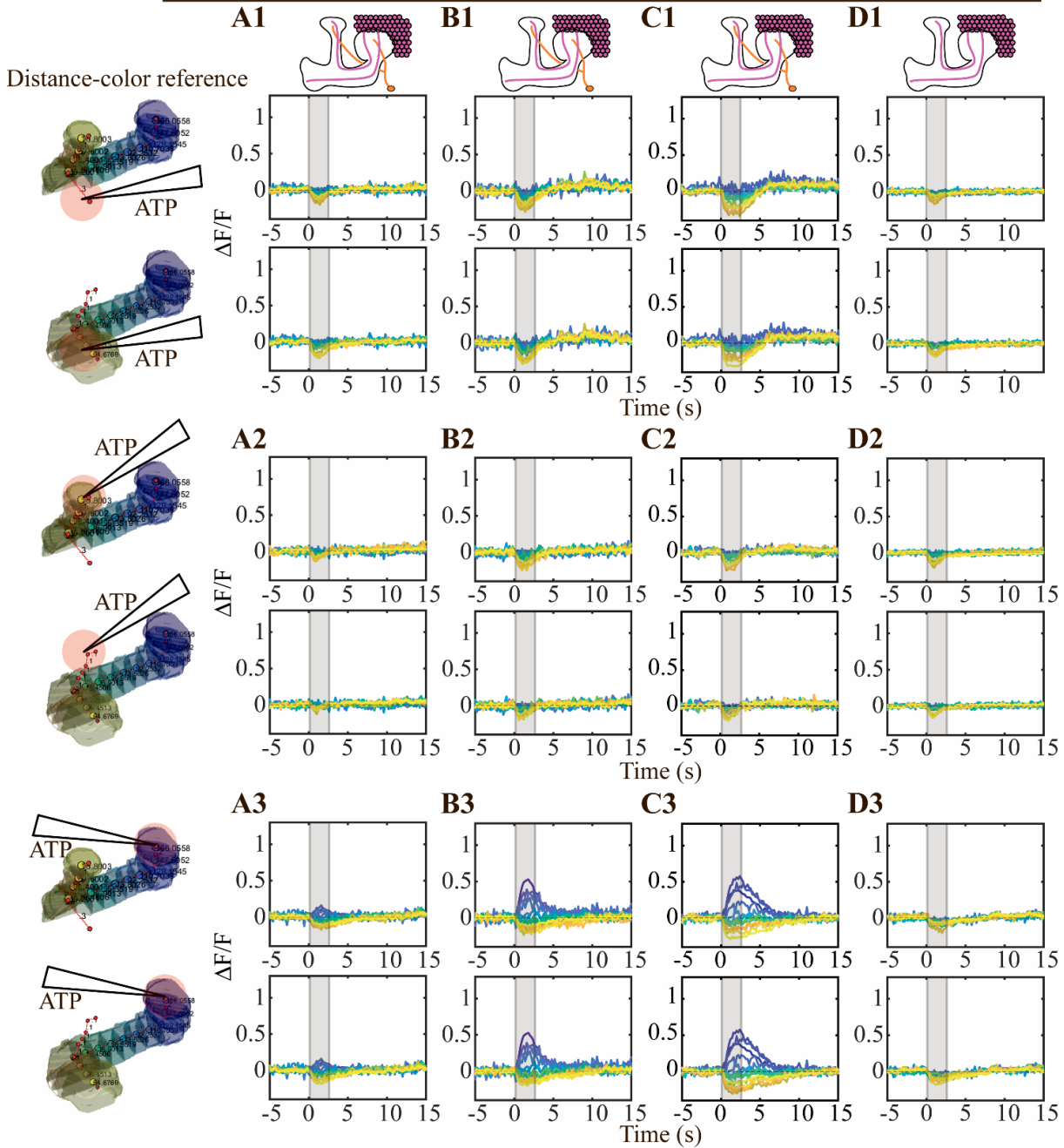


**Figure 3.6 Time courses showing inhibition of KC activity caused by activation of the APL neuron or GABA application**

Fly genotypes: (A-C) VT43924-Gal4.2>UAS-P2X2, MB247-LexA>LexAop-GCaMP6f. (D) OK107-Gal4>UAS-GCaMP6. n (A1-A3) = 10 (9 flies), n (B1-B2) = 10 (9 flies), n (B3) = 9 (8 flies), n (C1-C3) = 9 (7 flies), n (D1, D2) = 13 (8 flies), n (D3) = 11 (6 flies). Grey shading indicates time window used for quantification in **Fig. 3.6**. See legend for **Fig. 3.3** for further details.

The time courses for these figures are described further below (**Fig. 3.11-3.16**). **For clarity, it should be noted that the normalizations described above for the spatial analysis were not carried out for time courses, only spatial analysis.**

The inhibitory effect of stimulating the horizontal lobe was most prominent locally, the effect decreasing towards C and V, with higher concentrations evoking a more widespread effect. For 1.5 mM ATP there was not statistically significant difference between H and V in terms of the decrease in baseline activity (**Fig. 3.7 A1-C1**). Stimulation of the APL neuron in the horizontal lobe had a more far-reaching effect on KC baseline activity than the extent of activity spread observed in the APL neuron, which attenuated as it propagated through the peduncle and the vertical lobe (Compare panel **A1** and **B1** in **Fig. 3.8-3.10**).

Puffing ATP on the vertical lobe had a strong local effect on KC baseline activity that attenuated with distance. Higher concentrations had a stronger and more far-reaching effect (**Fig. 3.7 A2-C2**). The decrease in baseline activity was only significantly different between V and H for 0.3 mM ATP. This effect was considerably more widespread than what I observed for activity spread in the APL neuron (Compare **A2** to **B2** in **Fig. 3.8-3.10**). Whereas activity in the APL neuron evoked by puffing on the vertical lobe evoked a strong local response that attenuated before even reaching the horizontal lobe (panel **A2** in **Fig. 3.8-3.10**), the inhibitory effect on KC baseline activity was much broader. It affected baseline activity in parts of the peduncle and horizontal lobe, albeit to gradually weaker extent as it propagated away from the puff site (panel **B2** in **Fig. 3.8-3.10**).

Spatial analysis confirmed the observation that calyceal stimulation of the APL neuron evoked an increase in GCaMP6f signal locally in the calyx, but otherwise decreased baseline activity elsewhere in KC projections (**Fig. 3.7 A3-C3**). Puffing ATP on the calyx in flies with no P2X2 driver evoked an increase in GCaMP6f throughout the KC projections, while puffing ATP on the lobes had no clear effect (**Fig. 3.8-3.10 C1-C3**). This was likely due to leaky expression of P2X2 in the PNs or KCs. In the experimental flies, puffing ATP on the calyx activated the APL neuron, which locally releases GABA onto the KCs in the calyx. It is likely that this leaky expression causes a local increase in calcium influx in the calyx, but the simultaneous inhibition from the APL neuron likely blocked spikes from occurring, which would explain why there was a concurrent decrease in baseline activity in the lobes (**Fig. 3.7 A3-C3**).

Imaged	KC	KC	KC	KC
Genotype	KC>GCaMP6f APL>P2X2	KC>GCaMP6f APL>P2X2	KC>GCaMP6f APL>P2X2	KC>GCaMP6f
Stimulus	0.3 mM ATP	0.75 mM ATP	1.5 mM ATP	7.5 mM GABA

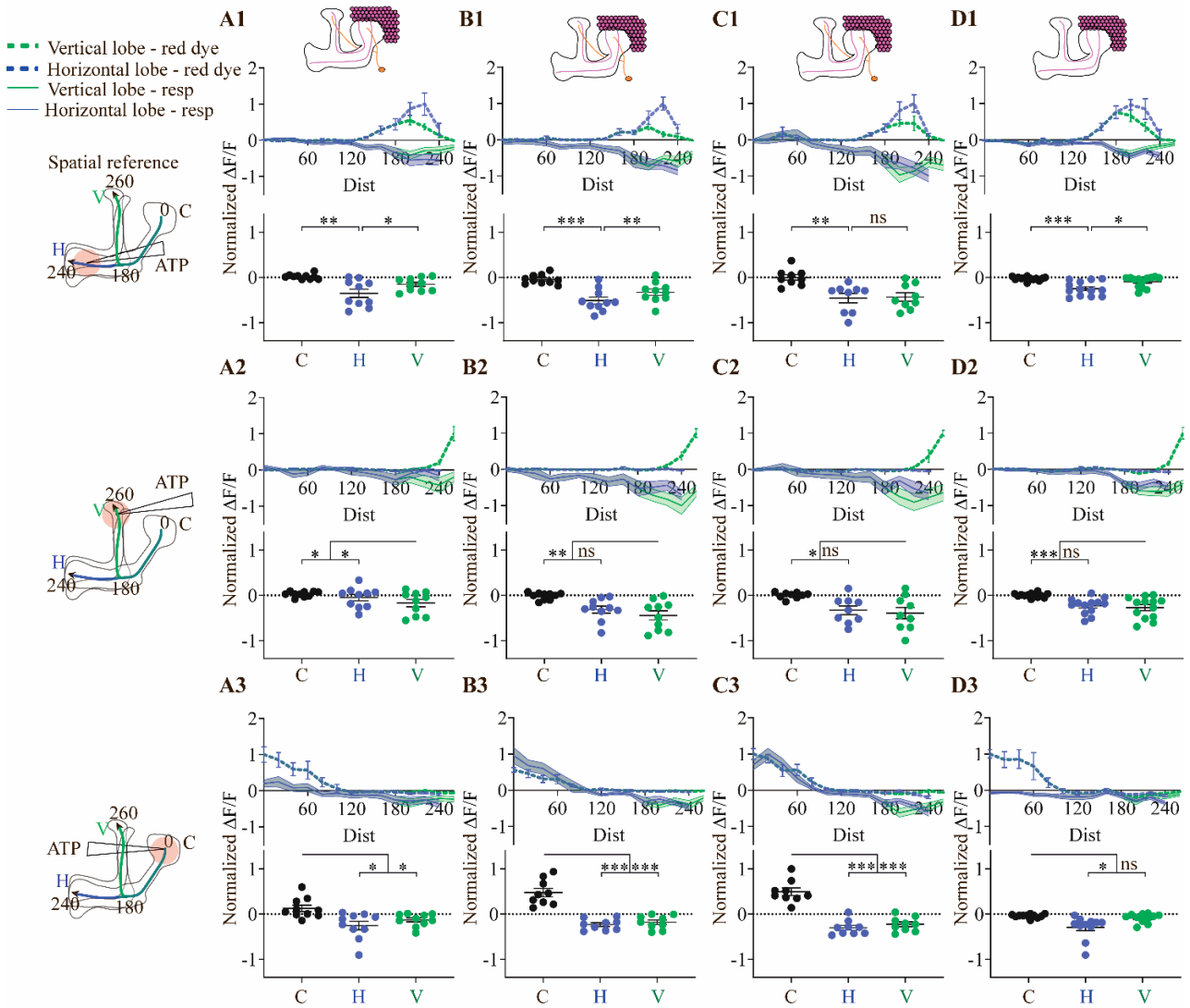


**Figure 3.7 Spatial quantification showing inhibition of KC activity caused by GABA application or activation of the APL neuron with different ATP concentrations**

Fly genotypes: (A-C) VT43924-Gal4.2>UAS-P2X2, MB247-LexA>LexAop-GCaMP6f. (D) OK107-Gal4>UAS-GCaMP6f. n (A1-A3) = 10 (9 flies), n (B1-B2) = 10 (9 flies), n (B3) = 9 (8 flies), n (C1-C3) = 9 (7 flies), n (D1, D2) = 13 (8 flies), n (D3) = 11 (6 flies). See legend for Fig. 3.4 for further details.

Imaged	APL	KC	KC
Genotype	APL>GCaMP6f APL>P2X2	KC>GCaMP6f APL>P2X2	KC>GCaMP6f P2X2 (No driver)
Stimulus	0.3 mM ATP	0.3 mM ATP	0.3 mM ATP

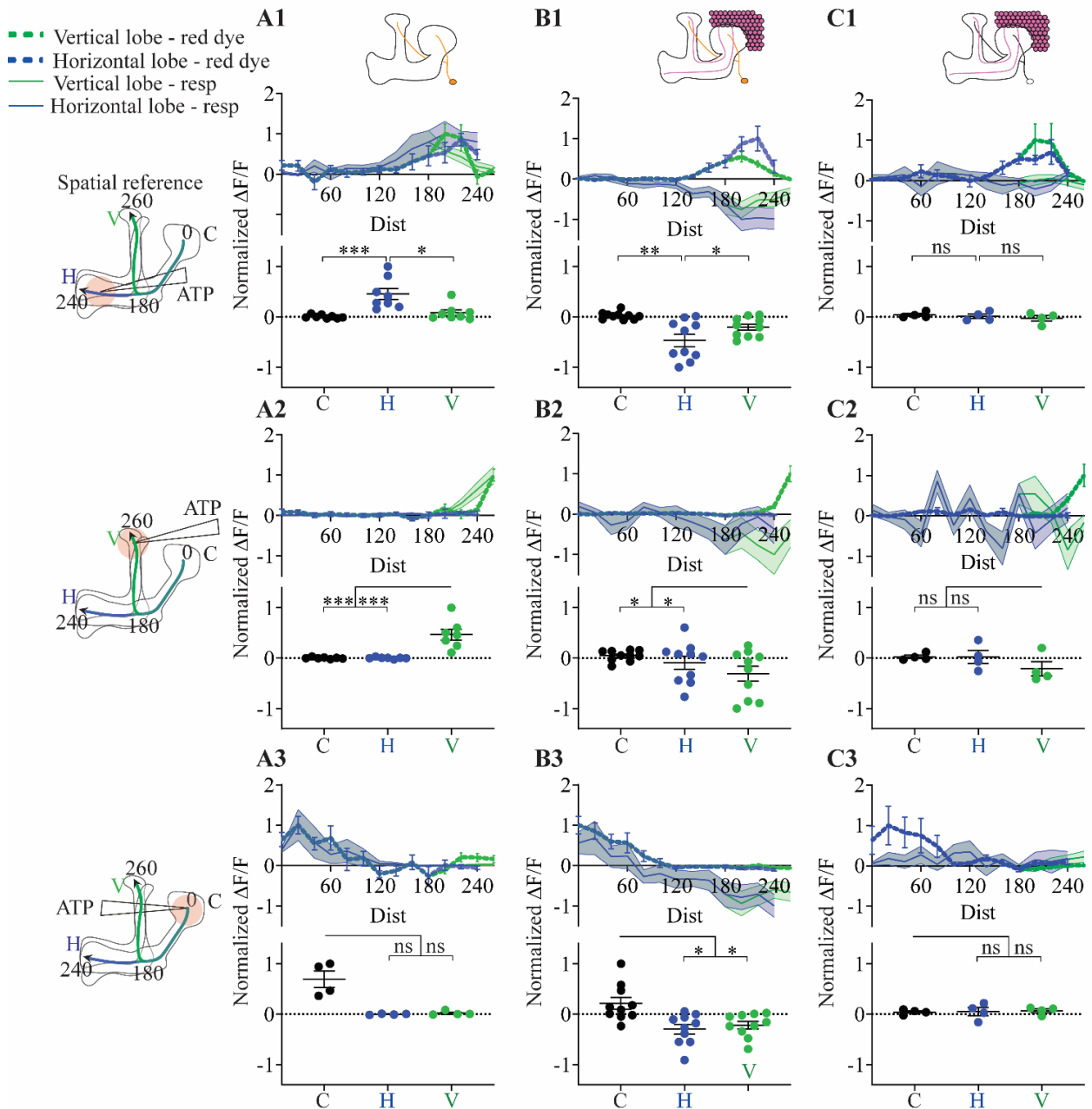


**Figure 3.8 Spatial comparison of activity spread in the APL neuron to the inhibition of KC activity caused by APL neuron activation or negative control (0.3 mM ATP)**

Fly genotypes: (A1-A3) VT43924-Gal4.2>UAS-GCaMP6f, UAS-P2X2, MB247-DsRed. (B1-B3) VT43924-Gal4.2>UAS-P2X2, MB247-LexA>LexAop-GCaMP6f. (C1-C3) UAS-P2X2, MB247-LexA>LexAop-GCaMP6f. n (A1) = 8 (5 flies), n (A2) = 7 (4 flies), n (A3) = 4 (4 flies), n (B1-B3) = 10 (9 flies), n (C1-C3) = 4 (2 flies). See legend for Fig. 3.4 for further details.

Imaged	APL	KC	KC
Genotype	APL>GCaMP6f APL>P2X2	KC>GCaMP6f APL>P2X2	KC>GCaMP6f P2X2 (No driver)
Stimulus	0.75 mM ATP	0.75 mM ATP	0.75 mM ATP

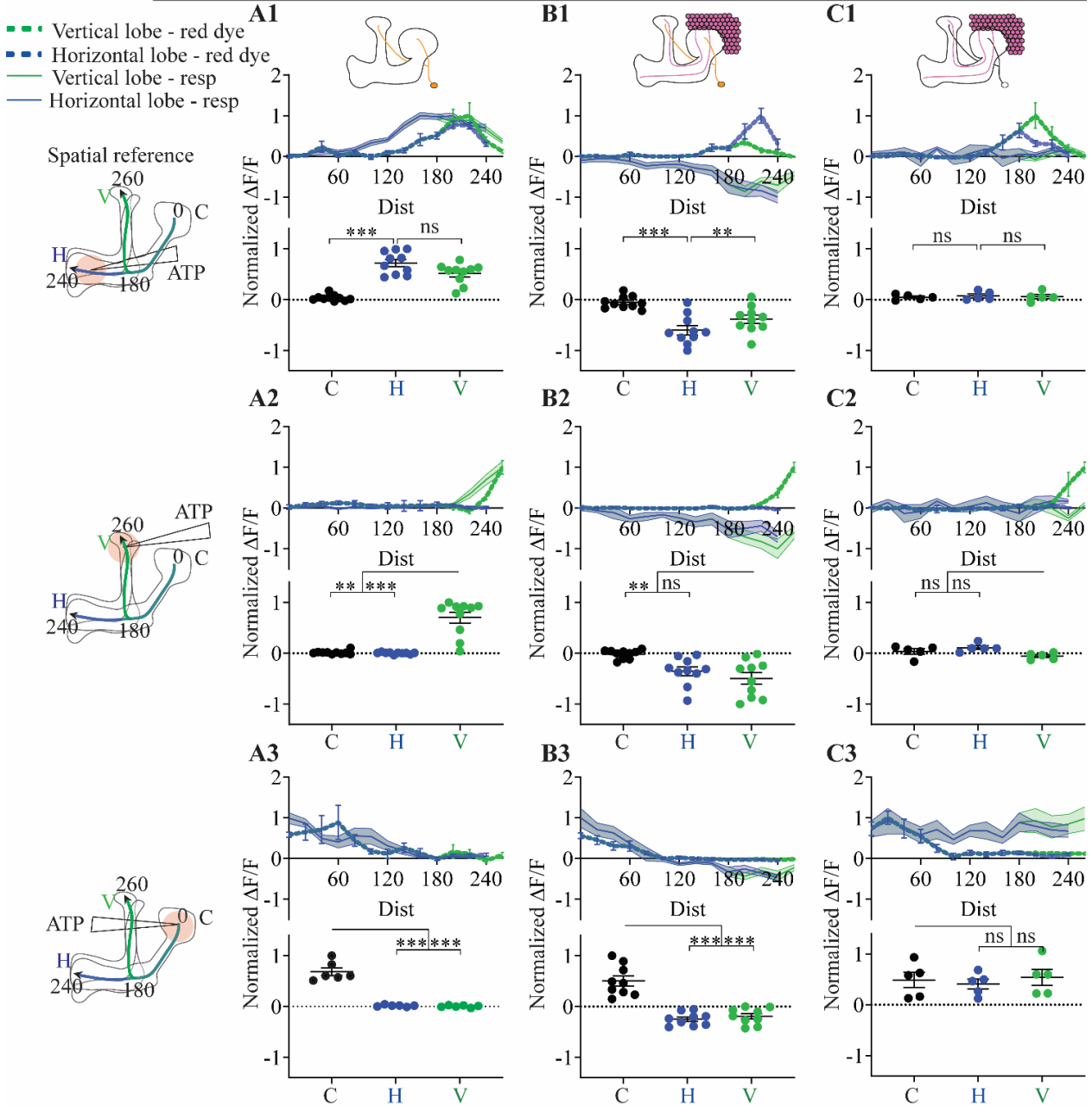


**Figure 3.9 Spatial comparison of activity spread in the APL neuron, to the inhibition of KC activity caused by APL neuron activation or negative control (0.75 mM ATP).**

Fly genotypes: **(A1-A3)** VT43924-Gal4.2>UAS-GCaMP6f, UAS-P2X2, MB247-DsRed. **(B1-B3)** VT43924-Gal4.2>UAS-P2X2, MB247-LexA>LexAop-GCaMP6f. **(C1-C3)** UAS-P2X2, MB247-LexA>LexAop-GCaMP6f. n **(A1, A2)** = 10 (6 flies), n **(A3)** = 6 (4 flies), n **(B1, B2)** = 10 (9 flies), n **(B3)** = 9 (8 flies), n **(C1-C3)** = 5 (3 flies). See legend for **Fig. 3.4** for further details.

Imaged	APL	KC	KC
Genotype	APL>GCaMP6f APL>P2X2	KC>GCaMP6f APL>P2X2	KC>GCaMP6f P2X2 (No driver)
Stimulus	1.5 mM ATP	1.5 mM ATP	1.5 mM ATP

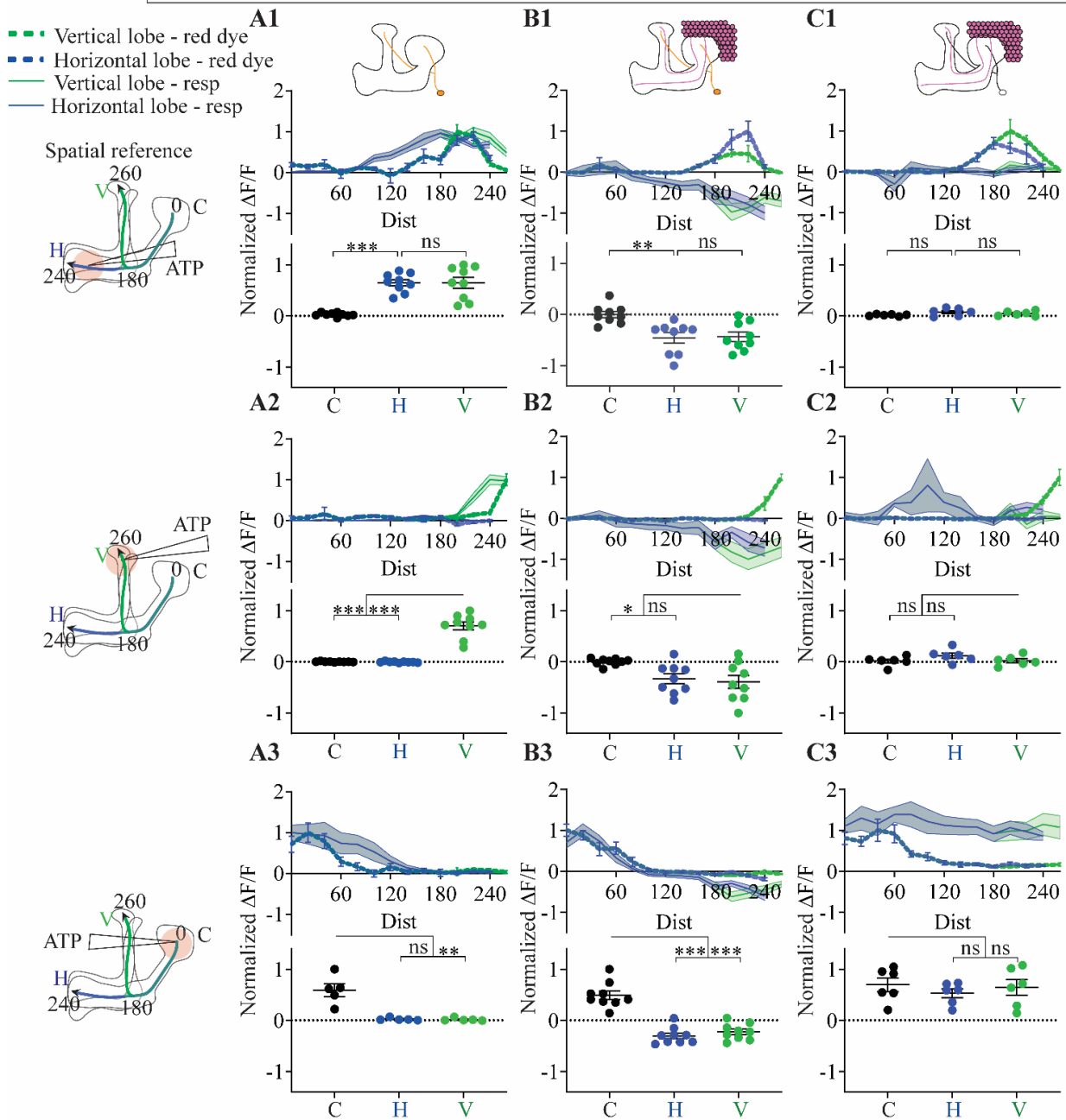


**Figure 3.10 Spatial comparison of activity spread in the APL neuron, to the inhibition of KC activity caused by APL neuron activation or negative control (1.5 mM ATP)**

Fly genotypes: (A1-A3) VT43924-Gal4.2>UAS-GCaMP6f, UAS-P2X2, MB247-DsRed. (B1-B3) VT43924-Gal4.2>UAS-P2X2, MB247-LexA>LexAop-GCaMP6f. (C1-C3) UAS-P2X2, MB247-LexA>LexAop-GCaMP6f See legend for Fig. 3.4. n (A1, A2) = 9 (6 flies), n (A3) = 5 (4 flies), n (A3) = 9 (7 flies), n (C1-C3) = 6 (4 flies), n (D1-D3) = 11 (6 flies).

In summary, the effect of local activation of the APL neuron with ATP locally decreased baseline activity in KCs, attenuating as it propagated from the stimulus site. In the lobes, the effect was strongest and more sustained for puffing ATP on the horizontal lobe compared to the vertical lobe. This difference between the puff sites in suppression of KC baseline activity could be due to the same reasons that contribute to differential activity spread in the APL neuron when puffing ATP on different sites, i.e. differences in ATP dispersion or ion channel expression. This observation is further discussed in section 3.3.2. The results for calyceal stimulation are difficult to interpret due to the leaky expression causing an increase in KC baseline activity in the calyx, but the concurrent decrease in the lobes suggests that inhibition from the APL neuron onto KCs in the calyx does affect baseline activity throughout the MB.

### 3.2.4 Local stimulation of the APL neuron inhibits KC odour responses beyond the spatial extent to which it is activated

The next step was to determine how local activation of the APL neuron would affect KC odour responses. Before I was looking at KC baseline activity, where the feedback loop between KCs and the APL neuron is unlikely to play a significant role. With odour stimulus, a broader network of neurons is recruited, including the feedback loop between KCs and the APL neuron, making interpretation of the results more complicated. First, I wanted to compare the time courses of KC odour responses with (Fig. 3.11-3.16 C1-C3) and without ATP (Fig. 3.11-3.16 A1-A3), relative to the time course of KC baseline activity inhibition evoked by activation of the APL neuron (Fig. 3.11-3.16 B1-B3)..

Fig#	type	Neurons imaged	APL> P2X2?	Odour?	Stim	ATP conc
3.11	Traces	KC	Y	Y v N	ATP, IAA	0.3 mM
3.12	Traces	KC	N	Y v N	ATP, IAA	0.3 mM
3.13	Traces	KC	Y	Y v N	ATP, IAA	0.75 mM
3.14	Traces	KC	N	Y v N	ATP, IAA	0.75 mM
3.15	Traces	KC	Y	Y v N	ATP, IAA	1.5 mM
3.16	Traces	KC	N	Y v N	ATP, IAA	1.5 mM

**Table 3.2 Overview of figures below**

See legend for Table 3.1 for details.

This allowed me to determine how well the temporal decrease in KC odour responses matches the effect of APL activation on KC baseline activity

For 0.3 mM ATP puffing on the horizontal lobe and vertical lobe, the inhibitory effect on odour responses was most prominent just before the odour response, and during the peak of the response. (compare panels **A1-C1** to **A2-C2** in **Fig. 3.11**). This matches well with the time course of KC baseline activity during activation of the APL neuron (**Fig. 3.11 B1** and **B2**). Compared to 0.3 mM ATP, puffing 0.75 and 1.5 mM ATP on the lobes showed a stronger and longer lasting decrease in KC baseline activity, which was reflected in the inhibitory effect on KC odour responses (**Fig. 3.13 and 3.15, A1-C1 and A2-C2**). There was no such clear effect from ATP application on the lobes in the corresponding negative controls (**Fig. 3.12, 3.14, and 3.16, A1-C1 and A2-C2**).

0.3 mM ATP evoked a relatively modest increase in GCaMP6f signal in the calyx (**Fig. 3.11 B3** vs **Fig. 3.13 B3** and **3.15 B3**), and an overall strong decrease in odour responses throughout the MB (**Fig. 3.11 A3** vs **C3**). This suggests that the local increase calcium influx evoked by puffing ATP on the calyx did not reflect actual depolarisation of the KCs, as this would likely have resulted in some level of increased GCaMP6f signal in the KC lobular projections. The observed decrease in the KC lobular projections is likely because activation of the APL neuron simultaneously inhibited the KCs in the calyx (further elaborated in section **3.3.2**).

Compared to 0.3 mM ATP, puffing 0.75 or 1.5 mM ATP on the calyx evoked a stronger and longer-lasting response (**Fig. 3.11 C3** vs **C3** in **Fig. 3.13** and **Fig. 3.15**). In view of the leaky expression of P2X2 that likely causes a local increase in calcium influx in the calyx, this response was not as large as would be expected if there was a summation of the ATP- and odour-evoked calcium influx (**A3** vs **C3** in **Fig. 3.13** and **Fig. 3.15**). This supports the notion that the increased calcium influx caused by ATP activating P2X2 channels in the KCs in the calyx does not represent a matching depolarisation of KCs. In the negative control flies, however, I observed that there was summation of the ATP- and odour-evoked increase in calcium influx throughout the KC projections when puffing ATP on the calyx (**Fig 3.14** and **Fig. 3.16, A3** vs **C3**), suggesting that puffing ATP on the calyx in the negative control flies did depolarise the KCs.



Imaged	KC	KC	KC
Genotype	KC>GCaMP6f P2X2 (no driver)	KC>GCaMP6f P2X2 (no driver)	KC>GCaMP6f P2X2 (no driver)
Stimulus	IAA	0.3 mM ATP	0.3 mM ATP IAA

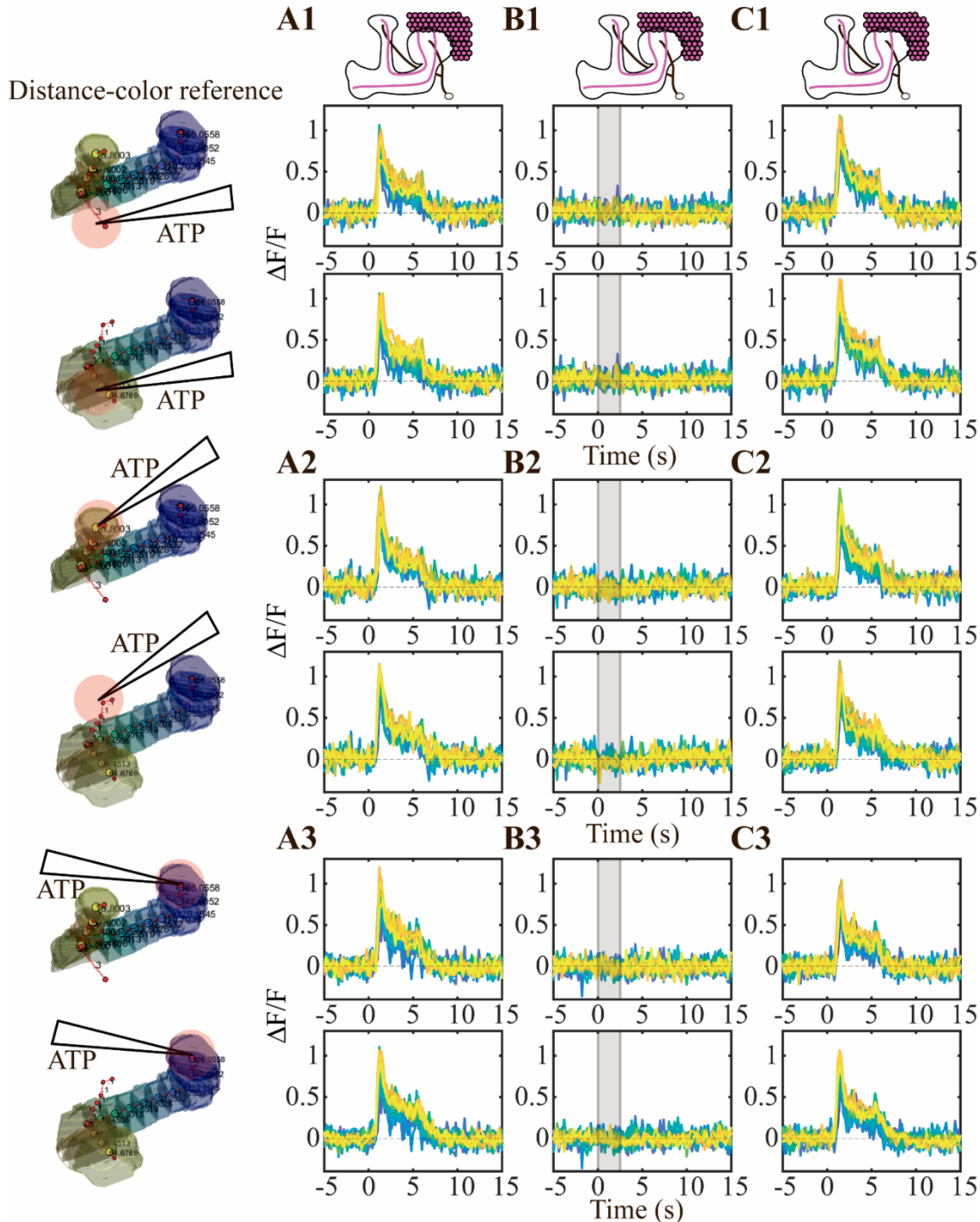


**Figure 3.12 Time courses showing the effect of ATP application on KC baseline activity or odour responses (no P2X2 driver, 0.3 mM ATP)**

Fly genotype: UAS-P2X2, MB247-LexA>LexAop-GCaMP6f. n (all graphs) = 4 (2 flies). Grey shading indicates time window used for quantification in **Fig. 3.8**. See legend for **Fig. 3.3** for further details.

Imaged	KC	KC	KC
Genotype	KC>GCaMP6f APL>P2X2	KC>GCaMP6f APL>P2X2	KC>GCaMP6f APL>P2X2
Stimulus	IAA	0.75 mM ATP	0.75 mM ATP IAA

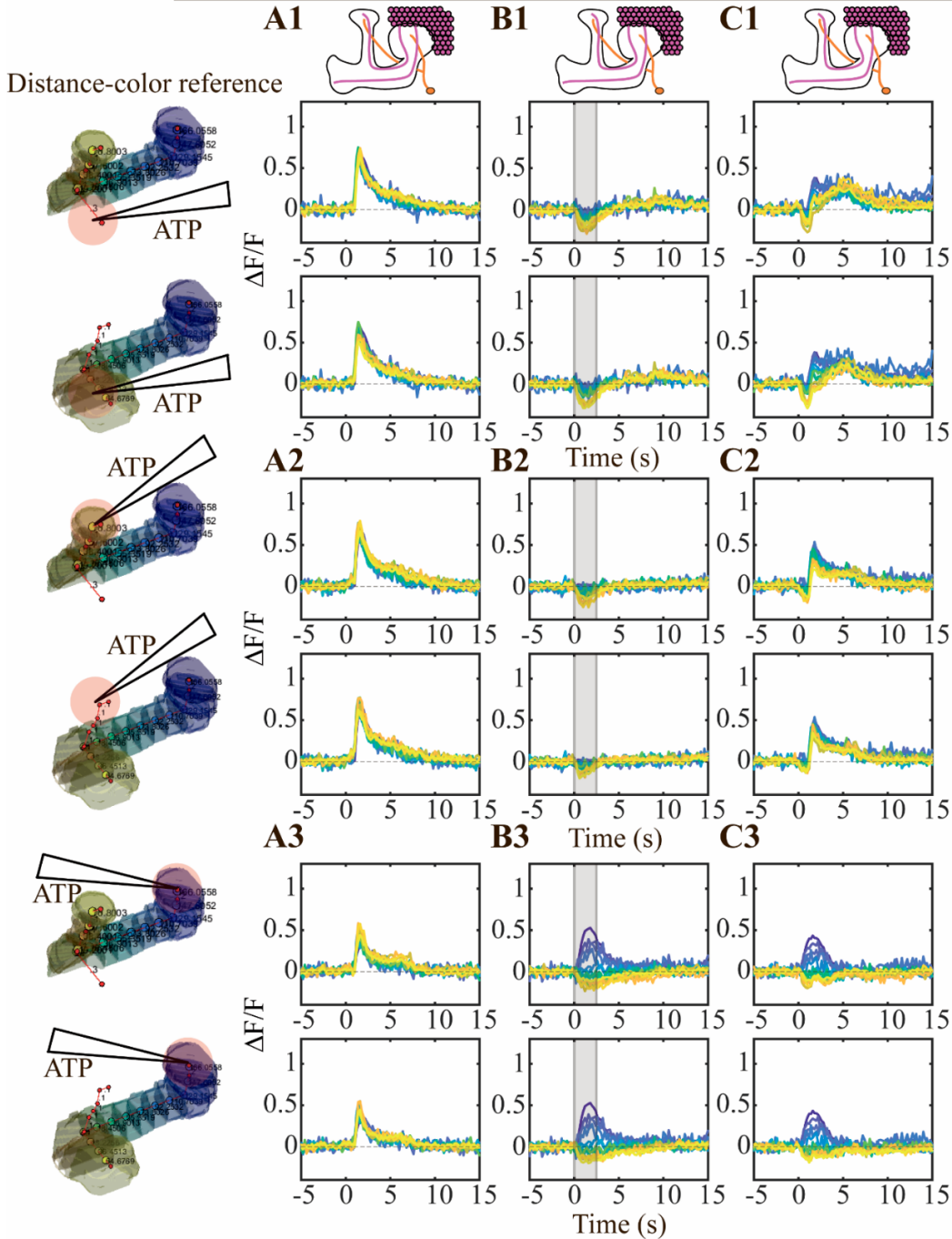


**Figure 3.13 Time courses showing inhibition of KC baseline activity or odour responses caused by APL neuron activation (0.75 mM ATP)**

Fly genotype: VT43924-Gal4.2>UAS-P2X2, MB247-LexA>LexAop-GCaMP6f. n (A1-C1, A2-C2) = 10 (9 flies), n (A3-C3) = 9 (8 flies). Grey shading indicates time window used for quantification in **Fig. 3.9**. See legend for **Fig. 3.3** for further details.

Imaged	KC	KC	KC
Genotype	KC>GCaMP6f P2X2 (no driver)	KC>GCaMP6f P2X2 (no driver)	KC>GCaMP6f P2X2 (no driver)
Stimulus	IAA	0.75 mM ATP	0.75 mM ATP IAA

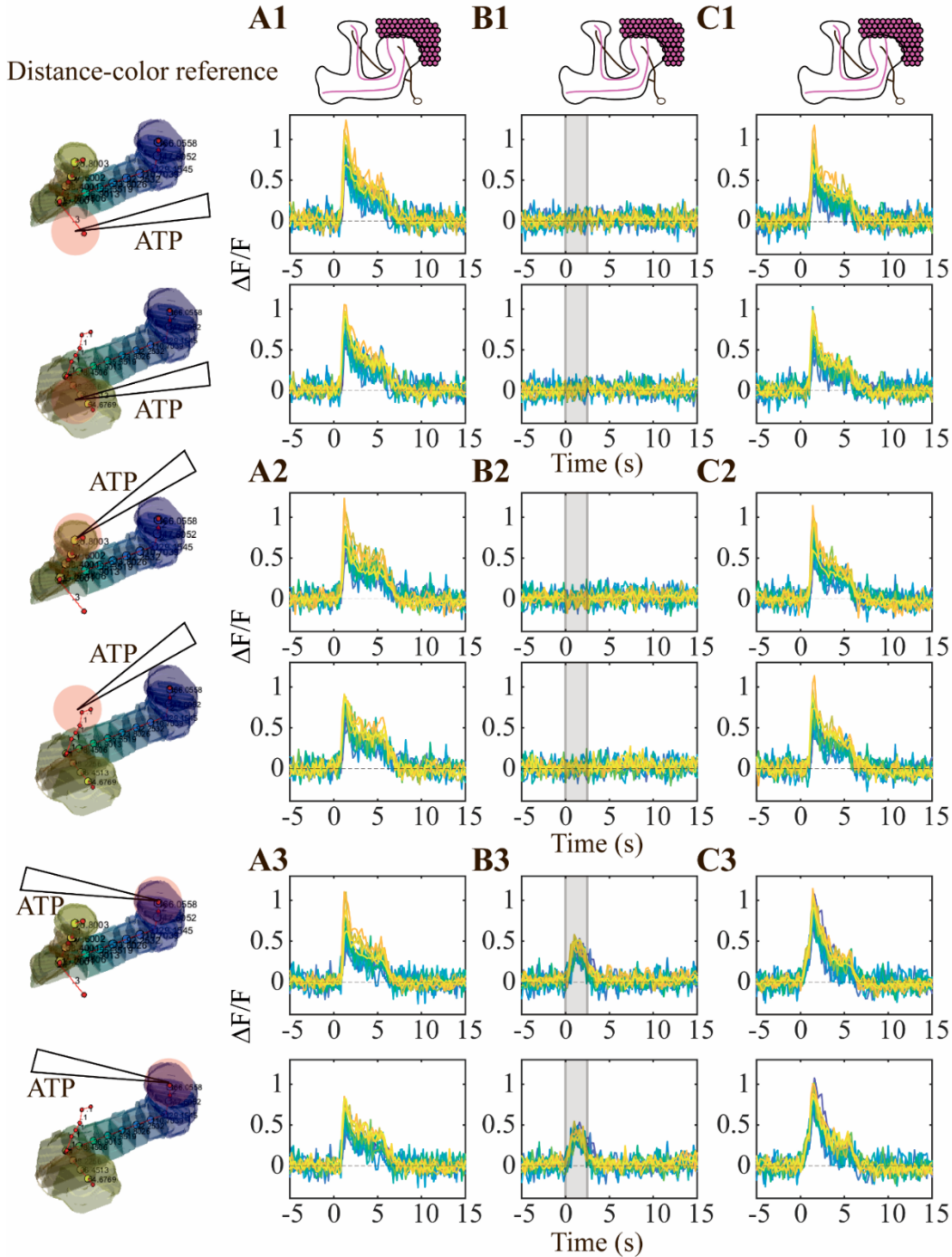


**Figure 3.14 Time courses showing the effect of ATP application on KC baseline activity or odour responses (no P2X2 driver, 0.75 mM ATP)**

Fly genotype: UAS-P2X2, MB247-LexA>LexAop-GCaMP6f. n (all graphs) = 5 (3 flies). Grey shading indicates time window used for quantification in Fig. 3.9. See legend for Fig. 3.3 for further details.

Imaged	KC	KC	KC
Genotype	KC>GCaMP6f APL>P2X2	KC>GCaMP6f APL>P2X2	KC>GCaMP6f APL>P2X2
Stimulus	IAA	1.5 mM ATP	1.5 mM ATP IAA

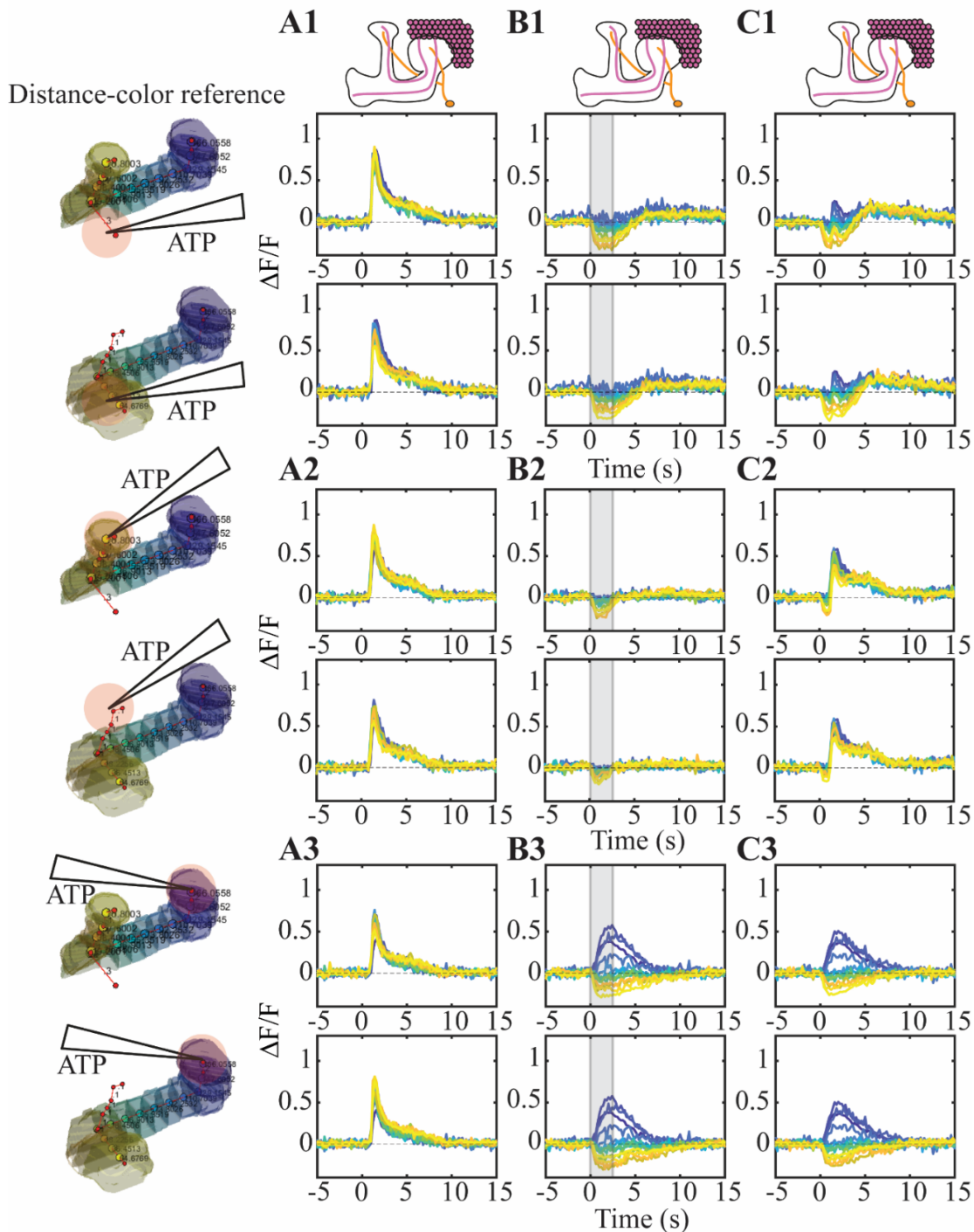


**Figure 3.15 Time courses showing inhibition of KC baseline activity or odour responses caused by APL neuron activation (1.5 mM ATP)**

Fly genotype: VT43924-Gal4.2>UAS-P2X2, MB247-LexA>LexAop-GCaMP6f. n (all graphs) = 9 (7 flies). Grey shading indicates time window used for quantification in **Fig. 3.10**. See legend for **Fig. 3.3** for further details.

Imaged	KC	KC	KC
Genotype	KC>GCaMP6f P2X2 (no driver)	KC>GCaMP6f P2X2 (no driver)	KC>GCaMP6f P2X2 (no driver)
Stimulus	IAA	1.5 mM ATP	1.5 mM ATP IAA

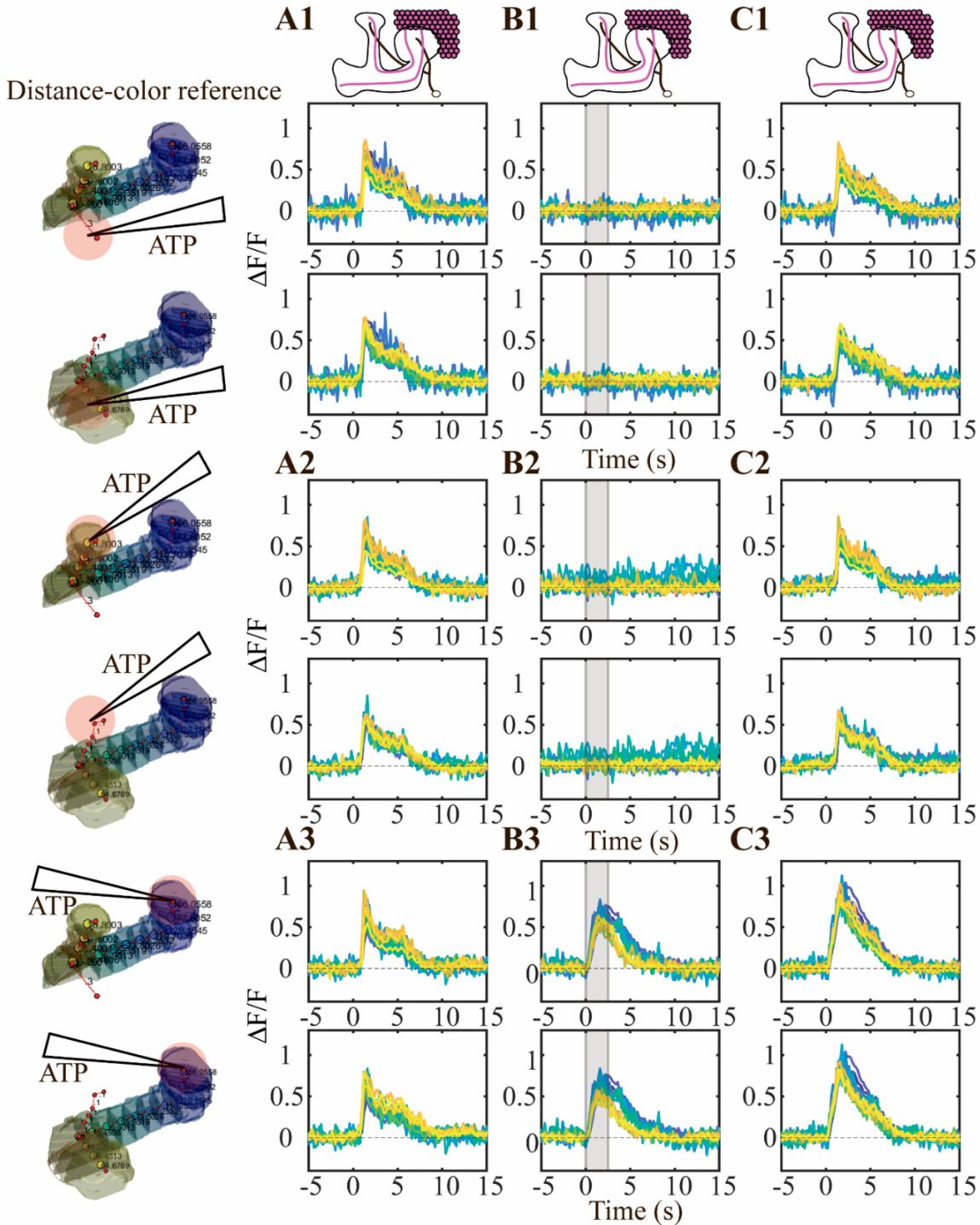


**Figure 3.16 Time courses showing the effect of ATP application on KC baseline activity or odour responses (no P2X2 driver, 1.5 mM ATP)**

Fly genotype: UAS-P2X2, MB247-LexA>LexAop-GCaMP6f. (all graphs) = 6 (4 flies). Grey shading indicates time window used for quantification in Fig. 3.10. See legend for Fig. 3.3 for further details.

How well did the spatial extent of the APL neuron’s inhibitory effect correspond to the spread of activity in the APL neuron? Addressing this question would be insightful in terms of assessing how reliable my characterisation of activity spread in the APL neuron is. If the APL neuron’s inhibitory output is more widespread, the GCaMP6f signal might underestimate the actual extent of activity spread in the APL neuron. Alternatively, my estimate of activity spread is accurate, and other mechanisms could facilitate a more widespread inhibitory effect (discussed in section 3.3.2). First, I looked at the time courses to see how these two measurements matched temporally. For each segment at each time point, the inhibitory effect of activating the APL neuron on KC odour responses was quantified as the difference between the KC odour response with and without ATP stimulation of the APL neuron, normalized to the peak odour response without ATP stimulation:  $\frac{(Odor_{ATP} - Odor)}{MAX_{Odor}}$ . Using the peak odour response instead of the average for normalizing was more robust for recordings where the odour response was low, where normalizing to the average caused extreme magnification of small changes.

Fig#	type	Neurons imaged	APL> P2X2?	Odour?	Stim	ATP conc
3.17	Traces	APL v KC	Y	Y v N	ATP, IAA	0.3 mM
3.18	Traces	APL v KC	N	Y v N	ATP, IAA	0.75 mM
3.19	Traces	APL v KC	Y	Y v N	ATP, IAA	1.5 mM
3.20	Quantification (3.17)	APL v KC	N	Y v N	ATP, IAA	0.3 mM
3.21	Quantification (3.18)	APL v KC	Y	Y v N	ATP, IAA	0.75 mM
3.22	Quantification (3.19)	APL v KC	N	Y v N	ATP, IAA	1.5 mM

**Table 3.3 Overview of figures below**

See legend for Table 3.1 for details.

For 0.3 mM ATP puffing on the lobes, there was a strong match between activity spread in the APL neuron and the inhibition time courses for the horizontal lobe (**Fig. 3.17 A1 vs B1**),

Imaged	APL	KC	KC
Genotype	APL>GCaMP6f APL>P2X2	KC>GCaMP6f APL>P2X2	KC>GCaMP6f P2X2 (No driver)
Stimulus	0.3 mM ATP	0.3 mM ATP IAA	0.3 mM ATP IAA

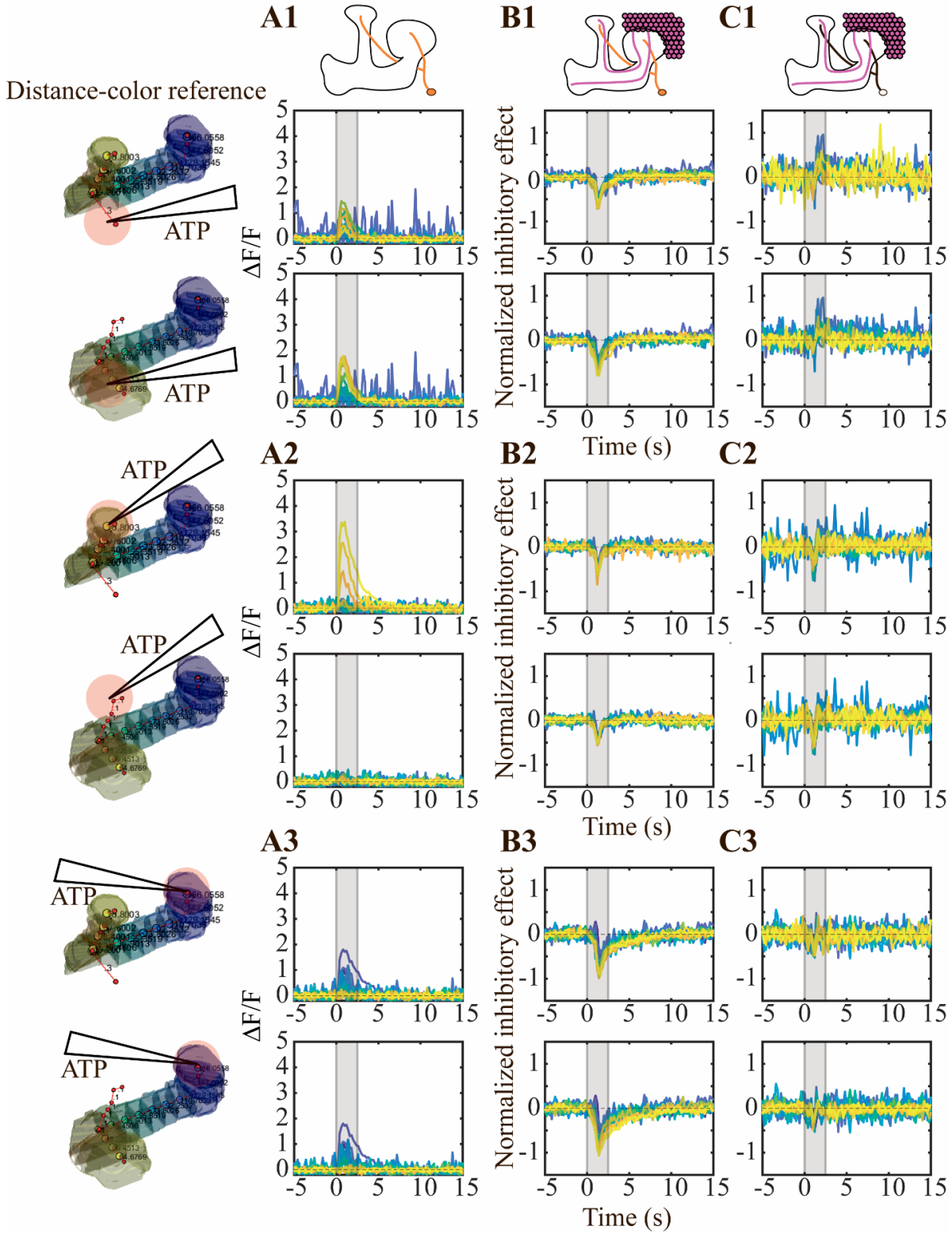


**Figure 3.17 Time courses showing APL neuron activity spread or inhibition of KC odour responses caused by APL neuron activation or negative control (0.3 mM ATP)**

(A1-A3) APL neuron  $\Delta F/F$  responses to ATP stimulation (10 ms pressure ejection at 12.5 psi), or (B1-B3, C1-C3) normalized inhibitory effect of ATP stimulation of the APL neuron on KC odour responses. This is quantified as the difference between KC odour responses with and without ATP stimulation of the APL neuron, normalized to the odour responses without ATP stimulation, for each individual segment, at each timepoint. (A-C) top: Table showing which neurons were imaged, fly genotype, and stimulus type, with MB schematics below showing which neuron expresses what transgene(s). Left: Example 3D-skeletons divided into the vertical (top) and horizontal (bottom) lobular branches, with distance-coloured segments, and an arrow showing where the ATP was puffed. The curves show the  $\Delta F/F$  (A1-A3) or normalized inhibitory effect (B1-B3 and C1-C3) vs time averaged across all recordings with the same conditions (ATP concentration and puff site) in the branch indicated by the 3D-skeleton on the left. Each curve shows the response or effect of its colour-matched segment. Stimulation occurred at 0 s. Grey shading indicates the time window used for quantification in Fig. 3.20. Fly genotypes: (A1-A3) VT43924-Gal4.2>UAS-GCaMP6f, UAS-P2X2, MB247-DsRed. (B1-B3) VT43924-Gal4.2>UAS-P2X2, MB247-LexA>LexAop-GCaMP6f. (C1-C3) UAS-P2X2, MB247-LexA>LexAop-GCaMP6f n (A1) = 8 (5 flies), n (A2) = 7 (4 flies), n (A3) = 4 (4 flies), n (B1-B3) = 10 (9 flies), n (C1-C3) = 4 (2 flies).

while activity spread in the APL neuron evoked by puffing on the vertical lobe lasted considerably longer than its inhibitory effect on KC odour responses, with the latter showing a sharp peak and quick decay compared to the former (Fig. 3.17 A2 vs B2).

For 0.75 and 1.5 mM ATP, the results were quite similar, with the disparity between activation of the APL neuron and its inhibitory effect on KC odour responses becoming more obvious (Fig. 3.18 and Fig. 3.19, A2 vs B2).

For 0.3 mM ATP KCs in the negative control flies showed an effect of similar magnitude to KCs in the experimental flies, although this was biphasic, with a brief decrease followed by a rise (Fig. 3.17 C1 and C2). This could be due to the leaky expression of the P2X2 driver in the APL neuron, KCs, or other unknown neurons. Interestingly, at higher concentrations, this effect was smaller relative to the effect observed in the experimental flies (Fig. 3.18 and Fig. 3.19, C1-C2 vs B1-B2). As the spatial analysis further below will show, puffing ATP on the lobes in the experimental flies had a clear spatially differential effect for 0.75 and 1.5 mM ATP in particular, whereas for the negative controls the effect was comparably negligible, and spatially indistinguishable (Fig. 3.20-3.22).

Imaged	APL	KC	KC
Genotype	APL>GCaMP6f APL>P2X2	KC>GCaMP6f APL>P2X2	KC>GCaMP6f P2X2 (No driver)
Stimulus	0.75 mM ATP	0.75 mM ATP IAA	0.75 mM ATP IAA

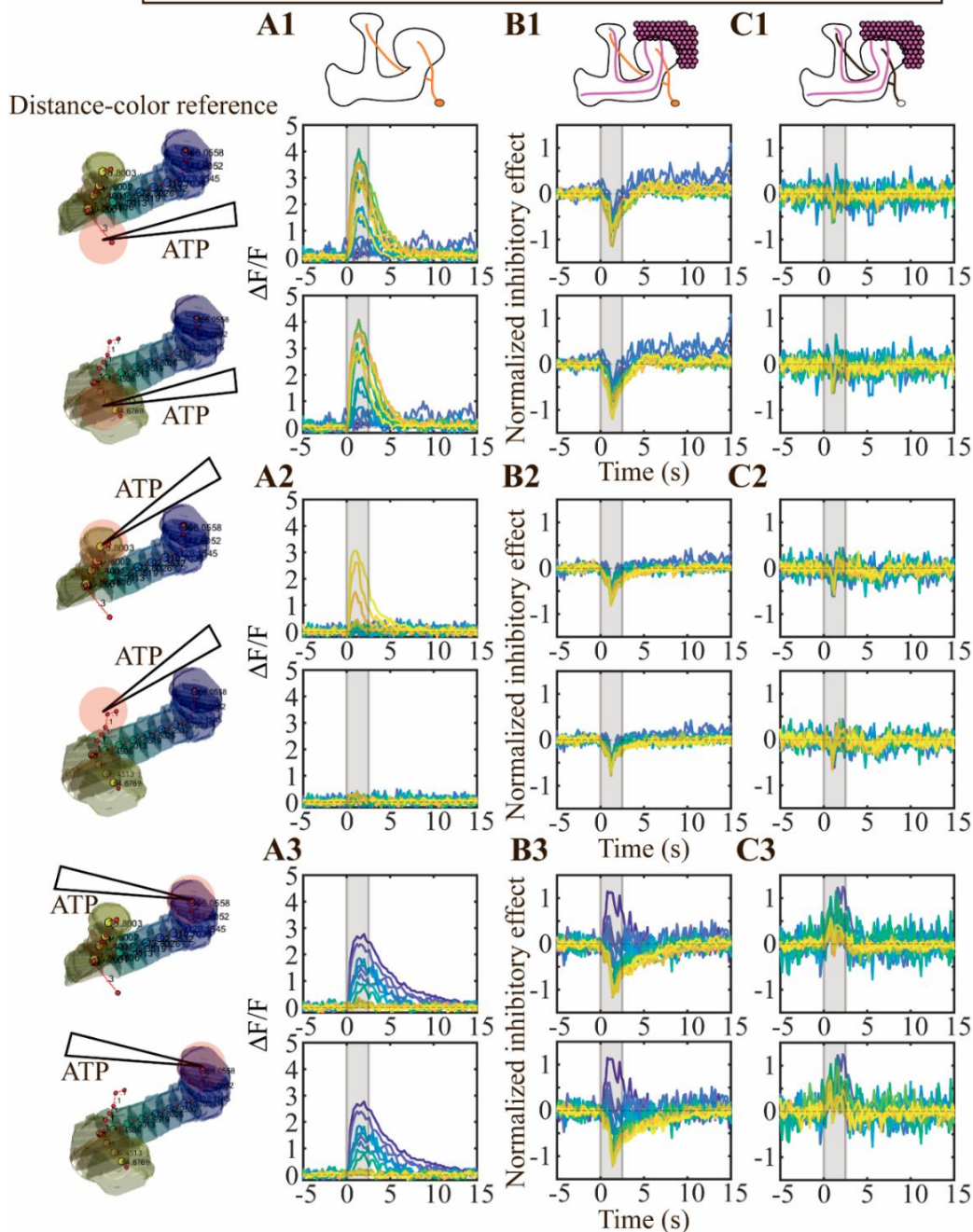


**Figure 3.18 Time courses showing APL neuron activity spread or inhibition of KC odour responses caused by APL neuron activation or negative control (0.75 mM ATP)**

Fly genotypes: (A1-A3) VT43924-Gal4.2>UAS-GCaMP6f, UAS-P2X2, MB247-DsRed. (B1-B3) VT43924-Gal4.2>UAS-P2X2, MB247-LexA>LexAop-GCaMP6f. (C1-C3) UAS-P2X2, MB247-LexA>LexAop-GCaMP6f n (A1, A2) = 10 (6 flies), n (A3) = 6 (4 flies), n (B1, B2) = 10 (9 flies), n (B3) = 9 (8 flies), n (C1-C3) = 5 (3 flies). Grey shading indicates time window used for quantification in Fig. 3.21. See legend for Fig. 3.17 for further details.

Imaged	APL	KC	KC
Genotype	APL>GCaMP6f APL>P2X2	KC>GCaMP6f APL>P2X2	KC>GCaMP6f P2X2 (No driver)
Stimulus	1.5 mM ATP	1.5 mM ATP IAA	1.5 mM ATP IAA

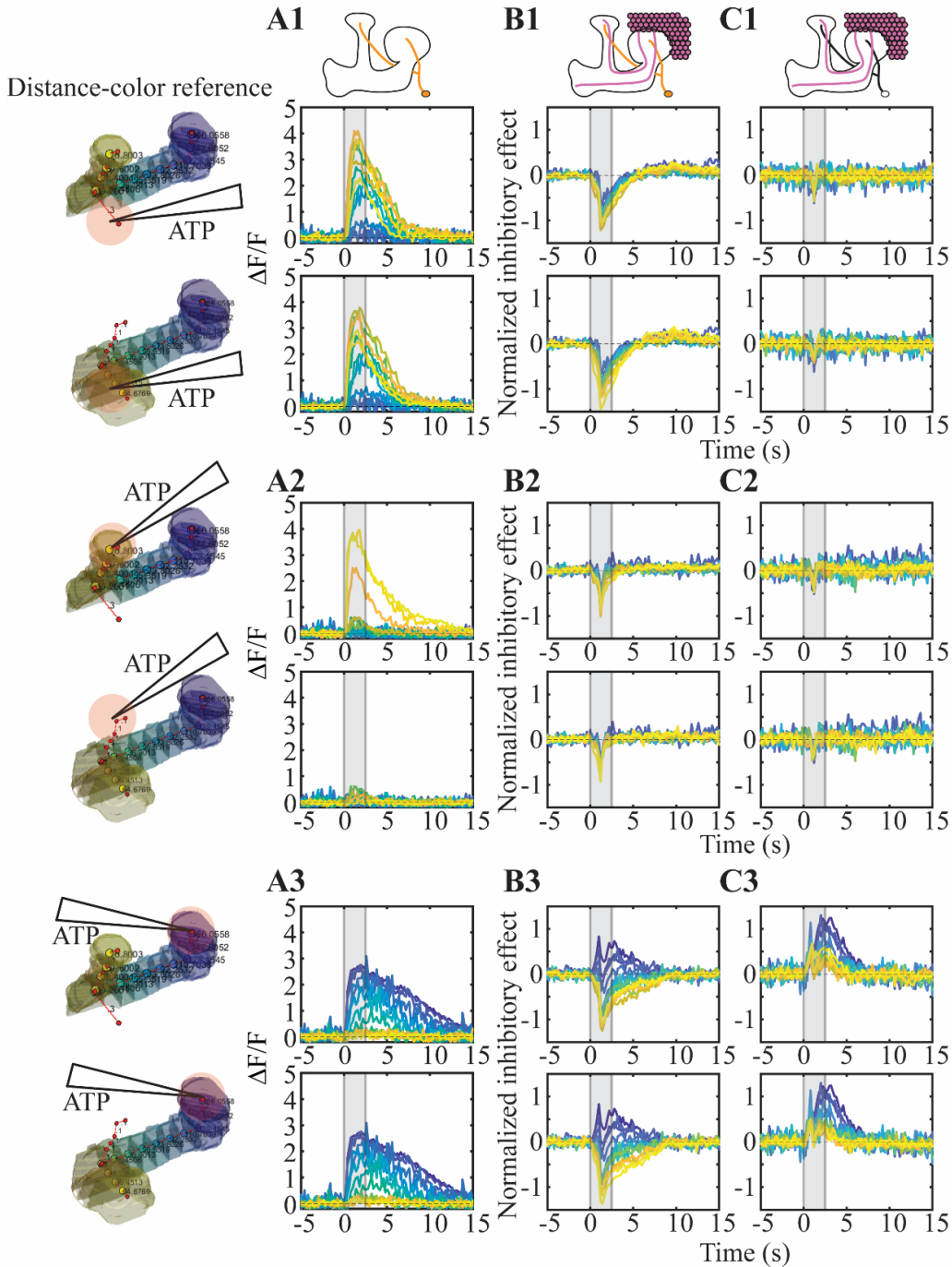


**Figure 3.19 Time courses showing APL neuron activity spread or inhibition of KC odour responses caused by APL neuron activation or negative control (1.5 mM ATP)**

Fly genotypes: (A1-A3) VT43924-Gal4.2>UAS-GCaMP6f, UAS-P2X2, MB247-DsRed. (B1-B3) VT43924-Gal4.2>UAS-P2X2, MB247-LexA>LexAop-GCaMP6f. (C1-C3) UAS-P2X2, MB247-LexA>LexAop-GCaMP6f. n (A1, A2) = 9 (6 flies), n (A3) = 5 (4 flies), n (B1-B3) = 9 (7 flies), n (C1-C3) = 6 (4 flies). Grey shading indicates time window used for quantification in Fig. 3.22. See legend for Fig. 3.17 for further details.

For puffing on the calyx, activation of the APL neuron was longer-lasting than the corresponding activation observed when puffing in other regions (**Fig. 3.17-3.19, A3 vs A1 and A2**). The inhibitory effect on KC odour responses was also notably lengthy, lasting ~3-4s longer than the odour pulse (**Fig. 3.17-3.19, B3 vs B1 and B2**).

I then carried out spatial analysis to properly determine how widespread the inhibitory effect of local activation of the APL neuron was, and to make direct comparisons between specific parts of the MB (**Fig. 3.2**, regions V, H, and C). For **Fig. 3.20-3.22**, the inhibitory effect was quantified as previously described (page 95), except that the time domain was collapsed into a single interval where the inhibitory effect was quantified, highlighted by the grey shading in **Fig 3.17-3.19**. Additionally, for each puff site, the inhibitory effect plots for the experimental and negative control flies were normalized to the largest absolute value in the experimental fly plots (Compare **C1 to B1, C2 to B2, C3 to B3**, in **Fig. 3.20-3.22**) to make comparisons between the experimental and negative control flies.

Activating the APL neuron in either the vertical or horizontal lobes had a considerably more widespread effect on KC odour responses than the activity spread evoked in the APL neuron (**Fig. 3.20-3.22 A1 vs B1 and A2 vs B2**).

This disparity in spatial extent between the activity propagation in the APL neuron and the inhibitory effect on KC odour responses was particularly prominent in the case of puffing ATP on the vertical lobe, considering that activity in the APL neuron did not spread any further than the junction with any ATP concentration for this puff site (**Fig. 3.20-3.22, A2**). Puffing 0.3 mM ATP on the vertical lobe showed similarly sized effects for the experimental and negative control flies (**3.20 B2 and C2**), which reflects the dip observed in the time courses of the inhibitory effect for these recordings (**Fig. 3.17 B2 and C2**). The raw odour response traces show that, for the experimental flies, there was a modest decrease in odour response from puffing ATP on the vertical lobe (**Fig. 3.11 A2 vs C2**), while for the negative control flies it is hard to make out any difference by looking at the raw odour response time courses (**Fig. 3.12 A2 vs C2**). The reason the effect looks prominent in the spatial analysis (**Fig. 3.20 C2**) is because the negative control values in the spatial analysis are normalized to the experimental values (**Fig. 3.17 B2**), which had a modest maximum effect size itself. There was no obvious effect of puffing 0.75 or 1.5 mM ATP on the lobes in the negative control flies (**Fig. 3.21-3.22 C1 and C2**).

Imaged	APL	KC	KC
Genotype	APL>GCaMP6f APL>P2X2	KC>GCaMP6f APL>P2X2	KC>GCaMP6f P2X2 (No driver)
Stimulus	0.3 mM ATP	0.3 mM ATP IAA	0.3 mM ATP IAA

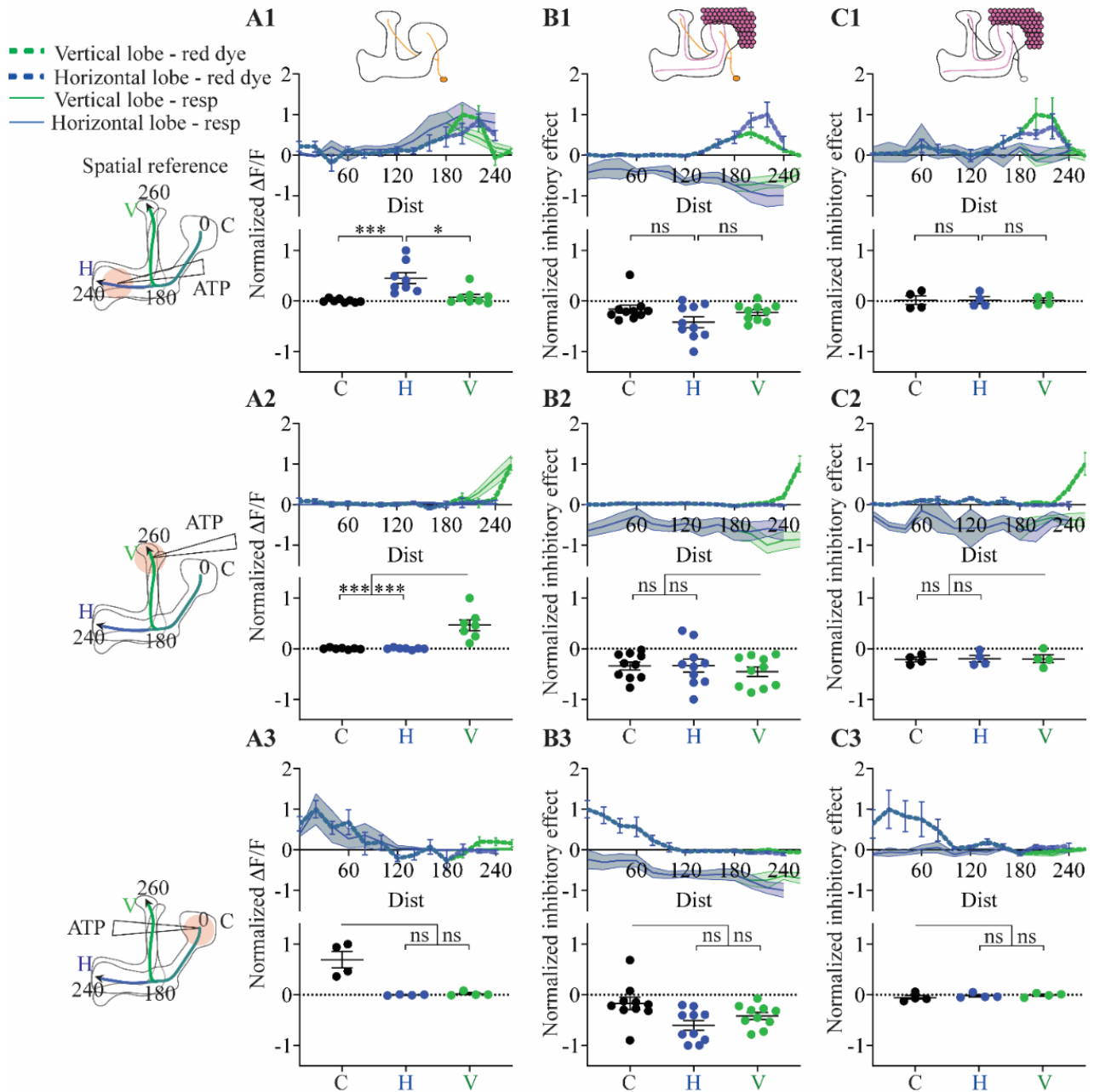


**Figure 3.20 Spatial comparison of activity spread in the APL neuron to the inhibition of KC odour responses caused by APL neuron activation or negative control (0.3 mM ATP)**

(A-C) top: Table showing which neurons were imaged, fly genotype, and stimulus type, with MB schematics below showing which neuron expresses what transgene(s). Left: MB schematics showing the 3D-skeleton distance measurements, with the calyx represented by 0, and the vertical and horizontal branches represented in green and blue colours, respectively. Top panels: Response curves showing mean  $\Delta F/F$  responses of the APL neuron to ATP stimulation (A1-A3), or the normalized inhibitory effect on KC odour responses caused by ATP stimulation of the APL neuron (B1-B3, C1-C3), vs distance from the calyx to the tip of the two lobular branches, in the grey-shaded periods

shown in Fig. 3.15 (2.5s from stimulus onset). The colour of the curves matches the vertical (green) and horizontal (blue) lobular branches depicted in the schematics shown on the left. The normalized inhibitory effect was quantified as the difference between KC odour responses with and without ATP stimulation of the APL neuron, normalized to KC odour responses without ATP stimulation, for each individual segment. Data shown is for responses averaged across all recordings for that condition  $\pm$ SEM shading. Bottom panels: Scatter plots showing the average response of the two most distal segments of the calyx (C), vertical (V), and horizontal lobe (H), quantified from the same period as the top panels. Each dot represents an individual recording. Data shown is mean. Error bars show mean  $\pm$ SEM. Fly genotypes: (**A1-A3**) VT43924-Gal4.2>UAS-GCaMP6f, UAS-P2X2, MB247-DsRed. (**B1-B3**) VT43924-Gal4.2>UAS-P2X2, MB247-LexA>LexAop-GCaMP6f. (**C1-C3**) UAS-P2X2, MB247-LexA>LexAop-GCaMP6f. n (**A1**) = 8 (5 flies), n (**A2**) = 7 (4 flies), n (**A3**) = 4 (4 flies), n (**B1-B3**) = 10 (9 flies), n (**C1-C3**) = 4 (2 flies).

For puffing 0.75 and 1.5 mM ATP on the horizontal lobe, the inhibitory effect was statistically significantly different for H compared to V and C, while no difference was found for 0.3 mM ATP. This suggests that, while the inhibitory effect was widespread, it was strongest locally. For vertical lobe stimulation with 0.75 and 1.5 mM ATP, there was only a statistically significant difference between V and C (**Fig. 3.21-3.22 B2**), emphasizing the contrast with the strictly localised activity spread in the APL neuron when puffing on the vertical lobe (**Fig. 3.20-3.22 A2**). No difference was found for 0.3 mM ATP stimulation (**Fig. 3.20 B2**).

Puffing ATP on the calyx decreased KC odour responses in the lobes (**Fig. 3.20-3.22 B3**), but similarly to the effect I observed on baseline activity (**Fig. 3.7 A3-C3**), it increased the GCaMP6f signal in the calyx (**Fig. 3.21-3.22 B3**). The exception was 0.3 mM ATP, where there was a decrease in odour responses throughout the KC projections (**Fig. 3.20 B3**), reflecting the modest local increase in calcium influx resulting from puffing 0.3 mM ATP on the calyx (**Fig. 3.11 A3-C3** and **Fig. 3.20-3.22 A1**). The results for the calyceal stimulation must be interpreted with caution, as the leaky expression meant that the ATP puff stimulated the KCs in the calyx, but to a smaller extent for 0.3 mM ATP. I observed an inhibitory effect on the lobes from stimulating the APL neuron in the calyx for all concentrations, suggesting that inhibition from the APL neuron onto KCs in the calyx has a widespread effect (**Fig. 3.24 A3-C3**).

Imaged	APL	KC	KC
Genotype	APL>GCaMP6f APL>P2X2	KC>GCaMP6f APL>P2X2	KC>GCaMP6f P2X2 (No driver)
Stimulus	0.75 mM ATP	0.75 mM ATP IAA	0.75 mM ATP IAA

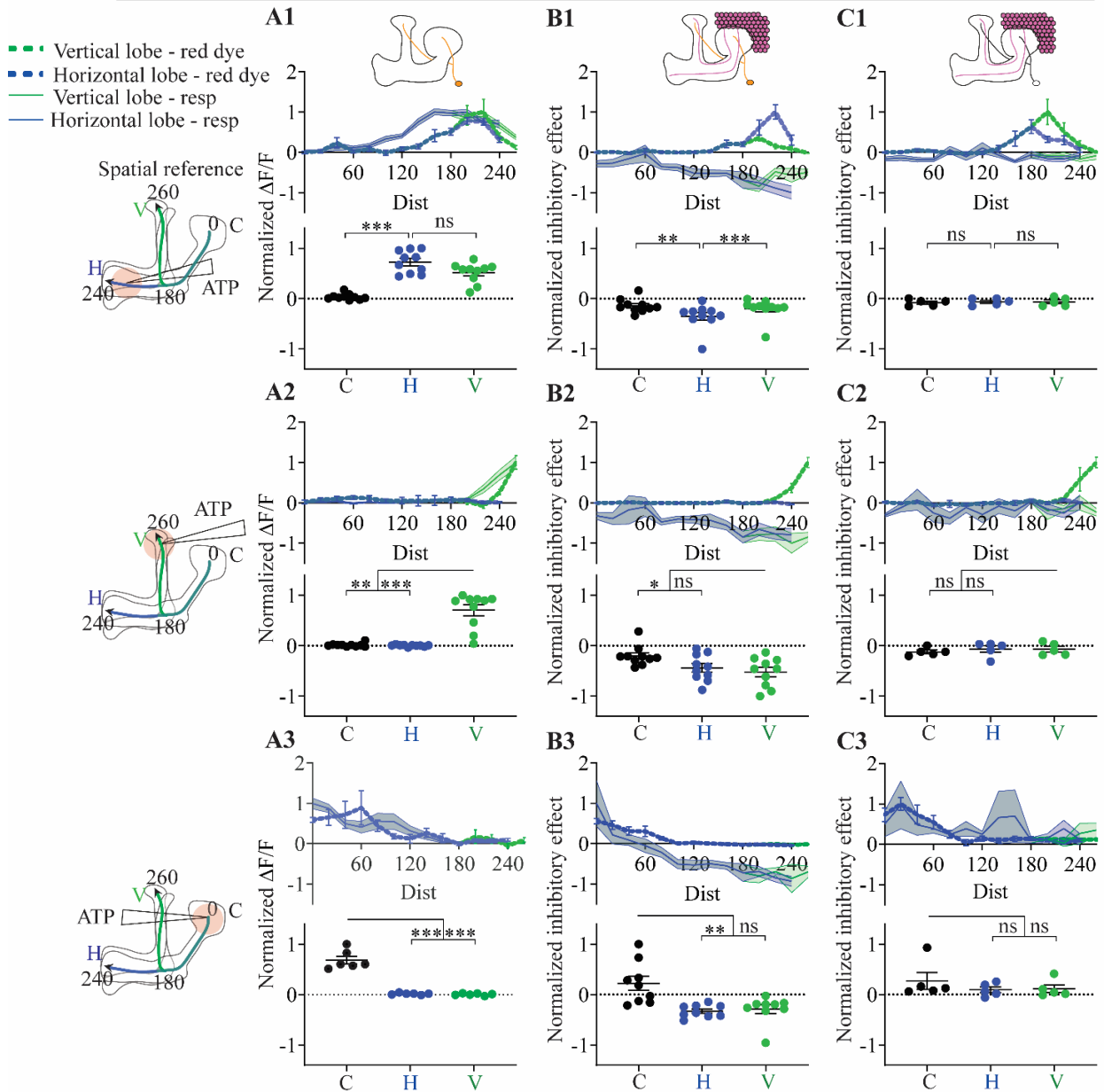


**Figure 3.21 Spatial comparison of activity spread in the APL neuron to the inhibition of KC odour responses caused by APL neuron activation or negative control (0.75 mM ATP)**

Fly genotypes: **(A1-A3)** VT43924-Gal4.2>UAS-GCaMP6f, UAS-P2X2, MB247-DsRed. **(B1-B3)** VT43924-Gal4.2>UAS-P2X2, MB247-LexA>LexAop-GCaMP6f. **(C1-C3)** UAS-P2X2, MB247-LexA>LexAop-GCaMP6f. n **(A1, A2)** = 10 (6 flies), n **(A3)** = 6 (4 flies), n **(B1, B2)** = 10 (9 flies), n **(B3)** = 9 (8 flies), n **(C1-C3)** = 5 (3 flies). See legend for **Fig. 3.20** for further details.

Imaged	APL	KC	KC
Genotype	APL>GCaMP6f APL>P2X2	KC>GCaMP6f APL>P2X2	KC>GCaMP6f P2X2 (No driver)
Stimulus	1.5 mM ATP	1.5 mM ATP IAA	1.5 mM ATP IAA

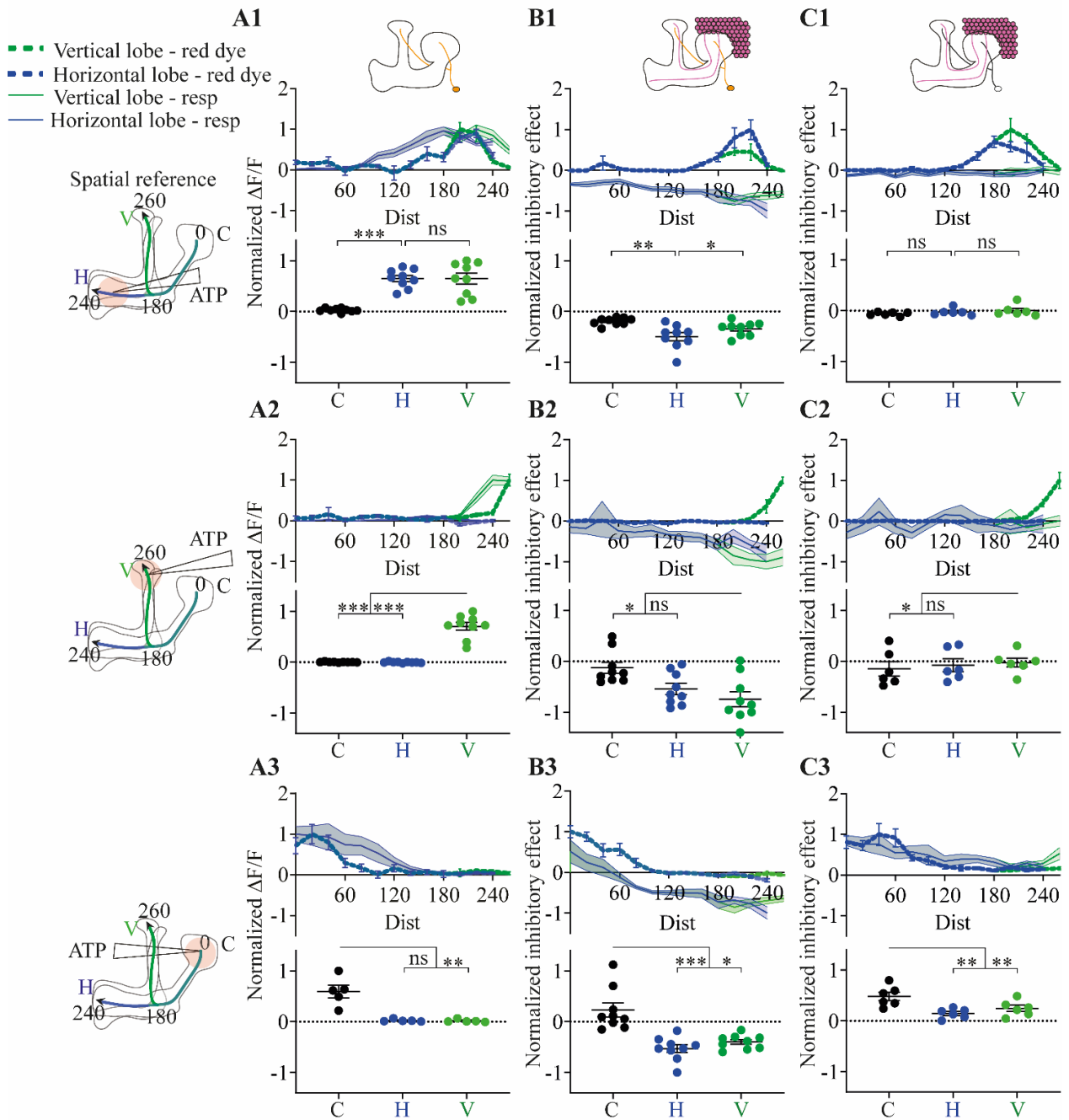


**Figure 3.22 Spatial comparison of activity spread in the APL neuron to the inhibition of KC odour responses caused by APL neuron activation or negative control (1.5 mM ATP)**

Fly genotypes: (A1-A3) VT43924-Gal4.2>UAS-GCaMP6f, UAS-P2X2, MB247-DsRed. (B1-B3) VT43924-Gal4.2>UAS-P2X2, MB247-LexA>LexAop-GCaMP6f. (C1-C3) UAS-P2X2, MB247-LexA>LexAop-GCaMP6f. n (A1, A2) = 9 (6 flies), n (A3) = 5 (4 flies), n (B1-B3) = 9 (7 flies), n (C1-C3) = 6 (4 flies). See legend for Fig. 3.20 for further details.

In summary, local stimulation of the APL neuron in the lobes and the calyx decreased KC odour responses (with the caveat that there was a local influx of calcium due to leaky P2X2 expression), suggesting that the APL neuron can inhibit KCs in both the MB lobes and the calyx. The inhibitory output of the APL neuron seemed to be more widespread than my estimates of its internal activity spread would suggest. This could be either due to an underestimation of activity spread in the APL neuron, widespread release of GABA from the APL neuron, or other mechanisms that facilitate widespread inhibition (discussed in section 3.3.2).

### 3.2.5 Local puffing of GABA and local activation of the APL neuron have similar effects on KC activity

Does the APL neuron release GABA more widely than my estimates of its activity spread suggests? This could occur if there is a level of calcium spread that is too low for GCaMP6f to detect, but sufficient to evoke vesicle release, and thereby inhibit KCs. To address this question, I attempted to reproduce the increased inhibition onto KCs by locally stimulating the APL neuron through locally applying GABA. To my knowledge, the APL neuron is the only known neuron that targets KCs with GABA release. One study suggested that the DPM neuron is GABAergic and can inhibit KCs (Haynes et al., 2015). This was based on GABA antibody staining showing colocalization with the DPM neuron and using a chloride sensor to show that activation of the DPM neuron increases chloride levels in KCs. However, a recent transcriptome study found no *Gad1* expression in the DPM neuron (Aso et al., 2019). The increased chloride in KCs observed from DPM activation could be indirectly mediated by GABA release from the APL neuron, as the two neurons are coupled by gap junctions (Wu et al., 2011).

Thus, puffing GABA on the MB can be used as an approach to approximate GABA release from the APL neuron. If puffing GABA on the MB has a considerably more localised effect, it would suggest that activity propagates further in the APL neuron than the calcium transients show, or that its inhibitory effect is not as localised as its spread of intracellular activity. Thus, puffing GABA on the MB could have a similar effect on KCs as activation of the APL neuron, depending on how far it spreads from the application site, and the amplitude of its effect. First, I looked at the time courses of the KC raw odour responses to odour stimulus with and without locally puffing GABA on the MB to characterise the temporal nature of its inhibitory effect on different segments (**Fig. 3.23**).



I observed modest decreases in KC odour responses when puffing GABA on the lobes (**Fig. 3.23 A1 vs C1 and A2 vs C2**), while puffing on the calyx strongly decreased KC odour responses (**Fig. 3.23 A3 vs C3**). For puffing GABA on the lobes, the inhibitory effect mainly affected the peak of the odour responses, which corresponded well with the brief dip in KC baseline activity evoked by GABA application in absence of odour stimulus (**Fig. 3.23 B1 vs C1 and B2 vs C2**). Puffing GABA on the calyx had a longer-lasting effect on KC baseline activity, and a corresponding longer effect on KC odour responses (**Fig. 3.23 B3 vs C3**).

The next two figures show the time courses from **Fig. 3.17-3.19** column **B** (**Fig. 3.24**) and the spatial analysis graphs from **Fig. 3.20-3.22** column **B** (**Fig. 3.25**) side-by-side, respectively, to compare the effects of locally activating the APL neuron with local application of GABA. For the time courses, the inhibitory effect was calculated and normalized as previously described (page 112). No normalization was carried out between individual panels.

For puffing GABA on the horizontal lobe, the result was most similar to that of activating the APL neuron with 0.3 mM ATP (**Fig. 3.24 A1 vs D1**), while puffing GABA on the vertical lobe looked more similar to 0.75 or 1.5 mM ATP, but broadened the inhibitory effect over a longer duration (**Fig. 3.24 A2-C2 vs D2**). Puffing GABA on the calyx closely resembled the inhibitory effect evoked by activating the APL neuron with 0.3 mM ATP, but seemed to have a longer-lasting effect for the calyceal segments (**Fig. 3.24 A3 vs D3**), and as expected, did not show the local increase in calcium influx in KC calyceal projections due to leaky P2X2 expression that I observed when I activated the APL neuron with higher concentrations (**Fig. 3.24 B3-C3 vs D3**).

To characterise the spatial differences in the inhibitory effect and make direct comparisons between specific segments of the MB (**Fig. 3.2**, regions V, H, and C), I carried out spatial analysis of the 3D skeleton (**Fig. 3.25**). The inhibitory effect was quantified as previously described (page 112), except that the time domain was collapsed into a single interval where the inhibitory effect was quantified, highlighted by the grey shading in **Fig 3.24**. Furthermore, for each puff site, the responses are normalized to the largest absolute value within that group (**A1-D1, A2-D2, and A3-D3**), for comparison between local activation of the APL neuron and local GABA application. This section will also cover the effect of locally puffing GABA on KC baseline activity (panels **D1-D3** in **Fig. 3.6 and 3.7**).

Imaged	KC	KC	KC	
Genotype	KC>GCaMP6f APL>P2X2	KC>GCaMP6f APL>P2X2	KC>GCaMP6f APL>P2X2	KC>GCaMP6f
Stimulus	0.3 mM ATP IAA	0.75 mM ATP IAA	1.5 mM ATP IAA	7.5 mM GABA IAA

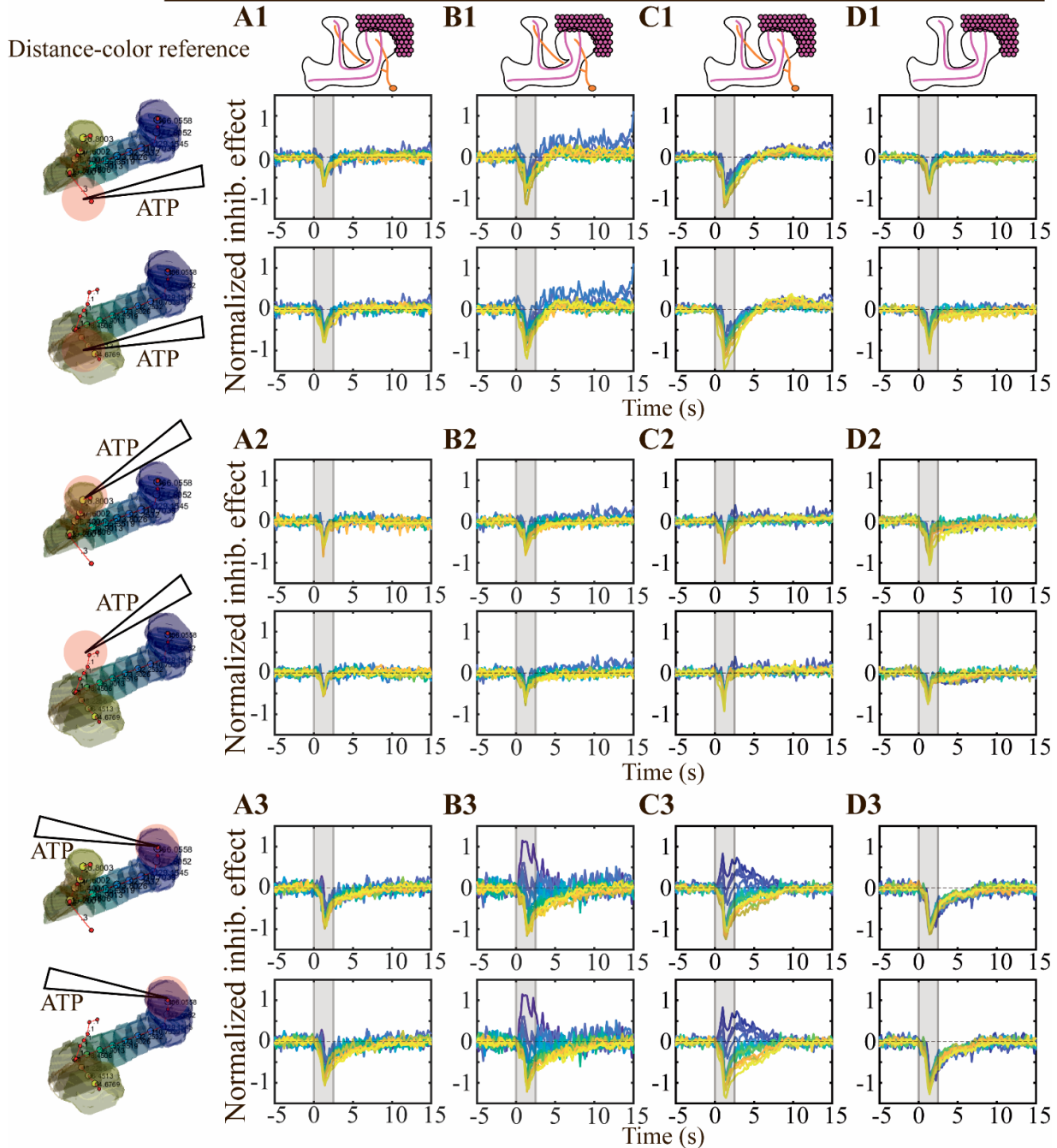


**Figure 3.24 Time courses showing inhibition of KC odour responses caused by GABA application or APL neuron activation with different ATP concentrations**

Fly genotypes: (All but **D1-D3**) VT43924-Gal4.2>UAS-P2X2, MB247-LexA>LexAop-GCaMP6f. (**D1-D3**) OK107-Gal4>UAS-GCaMP6f. n (**A1-A3**) = 10 (9 flies), n (**B1-B2**) = 10 (9 flies), n (**B3**) = 9 (8 flies), n (**C1-C3**) = 9 (7 flies), n (**D1, D2**) = 13 (8 flies), n (**D3**) = 11 (6 flies). Grey shading indicates time window used for quantification in **Fig. 3.25**. See legend for **Fig. 3.17** for further details.

Imaged	KC	KC	KC	KC
Genotype	KC>GCaMP6f APL>P2X2	KC>GCaMP6f APL>P2X2	KC>GCaMP6f APL>P2X2	KC>GCaMP6f
Stimulus	0.3 mM ATP IAA	0.75 mM ATP IAA	1.5 mM ATP IAA	7.5 mM GABA IAA

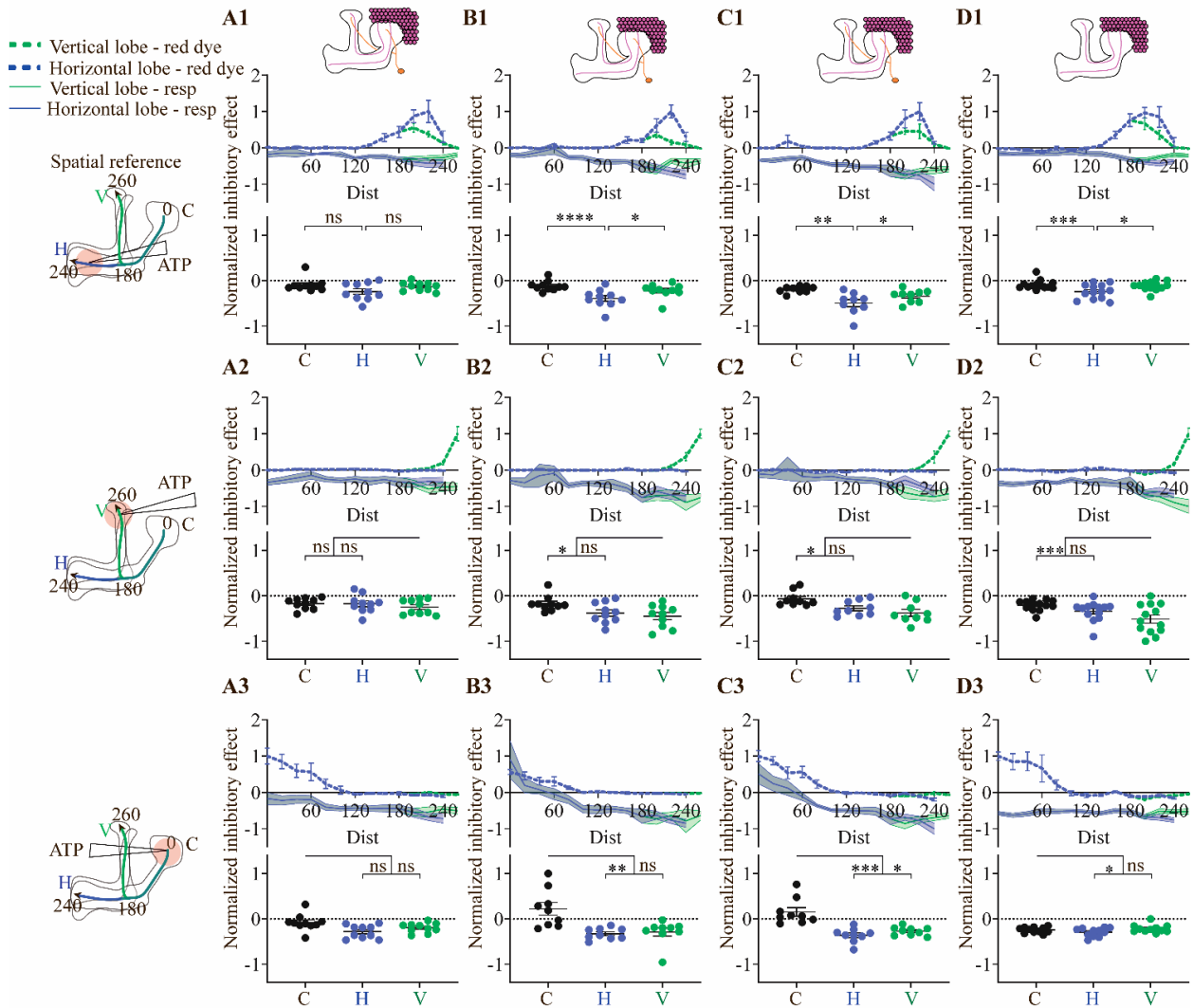


**Figure 3.25 Spatial quantification showing inhibition of KC odour responses caused by GABA application or activation of the APL neuron with different ATP concentrations**

Fly genotypes: (All but **D1-D3**) VT43924-Gal4.2>UAS-P2X2, MB247-LexA>LexAop-GCaMP6f. (**D1-D3**) OK107-Gal4>UAS-GCaMP6f. n (**A1-A3**) = 10 (9 flies), n (**B1-B2**) = 10 (9 flies), n (**B3**) = 9 (8 flies), n (**C1-C3**) = 9 (7 flies), n (**D1, D2**) = 13 (8 flies), n (**D3**) = 11 (6 flies). See legend for **Fig. 3.20** for further details.

Puffing GABA on the MB lobes had largely similar effects on KC baseline activity as activation of the APL neuron with ATP. The effect size was most like 0.3 mM ATP activation of the APL neuron (compare panels **D1-D3** to **A1-A3**, **B1-B3**, and **C1-C3** in **Fig. 3.6**). The decrease in KC baseline activity at H was statistically significantly stronger than V or C for puffing GABA on the horizontal lobe (**Fig. 3.7 D1**), while the statistics for puffing on the vertical lobe were similar to the results for 0.75 and 1.5 mM ATP (**Fig. 3.7 A2-D2**). In contrast to ATP, GABA puffing on the calyx

did not increase the baseline activity at C, but rather caused a decrease throughout the MB (**Fig. 3.7 D3**).

GABA puffing on the MB lobes had a strong local, but also widespread, effect on KC odour responses (**Fig. 3.24** and **Fig. 3.25**). Puffing on the horizontal lobe strongly decreased odour responses at H, but also decreased the responses at C and V to a lower extent (**Fig. 3.25 D1**). This effect size was most similar to 0.3 mM ATP. Puffing GABA on the vertical lobe had a strong inhibitory effect on V, but also affected odour responses at C and H, with no statistically significant difference between V and H. Interestingly, the effect size at V was stronger than that observed with any concentration of ATP (**Fig. 3.25 A2-D2**). Puffing GABA on the calyx reduced KC odour responses throughout the MB (panel **D3** in **Fig. 3.24** and **Fig. 3.25**).

In summary, the inhibitory effect of puffing GABA on the MB lobes had a strong local, but also weaker distal effects on KC odour responses, similar to the observations made for APL activation. As expected, puffing GABA on the calyx inhibited KC odour responses throughout the MB. These findings do not directly demonstrate how widely the APL neuron releases GABA. However, they suggest that the widespread inhibitory effect observed from locally stimulating the APL neuron is not due to an underestimation of activity spread in the APL neuron, or widespread release of GABA. In section **6.5.1** I discuss other ways of addressing the spatial extent of the APL neuron's inhibitory output.

### 3.2.6 Comparison of activity or effect spread vs red dye spread

One of the main limitations of my method of stimulating the APL neuron is the lack of a direct measure of ATP spread from the point of fluid ejection from the pipette. The smaller molecular weight of ATP vs the red dye means that quantification of red dye spread is at best an approximation of ATP spread.

To determine how well the red dye reflected the release of ATP and concomitant spread of activity in the APL neuron, I created scatter plots of red dye  $\Delta F/F$  against the GCaMP6f  $\Delta F/F$  or the inhibitory effect. The spread of the red dye was a reasonable approximation of activity spread in the APL neuron, particularly so for puffing on the vertical lobe, where the neuronal response and the red dye both show a steep drop from the puff site (**Fig. 3.26 A2**). For puffing on the horizontal lobe

and the calyx, the more widespread red dye signal was reflected in the widespread response (**Fig. 3.26 A1 and A3**). The highest-responding segment was rarely the same as the one with highest red dye signal, but there was a general trend to observe.

For the suppression of KC baseline activity observed with APL activation, the plots reflect the more widespread effect, particularly for puffing on the vertical lobe. Even when the red dye signal is at 0, there are still many segments with a large response (**Fig. 3.26 B2**). This was also the case for the horizontal lobe, although to a lesser extent (**Fig. 3.26 B1**). For puffing on the calyx, the plot shows the opposite effects on the calyx and the lobes due to the leaky expression of P2X2, with a peak response coinciding at or near the segment with the highest red dye signal (**Fig 3.26 B3**).

Plotting the inhibitory effect on odour responses vs the red dye signal showed a similar trend to what was observed for the suppressive effect on KC baseline activity (**Fig. 3.27**). Many of the segments showed responses despite there being no red dye signal, for both puffing on the vertical lobe and the horizontal lobe (**Fig. 3.27 A1 and A2**).

For the effect of GABA puffing on KC baseline activity and odour responses, I observed similar behaviour when puffing on the vertical lobe (**Fig. 3.26 and 3.27 A2 vs D2**). There was a clearer correlation between effect size and red dye signal with GABA puffing on the horizontal lobe, compared to ATP (Compare panel **A1 vs D1** in **Fig. 3.26 and 3.27**).

For both GABA and ATP puffing on horizontal lobe, there was the characteristic ‘loop’, where the plot reaches the maximum red dye signal, but then loops back to the left on the x-axis to reach the maximum effect size. This represents the segment at the tip of the horizontal lobe which showed the largest effect size when puffing on the horizontal lobe (**Fig. 3.6 and 3.25 A1-D1**).

To summarize, the red dye signal spread was a reasonable estimate of activity spread in the APL neuron (**Fig. 3.26 A1-A3**). It is plausible that the red dye would underestimate the activity spread to a degree, because activity is likely to propagate away from the stimulus site, and the ATP is likely to diffuse away from the stimulus site to some extent.

Imaged	APL	KC	KC	KC
Genotype	APL>GCaMP6f APL>P2X2	KC>GCaMP6f APL>P2X2	KC>GCaMP6f P2X2 (No driver)	KC>GCaMP6f
Stimulus	ATP	ATP	ATP	7.5 mM GABA

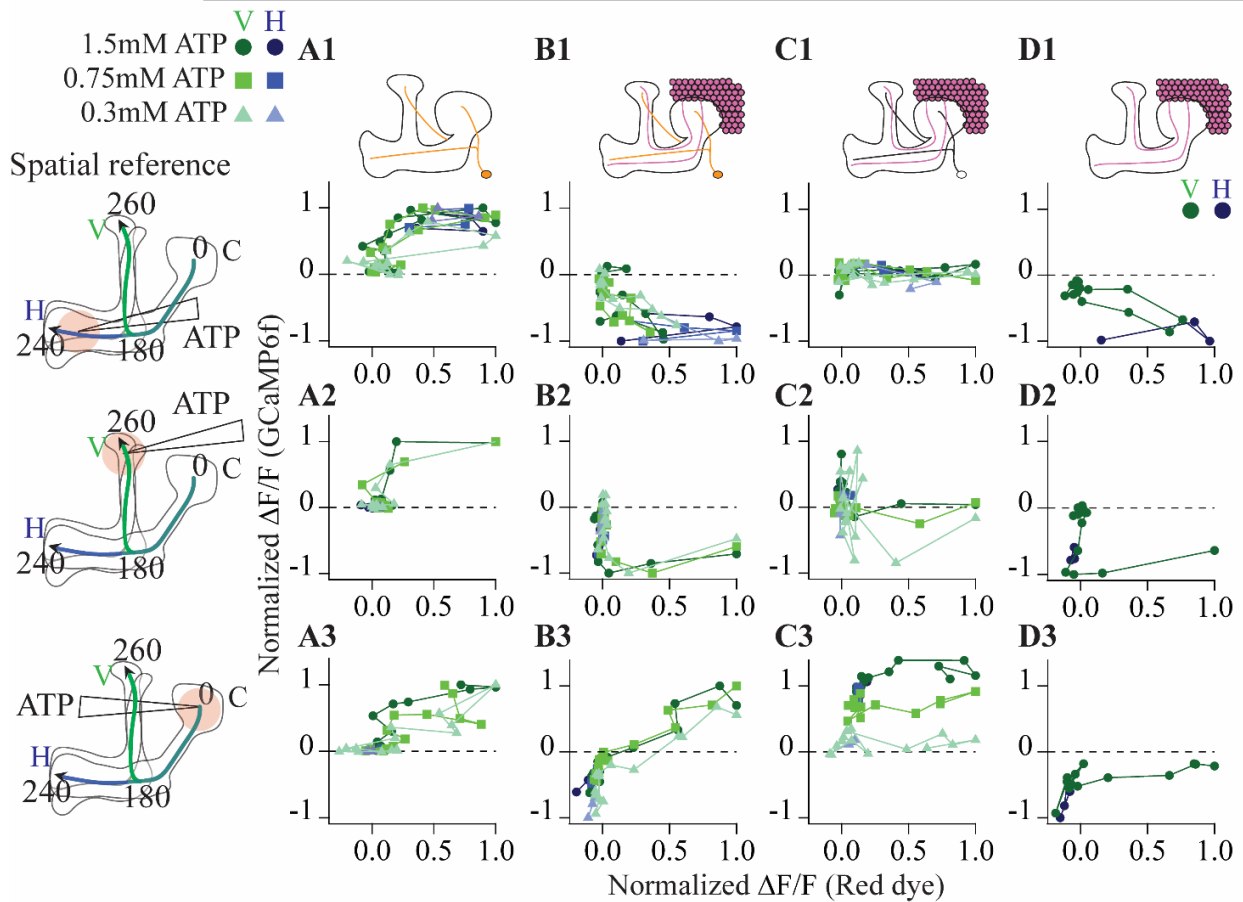


**Figure 3.26 GCaMP6f vs red dye plot for APL neuron activation/GABA application**

Plots of neuronal responses measured by GCaMP6f signal vs red dye signal of data from (A1-A3) Fig. 3.4, (B1-B3, D1-D3) Fig. 3.7, (C1-C3) Fig. 3.8, 3.9, and 3.10. The points represent individual 3D skeleton segments. Horizontal and vertical branch segments are shown in blue and green, respectively. (A-D) top: Table showing which neurons were imaged, fly genotype, and stimulus type, with MB schematics below showing which neuron expresses what transgene(s). Left: MB schematics showing the 3D-skeleton distance measurements, with the calyx represented by 0, and the vertical and horizontal branches represented in green and blue colours, respectively. Fly genotype: (A1-A3) VT43924-Gal4.2>UAS-GCaMP6f, UAS-P2X2, MB247-DsRed. (B1-B3) VT43924-Gal4.2>UAS-P2X2, MB247-LexA>LexAop-GCaMP6f. (C1-C3) UAS-P2X2, MB247-LexA>LexAop-GCaMP6f. (D1-D3) OK107-Gal4>UAS-GCaMP6f. The legend above the schematics shows the colour-coding of the different concentrations.

Imaged	KC	KC	KC
Genotype	KC>GCaMP6f APL>P2X2	KC>GCaMP6f P2X2 (No driver)	KC>GCaMP6f
Stimulus	ATP IAA	ATP IAA	7.5 mM GABA IAA

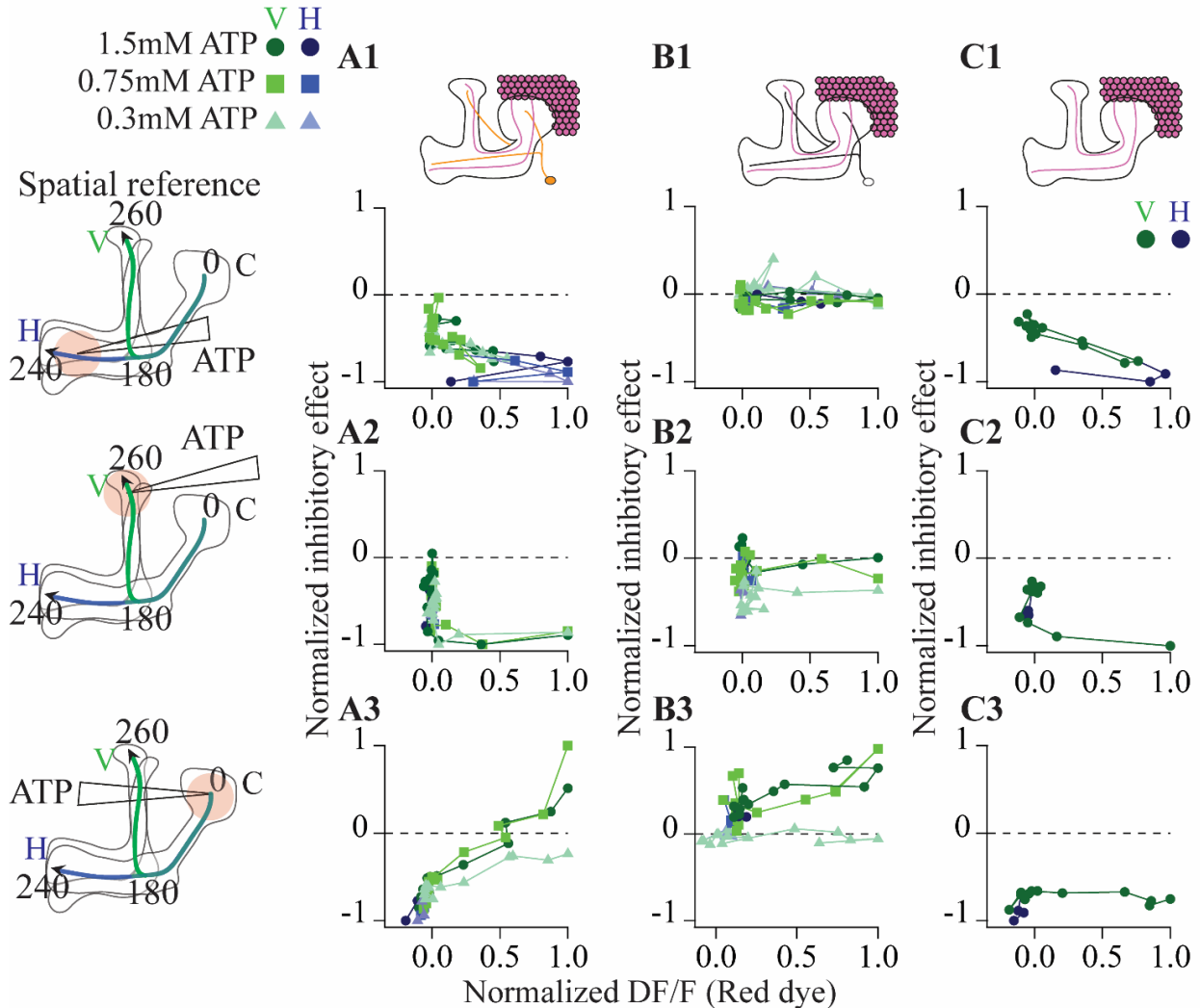


**Figure 3.27 Normalized inhibitory effect vs red dye plot for APL neuron activation/GABA application recordings**

Plots of normalized inhibitory effect vs red dye signal of data from **Fig. 3.24**. The points represent individual 3D skeleton segments. Horizontal and vertical branch segments are shown in blue and green, respectively. (**A-D**) top: Table showing which neurons were imaged, fly genotype, and stimulus type, with MB schematics below showing which neuron expresses what transgene(s). Left: MB schematics showing the 3D-skeleton distance measurements, with the calyx represented by 0, and the vertical and horizontal branches represented in green and blue colours, respectively. Fly genotype: (**A1-A3**) VT43924-Gal4.2>UAS-P2X2, MB247-LexA>LexAop-GCaMP6f. (**B1-B3**) UAS-P2X2, MB247-LexA>LexAop-GCaMP6f. (**C1-C3**) OK107-Gal4>UAS-GCaMP6f. The legend above the schematics shows the colour-coding of the different concentrations.

In contrast, the red dye signal spread was a poor indicator of how widespread the suppressive effect on KC baseline activity (**Fig. 3.26 B1-B3**) and the inhibitory effect on KC odour responses were (**Fig. 3.27 A1-A3**). This was particularly evident when puffing ATP on the vertical lobe (panel **A** in **Fig. 3.26** and **3.27**). However, the fact that ATP stimulation evoked spatially restricted activity in the APL neuron (**Fig. 3.4**, **Fig. 3.26 A1-A3**) argues that the widespread inhibitory effect was not caused by the ATP diffusing extensively. Instead, there are other possible explanations for the widespread inhibitory effect (discussed below).

### 3.3 Discussion

#### 3.3.1 Whole-MB characterisation of activity spread in the APL neuron

My findings characterise activity propagation in the APL neuron throughout its projections in the MB. My initial experiment showed that activity originating in the vertical lobe or the calyx attenuates before it reaches the other region (**Fig. 3.1**). This experiment built on the evidence in Papadopoulou et al., 2011 that no spikes were observed in the APL neuron when recording from the cell soma with a sharp electrode. Instead of relying on measurements from the cell soma, however, this was based on direct imaging of the APL neuron's projections in the MB.

I expanded upon these findings by using a custom-written MATLAB code to generate a 3D-skeleton of the entire MB, allowing me to characterise activity spread in the APL neuron in equally spaced segments. This demonstrated how activity attenuates as it propagates from the puff site and outwards (**Fig. 3.3** and **Fig. 3.4**). Additionally, I observed that activity evoked by stimulation of the different puff sites propagated to varying extents. Puffing on the vertical lobe evoked strongly restricted activity in comparison to puffing on the horizontal lobe or the calyx (**Fig. 3.4 A1 vs A2 and A3**). The comparatively lower activity propagation for puffing ATP on the vertical lobe could be explained by differences in tissue structure that affect the extent to which ATP disperses when puffed onto the different regions, as suggested by the spread of the red dye. For puffing on the vertical lobe, the red dye signal was undetectable after propagating only ~20-30  $\mu\text{m}$  from the peak of the signal (green dashed line in **Fig. 3.4 A2-C2**) compared to puffing on the horizontal lobe or calyx (blue dashed lines in **Fig. 3.4 A1-C1** and **A3-C3**) where the signal persists until ~100  $\mu\text{m}$ . Another contributing factor could be that there are spatial differences in expression of the ion

channels that drive activity spread in the APL neuron, such that activity originating from different regions can propagate to a different extent.

The spread of the red dye signal followed the spread of activity, but somewhat underestimated activity spread in the APL neuron (striped blue and green lines in **Fig. 3.4**, and further analysed in section **3.2.6**). This could be explained by the greater molecular mass of the red dye compared to the ATP, making the dye spread less extensively. Or it could simply be due to the level of passive spread that occurs within the APL neuron. Most likely it is a combination of both. Therefore, it is plausible that local excitatory input from KCs to the APL neuron during odour stimulus is even more localised than what I observed with artificial activation. This possibility is further supported by the observation that ATP stimulation with the lowest concentration evoked a stronger response than that observed with odour stimulus (**Fig. 3.3 A1-A3** vs **Fig. 3.5**).

It is possible that part of the activation of the APL neuron observed in **Fig. 3.3** arose from feedforward excitation from KCs, because UAS-P2X2 showed leaky expression (**Fig. 3.6** and **Fig. 3.7**), which led to local activation of KCs when ATP was applied to the MB. This was mainly the case when puffing on the calyx, and not the lobes (**Fig. 3.8**, **Fig. 3.13**, and **Fig. 3.17**). Thus, it is unlikely to play any role for the results observed for puffing on the lobes.

Do these findings exclude the possibility that there are spikes in the APL neuron? It is possible that spikes restricted to individual neurites are not detected when recording from the cell soma, as electrical signals evoked by synaptic inputs to dendrites can be spatially restricted. This implies that the APL neuron has only been electrically recorded from by sharp electrode in the cell soma (Papadopoulou et al., 2011). Thus, it is feasible that spikes are generated in segregated projections of the APL neuron, and that they simply do not reach very far due to limited active conductance. It follows that I cannot exclude from my GCaMP6f recordings of activity in the APL neuron that it operates by graded potentials only. Visualisation of ion channel expression throughout the APL neuron's neurites could provide further clues to this question.

What do these findings indicate about where the APL neuron imposes sparse coding on KC cell soma odour responses? The spatial segregation between activity in the calyx and the MB lobes (**Fig. 3.4**), together with the finding that local stimulation of the APL neuron in the calyx inhibits KC odour responses (**Fig. 3.25**), suggests that the sparse coding observed in KC cell soma arises from feedback inhibition onto KC dendrites in the calyx.

Finally, I cannot exclude that there is a difference between the spread of the calcium signal observed in the APL neuron and the extent to which local stimulation depolarises the APL neuron. As noted in section **1.2.11**, there can be differences between changes in membrane potential and calcium fluctuations. A small change in membrane potential does not necessarily equal a change in calcium influx. It follows that there could be more widespread depolarisation in the APL neuron than the calcium signal I recorded would suggest. This point and other limitations of my experimental approach are further discussed in section **6.5.1**

### 3.3.2 Local and distal effects of APL activation on KC activity

The prospect of the APL neuron operating locally, both in terms of input and output, is of great interest with regards to the compartmentalised architecture of the MB lobes, as this is where the reinforcement signal from DANs and the odour identity carried in the KC axons coincide, giving rise to plasticity in the KC-MBON synapse (Cognigni et al., 2018, Hige, 2018).

Having established that input to the APL neuron is localised to a degree, I then characterised the spatial extent of feedback inhibition from the APL neuron onto KCs. Local activation of the APL neuron with ATP while imaging KC baseline fluorescence levels revealed that there was baseline activity in the KCs (**Fig. 3.6** and **Fig. 3.7**). This is in agreement with previous studies showing that there is subthreshold activity and spontaneous spikes in KCs (Gu and O'Dowd, 2006, Turner et al., 2008).

When puffing ATP on the horizontal lobe, KC baseline activity was suppressed locally, but also to a lesser and declining extent distally (**Fig. 3.7 A1-C1**). The spatial extent of this effect was largely similar to the extent of activity spread in the APL neuron for all ATP concentrations (compare panel **A1** to **B1** in **Fig. 3.8-3.10**). APL activation in the horizontal lobe had a more widespread effect on KC odour responses compared to the effect on KC baseline activity (compare panels **A1-C1** in **Fig. 3.7** to **A1-C1** in **Fig. 3.25**), but the effect was still strongest locally for 0.75 and 1.5 mM ATP (**Fig. 3.25 B1** and **C1**).

Surprisingly, puffing on the vertical lobe also had a widespread effect on KC baseline activity that almost reached the calyx (**Fig. 3.7 A2-C2**), in stark contrast to its strongly attenuating activity spread in the APL neuron (compare panel **A2** to **B2** in **Fig. 3.8-3.10**). Similar results were obtained

for the inhibitory effect of APL neuron activation on KC odour responses, but here the distal effect seemed even more pronounced (**Fig. 3.25 A2-C2**).

What could explain this widespread inhibitory effect? First, it is unlikely that this effect is due to widespread diffusion of ATP from the puff site, because locally activating the APL neuron with ATP mainly evoked a strong local response that decayed with distance from the puff site, particularly when puffing on the vertical lobe (**Fig. 3.4, Fig. 3.26 A1-A3**). Thus, although the red dye spread was a poor estimator of how widespread KC odour responses were inhibited by activating the APL neuron (**Fig. 3.27 B1-B3**), it is unlikely to mean that the ATP spread or diffused widely.

Another possibility is that ATP stimulation of the APL neuron evoked activity and elicited neurotransmitter release in a more widespread manner than the GCaMP6f signal in the APL neuron suggested. If so, I would have expected local GABA puffing on the MB to have a more local effect. However, this explanation also seems unlikely, because locally puffing GABA on the MB lobes had widespread effects on KC baseline activity and odour responses (panel **D1** in **Fig. 3.7** and **3.25**). This suggests that the widespread inhibitory effect of local activation of the APL neuron is not due to widespread release of GABA from the APL neuron, because a similar inhibitory effect was observed with local application of GABA.

Although the spread of activity did not propagate farther than the peduncle in the APL neuron when puffing ATP on the horizontal lobe (**Fig. 3.4 A1-C1**), it is possible that the inhibitory effect reached the axon initial segment-like region in KCs (Trunova et al., 2011). There is some evidence to suggest that action potentials can backpropagate from this region to the dendritic branches of KCs: odour stimulus that evokes a response in the vertical lobe is correlated with widespread calcium influx in the dendrites, while only local calcium transients are observed in the calyx when the odour stimulus does not evoke any response in the lobes (Li et al., 2013). This could be due to backpropagation of spikes, or it could simply mean that KCs require multiple inputs to spike (Gruntman and Turner, 2013).

If KC spikes do backpropagate from their generation site, it could explain why I observed an inhibitory effect on KC neurites in the calyx when I puffed ATP on the horizontal lobe (**Fig. 3.25 A1-C1**). However, this cannot explain why puffing ATP on the vertical lobe influenced KC odour

responses in the calyx, because there is hardly any spread of activity in the APL neuron when puffing on the vertical lobe (**Fig. 3.4 A2-C2**)

Since neurotransmitter vesicle release is dependent on calcium influx, it seems reasonable to assume that the APL neuron only releases GABA where there is a detectable increase in GCaMP6f signal when it is artificially activated. However, it is possible that the dynamics of activity spread in the APL neuron differ during odour stimulus, either because the widespread activation of the APL neuron evoked by KC spikes facilitates propagation of activity spread to a greater extent, or because other, unspecified neurons can modulate activity spread in the APL neuron during odour stimulus. But if the widespread effect was due to modulation of activity spread in the APL neuron during odour stimulus, then local GABA application should not have recapitulated the results of ATP application. And yet it did (compare panel **A1-C1** to **D1** and **A2-C2** to **D2** in **Fig. 3.25**). Instead, a different mechanism must be responsible.

A previous study found that PNs and LNs are excited by artificial activation of KCs in the MB lobes using P2X2 and identified several neurons with processes in the MB lobes and AL as potential candidates that could convey this positive feedback from KCs to PNs (Hu et al., 2010). The study did not quantify to what extent this feedback from KCs to PNs affects KC odour responses. Regardless, this could explain the widespread inhibitory effect that activating the APL neuron in the lobe has on KC odour responses throughout the MB.

Another factor could be that homeostatic control mechanisms are disrupted when the APL neuron is artificially stimulated to release excess GABA during odour exposure. Dysfunction of glial cells is known to play an important role in epileptic seizures, possibly due to their role in regulating ion balance (Kunduri et al., 2018, Mazaud et al., 2019, Weiss et al., 2019, Rusan et al., 2014) Perhaps the local increase in GABA concentration exceeds the capacity of mechanisms that control neuronal excitability by regulating ion balance. It is unclear how glial cells could mechanistically propagate an effect of excess GABA, but a previous study has shown that calcium waves can propagate through neighbouring glial cells (Newman, 2001), and there are networks of glial cells innervating the fly brain, including ones that specifically surround the mushroom body (Awasaki et al., 2008).

What differences were there between the inhibitory effect of puffing ATP vs GABA on the MB? The suppression of KC baseline activity and odour responses were stronger when puffing ATP on the horizontal lobe compared to puffing on the vertical lobe (compare panel **A1-C1** to **A2-C2** in

**Fig. 3.6** and **3.24**), whereas with GABA the suppression observed when puffing on either region was similar. (compare panel **D1** to **D2** in **Fig. 3.6** and **3.24**). This could be explained by the APL neuron forming more or stronger synapses with KCs in the horizontal lobe. It seems more plausible than the horizontal lobe being more sensitive to inhibition or expressing a higher density of GABA receptors. If either of these alternatives were true, the GABA puffing should then also have affected the horizontal lobe more strongly than the vertical lobe. Another possibility is that the density of P2X2 channels is higher in the horizontal lobe. However, there was not a great difference in the amplitude or duration of evoked activity in the APL neuron between stimulation of the vertical and horizontal lobe (compare panels **A1-C1** to **A2-C2** in **Fig. 3.3**).

During my experiments, I obtained results indicating that there was leaky expression of the P2X2 construct (**Fig 3.6 A3-C3**). Leakiness can arise from activation of the transgene construct promoter by endogenous transcription factors (Akmammedov et al., 2017). Although the leaky expression of P2X2 meant that puffing ATP on the calyx locally stimulated KCs, their lobular projections showed a decrease. This is likely due to P2X2 opening creating an influx of calcium to enter the KCs locally where the ATP is applied, leading to an increased signal from GCaMP6f in the calyx. At the same time the APL neuron is activated, inhibiting the KCs in the calyx, but not blocking the calcium influx. The decrease in KC activity in the lobes likely arises from the inhibition of KCs in the calyx, blocking or reducing spike generation. This is supported by the results obtained from the negative control flies when applying 0.75 and 1.5 mM ATP. Without the APL neuron driver, puffing ATP on the calyx mainly evokes an increase in calcium throughout the KC projections, suggesting that the KCs are depolarised in the calyx, presumably generating spikes (panel **C3** in **Fig. 3.9** and **3.10**).

## 4 Characterising electric shock responses and plasticity in the APL neuron

### 4.1 Introduction

What is the role of the APL neuron in MB memory formation, and where in the neuron are memory traces formed? We know from a previous study that the APL neuron is required for 3h labile memory (Pitman et al., 2011). The APL neuron responds to ES, and punishment learning with ES reinforcement induces plasticity in the APL neuron (Liu and Davis, 2009, Zhou et al., 2019).

This is of great interest in relation to the architecture of the MBON and DAN projections, because the plasticity induced in KC-MBON synapses is compartment-specific, depending on the type of stimulus and the training protocol (Aso et al., 2012, Lin et al., 2014b, Huetteroth et al., 2015, Hige et al., 2015, Aso and Rubin, 2016). If there are spatially differential ES responses and plasticity in the APL neuron, it would suggest that, within the APL neuron, information related to memory formation remains localised.

Zhou et al. found that the APL neuron showed an increase in calcium signal upon activation of dopaminergic neurons, which was enhanced by knocking down the dopamine 2-like receptor, suggesting that activation of dopaminergic neurons has, directly or indirectly, both an excitatory and inhibitory effect on the APL neuron. This study also confirmed a previous finding that the APL neuron responds to electric shocks ((Liu and Davis, 2009), and went further to show that electric shock-odour coupling induces plasticity in the APL neuron in a dopamine 2-like receptor dependent manner, leading to a reduced response in the APL neuron to the odour paired with electric shock. However, the authors only imaged APL neuron responses in a single plane of the vertical lobe (Zhou et al., 2019). Thus, it is unclear if there are spatial differences in ES responses and plasticity in the APL neuron.

## 4.2 Results

### 4.2.1 APL neuron ES responses are spatially differential

To determine the spatial nature of the APL neuron's response to ES stimulus, I subjected flies expressing GCaMP6f in the APL neuron to electric shocks by placing a copper grid coupled to a current stimulator against the abdomen of the flies, and stimulated them with 32 mA 1.2s pulses. To quantify the responses, I subdivided the MB into the top-middle part of the vertical lobe (V), the lower part, or stalk, of the vertical lobe (S), the  $\gamma 1$ - $\gamma 3$  compartments, and the remainder of the horizontal lobe (H). This subdivision was based on the findings in a previous study, suggesting that the vertical stalk region is particularly responsive to ES stimulus, and undergoes plasticity (Zhou et al., 2019), and other studies that found the dopaminergic neurons innervating the  $\gamma 1$ - $\gamma 3$  compartments to respond to electric shocks or drive negative reinforcement when activated (Aso et al., 2012, Cohn et al., 2015).

Visual inspection of the results suggests that there may be electric shock responses, albeit a small one, in all the ROIs I selected. However, due to noisy data and generally low amplitude responses, it was difficult to determine if there was an actual response to electric shocks in any region other than V. Electric shock stimulus elicited a clear response in the V region, but otherwise only the response in the  $\gamma$  region was statistically significantly different from zero (**Fig. 4.1 C**, indicated by hash symbols). The mean values for the regions were quite similar, apart from V: V (0.2568), S (0.07730),  $\gamma$  (0.07346), H (0.06847). The response in V was statistically significantly different to the response in any other region, while the response in  $\gamma$  was not different from the responses in S and H (**Fig. 4.1 C**, indicated by asterisks). Based on these findings it seems that the APL neuron's responses to electric shock stimulus is spatially distinct.

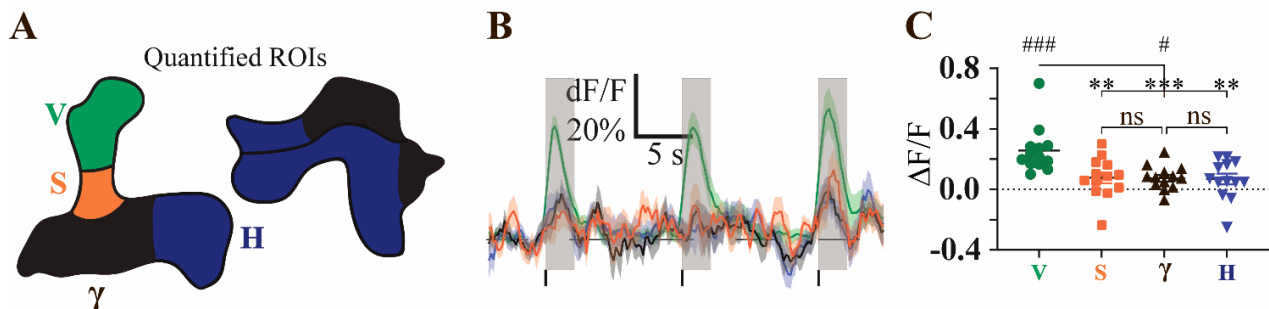


**Figure 4.1 Spatially differential responses to ES in the APL neuron**

Imaging responses of the APL neuron to ES in 474-Gal4>GCaMP6f flies. **(A)** Schematic of the ROIs that were used for quantification of the APL neuron's responses. The colour-coded letters represent these regions. **(B)** APL neuron response traces to ES stimulus. Three shocks lasting 1.2 s at 32 mA were delivered with a 12s interval. Black vertical bar indicates onset of the electric shock. Grey-shaded time windows indicate the interval (2.5s) that was used for quantification of the average response. **(C)** Scatter plot showing quantification of APL neuron responses to ES. Data shown is the mean response of each ROI during the grey-shaded time windows, averaged across all three stimulus trials. Each point represents an individual recording. One sample t-test vs null hypothesis (0) with Bonferroni correction for multiple comparisons, ### $p < 0.001$ , # $p < 0.05$ . One-way ANOVA for V against H, S, and  $\gamma$ , and  $\gamma$  against H and S \*\*\* $p < 0.001$ , \* $p < 0.05$ .  $n = 12$  flies.

## 4.2.2 Characterising plasticity in the APL neuron

Having characterised the APL neuron's responses to electric shock stimulus, I used the same approach to determine if there were any spatial differences in the plasticity induced in the APL neuron from electric shock-odour coupling. To validate that the experimental setup was able to induce plasticity, I first conducted a control experiment where I looked at the odour responses of MBON  $\gamma 2\alpha'1$ , where a memory trace is formed after electric shock-odour coupling, leading to a decreased response to the CS+ odour (Berry et al., 2018).

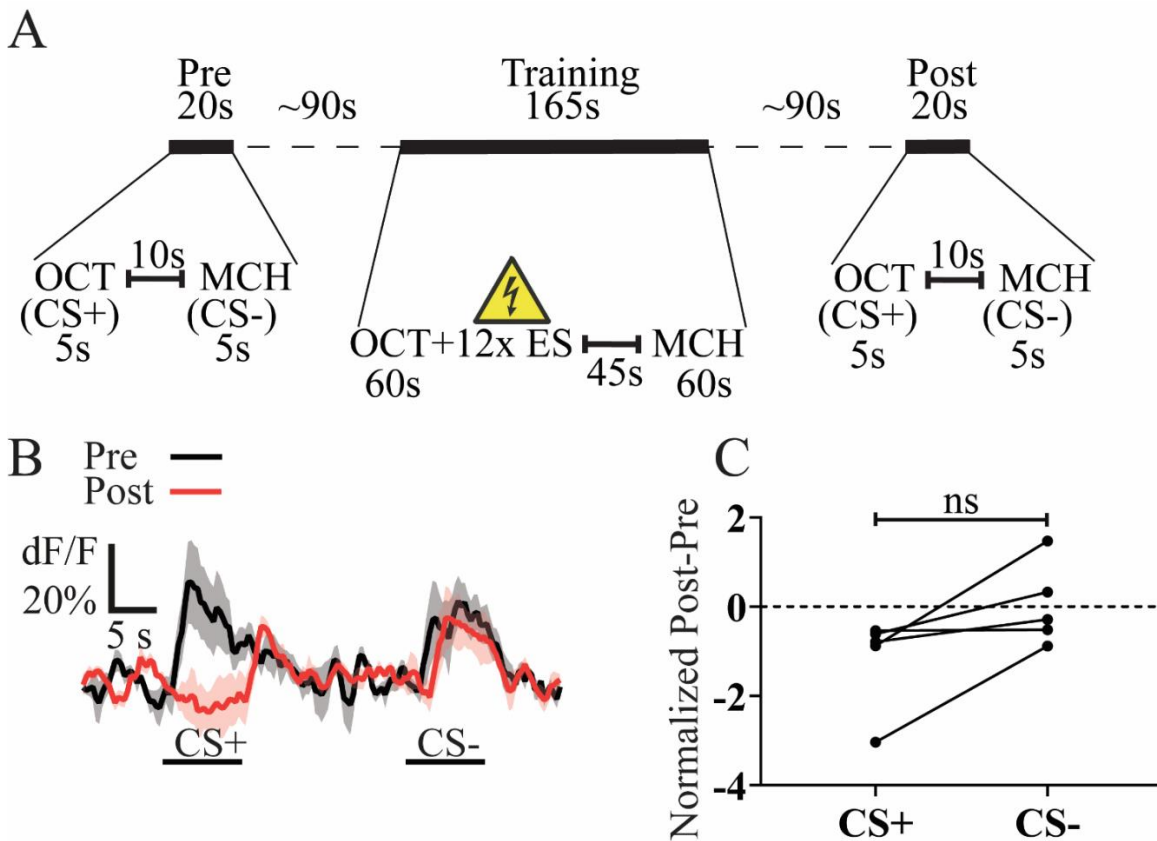


**Figure 4.2 ES-odour pairing reduces odour response to CS+ in MBON $\gamma 2\alpha'1$**

Imaging and quantifying responses of MBON $\gamma 2\alpha'1$  in MB077B>UAS-GCaMP6f flies to OCT and MCH pre and post conditioning. ROIs were drawn around all visible neurites through a whole-MB scan. (A) Flies were exposed to OCT for 5s, then MCH for 5s, with a 10s interval between the two odour pulses. After approximately 90s the flies were subjected to the training protocol, which consisted of 12x electric shocks coupled to 60s of OCT exposure, followed by 60s MCH exposure, with a 45s interval between the two odour pulses. This was followed by a post-conditioning test that was identical to the pre-conditioning protocol. (B) MBON $\gamma 2\alpha'1$  pre- (black) and post-conditioning (red) response traces showing the average response across all recordings (SEM shading. Black horizontal bar shows the onset and duration of CS+ and CS-. (C) Plot showing the difference between post- and pre-conditioned average responses of MBON $\gamma 2\alpha'1$  to CS+ and CS-, normalized to the peak CS+ and CS- pre-conditioning responses, respectively. The responses were quantified by taking the average from 0.5 s after odour pulse onset to 4 s into the odour pulse. Paired data are connected with lines. Paired t-test.  $n = 5$  (4 flies).

For training, the flies were subjected to 12 electric shock stimuli coupled to OCT and then exposed to MCH in absence of any shock stimulus (**Fig. 4.2**). The protocol was adapted from (Berry et al., 2018).

There was a clear decrease in the CS+ response after training, while the CS- pre- and post-conditioning responses looked very similar (**Fig. 4.2 B**). However, I found no statistically significant difference between the CS+ and CS- (**Fig. 4.2 C**) likely due to low sample size. Power analysis revealed that with the observed effect size, a sample size of 10 would yield a statistically significant result with a significance level of  $p < 0.05$ .

Despite that the control experiment did not show a statistically significant result, I was confident that the protocol successfully induced plasticity in  $MBON\gamma2\alpha'1$  due to the visually obvious difference between CS+ and CS-, and because another member of our group observed a similar, but statistically significant, effect (personal communication, Andrew Lin).

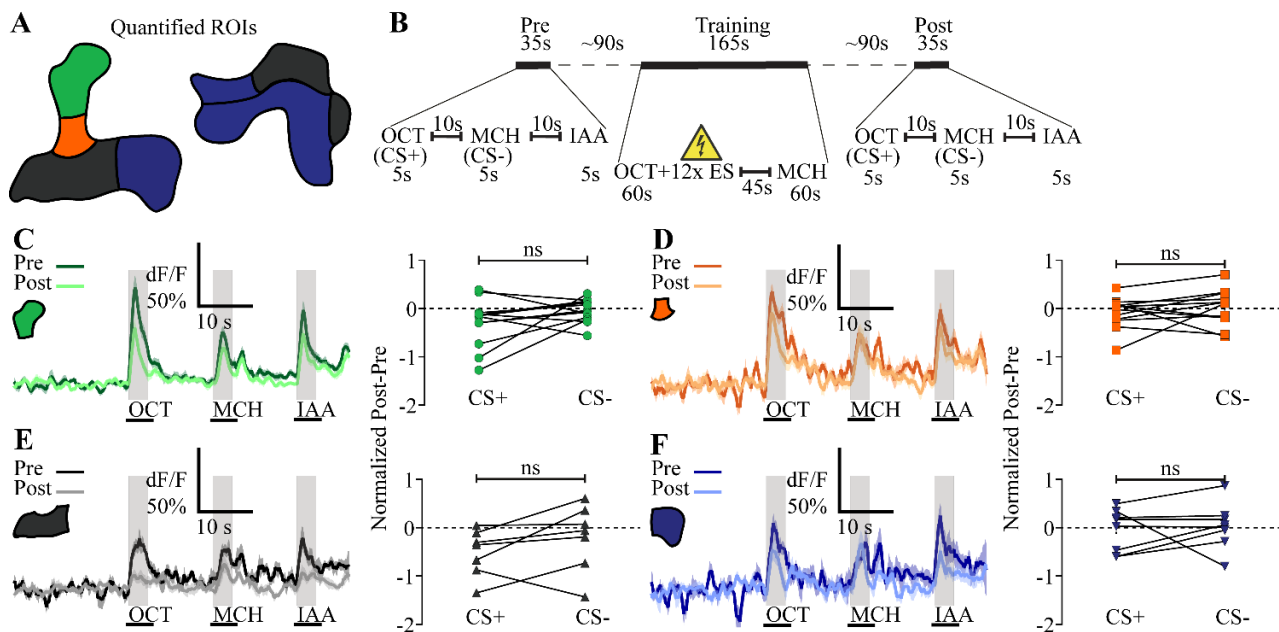


**Figure 4.3 ES-odour pairing in the APL neuron**

Imaging and quantifying responses of the APL neuron in 474-Gal4>UAS-GCaMP6f, MB247-DsRed and 474-Gal4>UAS-GCaMP6f, UAS-GCaMP6f, MB247-DsRed flies (pooled data) to OCT, MCH and IAA pre and post conditioning. (A) Schematic of the ROIs that were used for quantification of the APL neuron's responses. The colour-coded letters represent these regions. (B) Flies were exposed to OCT, MCH, and IAA consecutively for 5s each with a 10s interval between each odour pulse. After approximately 90s the flies were subjected to the training protocol, which consisted of 12x ESs coupled to 60s of OCT exposure, followed by 60s MCH exposure, with a 45s interval between the two odour pulses. This was followed by a post-conditioning test that was identical to the pre-conditioning protocol. (C-

**F)** Left: APL neuron pre- (dark) and post-conditioning (light) response traces showing the average response across all recordings (SEM shading). Traces are colour-coded to match the ROI they represent. Black vertical bar indicates onset of the odour pulses. Grey-shaded time windows indicate the interval that was used for quantification. Right: Plots showing the difference between post- and pre-conditioned responses of the APL neuron to CS+ and CS-, normalized to the peak IAA pre- and post-conditioning responses, respectively. Paired data are connected with lines. Paired t-test. n = 5 (4 flies). n (**C**, **D**) = 12 (10 flies). n (**E**) = 7 (6 flies). n (**F**) = 8 (6 flies)

Thus, I decided to apply the same protocol to see if this would induce plasticity in the APL neuron, and if the plasticity would be spatially differential (**Fig. 4.3**). I observed no statistically significant difference between CS+ and CS- for any of the ROIs that I quantified. While there was a clear decrease in the CS+ response for the  $\gamma$  region post conditioning, there was also a strong decrease in the AA response, suggesting that the effect was not specific for the conditioned odour (**Fig. 4.3 E**). The p-values for the V and  $\gamma$  ROIs indicated that, if anything, these regions showed the strongest trend towards a significant effect: V (p=0.3481),  $\gamma$  (p=0.3458), S (p=0.9077), H (p= 0.9856).

## 4.3 Discussion

### 4.3.1 Characterisation of electric shock responses in different regions of the APL neuron

My findings confirm that the APL neuron responds to ES. This expands on the previous findings in Liu, X., Davis, R. L., 2009 and Zhou et al., 2019 by recording the APL neuron's responses to electric shock throughout the MB simultaneously. Sampling the whole MB meant that the data for the deeper regions (S,  $\gamma$ , H) was very noisy. Light scattering increases as the beam passes through more tissue, and the sampling rate decreases the larger the imaged volume. Both of these factors lower the signal-to-noise ratio. Based on my results, I cannot exclude that there is a response to electric shock throughout the APL neuron in the ROIs I chose to quantify, despite only finding that the responses in the V and  $\gamma$  regions were statistically significantly different from zero, particularly when you consider that the means for S,  $\gamma$ , and H were quite similar, and that the spread of the data for these three regions are quite similar with the exception of one negative outlier for both S and H (**Fig. 4.1 C**).

It remains unclear from where the APL neuron receives the electric shock input. Dopaminergic neurons that respond to electric shocks are one of the main candidates. Dopaminergic neurons

innervating various parts of the MB lobes respond to electric shocks, including the  $\gamma 1$ -  $\gamma 3$  compartments, and parts of the vertical lobe (Mao and Davis, 2009, Cohn et al., 2015, Dylla et al., 2017). It is not yet established if the response profiles of different DANs are specific to punishment or reward, or what functional significance their varying degrees of response hold. Activation of PPL1 DANs can substitute for aversive learning (Aso et al., 2010, Claridge-Chang et al., 2009), suggesting that they carry the aversive teaching signal. EM data has confirmed that the APL neuron receives inputs from the PPL1 cluster DANs in the  $\alpha 2$  and  $\alpha 3$  compartments (Takemura et al., 2017). Zhou et al. 2019 used nsyb-GRASP to identify potential synapses between DANs (labelled by TH-LexA) and the APL neuron (labelled by GH146-Gal4), and found that, upon electric shock stimulation, the signal strongly increased in the medial region of the vertical lobe, but also to a smaller extent in the “heel” (roughly  $\gamma 1$ -  $\gamma 2$ ,  $\alpha'1/\beta'1$ , and  $\alpha 1/\beta 1$  compartments) and the “tip” of the horizontal lobe (the rest of the horizontal lobe), suggesting that the APL neuron is broadly connected to various DANs. They confirmed that the APL neuron receives dopaminergic input from the DANs broadly labelled by TH-LexA, by using a G protein-coupled receptor-activation-based DA sensor. The signal from the sensor in the APL neuron increased when the DANs were activated.

However, their findings suggested that dopamine signalling onto the APL neuron through the DD2R receptor is at least partially suppressive: knockdown of this receptor increased the APL neuron's response to electric shock (Zhou et al., 2019). It is also possible that the APL neuron is indirectly activated by DANs through KCs, for which there is some evidence to suggest that this could evoke responses in the APL neuron (Akalal et al., 2010, Dylla et al., 2017).

I intend to repeat the experiment with another APL driver, GH146-Gal4, or the original intersectional approach (Fig. 3.1) to see if I can obtain a better signal. I decided to use 474-Gal4 for the electric shock and plasticity experiments instead of VT43924-Gal4.2 because I was unable to drive expression of GCaMP6f towards the end of my experimental work. This could be due to contamination of the parent stocks, but I did not manage to determine this yet.

#### 4.3.2 No plasticity observed in the APL neuron following electric shock-odour coupling

Despite not finding a statistically significant difference between the change in CS+ response compared to the change for CS- from pre- to post-conditioning, the visually striking difference

between CS+ and CS- reassured me that the training protocol for inducing plasticity in MBON $\gamma$ 2 $\alpha$ '1 was working (**Fig. 4.2**), particularly because another person in our group had used the same protocol and obtained a statistically significant result (Andrew Lin, personal communication).

However, when I used the same training protocol and imaged odour responses in the APL neuron, I observed no statistically significant difference between CS+ and CS- for the difference in pre- to post-conditioning responses for any of the ROIs I chose (**Fig. 4.3 C-F**). It should be noted that for about half of the recordings I had to exclude the responses measured from the  $\gamma$  and H regions, on the criterion that the IAA response, or lack thereof, was within 1 standard deviation of the noise (measured as the mean fluorescence signal during the pre-stimulus period). In these cases, the IAA response was also visually absent from the traces. Therefore, there is a discrepancy in the number of recordings for the different ROIs that I quantified. **It was my intention to do the reverse pairing of the odours (MCH as CS+ and OCT as CS-), but due to time constraints I had to omit this part of the experiment.**

The remaining data is a sparse basis for drawing any conclusions, other than that I cannot reject the null hypothesis that there is no statistically significant difference between the change in CS+ and CS- from pre- to post-conditioning. It is possible that a larger data set would reveal a significant difference for one or more of these regions, but it is also possible that the training protocol induces plasticity in MBON $\gamma$ 2 $\alpha$ '1 without affecting the APL neuron. There is, to my knowledge, no studies showing that a protocol that induces plasticity in any given MBON necessarily leads to formation of plasticity in the APL neuron.

I also carried out a preliminary experiment using the training protocol in Zhou et al., 2019, with which the authors observed a depressed CS+ response in the APL neuron. However, my initial data from using this protocol did not show any learning in the APL neuron. Liu et al., 2009 looked at the APL neuron's responses in the horizontal lobe, while Zhou et al., 2019 imaged its responses in a transverse plane of the lower part of the vertical lobe. In contrast, I quantified the APL neuron's responses in volume ROIs. It is possible that I did not find a stimulus-specific suppression because the plasticity is restricted to very specific regions. It is possible that my choice of ROIs masks or averages out formation of plasticity in the APL neuron in one or more regions. A different approach would be to quantify the  $\gamma$ 2 and  $\alpha$ '1 compartments specifically. However, due to how noisy the data is, and these compartments being smaller than the ROIs I chose, this could prove even more difficult to quantify.

Finally, I considered analysing the data with the MATLAB 3D skeleton, but initial attempts at this suggested that the data was too noisy with the level of segmentation that I used for looking at activity spread. Using larger segments could have solved this, as averaging over a larger area could reduce the noise, but that would have defeated the purpose of trying to determine where plasticity in the APL neuron is induced, and also does not differentiate between different parts of the MB, like I was able to by selecting an ROI that corresponds to the  $\gamma 1$ -  $\gamma 3$  compartments.

## 5 Local muscarine application differentially affects KC subsets

### 5.1 Introduction

Metabotropic receptors for glutamate, the main excitatory neurotransmitter in mammals, play an important role in formation of synaptic plasticity (Jörntell and Hansel, 2006, Lüscher and Huber, 2010). However, the complexity of mammalian systems makes it difficult to link the role of metabotropic receptors in synaptic plasticity to subsequent behavioural changes. The fruit fly, *Drosophila*, offers a genetically malleable model system with a simple and well-established behavioural readout for learning-related changes. Memory formation has been extensively studied in fruit flies, particularly in the context of olfactory learning (Cognigni et al., 2018, Amin and Lin, 2019, Hige, 2018), where acetylcholine is the primary excitatory neurotransmitter, which is also the neurotransmitter used by KCs, the principal cells of the MB (Barnstedt et al., 2016). KCs themselves express both the nicotinic (ionotropic) and muscarinic (metabotropic) acetylcholine receptors (Crocker et al., 2016, Croset et al., 2018, Shih et al., 2019). Nicotinic acetylcholine receptors are involved in fast excitatory neurotransmission (Su and O'Dowd, 2003), but little is known about its role in cognitive processes.

Mammalian muscarinic acetylcholine receptors (mAChRs) are subdivided into the generally excitatory ones that signal through the G-protein  $G_{q/11}$  ( $M_1$ -type) and ones that are generally inhibitory ( $M_2$ -type) and signal through  $G_{i/o}$  G protein. *Drosophila* has three known mAChRs, mAChR-A, -B, and -C. Of these, mAChR-A is the most homologous to the mammalian mAChRs. Previous studies suggest that it works like the  $M_1$ -type mAChRs, where activation of the receptor leads to release of calcium from internal stores through  $G_{q/11}$  signalling (Ren et al., 2015, Collin et al., 2013).

A previous study found that knocking down expression of mAChR-A impairs memory formation in *Drosophila* larvae (Silva et al., 2015). However, it is unknown if mAChR-A plays any role in olfactory learning in *Drosophila* adults.

During my PhD I worked on a side-project with collaborators in the laboratory of Dr. Moshe Parnas. We investigated the role of metabotropic acetylcholine receptors in memory formation. We found that the mAChR-A is required for aversive conditioning. RNAi knockdown of the receptor impaired aversive memory formation. The expression of mAChR-A was specifically required in  $\gamma$  KCs. Next, we showed that knockdown of the receptor increased  $\gamma$  KC odour responses, suggesting that the receptor has an inhibitory effect on KCs. In fact, bath application of the mAChR-agonist, muscarine, suggested that the signalling through the receptor has an inhibitory effect on all KC subtypes. Using an mAChR-A construct with a FLAG-tag at the 3'-terminal, we showed that mAChR-A localizes to the calyx, and that overexpression of this construct rescues learning in flies depleted of m-AChR-A, suggesting that mAChR-A exerts its effect on learning in the MB calyx. Finally, we showed that knockdown of mAChR-A impairs aversive memory formation in MBON- $\gamma$ 1pedc $>\alpha/\beta$ .

We initially had not carried out the mAChR-A FLAG-tag localization experiment, and instead relied on a different approach to address this question. While the bath application of muscarine showed that it had an effect on KC odour responses, it provided no information as to where in the MB muscarine had this effect. To pin down where in the MB muscarine affects KC odour responses, we locally puffed muscarine on the calyx and the horizontal lobe to observe if this would differentially affect KC odour responses.

My personal contribution to the study was to demonstrate the effects of locally puffing muscarine on the MB calyx and horizontal lobe. I found that puffing muscarine on either region differentially affected the baseline activity of KC subsets in a time-dependent manner. Muscarine broadly inhibited odour responses when puffed on the calyx, while the effects observed from puffing on the horizontal lobe seemed to mainly affect odour responses in the  $\gamma$  and  $\beta$  lobes.

## 5.2 Results

### 5.2.1 Muscarine differentially affects the baseline activity of KC subsets, but overall inhibits odour responses throughout the MB

To determine the effects of muscarine on KC baseline activity, I locally puffed muscarine on either the calyx or the horizontal lobe and quantified odour responses in the lobes and the calyx (**Fig. 5.1 A**).

The red dye did not spread to the lobes when I puffed muscarine on the calyx. Likewise, I did not observe any red dye signal in the vertical lobe or the calyx when I puffed muscarine on the horizontal lobe (**Fig. 5.1 B**). This suggests that the muscarine remained localised. Puffing muscarine on the horizontal lobe differentially affected the KC subtypes. The  $\gamma$  and  $\beta$  lobes showed a significant decrease in baseline activity 0.5-1.5 s after muscarine application, followed by a gradual rise (**Fig. 5.1 A and C**), while the  $\alpha'\beta'$  lobes showed a significant increase in baseline activity around 3-4 s after muscarine application (**Fig. 5.1 D**). Puffing muscarine on the calyx elicited a significant increase in baseline activity in the calyx and the  $\alpha$  lobe (**Fig. 5.1 E**).

The local increase in calcium levels evoked by puffing muscarine on the calyx (**Fig. 5.1 A**) could be due to release of calcium from internal stores through  $G_{q/11}$  signalling. The effect of puffing muscarine on the calyx seemed to have an opposite effect on the  $\alpha'$  and  $\beta'$  lobes compared to puffing on the horizontal lobe, causing a nonsignificant decline in baseline activity (**Fig. 5.1 A and E**). These results suggested that muscarine differentially affects KC subtypes, on different timescales.

Next, I applied muscarine to the calyx or the horizontal lobe together with odour stimulus (**Fig. 5 F and G**). The muscarine was applied 1 s before the odour stimulus, as this had a stronger impact on the odour responses compared to applying it directly at odour onset (data not shown). Muscarine application on the horizontal lobe significantly decreased responses to OCT throughout the lobes and the calyx, while only decreasing odour responses in the  $\gamma$  and  $\beta$  lobes for MCH stimulus (**Fig. 5.1 G**). This discrepancy is addressed in section 5.3.

Puffing muscarine on the calyx strongly decreased responses to OCT throughout the lobes, except for the  $\alpha$  lobe and the calyx. This is further discussed in section 5.3. Although the responses to MCH were only statistically significantly decreased for the  $\alpha'$  and  $\beta$  lobes, there was a clear decrease in all regions except for the calyx, as is visible from the time courses **Fig. 5.2** panel **C**. The stronger decrease for OCT compared to MCH is possibly because more KCs respond to OCT, and so the effect would be more pronounced (Perisse et al., 2013, Lin et al., 2014a).

The decreased odour response in the calyx evoked by muscarine application suggest that the increase in baseline activity evoked by applying muscarine to the calyx (**Fig. 5.1 A**) is not excitatory. If it was excitatory, it should have summed to cause increase in odour responses, as the calyceal increase in GCaMP6f signal lasted more than 5 seconds, well into the timing of the odour response.

Generally speaking, muscarine application to the MB had no effect on odour responses in the opposite hemisphere (**Fig. 5.1 G** and **Fig 5.2 B, C**). Although there were some regions in the opposite hemisphere that seemed to be affected, it is more likely to be experimental noise than a genuine functional effect, as neither the quantification or the raw time courses showed a consistent effect across odours or across regions (**Fig. 5.1 G** and **Fig. 5.2 B** and **C**).

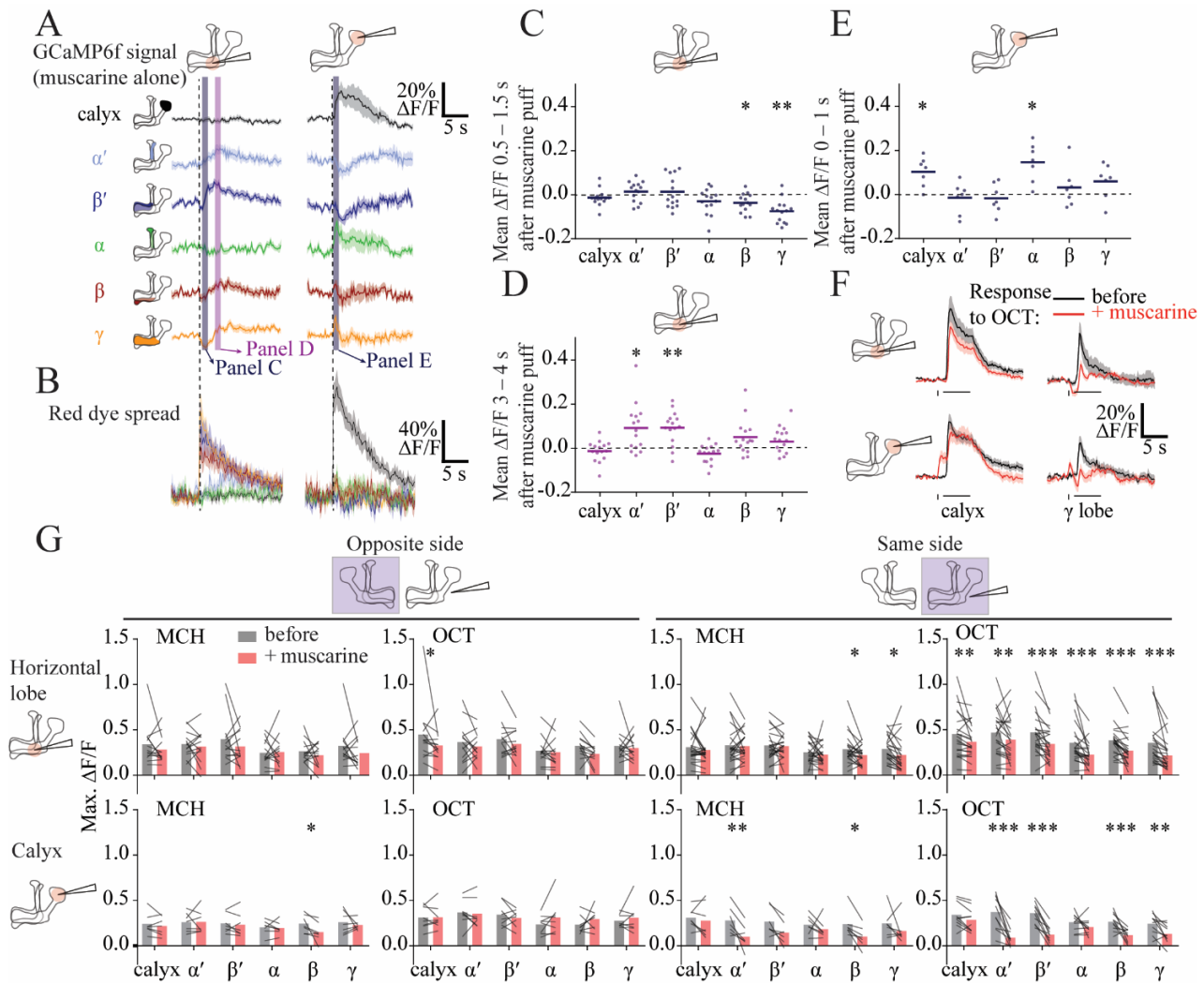


**Figure 5.1 Local muscarine application to the calyx and horizontal lobe differentially affects KC subtypes**

(A) Left: Schematic of MB, showing colour scheme for the different regions where responses were quantified. Right: Average  $\Delta F/F$  GCaMP6f signal in different areas of the MB of OK107>GCaMP6f flies in response to a 10 ms pulse of 20 mM muscarine on the horizontal lobe (left column) or the calyx (right column). Data are mean (solid line)  $\pm$  SEM (shaded area) of all recordings. Dashed vertical line shows the timing of muscarine application. Grey and purple shaded bars indicate time windows used to quantify responses in panel 7C-E. n given as number of hemispheres (number of flies): 15 (8) for pulsing on the horizontal lobe, 7 (5) for calyx.

(B)  $\Delta F/F$  traces of red dye indicator, estimating which MB regions the muscarine spread to. The traces follow the same colour scheme and visuals as shown in panel A.

(C-E) Scatter plot showing average  $\Delta F/F$  of GCaMP6f signal of the different MB regions at time 0.5-1.5 s (C) and 3-4 s (D) following 10 ms pulse of 20 mM on the horizontal lobe or the calyx (E, time 0-1 s), quantified from traces shown in (A). Colours match the shaded time windows in A. n: 15 (8) for pulsing on the horizontal lobe, 7 (5) for calyx. \*  $p < 0.05$ , \*\*  $p < 0.01$ , one-sample t-test (different from 0), Bonferroni correction for multiple comparisons.

(F) Average  $\Delta F/F$  GCaMP6f signal of the calyx and  $\gamma$  lobe during odour pulses of OCT (horizontal bar), before (black) and after (red) muscarine application on the horizontal lobe (top), or the calyx (bottom), 1 s before the odour pulse

(vertical bar). Data are mean (solid line)  $\pm$  SEM (shaded area). n: 12 (8) for pulsing on the horizontal lobe, 7 (5) for calyx. See Figure 5.2 for all traces.

**(G)** Line-bar plots showing paired peak  $\Delta F/F$  GCaMP6f responses of the different MB regions during 5 s odour pulses of MCH or OCT, before (grey) and after (pink) muscarine application to the calyx or the horizontal lobe, in the hemisphere where the muscarine was applied (same side, right) or the opposite (opposite side, left). Muscarine was applied 1 s before the odour pulse. Bars show mean value. n: Horizontal lobe same side MCH 23 (15), OCT 22 (15), opposite side MCH 13 (7), OCT 13 (7). Calyx same side MCH 8(6), OCT 10 (8), opposite side MCH 7 (5), OCT 7 (5). \*  $p < 0.05$ , \*\*  $p < 0.01$ , \*\*\*  $p < 0.001$  by 2-way repeated measures ANOVA with Holm-Sidak multiple comparisons test. n differs for panel **F** vs **G** because a scripting error meant that for 10 of the recordings, the odour pulse paired with muscarine presentation lasted 4 s, not 5 s. These data are included in **G**, because the peak  $\Delta F/F$  always occurred within the first 4 s of the odour pulse and thus was unaffected by the scripting error, but they are excluded from **F** because the stimuli do not match. Adapted from (Bielopolski et al., 2019)

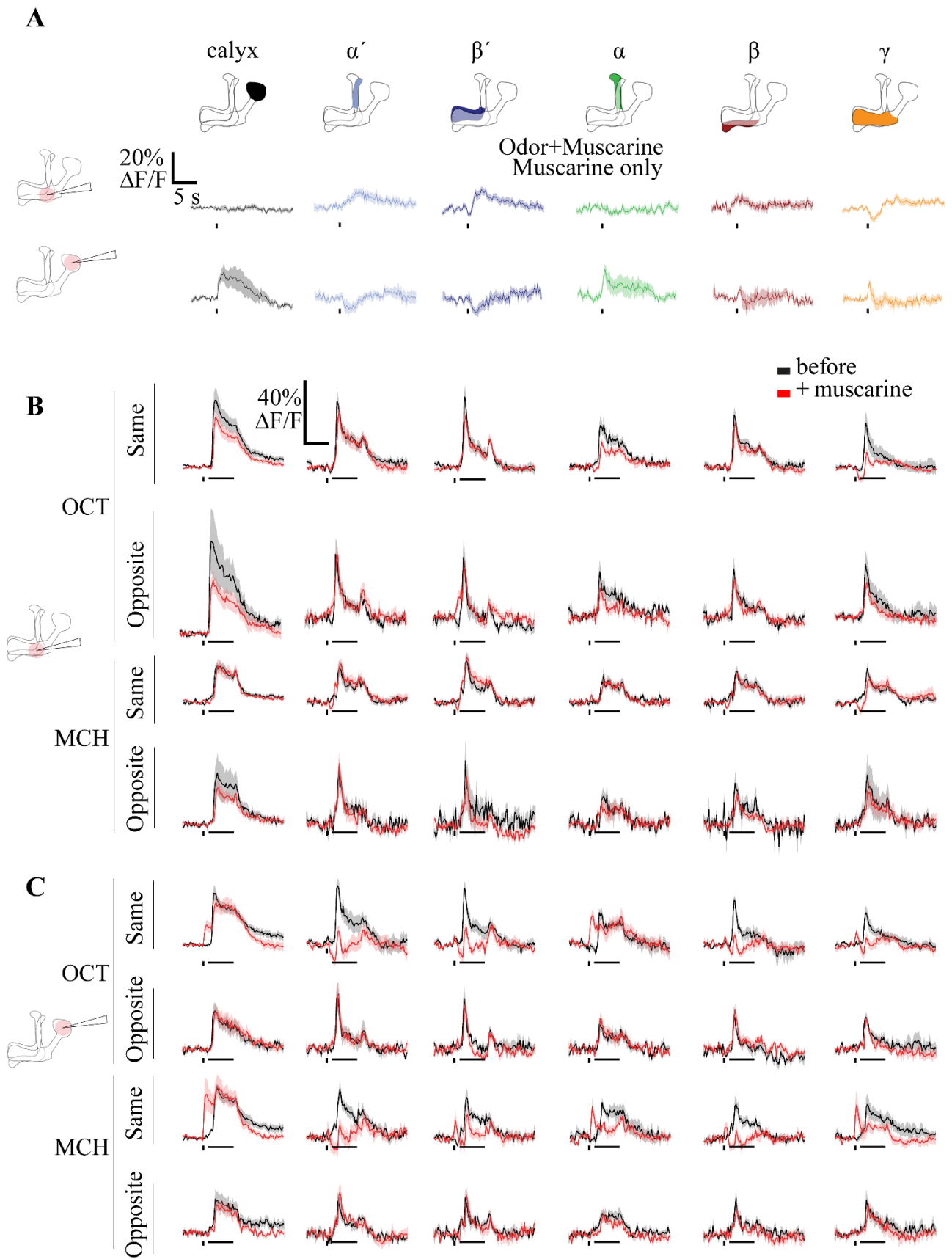


## Figure 5.2 Response traces for local muscarine application

Average  $\Delta F/F$  GCaMP6f traces of the different MB regions of OK107>GCaMP6f flies that only received the muscarine pulse (**A**) or received an odour pulse (MCH or OCT) before (black) or after (red) 10 ms pulse of 20 mM muscarine (**B, C**). Panel **A** is duplicated from **Figure 5.1A**; panels **B, C** are the traces corresponding to the **Figure 5.1G**.

Muscarine was applied either in the horizontal lobe or calyx, 1 s before the odour pulse where applicable. Traces are from the same side or the opposite side that muscarine was applied. Data are mean (solid line)  $\pm$  SEM (shaded area). Horizontal bars indicate odour pulse timing and duration. Vertical bars indicate timing of muscarine pulse. n, by number of hemispheres (number of flies): Horizontal lobe same side MCH 13 (8), OCT 12 (8), opposite side MCH 6 (3), OCT 6 (3), muscarine alone 15 (8). Calyx same side MCH 6 (4), OCT 7 (5), opposite side MCH 5 (3), OCT 5 (3), muscarine alone 7 (5). n for odour + muscarine traces differs between this figure vs. **Figure 5.1 G** because a scripting error meant that for 10 of the recordings, the odour pulse paired with muscarine presentation lasted 4 s, not 5 s. These data are included in **Figure 5.1 G**, because the peak  $\Delta F/F$  always occurred within the first 4 s of the odour pulse and thus was unaffected by the scripting error, but they are excluded from traces shown in this figure because the stimuli do not match.

## 5.3 Discussion

My results from puffing muscarine on the calyx and the horizontal lobe without odour stimulus suggest that the KC subtypes are differentially affected by muscarine signalling. Puffing muscarine on the horizontal lobe decreased the baseline activity in the  $\gamma$  and  $\beta$  lobes, while increasing the signal in the  $\alpha'$  and  $\beta'$  lobes, but at different times after muscarine application (**Fig. 5.1 A, C and D**). For puffing on the calyx, there was an increase in GCaMP6f signal locally and in the  $\alpha$  lobe, nonsignificant decreases in the  $\alpha'$  and  $\beta'$  lobes, and nonsignificant increases in the  $\gamma$  and  $\beta$  lobes (**Fig. 5.1 A and E**).

Muscarine had an inhibitory effect on KC odour responses (**Fig. 5.1 F and G, Fig. 5.1 B and C**). There was a decrease in all regions when puffing muscarine on the calyx. Judging by the raw data, odour responses in all regions decreased (**Fig. 5.2 C**), but only to a modest extent in the calyx. Although the decreased responses in the calyx and  $\alpha$  lobe were not statistically significant for the calyx and the  $\alpha$  lobe (**Fig. 5.1 G**), it is likely that there was a genuine decrease in these two regions, as puffing muscarine on the calyx in absence of odour stimulus increased GCaMP6f signal in these two regions (**Fig. 5.1 A**), but nevertheless led to decreased odour responses in both regions (**Fig. 5.1 G**).

Based on the quantification, puffing muscarine on the horizontal lobe significantly decreased odour responses to OCT in all regions. The time courses showed clear decreases for the calyx,  $\alpha$  lobe, and  $\gamma$  lobe, with only modest decreases in the other regions. For MCH, the quantification suggests that there were significant decreases in the  $\beta$  and  $\gamma$  lobes. Judging by the raw data there was a modest decrease in the  $\gamma$  lobe only (**Fig. 5.2 B**). However, it should be noted that the datasets in **Fig. 5.1 G** and **Fig. 5.2 B** are not identical. Due to a script error, the odour pulse only lasted 4 seconds for 10 of the recordings. This did not matter for the quantification, because the peak response occurred within the first 4 seconds regardless. However, these 10 recordings are not included in the data shown in **Fig. 5.2**, because the stimuli between the dataset with 4 and 5 s odour pulses, respectively, are temporally mismatched. In time courses of these 10 excluded recordings, there is a decreased response to MCH in the  $\beta$  lobe. This explains why quantification of the MCH response in the  $\beta$  lobe shows a decrease (**Fig. 5.1 G**). Therefore, the data suggest that puffing muscarine on the horizontal lobe at least affects odour responses in the  $\beta$  and  $\gamma$  lobes (**Fig. 5.1 G** and **Fig. 5.2 B**). Because there is not a consistent effect for all regions for both odours (**Fig. 5.1 G** and **Fig. 5.2 B**), it remains possible that other regions are also affected, but the data are not conclusive on this point.

What could explain that puffing muscarine on the calyx broadly affected KC odour responses while puffing on the lobe only affected the  $\beta$  and  $\gamma$  lobes? First, puffing on the calyx is likely to affect integration of inputs from the KC dendrites. This means that muscarine signalling in the calyx could affect KC spike generation, which would explain the widespread effect on odour responses.

Puffing muscarine on the horizontal lobe significantly decreased both MCH and OCT odour responses in the  $\beta$  and  $\gamma$  lobes, but not in the  $\beta'$  lobe. This could be due to the lower level of mAChR-A expression in the  $\alpha'\beta'$  KCs as revealed by single transcriptome analysis (Croset et al., 2018, Davie et al., 2018). Another possibility is that there are unknown, intrinsic differences between KC subtypes that causes muscarine signalling to have different effects.

If puffing muscarine on the horizontal lobe genuinely affects KC responses broadly, then it is interesting to note that the effect I observed spread beyond the lobes to the calyx (**Fig. 5.1 G**). One possible explanation is that the muscarine spreads further than the red dye. The MW of muscarine is 174.26 g/mol, which is roughly 1/10<sup>th</sup> of the MW of the red dye (1780 g/mol). Thus, it is likely that the muscarine spreads farther than the red dye. However, puffing muscarine on the horizontal lobe did not evoke any detectable change in the baseline activity in the calyx (**Fig. 5.1 A**). If any

muscarine reached the calyx, it had a considerably weaker effect than what I observed when puffing muscarine directly on the calyx (**Fig. 5.1 A**).

Another possibility is that the inhibitory effect of muscarine on the lobes indirectly affects odour responses in the KC calyceal projections. This far-reaching inhibitory effect is reminiscent of what I observed when I locally activated the APL neuron with ATP in the lobes or puffed GABA on the lobes and observed its effect on KC odour responses (**Fig. 3.25 A1-D1 and A2-D2**).

The far-reaching effect of puffing muscarine on the horizontal lobe could also be mediated through the indirect feedback from KCs to the PNs demonstrated in Hu et al., 2010. This could happen by muscarine inhibiting the KCs locally in the lobes, causing the indirect excitatory feedback from the KCs to PNs to decrease, leading to an overall widespread reduction in KC odour responses.

When we initially submitted the paper, the reviewers argued that, based on the red dye alone, we could not draw conclusions of where muscarine exerts its effect, because we could not exclude that muscarine applied to the lobes simply spread to the calyx, and vice versa. Because muscarine has a considerably lower MW than the red dye, it likely spreads further than the red dye. However, as mentioned before, puffing muscarine on the lobes did not affect KC baseline activity in the calyx, whereas puffing muscarine on the calyx evoked a substantial local increase in baseline activity (**Fig. 5.1 A**), which to me suggests that, if anything did propagate from the lobes to the calyx, it is a negligible amount in terms of baseline activity.

The reviewers further argued that the data did not support our claims about the muscarine differentially affecting KC subtypes, because the observed differences could be due to non-uniform distribution of muscarine to the different KC subtypes. They suggested the data be re-analysed so that only GCaMP6f signal from neuropil where the red dye is present should be included. This is a sound objection to raise, although I think it is likely that the muscarine spreads to neuropil where the red dye does not spread to, or regions where the signal gets canceled out by noise. Regardless, it would be interesting to re-analyse the data to quantify differences in red dye signal between the ROIs, and normalize the effect observed in different subsets to the amplitude of the red dye signal.

To address the issues raised by the reviewers, we conducted a rescue experiment of impaired learning in flies with an mAChR-A deficiency using a FLAG-tagged mAChR-A construct (Bielopolski et al., 2019). The tag allowed us to assess where the mAChR-A localised to, which

could provide a clue as to where it exerts its function. Overexpression of a FLAG-tagged mAChR-A construct rescued the learning deficiency in these flies. The FLAG-tagged mAChR-A only localised to the calyx, suggesting that it exerts its learning-related function in the calyx (Bielopolski et al., 2019).

Considering these findings, it is possible that the results I observed from puffing muscarine arise from muscarine exerting its effect through other receptors than mAChR-A, such as mAChR-B, or unidentified receptors. mAChR-B is 1000-fold less sensitive to muscarine (Collin et al., 2013), but it is possible that muscarine could exert an effect on KC odour responses through mAChR-B if it is expressed in the MB lobes (Bielopolski et al., 2019). Another possibility is that the level of mAChR-A in the lobes was too low to detect with the FLAG-tagged construct, or that the construct mis localised, and failed to be transported to the lobes. The last possibility seems unlikely, as other overexpressed proteins seem to properly localize to KC axons (Trunova et al., 2011, Bielopolski et al., 2019).

Finally, how does muscarine signalling reduce KC odour responses? Previous studies found that *Drosophila* mAChR-A signalling through the receptor works through  $G_{q/11}$  signalling to release calcium from internal stores (Ren et al., 2015, Collin et al., 2013), based on exogenous expression. It is difficult to explain how this on its own would cause a decrease in odour responses. It is possible that muscarine signalling simply has a different effect in KCs to what was observed in the Chinese hamster ovary cells. There are examples of  $G_{q/11}$  signalling inhibiting or reducing currents through calcium and sodium channels (Gamper et al., 2004, Kammermeier et al., 2000, Keum et al., 2014, Suh et al., 2010, Cantrell et al., 1996). Muscarine signalling could similarly inhibit depolarizing currents in KCs (Bielopolski et al., 2019).

## 6 Discussion

### 6.1 Summary of findings

This project aimed to establish whether the APL neuron in the fly olfactory system can locally compute information based on (1) spread of activity within the neuron, (2) the spatial extent of its output, and (3) the spatial nature of its responses to electric shock and learning-induced plasticity. This thesis also contains results from my experimental contributions to a joint publication, where I measured the effect of local muscarine application on KC activity.

I found that there is limited spread of activity between the vertical lobe and the calyx in the APL neuron (**Fig. 3.2**). Using a custom written MATLAB code, I visualised the MB as a 3D-skeleton (**Fig. 3.2**) and quantified activity spread in the APL neuron in the entire MB, and found that activity originating from different sites propagates to different extents (**Fig. 3.3** and **3.4**). Activating the APL neuron in either the lobes or the calyx inhibited KCs (**Fig. 3.6** and **3.7**), suggesting that there is feedback inhibition from the APL neuron to KCs in both the calyx and the lobes. Surprisingly, the inhibitory output of the APL neuron was more widespread than the spread of activity in the APL neuron (**Fig. 3.8-3.10** and **3.20-3.22**). I investigated if this widespread effect on KC activity could be due to more extensive GABA release from the APL neuron than my measurements of activity spread would suggest by locally applying GABA to the MB. However, this widespread inhibitory effect was also observed for local GABA application (**Fig. 3.25**).

My results show that there are spatially local differences in the APL neuron's response to electric shocks, with a strong response in the vertical lobe, but little or no response in other parts of the lobes (**Fig. 4.1**). I did not observe learning-induced plasticity, and thus could not determine if such plasticity in the APL neuron is spatially distinct.

I found that local application of muscarine to the horizontal lobe or the calyx differentially affected baseline activity of KC subsets (**Fig. 5.1 A, C and D**), while broadly inhibiting KC odour responses (**Fig. 5.1 F and G, Fig. 5.1 B and C**).

The following sections will discuss the implications of these findings, how the experimental approach could have been improved, and which experiments to conduct to expand on my findings.

## 6.2 Localised activity in the APL neuron

The implication of my findings on spread of activity in the APL neuron is that local excitatory input to the APL neuron evokes a response that attenuates as it propagates. My measurements are likely an overestimation of how widely activity spreads within the APL neuron, due to dispersion and diffusion of ATP and the large responses evoked by ATP application (discussed in section 3.3.2).

To what extent are inputs originating from different parts of the APL neuron functionally segregated? The results from puffing 1.5 mM ATP on the horizontal lobe evoked a response that attenuated to the extent that it did not reach the calyx, and vice versa for puffing on the calyx (**Fig. 3.4 C3**). Considering the amplitude of the response evoked by this stimulation compared to an odour response (compare panels **C1 and C3** in **Fig. 3.4** to **Fig. 3.5**), it is likely that activity arising in the lobes and the calyx are functionally segregated. Stimulating the APL neuron in the vertical lobe showed strong attenuation regardless of ATP concentration (**Fig. 3.4 B1-B3**). However, activity propagation from the horizontal lobe towards the tip of the vertical lobe was considerably less localised (**Fig. 3.4 A1-A3**). Thus, my data shows that local input to the APL neuron evokes strong local activity that diminishes as it propagates, but it is difficult to conclude from my data whether different parts of the lobes are functionally segregated or not without knowing how unitary excitatory inputs from KC axons are summed temporally and spatially.

How informative was this approach for addressing whether the APL neuron can operate locally? My approach towards characterising the spread of activity in the APL neuron was reductionist in the sense that, in a more physiologically relevant context, the APL neuron is active in concert with the whole olfactory circuit, not in isolation. I believe this is advantageous for determining whether spread of activity in the APL neuron **can** be restricted, and whether there are differences in the extent to which activity originating from different MB regions can spread. Thus, my results do not demonstrate to what extent activity in the APL neuron spreads during olfactory stimulus, but rather that input to the APL neuron evokes activity that can be spatially segregated, which could allow local processing of information.

## 6.3 Determining the spatial extent of the APL neurons output

What are the implications of the APL neuron's widespread inhibitory effect on KC activity compared to its more local activity spread for the possibility that it operates locally? In terms of locally computing inputs, one could argue that it is not relevant whether the effect of the APL neuron's inhibitory output from a single neurite is confined to only affect activity of neighbouring KC projections or if the inhibitory output globally affects KC activity, as the effect could arise from either local or global computation of input to the APL neuron.

However, in terms of operating locally, the widespread effect of its output suggests that it does not operate purely on a local level where input from KCs only translates into a local inhibitory effect on KC activity. Although the inhibitory effect is widespread, the stronger inhibitory effect observed proximally at the puff regions compared to the distal regions (H vs C and V in **Fig. 3.25 B1-C1**, and V vs C, in **Fig. 3.25 B2-C2**) shows that the inhibitory output is not spatially uniform. This difference could facilitate spatially distinct functions of the APL neurons output. As such, it is not necessary for the APL neuron's inhibitory effect to be strictly limited to the spatial extent of activity spread in the APL neuron to say that it operates locally.

Taken together, my findings on activity spread in the APL neuron and the proximal and distal effects of increasing feedback inhibition from the APL neuron onto KCs during odour stimulus support the notion that there is a degree of spatial segregation of activity in the APL neuron that could facilitate local computations. Despite the widespread inhibitory effect observed from locally stimulating the APL neuron, the spatially non-uniform strength of the effect suggests that the APL neuron can operate both locally and globally.

In sections **6.5.1** and **6.6**, I discuss other ways of estimating the spatial extent of the APL neuron's output, and the implications of my findings for the APL neuron's function in the MB, respectively.

## 6.4 Plasticity in the APL neuron

The third point I wanted to address was the spatial nature of electric shock responses, and the concomitant plasticity induced by aversive conditioning with electric shocks, in the APL neuron.

Previous studies reported that the APL neuron responds to electric shocks, but only imaged its response in a single imaging plane (Liu and Davis, 2009, Zhou et al., 2019). My results expanded on those reports by demonstrating the spatially distinct nature of the APL neuron's electric shock responses (**Fig. 4.1**).

My findings on the APL neuron's responses to electric shock agree with my characterisation of activity spread in the APL neuron, which shows that activity attenuates as it propagates throughout its neurites (**Fig. 3.4**). In fact, the attenuation was particularly pronounced for activity evoked by stimulating the APL neuron in the vertical lobe (**Fig. 3.4 A2-C2**). It is possible that the spatially distinct responses of the APL neuron to electric shock are facilitated by restricting spread of activity in its neurites. Taken together, these findings suggest that the APL neuron can locally compute the input it receives from electric shocks.

The increased calcium influx in the vertical lobe evoked by electric shock suggests that there might be a transient increase in GABA release from the APL neuron. It is possible that this plays a role during learning. My data from characterising the spatial extent of feedback inhibition from the APL neuron onto KCs suggests that this would have a strong local, albeit also widespread, inhibitory effect on KC odour responses. The increased calcium influx in the vertical lobe could possibly play a role in memory formation if this process depends on calcium influx in the APL neuron.

To investigate the spatial nature of plasticity in the APL neuron, I carried out aversive conditioning by coupling odour stimulus to electric shocks. I did not find a stimulus-specific suppression of responses in the APL neuron post conditioning with the protocol I employed and the ROIs I chose to quantify (**Fig. 4.3 C-F**). Two studies have previously documented a suppression in the APL neuron's responses to CS+ (Liu and Davis, 2009, Zhou et al., 2019). Liu et al. looked at the APL neuron's responses in the horizontal lobe, while Zhou et al. imaged its responses in a transverse plane of the lower part of the vertical lobe. In contrast, I quantified the APL neuron's responses in volume ROIs. This could be one reason I did not observe stimulus-specific depression post conditioning (further discussed in section **4.3.2**).

Another notable difference is that in Liu & Davis, 2009 and Zhou et al., 2019 the authors did not include a third odour that was not part of the training protocol to normalize the CS+ and CS- responses to. Neither did they make a comparison between the difference in the APL neuron's pre- and post-conditioning responses for CS+ and CS-. I quantified the difference between the APL

neuron's pre- and post-conditioning responses for CS+ and CS-, then compared this difference for CS+ vs CS- to determine if it was statistically significantly different (**Fig. 4.3 C-F**). This comparison was not made in the two previously mentioned studies (Zhou et al., 2019, Liu and Davis, 2009).

This point is particularly important for the findings in Zhou et al., 2019. They reported a drop in peak  $\Delta F/F$  odour responses for OCT (CS+) from ~ 15% pre-conditioning to ~ 12 % during- and ~ 11 % post-conditioning, but they also found a decline in MCH (CS-) peak  $\Delta F/F$  responses from ~ 18% pre-conditioning to ~ 17 % during- and ~ 15 % post-conditioning. It would have been very informative had they reported comparisons between the drop they observed for CS+ vs CS-.

What does this imply for the roles of the APL neuron in relation to memory formation proposed in section 1.2.9? To recapitulate, the model I proposed where suppression of the APL neuron opposes the depression of KC-MBON synapses induced by learning relies on (1) inhibition from the APL neuron locally affecting KCs and (2) learning-induced suppression of the APL neuron occurring locally (**Fig. 1.6 B**). The other possibility I proposed was that inhibition from the APL neuron gates memory formation. Suppression of the APL neuron would then allow the memory to be formed by increasing calcium influx in the KCs, leading to coincidental detection of calcium and the dopamine signal by the adenylyl cyclase, Rutabaga, which is required for memory formation.

My findings suggest that activity in the APL neuron remains spatially restricted in the lobes (**Fig. 3.4 A1-C1 and A2-C2**). The feedback inhibition had a more widespread effect on KC odour responses, but nevertheless was strongest proximally, decreasing in strength with distance (**Fig. 3.25 A1-C1 and A2-C2**). Although the feedback inhibition is not strictly localised, the gradual decline suggests that local learning-induced suppression of the APL neuron would mostly affect its output locally.

However, my results were inconclusive with regards to formation of a memory trace in the APL neuron in any of the ROIs I quantified (**Fig. 4.3 A**). Thus, based on my findings, I cannot say that both criteria are met. This does not mean that the model proposed in **Fig. 1.6** should be discounted. If suppression of the APL neuron is required only during training, and dispensable after, for immediate memory recall, then its suppression after training could still serve to locally counteract depression of KC-MBON synapses as the model suggests (**Fig. 1.6 B**). Thus, suppression of the APL neuron's response to the during training would explain its requirement for memory gating

(Zhou et al., 2019), but also explain why output from the APL neuron is required for reversal learning (Wu et al., 2012).

Contrary, if it is necessary to keep the APL neuron suppressed **after** training for immediate memory recall, it would suggest that increasing activity of the APL neuron would weaken or disrupt memory recall. This goes against the proposition that suppression of the APL neuron counteracts learning. As the exact temporal requirement for suppression of the APL neuron is not clear from the findings in Zhou et al., 2019, neither of the roles proposed in section **1.2.9** can be dismissed. Thus, the role(s) of the APL neuron with regards to memory formation remains unclear.

## 6.5 Expanding upon my findings and improving the experimental approach

### 6.5.1 Optical imaging of neuronal activity

How well did GCaMP6f serve the purpose of imaging neuronal activity? Estimating neuronal activity with GCaMP6f was adequate for characterising the spread of activity in the APL neuron and its inhibitory effect on KC activity in the entire MB (chapter 3), owing to its high dynamic range that allowed me to reliably demonstrate regional differences in activity spread and the APL neuron's inhibitory effect (discussed in sections **6.2** and **6.3**).

What are the limitations of using GCaMP6f to estimate neuronal activity? GECIs are inherently limited in their reliability as reporters of neuronal activity because they indirectly measure activity through changes in calcium levels. This leads to several drawbacks. One is the nonlinearities between cytoplasmic calcium levels to the spike frequency and to the fluorescence intensity of the fluorophore, meaning that calcium indicators at best approximately quantify neuronal activity (Akerboom et al., 2012, Chen et al., 2013). Another issue is the slow kinetics of the indicators compared to the duration of individual spikes. Even the fastest GECI, GCaMP6f can only resolve individual spikes if they are more than 50-75 ms apart (Chen et al., 2013), rendering the sensor unreliable for resolution of spikes at higher rates. Thus, there can be large disparities between voltage fluctuations and the activity reported by GECIs (Chen et al., 2013, Yang et al., 2016). This difference is most obvious in neurites with little to no spontaneous activity, where GECI signals are rectified and respond to depolarisations, but not hyperpolarisations (Yang et al., 2016). With that

said, in terms of determining where the APL neuron is active to the extent that it releases GABA, measuring calcium should provide a good estimate, under the assumption that calcium influx precedes vesicle release.

If the main priority of an experiment is to directly measure the spatial extent of depolarisation, using a GEVI would have been the better choice. At the time of my experiments, a recently developed voltage indicator, ASAP2f, with improved signal-to-noise ratio compared to its predecessor, was published (Yang et al., 2016). ASAP2f and GCaMP6f have been used to compare voltage and calcium fluctuations in fly visual system neurons evoked by visual stimulus (Yang et al., 2016). In terms of kinetics, the GCaMP6f signal took 5-fold longer than ASAP2f to reach peak response, and ~10-fold longer to decay to baseline levels. However, the superior temporal resolution offered by ASAP2f or other GEVIs would have been irrelevant due to the low sampling rate I used for acquiring volume imaging (5 Hz).

The main issue with GEVIs is the relatively low peak  $\Delta F/F$  evoked by activity, which can be 20-fold lower for ASAP2f compared to GCaMP6f (Yang et al., 2016), even though ASAP2f is amongst the highest-responding GEVIs available (Kannan et al., 2019). A 20-fold difference in  $\Delta F/F$  would likely have made some of the KC baseline activity or odour responses I measured more difficult to discern from the background noise, particularly when the responses were suppressed by inhibition from activating the APL neuron (panels **B1-B3** and **C1-C3** in **Fig. 3.11-3.15**). As such, I believe using GCaMP6f over a GEVI was the right decision for volume imaging.

Importantly, Yang et al., 2016 also showed that there are differences between GCaMP6f and ASAP2f signals across neuronal arbours, with region-specific disparity between the two indicators (Yang et al., 2016). These findings suggest that voltage and calcium fluctuations can vary widely within the same neuron, showing that GEVIs do not necessarily reproduce the spatial dynamics of membrane depolarisation faithfully.

Therefore, it would be valuable to characterise activity spread in MB neurons using a GEVI like ASAP2f in addition to GCaMP6f. The former directly reports changes in membrane potential (input), whereas the latter shows calcium influx, which precedes vesicle neurotransmitter release (output) (Grienberger et al., 2012). Using both sensors could reveal if there are spatial differences in the relationship between input and output in the APL neuron. If the peak  $\Delta F/F$  signal is too weak to record the entire MB volume simultaneously with a GEVI, one could image the spread of activity

longitudinally in the horizontal lobe (along the APL neuron's projections) in a single plane. This would not provide a global picture of activity spread throughout the APL neuron, but a comparison of activity spread as measured by ASAP2f and GCaMP6f from a single longitudinal imaging plane would be helpful to determine how faithfully GCaMP6f can report membrane depolarisation in the APL neuron. Alternatively, instead of measuring activity in the APL neuron using flies that express either ASAP2f or GCaMP6f (both GFP-based), one could express ASAP2f in conjunction with a red-shifted GECI like jRCaMP1b (Dana et al., 2016), so that calcium and voltage fluctuations can be captured and compared in the same recordings.

Finally, there are some concerns that GECI expression can perturb cell physiology. GCaMP variants with high calcium affinity can potentially function as strong calcium buffers, which could affect calcium dynamics in neurons. One study showed that expression of GCaMP6f in mouse cortical neurons perturbed calcium dynamics and calmodulin-dependent gene expression (Yang et al., 2018), while another study found that GCaMP6m expression could alter synaptic vesicle release probability in the mouse giant nerve terminal 'calyx of Held' (Singh et al., 2018).

I did not conduct any experiments to determine whether expression of GCaMP6f perturbed KC or APL neuron function. Thus, I cannot exclude that GCaMP6f perturbed the calcium dynamics or cell signalling in these neurons to some extent. However, I was able to record odour responses in both KCs (**Fig. 3.11-3.16**) and the APL neuron (**Fig. 3.5**) using GCaMP6f, suggesting that both types of neurons were at least in a functional state sufficient to respond to naturalistic stimulus

Another unresolved issue from my experiments is the discrepancy between the spatial extent of the APL neuron's inhibitory output on KC odour responses and the spread of activity in the APL neuron. To investigate whether this could be due to more widespread GABA release than my estimates of activity spread (**Fig. 3.4**) would suggest, I locally applied GABA to the MB. I found this to have a similarly widespread inhibitory effect on KCs as stimulation of the APL neuron (compare panels **D1-D3** to **A1-A3** in **Fig 3.25**). However, this approach does not directly address the spatial extent of the APL neuron's output. How could this be further substantiated? One way would be to look at vesicle release from the APL neuron during ATP stimulation, or by recording GABA signalling onto KCs.

The first option is possible through expression of synaptopHluorin in the APL neuron. This is a genetically encoded fluorescent probe that is a fusion protein of pH-sensitive GFP and the vesicle

protein VAMP2, which increases its fluorescence when it is released from the acidic lumen of vesicles (Miesenböck et al., 1998). Assuming that the fluorescent signal is strong enough, this method could visualise the spatial dynamics of GABA release from the APL neuron when it is artificially stimulated during odour exposure.

The other option is possible by expressing an intensity-based GABA sensing fluorescence reporter in KCs. This is a genetically encoded GABA sensor that is a fusion protein of a bacterial periplasmic GABA-binding protein and circularly permuted superfolder GFP that translocates to the cell membrane and emits increased fluorescence upon binding GABA (Marvin et al., 2019). This approach would not directly visualise GABA release from the APL neuron, but it would reveal to what spatial extent KCs receive the increased GABA signal evoked by local stimulation of the APL neuron.

### 6.5.2 Local activation of neurons

To locally activate neurons of interest, I expressed P2X2 in the neurons and locally applied ATP to the MB using a patch pipette coupled to a pressure system. This way, I was able to evoke local responses in the APL neuron (**Fig. 3.4**), and by changing the concentration of ATP in the patch pipette solution, I could alter the strength of the stimulus (**Fig. 3.3**).

This method of local artificial stimulation has several limitations. First, the procedure of positioning the patch pipette inside the brain to stimulate a specific region is difficult to accurately reproduce from one fly to another. This is greatly improved by expressing DsRed, a red-shifted fluorescent protein isolated from *Discosoma* coral (Matz et al., 1999), in the MB, instead of relying on the baseline fluorescent signal of GCaMP6f. Visualising the MB using DsRed allowed me to use its anatomical features as landmarks to direct the patch pipette to the same region in each fly.

However, because of the elasticity of the brain tissue, it is not possible to directly position the patch pipette in the desired location in the MB. As such, there will be slight variations in the puff site between flies.

Second, it is not possible to spatially restrict the stimulus to an exact region of interest. Irrespective of stimulus duration (determined by the duration of pressure applied by the Picospritzer and drug removal by continuous perfusion) and pressure, the bulk flow of the drug solution will disperse to

some extent. The dispersion will not be uniform, but instead depends on the way the tissue is organised around the puff site. This is another factor that contributes to variability between flies.

Third, it is difficult to determine how widely the ATP dispersed when it is ejected from the pipette, despite the co-ejection of a red dye to estimate the spread of patch pipette solution (covered in section 3.2.6 and 3.3.1). Furthermore, I found that P2X2 had leaky expression (Fig. 3.6 A3-C3), which complicated interpretation of the results from stimulating the calyx.

There are also potential concerns regarding the effect of ectopic expression of P2X2 in neurons. P2X2 is likely to change the intrinsic membrane properties due to its leak current (Fujiwara et al., 2009) which could change the resting membrane potential. I cannot exclude that this was the case when I expressed P2X2 in the APL neuron. Another issue is that uneven spatial distribution of P2X2 can give the false impression that there are regional differences in the extent of activity spread. Although I did observe differences in the spatial extent of activity spread originating from the vertical lobe and the horizontal lobe, this can be explained by the more restricted dispersion of the patch pipette solution when puffing on the vertical lobe (discussed in section 3.3.1).

What other approaches could have been used to locally stimulate neurons?

An alternative way to locally activate the APL neuron would have been to locally apply acetylcholine, a major excitatory neurotransmitter in insect brains (Dupuis et al., 2012), and the neurotransmitter released by KCs (Barnstedt et al., 2016), together with bath application of tetrodotoxin, a sodium channel blocker (Narahashi et al., 1964), to block KCs from spiking. Acetylcholine application would be more similar than ATP application to the excitatory input that the APL neuron receives from KCs, and therefore arguably more physiologically relevant. This would avoid the issue of expressing an ectopic ligand-gated ion channel in the cell membrane, which could change the resting membrane potential, or cause leaky expression. However, it is possible that acetylcholine application would also indirectly activate the APL neuron due to electrical coupling to the DPM neuron through gap junctions (Wu et al., 2011). Therefore, expressing the ectopic P2X2 ion channel and applying ATP offers a more controlled activation, barring leaky expression.

Another advantage of the approach I used is that I can relate the extent of activity spread in the APL neuron evoked by a certain concentration of ATP to its inhibitory effect on KC activity. The issue with acetylcholine application and bath perfusion with tetrodotoxin is that it precludes any

measurement of the inhibitory effect of the APL neuron on KC odour responses. I would have to use another means of locally stimulating the APL neuron. Activating the APL neuron with P2X2 by local ATP application allowed me to measure spread of activity in the APL neuron and to relate the spread of activity to the spatial extent of its inhibitory effect on KC odour responses. What would be a better way to achieve the same that overcomes the limitations of this drug application approach?

An optogenetics stimulation approach could be used to conduct the experiments I carried out that required local artificial activation of neurons. This approach offers greater control over stimulus parameters compared to ATP-mediated stimulation of P2X2-expressing neurons. First, there is no invasive procedure required to deliver the stimulus, and subsequently no difficulty with targeting the stimulus to a specific region, whereas the elasticity of the brain tissue makes it difficult to position the patch pipette in an exact location. Second, optogenetic stimulation circumvents the issue of uneven dispersion of the stimulation drug caused by the local tissue structure. Third, it offers greater control over stimulus duration and intensity, as optical stimulation can provide a pulse stimulus, rather than a stimulus with a time to peak and decay as with drug delivery. In terms of how small a stimulus region can be achieved using optogenetics, an optical stimulus decay distance to half intensity of 12  $\mu\text{m}$  laterally and  $\sim 24 \mu\text{m}$  axially has been reported (Packer et al., 2015), comparable to the decay distance to half intensity of  $\sim 10\text{-}25 \mu\text{m}$  for the red dye indicator I used when applying ATP with a patch pipette (Amin et al., 2020). It is possible to narrow the stimulus beam further, but there is a limit to how small a region must be stimulated to open enough channels to activate the target neuron (Packer et al., 2015). Thus, optogenetic stimulation does not necessarily provide more spatially confined activation, but offers the other advantages listed above.

Despite offering the above-mentioned advantages over ATP-mediated stimulation of P2X2-expressing neurons, optogenetic stimulation was not practically possible, as our two-photon microscopy setup does not feature a second laser and the scanning optics required for simultaneous optical stimulation and imaging.

Optogenetics also offers a different way to probe the spatial extent of the APL neuron's inhibitory effect. Instead of determining the spatial extent of the APL neuron's inhibitory output by recording KC odour responses while stimulating the APL neuron, one could locally inhibit the APL neuron to measure the spatial extent of KC disinhibition. What could we learn from this experiment? If the results would show that inhibition of the APL neuron locally increases KC odour responses, it

would suggest that the APL neuron's output can operate locally. Whereas if local inhibition of the APL neuron were to strongly disinhibit KCs proximally, but also to a smaller extent distally, it would confirm what I have already found by observing KC odour responses while locally activating the APL neuron. I initially attempted to conduct such an experiment by expressing a native histamine-gated chloride channel, in the APL neuron, and locally applying histamine to the MB. Bath application of histamine has previously been shown to efficiently inhibit Ort-expressing neurons in flies (Liu and Wilson, 2013). However, in the majority of my recordings, I was unable to observe any effect on KC odour responses from applying histamine and decided to abandon the experiment. What other ways could the APL neuron be locally inhibited?

This experiment could be conducted in the same way as the optogenetic stimulation approach described above, by driving the expression of an anion-gating channel, such as the *Guillardia theta* anion channelrhodopsins (GtACRs) (Govorunova et al., 2015) in the APL neuron and activating the channel in a small region with a separate laser. However, there are several reasons why this approach could be difficult to implement. GtACRs require excitation wavelengths in the 470-510 nm range, which holds for the majority of other optogenetic tools that have been used for suppression of neuronal activity (Wiegert et al., 2017). Excitation of these constructs could be difficult due to the limited penetrance of these wavelengths through the cuticle (Inagaki et al., 2014). Another issue is that this range of wavelengths would cross-activate GCaMP6f (Chen et al., 2013). This could possibly be circumvented by using a different GECI, like jRCaMP1b, whose excitation spectrum is red-shifted (Dana et al., 2016).

### 6.5.3 Measuring plasticity in the APL neuron

How could I improve my approach towards determining if and where associative conditioning leads to formation of plasticity in the APL neuron?

Intend to repeat the experiment shown in **Fig. 4.3** with the GH146-Gal4 driver that labels PNs and the APL neuron, and the APL neuron-specific intersectional approach that I used in for the experiment in **Fig. 3.1**, to determine if any of these approaches yields a stronger GCaMP6f signal in the APL neuron compared to the 474-Gal4 driver. This could solve the issues I had with noise in my recordings.

An alternative approach to studying the spatial nature of DAN-mediated suppression in the APL neuron would be to pair artificial activation of specific DAN types with odour stimulus. This approach has previously been shown to induce memory formation (Liu et al., 2012, Aso and Rubin, 2016, Aso et al., 2010, Aso et al., 2012, Burke et al., 2012, Claridge-Chang et al., 2009, Hige et al., 2015). One could then compare the APL neuron's response to the paired and an unpaired odour in the compartment(s) that are innervated by the activated DANs with those that are not, to determine if this induces compartment-specific potentiation or suppression of the APL neuron's odour response. This is not as physiologically relevant as actual aversive reinforcement and is unlikely to recapitulate the network activity evoked by a sugar reward or electric shock, but it can provide a clear link between DAN signalling and the spatial nature of memory formation in the APL neuron. My preliminary data for this experiment has confirmed that it is feasible to activate DANs locally using P2X2 (data not shown).

## 6.6 The implications of my findings for APL neuron function in the MB

Why would the APL neuron utilise graded potentials? What does it suggest for the APL neuron's function in the MB that there is localised activity in the APL neuron, while its inhibitory output is widespread, but non-uniform?

The use of graded potentials over spikes in the APL neuron could reflect a requirement for high rates of information transfer, as graded potentials have up to four-fold greater information capacity than action potentials (Laughlin and Sterling, 2015). However, KC firing rates evoked by odour stimulus are typically below 5 Hz (Turner et al., 2008), suggesting that the APL neuron is not required to transmit information at high rates. Another possibility is that the APL neuron's broad, but non-uniform feedback inhibition must be fine-tuned to the level of input it receives from KCs. The analogue nature of graded potentials can represent smaller levels of change in response compared to action potentials, and thus would be better suited to accurately adjust the level of inhibitory output.

Another possibility is that the use of analogue signalling in the APL neuron reflects a constraint in space or energy expenditure, rather than serving a particular function. As mentioned before, graded potentials are favourable to action potentials in terms of energy expenditure and utilised space (discussed in section 1.1.2). Due to the relatively small size of the fly brain, graded potentials could

suffice to transmit information at adequate speed and distance to meet the APL neuron's functional needs.

In section **1.2.10**, I speculated that, assuming that there was limited spread of activity between the calyx and the lobes in the APL neuron, the feedback inhibition could play distinct roles in these regions, due to differences in their anatomical organisation. My findings suggest that such a difference is possible. What could be the different roles of feedback inhibition in the calyx and the lobes?

As previously mentioned, feedback inhibition in the calyx could impose sparse coding on KC odour responses (see section **3.2.1**). This is plausible, considering that activity between the calyx and lobes are segregated, and that KC neurites are intermingled in the calyx, such that feedback inhibition from the APL neuron can affect all KC subsets. A role for the APL neuron to impose sparse coding in the calyx, where the KC neurites are intermingled, would agree with the previous finding that feedback inhibition from the APL neuron to KCs is all-to-all, such that reciprocal signalling between the APL neuron and any KC-subset inhibits odour responses in all KC subsets (Lin et al., 2014a).

What about the role of feedback inhibition in the MB lobes? My observation that the increased inhibitory output of the APL neuron from stimulation in the lobes was non-uniform, being stronger proximally than distally, could be interpreted to indicate that the APL neuron's output in the lobes plays distinct roles locally and globally. Although the inhibitory output is not purely local, the stronger, proximal effect suggests that suppression of the APL neuron's response to a conditioned odour could suffice to operate locally as a gating mechanism for memory formation or an 'anti-memory', as outlined in section **1.2.10**. The APL neuron presynapses onto MBONs (Takemura et al., 2017) could also play a role in memory formation or recall that so far remains unknown.

What could be the function of the widespread, or global, component of the inhibitory effect? This could contribute to maintaining sparse coding of odour responses in the KC axons. Alternatively, assuming that the APL neuron receives multimodal sensory input (see section **1.2.10**), the broader inhibition could also mediate crosstalk between the KCs representing different modalities. In this way, cross-inhibition of KCs through feedback inhibition by the APL neuron could be the mechanism by which the  $\alpha\beta$  posterior KCs that project their dendrites to the dorsal accessory calyx,

(Tanaka et al., 2008), who are thought to receive input from the visual system (Li et al., 2020), are inhibited by odour stimulus (Perisse et al., 2013).

## 6.7 Comparisons to other systems

In section **1.2.13**, I compared the fly MB to the vertebrate cerebellum, highlighting similarities between the two. However, one striking difference between these systems is that in the MB the APL neuron is the sole neuron that provides inhibition to the KCs, while in the cerebellum there are numerous Golgi cells that provide feedback inhibition to the granule cells. Another difference is that the Golgi cells encode information using spikes (D'Angelo et al., 2013), while the APL neuron is non-spiking. The cerebellum also contains other types of inhibitory interneurons, known as basket and stellate cells, that inhibit the Purkinje cells. The former synapse onto the cell bodies or axon initial segment, while the latter target the dendrites, of Purkinje cells (Prestori et al., 2019). Thus, inhibitory neurons in the vertebrate system are more numerous and diverse.

What could explain that the APL neuron is the sole inhibitory neuron that provides inhibition to the sparsely-coding KC population, while the cerebellum has numerous Golgi cells that provide feedback inhibition to the granule cells?

One obvious difference between the two systems is that the vertebrate brain has a larger volume available to occupy with neurons and their projections. For commonly used laboratory strains, the volume of a fly brain is  $\sim 8 \times 10^7 \mu\text{m}^3$  (Zheng et al., 2018), while the mouse brain measures  $415 \text{ mm}^3$  (Kovacevic et al., 2005), more than 5000-fold larger. Smaller brains cannot achieve the same level of complexity as larger brains because they must accomplish more with less: where the fly brain has space for a single neuron to encode a given piece of information, the vertebrate brain has multiple neurons which can specialise to represent different aspects or features of the same information. Increased specialisation of neuronal function has been proposed as the key feature that underlies the greater complexity of the tasks that the vertebrate nervous system performs (Laughlin and Sterling, 2015). The higher number of granule cells compared to KCs requires more inhibitory neurons. However, while the APL neuron forms synapses with all KCs (around 2000 per hemisphere), each Golgi cell only synapses onto a fraction of the granule cell population, down to a few hundred (D'Angelo et al., 2013). This difference could mean that there is a greater level of distribution of function by Golgi cells in the vertebrate cerebellum, compared to the APL neuron.

Likewise, the greater diversity of inhibitory neurons in the cerebellum could reflect a greater level of specialisation compared to the fly MB. Expanding the diversity of inhibitory interneurons allows each type of interneuron to encode more distinct information, but also to carry out a more diverse range of computations, facilitated by synapsing onto different regions of postsynaptic targets (Huang and Paul, 2019), like the basket and stellate cells.

The use of spikes in vertebrate interneurons vs graded potentials in the APL neuron could also be related to the considerable difference in brain size. At lengths above 1 mm (Dieudonne, 1998), the axonal projections of Golgi cells exceed the width of the fly brain (600  $\mu\text{m}$ ). Perhaps the spikes are necessary for activity in the interneurons in the cerebellum to reach their postsynaptic targets, while the reciprocal synapses between KCs and the APL neuron throughout the MB and the relatively small size of the fly brain mean that analogue signalling is sufficient for the APL neuron's function.

How could the smaller fly brain compensate for the lack of space? The APL neuron could fulfil more than a single function, or carry out different computations, by spatially segregating activity within its neurites. This way, a single inhibitory neuron could accomplish diverse functions and minimise energy expenditure. Of course, the disadvantage to having a single neuron carry out multiple functions is that there may be a degree of non-specificity or overlap in the local computations, and perhaps this is what is reflected in the more widespread inhibitory output of the APL neuron.

## References

- ABRAHAM, N. M., EGGER, V., SHIMSHEK, D. R., RENDEN, R., FUKUNAGA, I., SPRENGEL, R., SEEBURG, P. H., KLUGMANN, M., MARGRIE, T. W., SCHAEFER, A. T. & KUNER, T. 2010. Synaptic inhibition in the olfactory bulb accelerates odor discrimination in mice. *Neuron*, 65, 399-411.
- ACEVES-PIÑA, E. O. & QUINN, W. G. 1979. Learning in normal and mutant *Drosophila* larvae. *Science (New York, N.Y.)*, 206, 93-96.
- AKALAL, D.-B., YU, D. & DAVIS, R. 2010. A Late-Phase, Long-Term Memory Trace Forms in the gamma Neurons of *Drosophila* Mushroom Bodies after Olfactory Classical Conditioning. *Journal of Neuroscience*, 30, 16699-16708.
- AKERBOOM, J., CHEN, T. W., WARDILL, T. J., TIAN, L., MARVIN, J. S., MUTLU, S., CALDERÓN, N. C., ESPOSTI, F., BORGHUIS, B. G., SUN, X. R., GORDUS, A., ORGER, M. B., PORTUGUES, R., ENGERT, F., MACKLIN, J. J., FILOSA, A., AGGARWAL, A., KERR, R. A., TAKAGI, R., KRACUN, S., SHIGETOMI, E., KHAKH, B. S., BAIER, H., LAGNADO, L., WANG, S. S., BARGMANN, C. I., KIMMEL, B. E., JAYARAMAN, V., SVOBODA, K., KIM, D. S., SCHREITER, E. R. & LOOGER, L. L. 2012. Optimization of a GCaMP calcium indicator for neural activity imaging. *J Neurosci*, 32, 13819-40.
- AKERBOOM, J., RIVERA, J. D., GUILBE, M. M., MALAVÉ, E. C., HERNANDEZ, H. H., TIAN, L., HIRES, S. A., MARVIN, J. S., LOOGER, L. L. & SCHREITER, E. R. 2009. Crystal structures of the GCaMP calcium sensor reveal the mechanism of fluorescence signal change and aid rational design. *J Biol Chem*, 284, 6455-64.
- AKMAMMEDOV, A., GEIGGES, M. & PARO, R. 2017. Single vector non-leaky gene expression system for *Drosophila melanogaster*. *Sci Rep*, 7, 6899.
- ALBUS, J. S. 1971. A theory of cerebellar function. *Mathematical Biosciences*, 10, 25-61.
- ALLE, H. & GEIGER, J. R. 2006. Combined analog and action potential coding in hippocampal mossy fibers. *Science*, 311, 1290-3.
- AMIN, H. & LIN, A. C. 2019. Neuronal mechanisms underlying innate and learned olfactory processing in *Drosophila*. *Curr Opin Insect Sci*, 36, 9-17.
- AMIN, H., SUÁREZ-GRIMALT, R., VRONTOU, E. & LIN, A. 2020. Localized inhibition in the *Drosophila* mushroom body. *BioRxiv*.
- APPS, R., HAWKES, R., AOKI, S., BENGTSSON, F., BROWN, A. M., CHEN, G., EBNER, T. J., ISOPE, P., JÖRNTELL, H., LACKEY, E. P., LAWRENSON, C., LUMB, B., SCHONEWILLE, M., SILLITOE, R. V., SPAETH, L., SUGIHARA, I., VALERA, A., VOOGD, J., WYLIE, D. R. & RUIGROK, T. J. H. 2018. Cerebellar Modules and Their Role as Operational Cerebellar Processing Units: A Consensus paper [corrected]. *Cerebellum*, 17, 654-682.
- ASO, Y., HATTORI, D., YU, Y., JOHNSTON, R. M., IYER, N. A., NGO, T.-T. B., DIONNE, H., ABBOTT, L. F., AXEL, R., TANIMOTO, H. & RUBIN, G. M. 2014a. The neuronal architecture of the mushroom body provides a logic for associative learning. *eLife*, 3, e04577.
- ASO, Y., HERB, A., OGUETA, M., SIWANOWICZ, I., TEMPLIER, T., FRIEDRICH, A. B., ITO, K., SCHOLZ, H. & TANIMOTO, H. 2012. Three dopamine pathways induce aversive odor memories with different stability. *PLoS Genet*, 8, e1002768.
- ASO, Y., RAY, R. P., LONG, X., BUSHEY, D., CICHEWICZ, K., NGO, T. T., SHARP, B., CHRISTOFOROU, C., HU, A., LEMIRE, A. L., TILLBERG, P., HIRSH, J., LITWIN-KUMAR, A. & RUBIN, G. M. 2019. Nitric oxide acts as a cotransmitter in a subset of dopaminergic neurons to diversify memory dynamics. *Elife*, 8.
- ASO, Y. & RUBIN, G. M. 2016. Dopaminergic neurons write and update memories with cell-type-specific rules. *Elife*, 5.
- ASO, Y., SITARAMAN, D., ICHINOSE, T., KAUN, K. R., VOGT, K., BELLART-GUÉRIN, G., PLAÇAIS, P. Y., ROBIE, A. A., YAMAGATA, N., SCHNAITMANN, C., ROWELL, W. J., JOHNSTON, R. M., NGO, T. T., CHEN, N., KORFF, W., NITABACH, M. N., HEBERLEIN, U., PREAT, T., BRANSON, K. M., TANIMOTO, H. & RUBIN, G. M. 2014b. Mushroom body output neurons encode valence and guide memory-based action selection in *Drosophila*. *Elife*, 3, e04580.

- ASO, Y., SIWANOWICZ, I., BRÄCKER, L., ITO, K., KITAMOTO, T. & TANIMOTO, H. 2010. Specific Dopaminergic Neurons for the Formation of Labile Aversive Memory. *Current Biology*, 20, 1445-1451.
- AWASAKI, T., LAI, S. L., ITO, K. & LEE, T. 2008. Organization and postembryonic development of glial cells in the adult central brain of *Drosophila*. *J Neurosci*, 28, 13742-53.
- BARNSTEDT, O., OWALD, D., FELSEBERG, J., BRAIN, R., MOSZYNSKI, J. P., TALBOT, C. B., PERRAT, P. N. & WADDELL, S. 2016. Memory-Relevant Mushroom Body Output Synapses Are Cholinergic. *Neuron*, 89, 1237-1247.
- BAYLEY, T. G. & HEDWIG, B. 2018. Dendritic Ca<sup>2+</sup> dynamics and multimodal processing in a cricket antennal interneuron. *Journal of Neurophysiology*, 120, 910-919.
- BEAN, B. P. 2007. The action potential in mammalian central neurons. *Nature Reviews Neuroscience*, 8, 451.
- BECHER, P. G. A. F. G. A. R. E. A. S. A. A. H. A. A. L. S. A. L. M. C. A. H. B. S. A. P. J. A. 2012. Yeast, not fruit volatiles mediate *Drosophila melanogaster* attraction, oviposition and development. *Functional Ecology*, 26, 822-828.
- BELL, J. S. & WILSON, R. I. 2016. Behavior Reveals Selective Summation and Max Pooling among Olfactory Processing Channels. *Neuron*, 91, 425-438.
- BENTON, R., VANNICE, K. S., GOMEZ-DIAZ, C. & VOSSHALL, L. B. 2009. Variant Ionotropic Glutamate Receptors as Chemosensory Receptors in *Drosophila*. *Cell*, 136, 149-162.
- BENZER, S. 1967. Behavioral Mutants of *Drosophila* Isolated by Countercurrent Distribution. *Proceedings of the National Academy of Sciences of the United States of America*, 58, 1112-1119.
- BERRIDGE, M. J. 1993. Inositol trisphosphate and calcium signalling. *Nature*, 361, 315-25.
- BERRY, J. A., PHAN, A. & DAVIS, R. L. 2018. Dopamine Neurons Mediate Learning and Forgetting through Bidirectional Modulation of a Memory Trace. *Cell Rep*, 25, 651-662.e5.
- BHANDAWAT, V., OLSEN, S. R., GOUWENS, N. W., SCHLIEF, M. L. & WILSON, R. I. 2007. Sensory processing in the *Drosophila* antennal lobe increases reliability and separability of ensemble odor representations. *Nat Neurosci*, 10, 1474-82.
- BIALEK, W., VAN STEVENINCK, R. D. R., RIEKE, F. & WARLAND, D. 1997. *Spikes: Exploring the neural code*, The MIT Press.
- BIELOPOLSKI, N., AMIN, H., APOSTOLOPOULOU, A. A., ROZENFELD, E., LERNER, H., HUETTEROTH, W., LIN, A. C. & PARNAS, M. 2019. Inhibitory muscarinic acetylcholine receptors enhance aversive olfactory learning in adult *Drosophila*.
- BLOSS, ERIK B., CEMBROWSKI, MARK S., KARSH, B., COLONELL, J., FETTER, RICHARD D. & SPRUSTON, N. 2016. Structured Dendritic Inhibition Supports Branch-Selective Integration in CA1 Pyramidal Cells. *Neuron*, 89, 1016-1030.
- BRAKE, A. J., WAGENBACH, M. J. & JULIUS, D. 1994. New structural motif for ligand-gated ion channels defined by an ionotropic ATP receptor. *Nature*, 371, 519-23.
- BRANCO, T. & HÄUSSER, M. 2010. The single dendritic branch as a fundamental functional unit in the nervous system. *Curr Opin Neurobiol*, 20, 494-502.
- BRAND, A. H. & PERRIMON, N. 1993. Targeted gene expression as a means of altering cell fates and generating dominant phenotypes. *Development*, 118, 401-15.
- BROWN, M. R., CRIM, J. W., ARATA, R. C., CAI, H. N., CHUN, C. & SHEN, P. 1999. Identification of a *Drosophila* brain-gut peptide related to the neuropeptide Y family. *Peptides*, 20, 1035-42.
- BRÄCKER, LASSE B., SIJU, K. P., VARELA, N., ASO, Y., ZHANG, M., HEIN, I., VASCONCELOS, MARIA L. & GRUNWALD KADOW, ILONA C. 2013. Essential Role of the Mushroom Body in Context-Dependent CO<sub>2</sub> Avoidance in *Drosophila*. *Current Biology*, 23, 1228-1234.
- BURKE, C. J., HUETTEROTH, W., OWALD, D., PERISSE, E., KRASHES, M. J., DAS, G., GOHL, D., SILIES, M., CERTEL, S. & WADDELL, S. 2012. Layered reward signalling through octopamine and dopamine in *Drosophila*. *Nature*, 492, 433.
- BURNSTOCK, G. 2018. Purine and purinergic receptors. *Brain Neurosci Adv*, 2, 2398212818817494.
- BURROWS, M. 1980. The control of sets of motoneurons by local interneurons in the locust. *Journal of Physiology (London)*, 298, 213-233.
- BURROWS, M. & SIEGLER, M. 1978. Graded synaptic transmission between local interneurons and motor neurons in the metathoracic ganglion of the locust. *Journal of Physiology (London)*, 285, 231-255.

- CAMPBELL, R. A. A., HONEGGER, K. S., QIN, H., LI, W., DEMIR, E. & TURNER, G. C. 2013. Imaging a population code for odor identity in the *Drosophila* mushroom body. *The Journal of neuroscience : the official journal of the Society for Neuroscience*, 33, 10568-10581.
- CANTRELL, A. R., MA, J. Y., SCHEUER, T. & CATTERALL, W. A. 1996. Muscarinic modulation of sodium current by activation of protein kinase C in rat hippocampal neurons. *Neuron*, 16, 1019-26.
- CARLSON, D. & CARIN, L. 2019. Continuing progress of spike sorting in the era of big data. *Curr Opin Neurobiol*, 55, 90-96.
- CARON, S., RUTA, V., ABBOTT, L. & AXEL, R. 2013. Random convergence of olfactory inputs in the *Drosophila* mushroom body. *Nature*, 497, 113-7.
- CASTELLS-NOBAU, A., EIDHOF, I., FENCKOVA, M., BRENNAN-SUTTNER, D. B., SCHEFFER-DE GOOYERT, J. M., CHRISTINE, S., SCHELLEVIS, R. L., VAN DER LAAN, K., QUENTIN, C., VAN NINHUIJS, L., HOFMANN, F., EJSMONT, R., FISHER, S. E., KRAMER, J. M., SIGRIST, S. J., SIMON, A. F. & SCHENCK, A. 2019. Conserved regulation of neurodevelopmental processes and behavior by FoxP in *Drosophila*. *PLoS One*, 14, e0211652.
- CASTRO, J. B. & URBAN, N. N. 2009. Subthreshold glutamate release from mitral cell dendrites. *J Neurosci*, 29, 7023-30.
- CERVANTES-SANDOVAL, I., CHAKRABORTY, M., MACMULLEN, C. & DAVIS, R. L. 2016. Scribble Scaffolds a Signalosome for Active Forgetting. *Neuron*, 90, 1230-1242.
- CERVANTES-SANDOVAL, I., PHAN, A., CHAKRABORTY, M. & DAVIS, R. L. 2017. Reciprocal synapses between mushroom body and dopamine neurons form a positive feedback loop required for learning. *Elife*, 6.
- CHEN, C. F., BARNES, D. C. & WILSON, D. A. 2011. Generalized vs. stimulus-specific learned fear differentially modifies stimulus encoding in primary sensory cortex of awake rats. *J Neurophysiol*, 106, 3136-44.
- CHEN, M., LEE, S. & ZHOU, Z. J. 2017. Local synaptic integration enables ON-OFF asymmetric and layer-specific visual information processing in vGluT3 amacrine cell dendrites. *Proc Natl Acad Sci U S A*, 114, 11518-11523.
- CHEN, T. W., WARDILL, T. J., SUN, Y., PULVER, S. R., RENNINGER, S. L., BAOHAN, A., SCHREITER, E. R., KERR, R. A., ORGER, M. B., JAYARAMAN, V., LOOGER, L. L., SVOBODA, K. & KIM, D. S. 2013. Ultrasensitive fluorescent proteins for imaging neuronal activity. *Nature*, 499, 295-300.
- CHIN, S. G., MAGUIRE, S. E., HUOVIOLA, P., JEFFERIS, G. S. X. E. & POTTER, C. J. 2018. Olfactory Neurons and Brain Centers Directing Oviposition Decisions in *Drosophila*. *Cell Reports*, 24, 1667-1678.
- CHRISTIANSEN, F., ZUBE, C., ANDLAUER, T. F., WICHMANN, C., FOUQUET, W., OWALD, D., MERTEL, S., LEISS, F., TAVOSANIS, G., LUNA, A. J., FIALA, A. & SIGRIST, S. J. 2011. Presynapses in Kenyon cell dendrites in the mushroom body calyx of *Drosophila*. *J Neurosci*, 31, 9696-707.
- CICHON, J. & GAN, W.-B. 2015. Branch-specific dendritic Ca(2+) spikes cause persistent synaptic plasticity. *Nature*, 520, 180-185.
- CLARIDGE-CHANG, A., ROORDA, R. D., VRONTOU, E., SJULSON, L., LI, H., HIRSH, J. & MIESENBOECK, G. 2009. Writing Memories with Light-Addressable Reinforcement Circuitry. *Cell*, 139, 405-415.
- CLARK, J. T., KALRA, P. S., CROWLEY, W. R. & KALRA, S. P. 1984. Neuropeptide Y and human pancreatic polypeptide stimulate feeding behavior in rats. *Endocrinology*, 115, 427-9.
- COESMANS, M., WEBER, J. T., DE ZEEUW, C. I. & HANSEL, C. 2004. Bidirectional parallel fiber plasticity in the cerebellum under climbing fiber control. *Neuron*, 44, 691-700.
- COGNIGNI, P., FELSEBERG, J. & WADDELL, S. 2018. Do the right thing: neural network mechanisms of memory formation, expression and update in *Drosophila*. *Curr Opin Neurobiol*, 49, 51-58.
- COHN, R., MORANTTE, I. & RUTA, V. 2015. Coordinated and Compartmentalized Neuromodulation Shapes Sensory Processing in *Drosophila*. *Cell*, 163, 1742-55.
- COLLIN, C., HAUSER, F., GONZALEZ DE VALDIVIA, E., DE VALDIVIA, E. G., LI, S., REISENBERGER, J., CARLSEN, E. M., KHAN, Z., HANSEN, N. O., PUHM, F., SØNDERGAARD, L., NIEMIEC, J., HENINGER, M., REN, G. R. & GRIMMELIKHUIJZEN, C. J. 2013. Two types of muscarinic acetylcholine receptors in *Drosophila* and other arthropods. *Cell Mol Life Sci*, 70, 3231-42.

- COLOMB, J., KAISER, L., CHABAUD, M. A. & PREAT, T. 2009. Parametric and genetic analysis of *Drosophila* appetitive long-term memory and sugar motivation. *Genes, Brain and Behavior*, 8, 407-415.
- COUTO, A., ALENIUS, M. & DICKSON, B. J. 2005. Molecular, Anatomical, and Functional Organization of the *Drosophila* Olfactory System. *Current Biology*, 15, 1535-1547.
- CRIVICI, A. & IKURA, M. 1995. Molecular and structural basis of target recognition by calmodulin. *Annu Rev Biophys Biomol Struct*, 24, 85-116.
- CROCKER, A., GUAN, X.-J., MURPHY, C. T. & MURTHY, M. 2016. Cell Type-Specific Transcriptome Analysis in the *Drosophila* Mushroom Body Reveals Memory-Related Changes in Gene Expression. *Cell reports*, 15, 1580-1596.
- CROSET, V., TREIBER, C. D. & WADDELL, S. 2018. Cellular diversity in the. *Elife*, 7.
- D'ANGELO, E., SOLINAS, S., MAPELLI, J., GANDOLFI, D., MAPELLI, L. & PRESTORI, F. 2013. The cerebellar Golgi cell and spatiotemporal organization of granular layer activity. *Front Neural Circuits*, 7, 93.
- DAN, O., HOPP, E., BORST, A. & SEGEV, I. 2018. Non-uniform weighting of local motion inputs underlies dendritic computation in the fly visual system. *Sci Rep*, 8, 5787.
- DANA, H., MOHAR, B., SUN, Y., NARAYAN, S., GORDUS, A., HASSEMAN, J. P., TSEGAYE, G., HOLT, G. T., HU, A., WALPITA, D., PATEL, R., MACKLIN, J. J., BARGMANN, C. I., AHRENS, M. B., SCHREITER, E. R., JAYARAMAN, V., LOOGER, L. L., SVOBODA, K. & KIM, D. S. 2016. Sensitive red protein calcium indicators for imaging neural activity. *Elife*, 5.
- DANA, H., SUN, Y., MOHAR, B., HULSE, B. K., KERLIN, A. M., HASSEMAN, J. P., TSEGAYE, G., TSANG, A., WONG, A., PATEL, R., MACKLIN, J. J., CHEN, Y., KONNERTH, A., JAYARAMAN, V., LOOGER, L. L., SCHREITER, E. R., SVOBODA, K. & KIM, D. S. 2019. High-performance calcium sensors for imaging activity in neuronal populations and microcompartments. *Nat Methods*, 16, 649-657.
- DASGUPTA, S., FERREIRA, C. H. & MIESENBOCK, G. 2014. FoxP influences the speed and accuracy of a perceptual decision in *Drosophila*. *Science (New York, N.Y.)*, 344, 901-904.
- DASGUPTA, S., STEVENS, C. F. & NAVLAKHA, S. 2017. A neural algorithm for a fundamental computing problem. *Science (New York, N.Y.)*, 358, 793-796.
- DAVIE, K., JANSSENS, J., KOLDERE, D., DE WAEGENEER, M., PECH, U., KREFT, Ł., AIBAR, S., MAKHZAMI, S., CHRISTIAENS, V., BRAVO GONZÁLEZ-BLAS, C., POOVATHINGAL, S., HULSELMANS, G., SPANIER, K. I., MOERMAN, T., VANSPAUWEN, B., GEURS, S., VOET, T., LAMMERTYN, J., THIENPONT, B., LIU, S., KONSTANTINIDES, N., FIERS, M., VERSTREKEN, P. & AERTS, S. 2018. A Single-Cell Transcriptome Atlas of the Aging *Drosophila* Brain. *Cell*.
- DEISSEROTH, K. 2015. Optogenetics: 10 years of microbial opsins in neuroscience. *Nat Neurosci*, 18, 1213-25.
- DIEUDONNE, S. 1998. Submillisecond kinetics and low efficacy of parallel fibre-Golgi cell synaptic currents in the rat cerebellum. *J Physiol*, 510 ( Pt 3), 845-66.
- DING, H., SMITH, R. G., POLEG-POLSKY, A., DIAMOND, J. S. & BRIGGMAN, K. L. 2016. Species-specific wiring for direction selectivity in the mammalian retina. *Nature*, 535, 105-110.
- DOLAN, M.-J., BATES, A., CHUNTAO, D., DIONNE, H., CHRISTOFOROU, C., CLOSE, K., SUTCLIFFE, B., LI, F., COSTA, M., MEISSNER, G., BOCK, D., RUBIN, G. & JEFFERIS, G. 2019. Neurogenetic dissection of the *Drosophila* lateral horn reveals major outputs, diverse behavioural functions, and interactions with the mushroom body. *eLife*, 8.
- DOLAN, M.-J., BELLIART-GUÉRIN, G., BATES, A. S., FRECHTER, S., LAMPIN-SAINT-AMAUX, A., ASO, Y., ROBERTS, R. J. V., SCHLEGEL, P., WONG, A., HAMMAD, A., BOCK, D., RUBIN, G. M., PREAT, T., PLAÇAIS, P.-Y. & JEFFERIS, G. S. X. E. 2018. Communication from Learned to Innate Olfactory Processing Centers Is Required for Memory Retrieval in *Drosophila*. *Neuron*, 100, 651-668.e8.
- DUDAI, Y., JAN, Y. N., BYERS, D., QUINN, W. G. & BENZER, S. 1976. *dunce*, a mutant of *Drosophila* deficient in learning. *Proceedings of the National Academy of Sciences of the United States of America*, 73, 1684.
- DUGUID, I. C., PANKRATOV, Y., MOSS, G. W. & SMART, T. G. 2007. Somatodendritic release of glutamate regulates synaptic inhibition in cerebellar Purkinje cells via autocrine mGluR1 activation. *J Neurosci*, 27, 12464-74.

- DUPUIS, J., LOUIS, T., GAUTHIER, M. & RAYMOND, V. 2012. Insights from honeybee (*Apis mellifera*) and fly (*Drosophila melanogaster*) nicotinic acetylcholine receptors: from genes to behavioral functions. *Neurosci Biobehav Rev*, 36, 1553-64.
- DWECK, HANY K. M., EBRAHIM, SHIMAA A. M., KROMANN, S., BOWN, D., HILLBUR, Y., SACHSE, S., HANSSON, BILL S. & STENSMYR, MARCUS C. 2013. Olfactory Preference for Egg Laying on Citrus Substrates in *Drosophila*. *Current Biology*, 23, 2472-2480.
- DYLLA, K., RAISER, G., GALIZIA, C. & SZYSZKA, P. 2017. Trace Conditioning in *Drosophila* Induces Associative Plasticity in Mushroom Body Kenyon Cells and Dopaminergic Neurons. *Frontiers in Neural Circuits*, 11.
- ELYADA, Y. M., HAAG, J. & BORST, A. 2009. Different receptive fields in axons and dendrites underlie robust coding in motion-sensitive neurons. *Nature Neuroscience*, 12, 327.
- ENELL, L., HAMASAKA, Y., KOLODZIEJCZYK, A. & NÄSSEL, D. R. 2007. gamma-Aminobutyric acid (GABA) signaling components in *Drosophila*: immunocytochemical localization of GABA(B) receptors in relation to the GABA(A) receptor subunit RDL and a vesicular GABA transporter. *J Comp Neurol*, 505, 18-31.
- ERBER, J. 1978. Response characteristics and after effects of multimodal neurons in the mushroom body area of the honey bee. *Physiological Entomology*, 3, 77-89.
- EULER, T., DETWILER, P. & DENK, W. 2002. Direction-selective calcium signals in starburst cell dendrites. *Invest. Ophthalmol. Vis. Sci.*, 43, U1343-U1343.
- EVANS, R. J., LEWIS, C., VIRGINIO, C., LUNDSTROM, K., BUELL, G., SURPRENANT, A. & NORTH, R. A. 1996. Ionic permeability of, and divalent cation effects on, two ATP-gated cation channels (P2X receptors) expressed in mammalian cells. *J Physiol*, 497 ( Pt 2), 413-22.
- FARRIS, S. M. 2011. Are mushroom bodies cerebellum-like structures? *Arthropod Struct Dev*, 40, 368-79.
- FELSENBERG, J., BARNSTEDT, O., COGNIGNI, P., LIN, S. & WADDELL, S. 2017. Re-evaluation of learned information in *Drosophila*. *Nature*, 544.
- FELSENBERG, J., JACOB, P. F., WALKER, T., BARNSTEDT, O., EDMONDSON-STAIT, A. J., PLEIJZIER, M. W., OTTO, N., SCHLEGEL, P., SHARIFI, N., PERISSE, E., SMITH, C. S., LAURITZEN, J. S., COSTA, M., JEFFERIS, G. S. X. E., BOCK, D. D. & WADDELL, S. 2018. Integration of Parallel Opposing Memories Underlies Memory Extinction. *Cell*, 175, 709-722.e15.
- FISHILEVICH, E. & VOSSHALL, L. B. 2005. Genetic and Functional Subdivision of the *Drosophila* Antennal Lobe. *Current Biology*, 15, 1548-1553.
- FRANK, D. D., JOUANDET, G. C., KEARNEY, P. J., MACPHERSON, L. J. & GALLIO, M. 2015. Temperature representation in the *Drosophila* brain. *Nature*, 519, 358-361.
- FRANSEN, J. W. & BORGHUIS, B. G. 2017. Temporally Diverse Excitation Generates Direction-Selective Responses in ON- and OFF-Type Retinal Starburst Amacrine Cells. *Cell Reports*, 18, 1356-1365.
- FRECHTER, S., BATES, A. S., TOOTOONIAN, S., DOLAN, M.-J., MANTON, J., JAMASB, A. R., KOHL, J., BOCK, D. & JEFFERIS, G. 2019. Functional and anatomical specificity in a higher olfactory centre. *eLife*, 8.
- FUJIWARA, Y., KECELI, B., NAKAJO, K. & KUBO, Y. 2009. Voltage- and [ATP]-dependent gating of the P2X(2) ATP receptor channel. *J Gen Physiol*, 133, 93-109.
- GAMPER, N., REZNIKOV, V., YAMADA, Y., YANG, J. & SHAPIRO, M. S. 2004. Phosphatidylinositol [correction] 4,5-bisphosphate signals underlie receptor-specific Gq/11-mediated modulation of N-type Ca<sup>2+</sup> channels. *J Neurosci*, 24, 10980-92.
- GERVASI, N., TCHÉNIÓ, P. & PREAT, T. 2010. PKA dynamics in a *Drosophila* learning center: coincidence detection by rutabaga adenylyl cyclase and spatial regulation by dunce phosphodiesterase. *Neuron*, 65, 516-29.
- GODFREY, P. A., MALNIC, B. & BUCK, L. B. 2004. The mouse olfactory receptor gene family. *Proc Natl Acad Sci U S A*, 101, 2156-61.
- GOHL, D. M., SILIES, M. A., GAO, X. J., BHALERAO, S., LUONGO, F. J., LIN, C.-C., POTTER, C. J. & CLANDININ, T. R. 2011. A versatile in vivo system for directed dissection of gene expression patterns. *Nature Methods*, 8, 231.

- GOVORUNOVA, E. G., SINESHCHEKOV, O. A., JANZ, R., LIU, X. & SPUDICH, J. L. 2015. NEUROSCIENCE. Natural light-gated anion channels: A family of microbial rhodopsins for advanced optogenetics. *Science*, 349, 647-50.
- GRABE, V., BASCHWITZ, A., DWECK, H. K. M., LAVISTA-LLANOS, S., HANSSON, B. S. & SACHSE, S. 2016. Elucidating the Neuronal Architecture of Olfactory Glomeruli in the Drosophila Antennal Lobe. *Cell Reports*, 16, 3401-3413.
- GRANGETEAU, C., YAHOU, F., EVERAERTS, C., DUPONT, S., FARINE, J. P., BENEY, L. & FERVEUR, J. F. 2018. Yeast quality in juvenile diet affects Drosophila melanogaster adult life traits. *Sci Rep*, 8, 13070.
- GRIENBERGER, C. & KONNERTH, A. 2012. Imaging calcium in neurons. *Neuron*, 73, 862-85.
- GRIMES, W. N., ZHANG, J., GRAYDON, C. W., KACHAR, B. & DIAMOND, J. S. 2010. Retinal parallel processors: more than 100 independent microcircuits operate within a single interneuron. *Neuron*, 65, 873-85.
- GROSCHNER, L. N., CHAN WAH HAK, L., BOGACZ, R., DASGUPTA, S. & MIESENBOCK, G. 2018. Dendritic Integration of Sensory Evidence in Perceptual Decision-Making. *Cell*, 173, 894-905.e13.
- GROVER, D., KATSUKI, T., LI, J., DAWKINS, T. J. & GREENSPAN, R. J. 2020. Imaging brain activity during complex social behaviors in Drosophila with Flyception2. *Nat Commun*, 11, 623.
- GRUNTMAN, E. & TURNER, G. C. 2013. Integration of the olfactory code across dendritic claws of single mushroom body neurons. *Nature neuroscience*, 16, 1821-1829.
- GU, H. & O'DOWD, D. K. 2006. Cholinergic synaptic transmission in adult Drosophila Kenyon cells in situ. *J Neurosci*, 26, 265-72.
- HALLEM, E. A. & CARLSON, J. R. 2006. Coding of Odors by a Receptor Repertoire. *Cell*, 125, 143-160.
- HAN, K.-A., MILLAR, N. S., GROTEWIEL, M. S. & DAVIS, R. L. 1996. DAMB, a Novel Dopamine Receptor Expressed Specifically in Drosophila Mushroom Bodies. *Neuron*, 16, 1127-1135.
- HANDLER, A., GRAHAM, T. G. W., COHN, R., MORANTE, I., SILICIANO, A. F., ZENG, J., LI, Y. & RUTA, V. 2019. Distinct Dopamine Receptor Pathways Underlie the Temporal Sensitivity of Associative Learning. *Cell*, 178, 60-75.e19.
- HATTORI, D., ASO, Y., SWARTZ, K. J., RUBIN, G. M., ABBOTT, L. F. & AXEL, R. 2017. Representations of Novelty and Familiarity in a Mushroom Body Compartment. *Cell*, 169, 956-969.e17.
- HAYASHI, S., ITO, K., SADO, Y., TANIGUCHI, M., AKIMOTO, A., TAKEUCHI, H., AIGAKI, T., MATSUZAKI, F., NAKAGOSHI, H., TANIMURA, T., UEDA, R., UEMURA, T., YOSHIHARA, M. & GOTO, S. 2002. GETDB, a database compiling expression patterns and molecular locations of a collection of gal4 enhancer traps. *genesis*, 34, 58-61.
- HAYNES, P. R., CHRISTMANN, B. L. & GRIFFITH, L. C. 2015. A single pair of neurons links sleep to memory consolidation in Drosophila melanogaster. *Elife*, 4.
- HEIDELBERGER, R. 2007. Mechanisms of tonic, graded release: lessons from the vertebrate photoreceptor. *Journal of Physiology*, 585, 663-667.
- HEISENBERG, M., BORST, A., WAGNER, S. & BYERS, D. 1985. Drosophila mushroom body mutants are deficient in olfactory learning. *J Neurogenet*, 2, 1-30.
- HIGE, T. 2018. What can tiny mushrooms in fruit flies tell us about learning and memory? *Neurosci Res*, 129, 8-16.
- HIGE, T., ASO, Y., MODI, M. N., RUBIN, G. M. & TURNER, G. C. 2015. Heterosynaptic Plasticity Underlies Aversive Olfactory Learning in Drosophila. *Neuron*, 88, 985-998.
- HILGEN, G., SORBARO, M., PIRMORADIAN, S., MUTHMANN, J. O., KEPIRO, I. E., ULLO, S., RAMIREZ, C. J., PUENTE ENCINAS, A., MACCIONE, A., BERDONDINI, L., MURINO, V., SONA, D., CELLA ZANACCHI, F., SERNAGOR, E. & HENNIG, M. H. 2017. Unsupervised Spike Sorting for Large-Scale, High-Density Multielectrode Arrays. *Cell Rep*, 18, 2521-2532.
- HIMMELREICH, S., MASUHO, I., BERRY, J. A., MACMULLEN, C., SKAMANGAS, N. K., MARTEMYANOV, K. A. & DAVIS, R. L. 2017. Dopamine Receptor DAMB Signals via Gq to Mediate Forgetting in Drosophila. *Cell Reports*, 21, 2074-2081.
- HODGKIN, A. L. & HUXLEY, A. F. 1952. A quantitative description of membrane current and its application to conduction and excitation in nerve. *Journal of Physiology*, 117, 500-544.

- HONEGGER, K. S., CAMPBELL, R. A. & TURNER, G. C. 2011. Cellular-resolution population imaging reveals robust sparse coding in the *Drosophila* mushroom body. *J Neurosci*, 31, 11772-85.
- HONG, ELIZABETH J. & WILSON, RACHEL I. 2015. Simultaneous Encoding of Odors by Channels with Diverse Sensitivity to Inhibition. *Neuron*, 85, 573-589.
- HU, A., ZHANG, W. & WANG, Z. 2010. Functional feedback from mushroom bodies to antennal lobes in the *Drosophila* olfactory pathway. *Proc Natl Acad Sci U S A*, 107, 10262-7.
- HUANG, Z. J. & PAUL, A. 2019. The diversity of GABAergic neurons and neural communication elements. *Nat Rev Neurosci*, 20, 563-572.
- HUETTEROTH, W., PERISSE, E., LIN, S., KLAPPENBACH, M., BURKE, C. & WADDELL, S. 2015. Sweet taste and nutrient value subdivide rewarding dopaminergic neurons in *Drosophila*. *Curr Biol*, 25, 751-758.
- ICHINOSE, T., ASO, Y., YAMAGATA, N., ABE, A., RUBIN, G. M. & TANIMOTO, H. 2015. Reward signal in a recurrent circuit drives appetitive long-term memory formation. *Elife*, 4, e10719.
- INADA, K., TSUCHIMOTO, Y. & KAZAMA, H. 2017. Origins of Cell-Type-Specific Olfactory Processing in the *Drosophila* Mushroom Body Circuit. *Neuron*, 95, 357-367.e4.
- INAGAKI, H. K., JUNG, Y., HOOPFER, E. D., WONG, A. M., MISHRA, N., LIN, J. Y., TSIEN, R. Y. & ANDERSON, D. J. 2014. Optogenetic control of *Drosophila* using a red-shifted channelrhodopsin reveals experience-dependent influences on courtship. *Nat Methods*, 11, 325-32.
- ISAACSON, J. S. & STROWBRIDGE, B. W. 1998. Olfactory reciprocal synapses: dendritic signaling in the CNS. *Neuron*, 20, 749-61.
- ITO, I., ONG, R. C., RAMAN, B. & STOPFER, M. 2008. Sparse odor representation and olfactory learning. *Nat Neurosci*, 11, 1177-84.
- IURILLI, G. & DATTA, S. R. 2017. Population Coding in an Innately Relevant Olfactory Area. *Neuron*, 93, 1180-1197.e7.
- JACKIE, S., YITZHAK, S. & DAVID, E. C. 1998. NMDA receptors amplify calcium influx into dendritic spines during associative pre- and postsynaptic activation. *Nature Neuroscience*, 1, 114.
- JAHR, C. E. & NICOLL, R. A. 1980. Dendrodendritic inhibition: demonstration with intracellular recording. *Science*, 207, 1473-5.
- JAHR, C. E. & NICOLL, R. A. 1982. Noradrenergic modulation of dendrodendritic inhibition in the olfactory bulb. *Nature*, 297, 227-9.
- JEANNE, J. M., FIŞEK, M. & WILSON, R. I. 2018. The Organization of Projections from Olfactory Glomeruli onto Higher-Order Neurons. *Neuron*, 98, 1198-1213.e6.
- JEFFERIS, G. S. X. E., POTTER, C. J., CHAN, A. M., MARIN, E. C., ROHLFING, T., MAURER, C. R. & LUO, L. 2007. Comprehensive Maps of *Drosophila* Higher Olfactory Centers: Spatially Segregated Fruit and Pheromone Representation. *Cell*, 128, 1187-1203.
- JEFFRY, S. I. 2001. Mechanisms governing dendritic  $\gamma$ -aminobutyric acid (GABA) release in the rat olfactory bulb. *Proceedings of the National Academy of Sciences of the United States of America*, 98, 337.
- JENETT, A., RUBIN, G. M., NGO, T. T., SHEPHERD, D., MURPHY, C., DIONNE, H., PFEIFFER, B. D., CAVALLARO, A., HALL, D., JETER, J., IYER, N., FETTER, D., HAUSENFLUCK, J. H., PENG, H., TRAUTMAN, E. T., SVIRSKAS, R. R., MYERS, E. W., IWINSKI, Z. R., ASO, Y., DEPASQUALE, G. M., ENOS, A., HULAMM, P., LAM, S. C., LI, H. H., LAVERTY, T. R., LONG, F., QU, L., MURPHY, S. D., ROKICKI, K., SAFFORD, T., SHAW, K., SIMPSON, J. H., SOWELL, A., TAE, S., YU, Y. & ZUGATES, C. T. 2012. A GAL4-driver line resource for *Drosophila* neurobiology. *Cell Rep*, 2, 991-1001.
- JUUSOLA, M., FRENCH, A. S., UUSITALO, R. O. & WECKSTRÖM, M. 1996. Information processing by graded-potential transmission through tonically active synapses. *Trends Neurosci*, 19, 292-7.
- JÖRNTELL, H. & HANSEL, C. 2006. Synaptic memories upside down: bidirectional plasticity at cerebellar parallel fiber-Purkinje cell synapses. *Neuron*, 52, 227-38.
- KAMMERMEIER, P. J., RUIZ-VELASCO, V. & IKEDA, S. R. 2000. A voltage-independent calcium current inhibitory pathway activated by muscarinic agonists in rat sympathetic neurons requires both  $G_{\alpha q/11}$  and  $G_{\beta\gamma}$ . *J Neurosci*, 20, 5623-9.
- KANDEL, E. R. 2013. *Principles of neural science*, New York, New York : McGraw-Hill, c2013.
- KANNAN, M., VASAN, G. & PIERIBONE, V. A. 2019. Optimizing Strategies for Developing Genetically Encoded Voltage Indicators. *Front Cell Neurosci*, 13, 53.

- KAZAMA, H. & WILSON, R. I. 2008. Homeostatic matching and nonlinear amplification at identified central synapses. *Neuron*, 58, 401-413.
- KEENE, A. C., KRASHES, M. J., LEUNG, B., BERNARD, J. A. & WADDELL, S. 2006. Drosophila dorsal paired medial neurons provide a general mechanism for memory consolidation. *Curr Biol*, 16, 1524-30.
- KEENE, A. C., STRATMANN, M., KELLER, A., PERRAT, P. N., VOSSHALL, L. B. & WADDELL, S. 2004. Diverse odor-conditioned memories require uniquely timed dorsal paired medial neuron output. *Neuron*, 44, 521-33.
- KEENE, A. C. & WADDELL, S. 2007. Drosophila olfactory memory: single genes to complex neural circuits. *Nature reviews. Neuroscience*, 8, 341-354.
- KELEMAN, K., VRONTOU, E., KRÜTTNER, S., YU, J. Y., KURTOVIC-KOZARIC, A. & DICKSON, B. J. 2012. Dopamine neurons modulate pheromone responses in Drosophila courtship learning. *Nature*, 489, 145-9.
- KEUM, D., BAEK, C., KIM, D. I., KWEON, H. J. & SUH, B. C. 2014. Voltage-dependent regulation of CaV2.2 channels by Gq-coupled receptor is facilitated by membrane-localized  $\beta$  subunit. *J Gen Physiol*, 144, 297-309.
- KIM, A., LAZAR, A. & SLUTSKIY, Y. 2015. Projection neurons in Drosophila antennal lobes signal the acceleration of odor concentrations. *eLife*, 4.
- KIM, Y.-C., LEE, H.-G., SEONG, C.-S. & HAN, K.-A. 2003. Expression of a D1 dopamine receptor dDA1/DmDOP1 in the central nervous system of Drosophilamelanogaster. *Gene Expression Patterns*, 3, 237-245.
- KIM, Y. K., SAVER, M., SIMON, J., KENT, C. F., SHAO, L., EDDISON, M., AGRAWAL, P., TEXADA, M., TRUMAN, J. W. & HEBERLEIN, U. 2018. Repetitive aggressive encounters generate a long-lasting internal state in. *Proc Natl Acad Sci U S A*, 115, 1099-1104.
- KIRKHART, C. & SCOTT, K. 2015. Gustatory learning and processing in the Drosophila mushroom bodies. *The Journal of neuroscience : the official journal of the Society for Neuroscience*, 35, 5950-5958.
- KLAPOETKE, N. C., MURATA, Y., KIM, S. S., PULVER, S. R., BIRDSEY-BENSON, A., CHO, Y. K., MORIMOTO, T. K., CHUONG, A. S., CARPENTER, E. J., TIAN, Z., WANG, J., XIE, Y., YAN, Z., ZHANG, Y., CHOW, B. Y., SUREK, B., MELKONIAN, M., JAYARAMAN, V., CONSTANTINE-PATON, M., WONG, G. K. & BOYDEN, E. S. 2014. Independent optical excitation of distinct neural populations. *Nat Methods*, 11, 338-46.
- KOVACEVIC, N., HENDERSON, J., CHAN, E., LIFSHITZ, N., BISHOP, J., EVANS, A., HENKELMAN, R. & CHEN, X. 2005. A Three-dimensional MRI Atlas of the Mouse Brain with Estimates of the Average and Variability. *Cerebral Cortex*, 15, 639-645.
- KRASHES, M. J., DASGUPTA, S., VREEDE, A., WHITE, B., ARMSTRONG, J. D. & WADDELL, S. 2009. A neural circuit mechanism integrating motivational state with memory expression in Drosophila. *Cell*, 139, 416-27.
- KRASHES, M. J., KEENE, A. C., LEUNG, B., ARMSTRONG, J. D. & WADDELL, S. 2007. Sequential use of mushroom body neuron subsets during drosophila odor memory processing. *Neuron*, 53, 103-15.
- KRASHES, M. J. & WADDELL, S. 2008. Rapid consolidation to a radish and protein synthesis-dependent long-term memory after single-session appetitive olfactory conditioning in Drosophila. *J Neurosci*, 28, 3103-13.
- KUNDURI, G., TURNER-EVANS, D., KONYA, Y., IZUMI, Y., NAGASHIMA, K., LOCKETT, S., HOLTHUIS, J., BAMBA, T., ACHARYA, U. & ACHARYA, J. K. 2018. Defective cortex glia plasma membrane structure underlies light-induced epilepsy in. *Proc Natl Acad Sci U S A*, 115, E8919-E8928.
- KVON, E. Z., KAZMAR, T., STAMPFEL, G., YÁÑEZ-CUNA, J. O., PAGANI, M., SCHERNHUBER, K., DICKSON, B. J. & STARK, A. 2014. Genome-scale functional characterization of Drosophila developmental enhancers in vivo. *Nature*, 512, 91-5.
- KÖNIG, C., KHALILI, A., GANESAN, M., NISHU, A. P., GARZA, A. P., NIEWALDA, T., GERBER, B., ASO, Y. & YARALI, A. 2018. Reinforcement signaling of punishment versus relief in fruit flies. *Learn Mem*, 25, 247-257.
- LAISSUE, P. P., REITER, C., HIESINGER, P. R., HALTER, S., FISCHBACH, K. F. & STOCKER, R. F. 1999. Three-dimensional reconstruction of the antennal lobe in Drosophila melanogaster. *J Comp Neurol*, 405, 543-52.

- LARGE, A. M., VOGLER, N. W., MIELO, S. & OSWALD, A. M. 2016. Balanced feedforward inhibition and dominant recurrent inhibition in olfactory cortex. *Proc Natl Acad Sci U S A*, 113, 2276-81.
- LAUGHLIN, S. & STERLING, P. 2015. Principles of Neural Design. The MIT Press.
- LEE, T., LEE, A. & LUO, L. 1999. Development of the Drosophila mushroom bodies: sequential generation of three distinct types of neurons from a neuroblast. *Development*, 126, 4065-4076.
- LEISS, F., GROH, C., BUTCHER, N. J., MEINERTZHAGEN, I. A. & TAVOSANIS, G. 2009. Synaptic organization in the adult Drosophila mushroom body calyx. *Journal of Comparative Neurology*, 517, 808-824.
- LEVIN, L. R., HAN, P. L., HWANG, P. M., FEINSTEIN, P. G., DAVIS, R. L. & REED, R. R. 1992. The Drosophila learning and memory gene rutabaga encodes a Ca<sup>2+</sup>/Calmodulin-responsive adenylyl cyclase. *Cell*, 68, 479-89.
- LEWIS, L. P., SIJU, K. P., ASO, Y., FRIEDRICH, A. B., BULTEEL, A. J., RUBIN, G. M. & GRUNWALD KADOW, I. C. 2015. A Higher Brain Circuit for Immediate Integration of Conflicting Sensory Information in Drosophila. *Curr Biol*, 25, 2203-14.
- LI, H., LI, Y., LEI, Z., WANG, K. & GUO, A. 2013. Transformation of odor selectivity from projection neurons to single mushroom body neurons mapped with dual-color calcium imaging. *Proc Natl Acad Sci U S A*, 110, 12084-9.
- LI, J., MAHONEY, B. D., JACOB, M. S. & CARON, S. J. C. 2020. Visual input into the Drosophila melanogaster mushroom body. *BioRxiv*.
- LIANG, L., LI, Y., POTTER, CHRISTOPHER J., YIZHAR, O., DEISSEROTH, K., TSIEN, RICHARD W. & LUO, L. 2013. GABAergic Projection Neurons Route Selective Olfactory Inputs to Specific Higher-Order Neurons. *Neuron*, 79, 917-931.
- LIM, J., FERNANDEZ, A. I., HINOJOS, S. J., ARANDA, G. P., JAMES, J., SEONG, C. S. & HAN, K. A. 2018. The mushroom body D1 dopamine receptor controls innate courtship drive. *Genes Brain Behav*, 17, 158-167.
- LIN, A. C., BYGRAVE, A. M., DE CALIGNON, A., LEE, T. & MIESENBOCK, G. 2014a. Sparse, decorrelated odor coding in the mushroom body enhances learned odor discrimination. *Nat Neurosci*, 17, 559-68.
- LIN, H. H., LAI, J. S., CHIN, A. L., CHEN, Y. C. & CHIANG, A. S. 2007. A map of olfactory representation in the Drosophila mushroom body. *Cell*, 128, 1205-17.
- LIN, J. Y., KNUTSEN, P. M., MULLER, A., KLEINFELD, D. & TSIEN, R. Y. 2013. ReaChR: a red-shifted variant of channelrhodopsin enables deep transcranial optogenetic excitation. *Nat Neurosci*, 16, 1499-508.
- LIN, S., OWALD, D., CHANDRA, V., TALBOT, C., HUETTEROTH, W. & WADDELL, S. 2014b. Neural correlates of water reward in thirsty Drosophila. *Nat Neurosci*, 17, 1536-42.
- LIN, S., SENAPATI, B. & TSAO, C. H. 2019. Neural basis of hunger-driven behaviour in Drosophila. *Open Biol*, 9, 180259.
- LITTLETON, J. T. & GANETZKY, B. 2000. Ion channels and synaptic organization: analysis of the Drosophila genome. *Neuron*, 26, 35-43.
- LIU, C., PLAÇAIS, P.-Y., YAMAGATA, N., PFEIFFER, B. D., ASO, Y., FRIEDRICH, A. B., SIWANOWICZ, I., RUBIN, G. M., PREAT, T. & TANIMOTO, H. 2012. A subset of dopamine neurons signals reward for odour memory in Drosophila. *Nature*, 488, 512.
- LIU, D. M. & ADAMS, D. J. 2001. Ionic selectivity of native ATP-activated (P2X) receptor channels in dissociated neurones from rat parasympathetic ganglia. *J Physiol*, 534, 423-35.
- LIU, Q., TABUCHI, M., LIU, S., KODAMA, L., HORIUCHI, W., DANIELS, J., CHIU, L., BALDONI, D. & WU, M. N. 2017. Branch-specific plasticity of a bifunctional dopamine circuit encodes protein hunger. *Science*, 356, 534-539.
- LIU, W. W. & WILSON, R. I. 2013. Transient and specific inactivation of Drosophila neurons in vivo using a native ligand-gated ion channel. *Curr Biol*, 23, 1202-8.
- LIU, X. & DAVIS, R. L. 2009. The GABAergic anterior paired lateral neuron suppresses and is suppressed by olfactory learning. *Nat Neurosci*, 12, 53-9.
- LIVINGSTONE, M. S., SZIBER, P. P. & QUINN, W. G. 1984. Loss of calcium/calmodulin responsiveness in adenylyl cyclase of rutabaga, a Drosophila learning mutant. *Cell*, 37, 205-215.
- LOSONCZY, A., JUDIT, K. M. & JEFFREY, C. M. 2008. Compartmentalized dendritic plasticity and input feature storage in neurons. *Nature*, 452, 436.

- LUDWIG, M., APPS, D., MENZIES, J., PATEL, J. C. & RICE, M. E. 2016. Dendritic Release of Neurotransmitters. *Compr Physiol*, 7, 235-252.
- LUDWIG, M. & STERN, J. 2015. Multiple signalling modalities mediated by dendritic exocytosis of oxytocin and vasopressin. *Philosophical transactions of the Royal Society of London. Series B, Biological sciences*, 370.
- LÜSCHER, C. & HUBER, K. M. 2010. Group 1 mGluR-dependent synaptic long-term depression: mechanisms and implications for circuitry and disease. *Neuron*, 65, 445-59.
- MAGNUSSON, A. K., PARK, T. J., PECKA, M., GROTHE, B. & KOCH, U. 2008. Retrograde GABA Signaling Adjusts Sound Localization by Balancing Excitation and Inhibition in the Brainstem. *Neuron*, 59, 125-137.
- MANJILA, S. B., KURUVILLA, M., FERVEUR, J. F., SANE, S. P. & HASAN, G. 2019. Extended Flight Bouts Require Disinhibition from GABAergic Mushroom Body Neurons. *Curr Biol*, 29, 283-293.e5.
- MAO, Z. & DAVIS, R. L. 2009. Eight different types of dopaminergic neurons innervate the Drosophila mushroom body neuropil: anatomical and physiological heterogeneity. *Frontiers in neural circuits*, 3, 5-5.
- MARCUS, D., REINHARD, W. & MARTIN, H. 1993. Visual pattern recognition in Drosophila involves retinotopic matching. *Nature*, 365, 751.
- MARDER, E. 2006. Neurobiology: Extending influence. *Nature*, 441, 702.
- MARIN, E., ROBERTS, R., THEISS, M., PLEIJZIER, M., SARKISSIAN, T., LAURSEN, W., SCHLEGEL, P., BATES, A., LI, F., LANDGRAF, M., COSTA, M., BOCK, D. & GARRITY, P. 2020. Connectomics analysis reveals first, second, and third order thermosensory and hygrosensory neurons in the adult Drosophila brain. *BioRxiv*.
- MARIN, E. C., JEFFERIS, G. S. X. E., KOMIYAMA, T., ZHU, H. & LUO, L. 2002. Representation of the Glomerular Olfactory Map in the Drosophila Brain. *Cell*, 109, 243-255.
- MARR, D. 1969. A theory of cerebellar cortex. *The Journal of physiology*, 202, 437-470.
- MARVIN, J. S., SHIMODA, Y., MAGLOIRE, V., LEITE, M., KAWASHIMA, T., JENSEN, T. P., KOLB, I., KNOTT, E. L., NOVAK, O., PODGORSKI, K., LEIDENHEIMER, N. J., RUSAKOV, D. A., AHRENS, M. B., KULLMANN, D. M. & LOOGER, L. L. 2019. A genetically encoded fluorescent sensor for in vivo imaging of GABA. *Nat Methods*, 16, 763-770.
- MATZ, M. V., FRADKOV, A. F., LABAS, Y. A., SAVITSKY, A. P., ZARAIKY, A. G., MARKELOV, M. L. & LUKYANOV, S. A. 1999. Fluorescent proteins from nonbioluminescent Anthozoa species. *Nat Biotechnol*, 17, 969-73.
- MAUSS, A. S., VLASITS, A., BORST, A. & FELLER, M. 2017. Visual Circuits for Direction Selectivity. *Annu. Rev. Neurosci.*, 40, 211-230.
- MAZAUD, D., KOTTLER, B., GONÇALVES-PIMENTEL, C., PROELSS, S., TÜCHLER, N., DENEUBOURG, C., YUASA, Y., DIEBOLD, C., JUNGBLUTH, H., LAI, E. C., HIRTH, F., GIANGRANDE, A. & FANTO, M. 2019. Transcriptional Regulation of the Glutamate/GABA/Glutamine Cycle in Adult Glia Controls Motor Activity and Seizures in. *J Neurosci*, 39, 5269-5283.
- MCGUIRE, S. E., DESHAZER, M. & DAVIS, R. L. 2005. Thirty years of olfactory learning and memory research in Drosophila melanogaster. *Progress in Neurobiology*, 76, 328-347.
- MEDAN, V., MÄKI-MARTTUNEN, T., SZTARKER, J. & PREUSS, T. 2018. Differential processing in modality-specific Mauthner cell dendrites. *J Physiol*, 596, 667-689.
- MIESENBÖCK, G., DE ANGELIS, D. A. & ROTHMAN, J. E. 1998. Visualizing secretion and synaptic transmission with pH-sensitive green fluorescent proteins. *Nature*, 394, 192-5.
- MOMBAERTS, P., WANG, F., DULAC, C., CHAO, S. K., NEMES, A., MENDELSON, M., EDMONDSON, J. & AXEL, R. 1996. Visualizing an olfactory sensory map. *Cell*, 87, 675-86.
- NAKAI, J., OHKURA, M. & IMOTO, K. 2001. A high signal-to-noise Ca(2+) probe composed of a single green fluorescent protein. *Nat Biotechnol*, 19, 137-41.
- NARAHASHI, T., MOORE, J. W. & SCOTT, W. R. 1964. TETRODOTOXIN BLOCKAGE OF SODIUM CONDUCTANCE INCREASE IN LOBSTER GIANT AXONS. *The Journal of general physiology*, 47, 965-974.

- NERN, A., PFEIFFER, B. D. & RUBIN, G. M. 2015. Optimized tools for multicolor stochastic labeling reveal diverse stereotyped cell arrangements in the fly visual system. *Proc Natl Acad Sci U S A*, 112, E2967-76.
- NEWMAN, E. A. 2001. Propagation of intercellular calcium waves in retinal astrocytes and Müller cells. *J Neurosci*, 21, 2215-23.
- OBIEN, M. E., DELIGKARIS, K., BULLMANN, T., BAKKUM, D. J. & FREY, U. 2014. Revealing neuronal function through microelectrode array recordings. *Front Neurosci*, 8, 423.
- OFSTAD, T. A., ZUKER, C. S. & REISER, M. B. 2011. Visual place learning in *Drosophila melanogaster*. *Nature*, 474, 204.
- OGAWA, H. & OKA, K. 2015. Direction-Specific Adaptation in Neuronal and Behavioral Responses of an Insect Mechanosensory System. *The Journal of neuroscience : the official journal of the Society for Neuroscience*, 35, 11644-11655.
- OLSEN, S. R., BHANDAWAT, V. & WILSON, R. I. 2007. Excitatory Interactions between Olfactory Processing Channels in the *Drosophila* Antennal Lobe. *Neuron*, 54, 89-103.
- OLSEN, S. R., BHANDAWAT, V. & WILSON, R. I. 2010. Divisive Normalization in Olfactory Population Codes. *Neuron*, 66, 287-299.
- OLSHAUSEN, B. A. & FIELD, D. J. 2004. Sparse coding of sensory inputs. *Current Opinion in Neurobiology*, 14, 481-487.
- OWALD, D., FELSEBERG, J., TALBOT, C. B., DAS, G., PERISSE, E., HUETTEROTH, W. & WADDELL, S. 2015. Activity of defined mushroom body output neurons underlies learned olfactory behavior in *Drosophila*. *Neuron*, 86, 417-27.
- PACKER, A. M., ROSKA, B. & HÄUSSER, M. 2013. Targeting neurons and photons for optogenetics. *Nat Neurosci*, 16, 805-15.
- PACKER, A. M., RUSSELL, L. E., DALGLEISH, H. W. & HÄUSSER, M. 2015. Simultaneous all-optical manipulation and recording of neural circuit activity with cellular resolution in vivo. *Nat Methods*, 12, 140-6.
- PALANCA, L., GASKETT, A. C., GÜNTHER, C. S., NEWCOMB, R. D. & GODDARD, M. R. 2013. Quantifying variation in the ability of yeasts to attract *Drosophila melanogaster*. *PLoS One*, 8, e75332.
- PAPADOPOULOU, M., CASSENAER, S., NOWOTNY, T. & LAURENT, G. 2011. Normalization for sparse encoding of odors by a wide-field interneuron. *Science*, 332, 721-5.
- PARNAS, M., LIN, ANDREW C., HUETTEROTH, W. & MIESENBOCK, G. 2013. Odor Discrimination in *Drosophila*: From Neural Population Codes to Behavior. *Neuron*, 79, 932-944.
- PASZTOR, V. M. & BUSH, B. M. H. 1982. Impulse-coded and analog signaling in single mechanoreceptor neurons. *Science*, 216, 1635-1637.
- PATEL, J. C., WITKOVSKY, P., AVSHALUMOV, M. V. & RICE, M. E. 2009. Mobilization of calcium from intracellular stores facilitates somatodendritic dopamine release. *J Neurosci*, 29, 6568-79.
- PAVLOWSKY, A., SCHOR, J., PLAÇAIS, P. Y. & PREAT, T. 2018. A GABAergic Feedback Shapes Dopaminergic Input on the *Drosophila* Mushroom Body to Promote Appetitive Long-Term Memory. *Curr Biol*, 28, 1783-1793.e4.
- PEREZ-ORIVE, J., MAZOR, O., TURNER, G. C., CASSENAER, S., WILSON, R. I. & LAURENT, G. 2002. Oscillations and sparsening of odor representations in the mushroom body. *Science*, 297, 359-65.
- PERISSE, E., OWALD, D., BARNSTEDT, O., TALBOT, C. B., HUETTEROTH, W. & WADDELL, S. 2016. Aversive Learning and Appetitive Motivation Toggle Feed-Forward Inhibition in the *Drosophila* Mushroom Body. *Neuron*, 90, 1086-99.
- PERISSE, E., YIN, Y., LIN, A. C., LIN, S., HUETTEROTH, W. & WADDELL, S. 2013. Different kenyon cell populations drive learned approach and avoidance in *Drosophila*. *Neuron*, 79, 945-56.
- PITMAN, J. L., DASGUPTA, S., KRASHES, M. J., LEUNG, B., PERRAT, P. N. & WADDELL, S. 2009. There are many ways to train a fly.
- PITMAN, J. L., HUETTEROTH, W., BURKE, C. J., KRASHES, M. J., LAI, S. L., LEE, T. & WADDELL, S. 2011. A pair of inhibitory neurons are required to sustain labile memory in the *Drosophila* mushroom body. *Curr Biol*, 21, 855-61.

- PLAÇAIS, P. Y. & PREAT, T. 2013. To favor survival under food shortage, the brain disables costly memory. *Science*, 339, 440-2.
- PLAÇAIS, P. Y., TRANNOY, S., ISABEL, G., ASO, Y., SIWANOWICZ, I., BELLIART-GUÉRIN, G., VERNIER, P., BIRMAN, S., TANIMOTO, H. & PREAT, T. 2012. Slow oscillations in two pairs of dopaminergic neurons gate long-term memory formation in *Drosophila*. *Nat Neurosci*, 15, 592-9.
- POIRAZI, P. & MEL, B. W. 2001. Impact of Active Dendrites and Structural Plasticity on the Memory Capacity of Neural Tissue. *Neuron*, 29, 779-796.
- POLEG-POLSKY, A., DING, H. & DIAMOND, J. S. 2018. Functional Compartmentalization within Starburst Amacrine Cell Dendrites in the Retina. *Cell Reports*, 22, 2898-2908.
- POO, C. & ISAACSON, J. S. 2009. Odor representations in olfactory cortex: "sparse" coding, global inhibition, and oscillations. *Neuron*, 62, 850-61.
- PRESTORI, F., MAPELLI, L. & D'ANGELO, E. 2019. Diverse Neuron Properties and Complex Network Dynamics in the Cerebellar Cortical Inhibitory Circuit. *Front Mol Neurosci*, 12, 267.
- PREŠERN, J., TRIBLEHORN, J. D. & SCHUL, J. 2015. Dynamic dendritic compartmentalization underlies stimulus-specific adaptation in an insect neuron. *Journal of neurophysiology*, 113, 3787-3797.
- PRICE, J. L. & POWELL, T. P. 1970. The mitral and short axon cells of the olfactory bulb. *J Cell Sci*, 7, 631-51.
- QUINN, W. G., HARRIS, W. A. & BENZER, S. 1974. Conditioned Behavior in *Drosophila melanogaster*. *Proceedings of the National Academy of Sciences of the United States of America*, 71, 708.
- QUINN, W. G., SZIBER, P. P. & BOOKER, R. 1979. The *Drosophila* memory mutant amnesiac. *Nature*, 277, 212-4.
- REGEHR, W. G., CAREY, M. R. & BEST, A. R. 2009. Activity-Dependent Regulation of Synapses by Retrograde Messengers. *Neuron*, 63, 154-170.
- REN, G. R., FOLKE, J., HAUSER, F., LI, S. & GRIMMELIKHUIJZEN, C. J. 2015. The A- and B-type muscarinic acetylcholine receptors from *Drosophila melanogaster* couple to different second messenger pathways. *Biochem Biophys Res Commun*, 462, 358-64.
- RICE, M. E. & PATEL, J. C. 2015. Somatodendritic dopamine release: recent mechanistic insights. *Philosophical transactions of the Royal Society of London. Series B, Biological sciences*, 370.
- RIEMENSBERGER, T., VÖLLER, T., STOCK, P., BUCHNER, E. & FIALA, A. 2005. Punishment Prediction by Dopaminergic Neurons in *Drosophila*. *Current Biology*, 15, 1953-1960.
- ROBERTS, A. & BUSH, B. M. H. 1981. *Neurons without Impulses: Their Significance for Vertebrate and Invertebrate Nervous Systems*. Cambridge University Press.
- ROOT, C. M., SEMMELHACK, J. L., WONG, A. M., FLORES, J. & WANG, J. W. 2007. Propagation of olfactory information in *Drosophila*. *Proceedings of the National Academy of Sciences*, 104, 11826.
- RUSAN, Z. M., KINGSFORD, O. A. & TANOUYE, M. A. 2014. Modeling glial contributions to seizures and epileptogenesis: cation-chloride cotransporters in *Drosophila melanogaster*. *PLoS One*, 9, e101117.
- SANTOS, M. E., ATHANASIADIS, A., LEITÃO, A. B., DUPASQUIER, L. & SUCENA, E. 2011. Alternative splicing and gene duplication in the evolution of the FoxP gene subfamily. *Mol Biol Evol*, 28, 237-47.
- SARDI, S., VARDI, R., SHEININ, A., GOLDENTAL, A. & KANTER, I. 2017. New Types of Experiments Reveal that a Neuron Functions as Multiple Independent Threshold Units. *Sci Rep*, 7, 18036.
- SCHEIDLER, N. H., LIU, C., HAMBY, K. A., ZALOM, F. G. & SYED, Z. 2015. Volatile codes: Correlation of olfactory signals and reception in *Drosophila*-yeast chemical communication. *Sci Rep*, 5, 14059.
- SCHEUNEMANN, L., PLAÇAIS, P. Y., DROMARD, Y., SCHWÄRZEL, M. & PREAT, T. 2018. Dunce Phosphodiesterase Acts as a Checkpoint for *Drosophila* Long-Term Memory in a Pair of Serotonergic Neurons. *Neuron*, 98, 350-365.e5.
- SEVELINGES, Y., GERVAIS, R., MESSAOUDI, B., GRANJON, L. & MOULY, A. M. 2004. Olfactory fear conditioning induces field potential potentiation in rat olfactory cortex and amygdala. *Learn Mem*, 11, 761-9.
- SHADLEN, MICHAEL N. & KIANI, R. 2013. Decision Making as a Window on Cognition. *Neuron*, 80, 791-806.
- SHANG, Y., CLARIDGE-CHANG, A., SJULSON, L., PYPART, M. & MIESENBOCK, G. 2007. Excitatory Local Circuits and Their Implications for Olfactory Processing in the Fly Antennal Lobe. *Cell*, 128, 601-612.
- SHIH, H. W., WU, C. L., CHANG, S. W., LIU, T. H., LAI, J. S., FU, T. F., FU, C. C. & CHIANG, A. S. 2015. Parallel circuits control temperature preference in *Drosophila* during ageing. *Nat Commun*, 6, 7775.

- SHIH, M. M., DAVIS, F. P., HENRY, G. L. & DUBNAU, J. 2019. Nuclear Transcriptomes of the Seven Neuronal Cell Types That Constitute the. *G3 (Bethesda)*, 9, 81-94.
- SHUAI, Y., LU, B., HU, Y., WANG, L., SUN, K. & ZHONG, Y. 2010. Forgetting is regulated through Rac activity in *Drosophila*. *Cell*, 140, 579-89.
- SHYU, W. H., CHIU, T. H., CHIANG, M. H., CHENG, Y. C., TSAI, Y. L., FU, T. F., WU, T. & WU, C. L. 2017. Neural circuits for long-term water-reward memory processing in thirsty *Drosophila*. *Nat Commun*, 8, 15230.
- SIEGEL, R. W. & HALL, J. C. 1979. Conditioned responses in courtship behavior of normal and mutant *Drosophila*. *Proceedings of the National Academy of Sciences of the United States of America*, 76, 3430.
- SILVA, B., MOLINA-FERNÁNDEZ, C., UGALDE, M. B., TOGNARELLI, E. I., ANGEL, C. & CAMPUSANO, J. M. 2015. Muscarinic ACh Receptors Contribute to Aversive Olfactory Learning in *Drosophila*. *Neural Plast*, 2015, 658918.
- SIMPSON, J. H. & LOOGER, L. L. 2018. Functional Imaging and Optogenetics in *Drosophila*. *Genetics*, 208, 1291-1309.
- SINGH, M., LUJAN, B. & RENDEN, R. 2018. Presynaptic GCaMP expression decreases vesicle release probability at the calyx of Held. *Synapse*, 72, e22040.
- STANLEY, B. G. & LEIBOWITZ, S. F. 1985. Neuropeptide Y injected in the paraventricular hypothalamus: a powerful stimulant of feeding behavior. *Proc Natl Acad Sci U S A*, 82, 3940-3.
- STETTLER, D. D. & AXEL, R. 2009. Representations of odor in the piriform cortex. *Neuron*, 63, 854-64.
- STOCKER, R., LIENHARD, M., BORST, A. & FISCHBACH, K. 1990. Neuronal architecture of the antennal lobe in *Drosophila melanogaster*. *Cell and Tissue Research*, 262, 9-34.
- SU, C.-Y., MENUZ, K. & CARLSON, J. R. 2009. Olfactory Perception: Receptors, Cells, and Circuits. *Cell*, 139, 45-59.
- SU, H. & O'DOWD, D. K. 2003. Fast synaptic currents in *Drosophila* mushroom body Kenyon cells are mediated by alpha-bungarotoxin-sensitive nicotinic acetylcholine receptors and picrotoxin-sensitive GABA receptors. *J Neurosci*, 23, 9246-53.
- SUH, B. C., LEAL, K. & HILLE, B. 2010. Modulation of high-voltage activated Ca(2+) channels by membrane phosphatidylinositol 4,5-bisphosphate. *Neuron*, 67, 224-38.
- SUH, G. S. B., WONG, A. M., HERGARDEN, A. C., WANG, J. W., SIMON, A. F., BENZER, S., AXEL, R. & ANDERSON, D. J. 2004. A single population of olfactory sensory neurons mediates an innate avoidance behaviour in *Drosophila*. *Nature*, 431, 854.
- SUN, F., ZENG, J., JING, M., ZHOU, J., FENG, J., OWEN, S. F., LUO, Y., LI, F., WANG, H., YAMAGUCHI, T., YONG, Z., GAO, Y., PENG, W., WANG, L., ZHANG, S., DU, J., LIN, D., XU, M., KREITZER, A. C., CUI, G. & LI, Y. 2018. A Genetically Encoded Fluorescent Sensor Enables Rapid and Specific Detection of Dopamine in Flies, Fish, and Mice. *Cell*, 174, 481-496.e19.
- SWANSON, N. & SWANSON, L. 1995. *Histology of the Nervous System of Man and Vertebrates*, Oxford University Press.
- SÉJOURNÉ, J., PLAÇAIS, P. Y., ASO, Y., SIWANOWICZ, I., TRANNOY, S., THOMA, V., TEDJAKUMALA, S. R., RUBIN, G. M., TCHÉNIO, P., ITO, K., ISABEL, G., TANIMOTO, H. & PREAT, T. 2011. Mushroom body efferent neurons responsible for aversive olfactory memory retrieval in *Drosophila*. *Nat Neurosci*, 14, 903-10.
- TAKEMURA, S. Y., ASO, Y., HIGE, T., WONG, A., LU, Z., XU, C. S., RIVLIN, P. K., HESS, H., ZHAO, T., PARAG, T., BERG, S., HUANG, G., KATZ, W., OLBRIS, D. J., PLAZA, S., UMayAM, L., ANICETO, R., CHANG, L. A., LAUCHIE, S., OGUNDEYI, O., ORDISH, C., SHINOMIYA, A., SIGMUND, C., TAKEMURA, S., TRAN, J., TURNER, G. C., RUBIN, G. M. & SCHEFFER, L. K. 2017. A connectome of a learning and memory center in the adult *Drosophila* brain. *Elife*, 6.
- TANAKA, N. K., AWASAKI, T., SHIMADA, T. & ITO, K. 2004. Integration of Chemosensory Pathways in the *Drosophila* Second-Order Olfactory Centers. *Current Biology*, 14, 449-457.
- TANAKA, N. K., ENDO, K. & ITO, K. 2012. Organization of antennal lobe-associated neurons in adult *Drosophila melanogaster* brain. *Journal of Comparative Neurology*, 520, 4067-4130.

- TANAKA, N. K., TANIMOTO, H. & ITO, K. 2008. Neuronal assemblies of the *Drosophila* mushroom body. *J Comp Neurol*, 508, 711-55.
- TANIMOTO, H., HEISENBERG, M. & GERBER, B. 2004. Experimental psychology: Event timing turns punishment to reward. *Nature*, 430, 983.
- TEMPEL, B. L., BONINI, N., DAWSON, D. R. & QUINN, W. G. 1983. Reward learning in normal and mutant *Drosophila*. *Proceedings of the National Academy of Sciences of the United States of America*, 80, 1482.
- TIAN, L., HIRES, S. A., MAO, T., HUBER, D., CHIAPPE, M. E., CHALASANI, S. H., PETREANU, L., AKERBOOM, J., MCKINNEY, S. A., SCHREITER, E. R., BARGMANN, C. I., JAYARAMAN, V., SVOBODA, K. & LOOGER, L. L. 2009. Imaging neural activity in worms, flies and mice with improved GCaMP calcium indicators. *Nat Methods*, 6, 875-81.
- TIRIAN, L. & DICKSON, B. 2017. The VT GAL4, LexA, and split-GAL4 driver line collections for targeted expression in the *Drosophila* nervous system. *BioRxiv*.
- TOMCHIK, S. M. & DAVIS, R. L. 2009. Dynamics of learning-related cAMP signaling and stimulus integration in the *Drosophila* olfactory pathway. *Neuron*, 64, 510-21.
- TRANNOY, S., REDT-CLOUET, C., DURA, J. M. & PREAT, T. 2011. Parallel processing of appetitive short- and long-term memories in *Drosophila*. *Curr Biol*, 21, 1647-53.
- TRUNOVA, S., BAEK, B. & GINIGER, E. 2011. Cdk5 regulates the size of an axon initial segment-like compartment in mushroom body neurons of the *Drosophila* central brain. *J Neurosci*, 31, 10451-62.
- TSAO, C.-H., CHIEN-CHUN, C., CHEN-HAN, L. & HAO-YU, Y. 2018. *Drosophila* mushroom bodies integrate hunger and satiety signals to control innate food-seeking behavior. *eLife*, 7.
- TULLY, T., PREAT, T., BOYNTON, S. C. & DEL VECCHIO, M. 1994. Genetic dissection of consolidated memory in *Drosophila*. *Cell*, 79, 35-47.
- TULLY, T. & QUINN, W. 1985. Classical conditioning and retention in normal and mutant *Drosophila melanogaster*. *Sensory, Neural and Behavioral Physiology*, 157, 263-277.
- TURNER, G. C., BAZHENOV, M. & LAURENT, G. 2008. Olfactory representations by *Drosophila* mushroom body neurons. *J Neurophysiol*, 99, 734-46.
- VALERA, S., HUSSY, N., EVANS, R. J., ADAMI, N., NORTH, R. A., SURPRENANT, A. & BUELL, G. 1994. A new class of ligand-gated ion channel defined by P2x receptor for extracellular ATP. *Nature*, 371, 516-9.
- VARELA, N., GASPAR, M., DIAS, S. & VASCONCELOS, M. L. 2019. Avoidance response to CO<sub>2</sub> in the lateral horn. *PLoS Biology*, 17.
- VENKEN, K. J., SIMPSON, J. H. & BELLEN, H. J. 2011. Genetic manipulation of genes and cells in the nervous system of the fruit fly. *Neuron*, 72, 202-30.
- VLASITS, ANNA L., MORRIE, RYAN D., TRAN-VAN-MINH, A., BLECKERT, A., GAINER, CHRISTIAN F., DIGREGORIO, DAVID A. & FELLER, MARLA B. 2016. A Role for Synaptic Input Distribution in a Dendritic Computation of Motion Direction in the Retina. *Neuron*, 89, 1317-1330.
- VOGT, K., ASO, Y., HIGE, T., KNAPEK, S., ICHINOSE, T., FRIEDRICH, A. B., TURNER, G. C., RUBIN, G. M. & TANIMOTO, H. 2016. Direct neural pathways convey distinct visual information to *Drosophila* mushroom bodies. *Elife*, 5.
- VOGT, K., SCHNAITMANN, C., DYLLA, K. V., KNAPEK, S., ASO, Y., RUBIN, G. M. & TANIMOTO, H. 2014. Shared mushroom body circuits underlie visual and olfactory memories in *Drosophila*. *eLife*, 3, e02395-e02395.
- VOGT, K., YARALI, A. & TANIMOTO, H. 2015. Reversing Stimulus Timing in Visual Conditioning Leads to Memories with Opposite Valence in *Drosophila*. *PLoS One*, 10, e0139797.
- VOSSHALL, L. B., WONG, A. M. & AXEL, R. 2000. An Olfactory Sensory Map in the Fly Brain. *Cell*, 102, 147-159.
- WADDELL, S., ARMSTRONG, J. D., KITAMOTO, T., KAISER, K. & QUINN, W. G. 2000. The amnesiac gene product is expressed in two neurons in the *Drosophila* brain that are critical for memory. *Cell*, 103, 805-13.
- WANG, Q., SHUI, B., KOTLIKOFF, M. I. & SONDERMANN, H. 2008. Structural basis for calcium sensing by GCaMP2. *Structure*, 16, 1817-27.
- WEISS, S., MELOM, J. E., ORMEROD, K. G., ZHANG, Y. V. & LITTLETON, J. T. 2019. Glial Ca. *Elife*, 8.

- WEIZHE, H., HAITAO, Z., CHRISTOPHER, J. P., GABRIELLE, B., MITSUHIKO, K., KAI, Z. & LIQUN, L. 2009. Leucine-rich repeat transmembrane proteins instruct discrete dendrite targeting in an olfactory map. *Nature Neuroscience*, 12, 1542.
- WIEGERT, J. S., MAHN, M., PRIGGE, M., PRINTZ, Y. & YIZHAR, O. 2017. Silencing Neurons: Tools, Applications, and Experimental Constraints. *Neuron*, 95, 504-529.
- WILSON, R. I. 2013. Early Olfactory Processing in *Drosophila*: Mechanisms and Principles. *Annual review of neuroscience*, 36, 217-241.
- WU, C. L., SHIH, M. F., LAI, J. S., YANG, H. T., TURNER, G. C., CHEN, L. & CHIANG, A. S. 2011. Heterotypic gap junctions between two neurons in the *Drosophila* brain are critical for memory. *Curr Biol*, 21, 848-54.
- WU, C. L., SHIH, M. F., LEE, P. T. & CHIANG, A. S. 2013. An octopamine-mushroom body circuit modulates the formation of anesthesia-resistant memory in *Drosophila*. *Curr Biol*, 23, 2346-54.
- WU, Y., REN, Q., LI, H. & GUO, A. 2012. The GABAergic anterior paired lateral neurons facilitate olfactory reversal learning in *Drosophila*. *Learn Mem*, 19, 478-86.
- WYBO, W. A. M., TORBEN-NIELSEN, B., NEVIAN, T. & GEWALTIG, M.-O. 2019. Electrical Compartmentalization in Neurons. *Cell Reports*, 26, 1759-1773.e7.
- XIAO, L. & SCHEIFFELE, P. 2018. Local and long-range circuit elements for cerebellar function. *Curr Opin Neurobiol*, 48, 146-152.
- XU, C. S., JANUSZEWSKI, M., LU, Z., TAKEMURA, S.-Y., HAYWORTH, K. J., HUANG, G., SHINOMIYA, K., MAITIN-SHEPARD, J., ACKERMAN, D., BERG, S., BLAKELY, T., BOGOVIC, J., CLEMENTS, J., DOLAFI, T., HUBBARD, P., KAINMUELLER, D., KATZ, W., KAWASE, T., KHAIRY, K. A., LEAVITT, L., LI, P. H., LINDSEY, L., NEUBARTH, N., OLBRIS, D. J., OTSUNA, H., TROUTMAN, E. T., UMayAM, L., ZHAO, T., ITO, M., GOLDAMMER, J., WOLFF, T., SVIRSKAS, R., SCHLEGEL, P., NEACE, E. R., KNECHT, C. J., ALVARADO, C. X., BAILEY, D. A., BALLINGER, S., BORYCZ, J. A., CANINO, B. S., CHEATHAM, N., COOK, M., DREHER, M., DUCLOS, O., EUBANKS, B., FAIRBANKS, K., FINLEY, S., FORKNALL, N., FRANCIS, A., HOPKINS, G. P., JOYCE, E. M., KIM, S., KIRK, N. A., KOVALYAK, J., LAUCHIE, S. A., LOHFF, A., MALDONADO, C., MANLEY, E. A., MCLIN, S., MOONEY, C., NDAMA, M., OGUNDEYI, O., OKEOMA, N., ORDISH, C., PADILLA, N., PATRICK, C., PATERSON, T., PHILLIPS, E. E., PHILLIPS, E. M., RAMPALLY, N., RIBEIRO, C., ROBERTSON, M. K., RYMER, J. T., RYAN, S. M., SAMMONS, M., SCOTT, A. K., SCOTT, A. L., SHINOMIYA, A., SMITH, C., SMITH, K., SMITH, N. L., SOBESKI, M. A., SULEIMAN, A., SWIFT, J., TAKEMURA, S., TALEBI, I., TARNOGORSKA, D., TENSCHAW, E., TOKHI, T., WALSH, J. J., YANG, T., HORNE, J. A., LI, F., PAREKH, R., RIVLIN, P. K., JAYARAMAN, V., ITO, K., SAALFELD, S., GEORGE, R., MEINERTZHAGEN, I., et al. 2020. A Connectome of the Adult *Drosophila* Central Brain. *bioRxiv*, 2020.01.21.911859.
- YA-HUI, C., SPLETTER, M. L., YAKSI, E., LEONG, J. C. S., WILSON, R. I. & LUO, L. 2010. Diversity and wiring variability of olfactory local interneurons in the *Drosophila* antennal lobe. *Nature Neuroscience*, 13, 439.
- YAGI, R., MABUCHI, Y., MIZUNAMI, M. & TANAKA, N. K. 2016. Convergence of multimodal sensory pathways to the mushroom body calyx in *Drosophila melanogaster*. *Sci Rep*, 6, 29481.
- YAKSI, E. & WILSON, R. I. 2010. Electrical Coupling between Olfactory Glomeruli. *Neuron*, 67, 1034-1047.
- YAMAGATA, N., ICHINOSE, T., ASO, Y., PLAÇAIS, P.-Y., FRIEDRICH, A. B., SIMA, R. J., PREAT, T., RUBIN, G. M. & TANIMOTO, H. 2015. Distinct dopamine neurons mediate reward signals for short- and long-term memories. *Proceedings of the National Academy of Sciences*, 112, 578.
- YAMAZAKI, D., HIROI, M., ABE, T., SHIMIZU, K., MINAMI-OHTSUBO, M., MAEYAMA, Y., HORIUCHI, J. & TABATA, T. 2018. Two Parallel Pathways Assign Opposing Odor Valences during *Drosophila* Memory Formation. *Cell Rep*, 22, 2346-2358.
- YANG, H. H., ST-PIERRE, F., SUN, X., DING, X., LIN, M. Z. & CLANDININ, T. R. 2016. Subcellular Imaging of Voltage and Calcium Signals Reveals Neural Processing In Vivo. *Cell*, 166, 245-57.
- YANG, Y., LIU, N., HE, Y., LIU, Y., GE, L., ZOU, L., SONG, S., XIONG, W. & LIU, X. 2018. Improved calcium sensor GCaMP-X overcomes the calcium channel perturbations induced by the calmodulin in GCaMP. *Nature communications*, 9, 1504-1504.

- YURKOVIC, A., WANG, O., BASU, A. C. & KRAVITZ, E. A. 2006. Learning and Memory Associated with Aggression in *Drosophila melanogaster*. *Proceedings of the National Academy of Sciences of the United States of America*, 103, 17519-17524.
- YUSTE, R. & DENK, W. 1995. DENDRITIC SPINES AS BASIC FUNCTIONAL UNITS OF NEURONAL INTEGRATION. *Nature*, 375, 682-684.
- ZBILI, M., RAMA, S. & DEBANNE, D. 2016. Dynamic Control of Neurotransmitter Release by Presynaptic Potential. *Frontiers in Cellular Neuroscience*, 10.
- ZHANG, X. 2016. Functional integration of a serotonergic neuron in the *Drosophila* antennal lobe. *eLife*, 5.
- ZHANG, X., COATES, K., DACKS, A., GÜNAY, C., LAURITZEN, J. S., LI, F., CALLE-SCHULER, S. A., BOCK, D. & GAUDRY, Q. 2019. Local synaptic inputs support opposing, network-specific odor representations in a widely projecting modulatory neuron. *eLife*, 8.
- ZHENG, Z., LAURITZEN, J. S., PERLMAN, E., ROBINSON, C. G., NICHOLS, M., MILKIE, D., TORRENS, O., PRICE, J., FISHER, C. B., SHARIFI, N., CALLE-SCHULER, S. A., KMECOVA, L., ALI, I. J., KARSH, B., TRAUTMAN, E. T., BOGOVIC, J. A., HANSLOVSKY, P., JEFFERIS, G. S. X. E., KAZHDAN, M., KHAIRY, K., SAALFELD, S., FETTER, R. D. & BOCK, D. D. 2018. A Complete Electron Microscopy Volume of the Brain of Adult *Drosophila melanogaster*. *Cell*, 174, 730-743.e22.
- ZHOU, M., CHEN, N., TIAN, J., ZENG, J., ZHANG, Y., ZHANG, X., GUO, J., SUN, J., LI, Y. & GUO, A. 2019. Suppression of GABAergic neurons through D2-like receptor secures efficient conditioning in. *Proc Natl Acad Sci U S A*.
- ZHOU, Z. J. & FAIN, G. L. 1996. Starburst amacrine cells change from spiking to nonspiking neurons during retinal development. *Proc Natl Acad Sci U S A*, 93, 8057-62.
- ZILBERTER, Y., KAISER, K. & SAKMANN, B. 1999. Dendritic GABA Release Depresses Excitatory Transmission between Layer 2/3 Pyramidal and Bitufted Neurons in Rat Neocortex. *Neuron*, 24, 979-988.